LEUPHANA
UNIVERSITÄT LÜNEBURG

A Thermochemical Heat Storage System for Households: Thermal Transfers Coupled to Chemical Reaction Investigations

Thermochemisches Wärmespeichersystem

Dissertation submitted in partial fulfilment of the requirements for the academic degree of
Doctor of Natural Sciences (Dr. rer. nat.)

at the Faculty of Sustainability (Fakultät Nachhaltigkeit)

by

Dipl.-Phys. Armand Fopah Lele

Lüneburg, 2015

Submitted on (Eingereicht am): 31/04/2015

Supervisor (Betreuer und Gutachter): Prof. Dr.-Ing. Wolfgang K. L. Ruck, Leuphana University of Lüneburg, Germany

Examiner (Gutachter): Prof. Dr. Frédéric Kuznik, National Institute of applied Sciecnes (INSA)-Lyon, France

Examiner (Gutachter): Prof. Dr.-Ing. Bernd Niemeyer, Helmut-Schmidt-University (HSU) / University of the Bundeswehr of Hamburg, Germany

Day of defense (Tag der Disputation): 08/12/ 2015

To my wife Marcelle *and our son* Yohann Alexandre

"If you are storing energy, you probably want it back..."

ACKNOWLEDGEMENTS

PUBLICATIONS

1) A. Fopah Lele, C. Rohde, K. Neumann, K. E. N'Tsoukpoe, T. Tietjen, T. Rönnebeck, T. Osterland, O. Opel, W. K. L. Ruck, (2016) Lab-scale experiment of closed thermochemical heat storage with inserted honeycomb heat exchanger, Energy, submitted on 27-10-2015 with reference: EGY-D-15-04223.

2) A. Fopah Lele, F. Kuznik, T. Osterland, W.K.L. Ruck, (2016) Thermal synthesis of thermochemical heat storage with heat exchanger optimization, Applied Thermal Engineering, submitted on 30-08-2015 in special issue from invitation of ASME-ATI-UIT conference, with reference: ATE-S-15-02572.

3) A. Fopah Lele, F. Kuznik, O. Opel, W.K.L. Ruck, (2015) Performance analysis of closed thermochemical heat storage as an addition to cogeneration systems, Energy Conversion and Management, Vol. 106, pp. 1327 – 1344. doi:10.1016/j.applthermaleng.2015.06.077.

4) A. Fopah Lele, K.E. N'Tsoukpoe, T. Osterland, F. Kuznik, W.K.L. Ruck, (2015) Thermal conductivity measurement of thermochemical storage materials, Applied Thermal Engineering, Vol. 89 pp. 916–926. doi:10.1016/j.applthermaleng.2015.06.077.

5) A. Fopah Lele, F. Kuznik, H.U. Rammelberg, T. Schmidt, W.K.L. Ruck, (2015) Thermal decomposition kinetic of salt hydrates for heat storage systems, Applied Energy, Vol. 154 pp. 447–458. doi:10.1016/j.apenergy.2015.02.011.

6) K. Korhammer, M.-M. Druske, A. Fopah Lele, H.U. Rammelberg, N. Wegscheider, O. Opel, et al., (2015) Sorption and thermal characterization of composite materials based on chlorides for thermal energy storage, Applied Energy. Accepted on 26-09-2015 for publication (APEN_6825). doi:10.1016/j.apenergy.2015.08.037.

7) A. Fopah Lele, T. Rönnebeck, C. Rohde, T. Schmidt, F. Kuznik, W.K.L. Ruck, (2014) Modelling of heat exchangers based on thermochemical material for solar heat storage systems, Energy Procedia. 61 pp. 2809–2813. doi:10.1016/j.egypro.2014.12.284.

ZUSAMMENFASSUNG

Heizung stellt wegen des hohen Energieverbrauchs in kalten Regionen den wichtigsten Teil des Wärmeenergiebedarfs. Die Bedeutung der erneuerbaren Energiequellen soll effizienter gemacht werden. Allerdings wird ihre Periodizität als problembehaftet angesehen. Deshalb werden werden nicht nur eine effizientere Verwaltung der Nachfrage, als auch leistungsfähige Speichersysteme erforderlich. Auf der Grundlage dieser Behauptung wurden thermische Anlagen in Verbindung mit Stromerzeugung effizienter gestaltet, und zwar unter einem Verfahren Namens „Kraft-Wärme-Kopplung" (Mikro-BHKW). Die Wärmeverluste des Wärmeanteils des Systems führen jedoch zu Elektrizitätsschwankungen. Daher ist die Verwendung von Mikro-BHKWs in Verbindung mit einer effizienten und nahezu verlustfreien Methode, um Stromschwankungen im Wärmespeicher entgegenzuwirken, als praktikable Lösung anzusehen.

Das Wärmespeichersystem dieser Arbeit wurde auf Basis reversibler thermochemischer Reaktion entwickelt. Ein großes Potenzial ergibt sich aus guter Leistungscharakteristika wie Dehydration und Hydrierung von anorganischen Salzen, die hohe Energiedichten aufweisen (bis zu 628 kWh·m^{-3}). Das gewählte anorganische Salz ($SrBr_2 \cdot 6H_2O$) wird mit reinem Wasserdampf innerhalb eines geschlossenen Systems reagieren. Ziel dieser Arbeit ist es, ein System, das thermodynamisch günstigen Geltungsbereich für die Kombination mit Mikro-BHKW entspricht, zu entwickeln. Daher wurden Untersuchungen auf das ganze Speichermaterial vom Mikromaßstab bis zum System im Labormaßstab durgeführt. Modelle wurden auf Basis von Wärme- und Stoffaustausch mit chemischen Reaktionen ausgearbeitet, um das System zu analysieren. Experimente wurden durchgeführt, um die numerischen Tools für zukünftige Studien zusätzlich zu konsolidieren. Charakterizierungsmethod und -experimente wurden entwickelt und durchgeführt. Thermophysikalische Eigenschaften (Wärmeleitfähigkeit, spezifische Wärmekapazität, Durchlässigkeit und chemische Kinetik) des reaktiven Salzes wurden dann bestimmt, um sie als Parameter in der so entwickelten Modelle verwenden zu können.

Die numerischen Simulationen führen zu der zeitlich-räumlichen Entwicklung der Heizungsflüssigkeit, der reaktiven Bett temperaturen und des Reaktordrucks. Vorliegende Studie ist insoweit original, als sie den gekoppelten Wärme- und Stoffaustausch mit der chemischen Reaktion auf einem realitätsnahen 3D-Geometrie-Muster modelliert. Die Ergebnisse helfen, die Leistungen der thermochemischen Wärmespeicher numerisch und experimentell zu analysieren. Die Energiedichte des Bettes wird experimentell auf 531 kWh·m^{-3} von Salzhydrat festgestellt. Basierend auf der Kondensationstemperatur während des Experiments wird eine thermische Effizienz von 0,78 erreicht. Dieses System weist eine Regenerationsfähigkeit von mehr als 2/3 der Eingangsenergie auf. Auf verschiedene Aspekte der Gestaltung und der empfohlenen Reaktorenergiedichte von 140 kWh·m^{-3}, sowie eine Speicherkapazität von 65 kWh, die während der Entwicklung von Prototypen helfen könnte, werden berücksichtigt. Der Vergleich von Simulations- und Versuchsergebnissen wird dann durchgeführt und diskutiert. Dieser zeigt ermutigende Ergebnisse, auch wenn diese Studie auf Labormaßstab beschränkt ist.

Stichwort: Wärmespecher; Mikro-BHKW; thermochemische Speicher; Strontiumbromid; Wärme- und Stoffstransport mit chemischen Reaktionen gekoppelt; 3D-Modellierung; Thermophysikalische Eigenschaften; chemische Kinetik; Energieffizienz; Leistungsanalyse.

ABSTRACT

Heating is most important part of thermal energy demand, and accounts for large amounts of energy consumption in cold regions. Renewable energy sources will be of great importance in order to cover future energy demands. However, their intermittency is rightly considered as inconvenient. Thus, a more effective management of demand, coupled with efficient storage systems is required. Based on this perception, thermal systems coupled with electricity production have been efficiently designed, they are the so called "combined heat and power" (micro-CHP). Nonetheless, heat losses from the thermal part of their system lead to electricity fluctuation. Therefore, the use of micro-CHP in combination with a volume-efficient and nearly lossless heat storage system to counteract electricity fluctuations is a viable solution.

The heat storage system in this work is based on reversible thermochemical reactions, such as dehydration and hydration of inorganic salts, which exhibits very high energy density (up to 628 kWh·m^{-3} of storage material). The chosen inorganic salt ($SrBr_2 \cdot 6H_2O$) reacting with pure water vapour operates within a closed system. The objective of this work is to design a system that thermodynamically matches the combination with micro-CHP. Therefore, investigations have been performed from the material at micro-scale to the system at lab-scale. Models were developed on the basis of heat and mass transfer with chemical reaction and were done in order to numerically analyse the system. Experiments were additionally performed to consolidate the numerical tools for future studies. Characterization experiments have been designed and tested. Thermo-physical properties (thermal conductivity, specific heat capacity, permeability, chemical kinetics) of the reactive salt were then determined to be used as parameters into the so developed models.

The numerical simulations lead to the time-space evolution of heating fluid, reactive bed temperatures and reactor pressure. The originality of this study is to model the coupled heat and mass transfer with chemical reaction on a 3D geometry to be close to the reality. Results help to numerically and experimentally analyse the thermochemical heat storage performances. The bed energy density is experimentally found to be 531 kWh·m^{-3} of salt hydrate. Based on the condensation temperature during the experimentation, a reactor energy density of 140 kWh·m^{-3} and a storage capacity of 65 kWh with a thermal efficiency of 0.78 are obtained. This system proves the recovery capacity of more than 2/3 of the input energy. Various aspects of design and recommendation for optimisation aspect that could help during prototype development are taken into account and addressed. Comparison simulation-experiment is then performed and discussed, showing encouraging results, even if limited at lab-scale.

Keywords: Thermal energy storage; micro-CHP; thermochemical storage; strontium bromide; coupled heat and mass transfer with chemical reactions; 3D modelling; thermos-physical properties; chemical kinetics; energy efficiency; performance analysis.

TABLE OF CONTENTS

LIST OF FIGURES

LIST OF TABLES

NOMENCLATURE

a: honeycomb cell size (m)

A, A_0: area, heat exchanger area (m²)

A_f: frequency factor of Arrhenius (s⁻¹)

b, c: constant kinetic parameters for the reaction rate

C_0: initial concentration of salt hydrate (mol·m⁻³)

C_f: final concentration of the salt hydrate (mol·m⁻³)

C: concentration of the salt hydrate (mol·m⁻³)

C_p: specific heat capacity (J·kg⁻¹·K⁻¹)

d: diameter (m)

D_g: effective gas diffusivity in solid (m²·s⁻¹)

E_a: activation energy (J·mol⁻¹)

$E_{a,w}$: activation energy of water (J·mol⁻¹)

E_d: storage energy density of the salt (J·m⁻³)

E_{st}: stored energy (J)

$f(\alpha)$: function describing the influence of conversion, independently of temperature

g: acceleration of the gravity (m²·s⁻¹)

$h(p)$: function describing the pressure effect during the chemical process

ΔH_r^0: standard enthalpy (J·mol⁻¹·K⁻¹)

ΔH_r: enthalpy of the reaction (J·mol⁻¹·K⁻¹)

$\boldsymbol{j}$: vapour mass flux (kg·m⁻²·s⁻¹)

$k(T)$: kinetic rate constant (s⁻¹)

k: permeability (m²)

K_{cp}: heat capacity calibration constant (-)

k_D: Darcy permeability (m²)

k_E: Ergun permeability (m²)

L: length or thickness (m)

l: length of the polygonal duct or cell wall length (m)

L_{du}: height of the honeycomb element (m)

M: molar mass (g·mol⁻¹)

$\dot{m}$: mass flow rate (kg·s⁻¹)

m_0: initial mass of salt hydrate (kg)

m_f: final mass salt hydrate (kg)

m: mass of salt hydrate (kg)

N: steam molar flux (mol·m⁻³·s⁻¹)

$\vec{\boldsymbol{n}}$: normal vector to a surface

p: vapour pressure (Pa)

p_{eq}: equilibrium pressure (Pa)

p_f: reaction front pressure (Pa)

P_{aver}: average thermal power during hydration (W)

P_{aver_sht}: average thermal power during hydration based on sorption heat (W)

P_{aver_v}: volumetric average thermal power during hydration (W)

P_{stored}: average thermal power during dehydration (W)

P_{stored_1}: average thermal power during dehydration based on salt energy density (W)

P_{stored_sht}: average thermal power during dehydration based on sorption heat (W)

q: power source (W)

$\mathcal{R}$: ideal gas constant (J·mol⁻¹·K⁻¹)

R_{cht}: convective heat transfer resistance (K·W⁻¹ or °C·W⁻¹)

R_{tc2}, R_{tc2}: conductive heat transfer resistance (K·W⁻¹ or °C·W⁻¹)

R_{kin}: kinetic factor (s⁻¹)

r_p: particle radius (m)

r_i: thermocouple position (m)

S: Sutherland temperature (K)

S_w: water vapour saturation (%)

ΔS_r: entropy of the reaction of dehydration (J·mol⁻¹·K⁻¹)

ΔS_r^0: entropy of formation (J·mol⁻¹·K⁻¹)

T: temperature (K)

T_{cg}: gas phase temperature at the critical point on equilibrium curve (K)

T_{cs}: solid phase temperature at the critical point on equilibrium curve (K)

T_{eq}: equilibrium temperature (K)

T_{HTF}: heat transfer fluid temperature (K)

T_p: peak temperature usually obtained in thermal analysis experiment (K)

t: time (s)

t_α: hydration time (s)

t_α': dehydration time (s)

$\boldsymbol{u}$ velocity vector (m·s^{-1})

$\boldsymbol{u_0}$ free stream velocity vector (m·s^{-1})

$\dot{V}_f$: volume flow rate of the vapour (m^{-3}·s^{-1})

V_g: gas atomic volume (m^3)

V_s: solid atomic volume (m^3)

x, y, z : spatial coordinates (also representing thickness and width) (m)

Greek symbols:

α: reaction conversion or advancement (%)

β: heating rate (K·s^{-1})

ρ: volumetric density (kg·m^{-3})

μ: viscosity (Pa·s)

σ: energy ratio between the sensible and the reaction energy (%)

ε: total porosity of the material bed (-)

η: thermal efficiency (-)

λ: thermal conductivity (W·m^{-1}·K^{-1})

λ_s: thermal conductivity of the salt bed (W·m^{-1}·K^{-1})

ς, χ: stoichiometric coefficient of water (-)

δ: constrictivity in the porous material ()

ξ: Archie's first exponent (generally between 1.3 and 2.0)

τ: tortuosity in the porous material (-)

μ: dynamic viscosity (Pa·s)

μ_0: dynamic viscosity at the temperature of the porous media surface T_0 (Pa·s)

$\frac{d\alpha}{dt}$: reaction rate (s^{-1})

Subscripts:

ads: adsorption (or hydration phase)

bed: salt bed

c: critical point

ch: charging

$cond$: condenser

d: dense (fluid)

dis: discharging

des: desorption (or dehydration phase)

e: electrical

e_{wall}: wall thickness (m)

eff: effective

ext: external to the material bed

eq, eql: equilibrium, equivalent

f: fluid, gas

g: gas phase

h: convective heat transfer coefficient

HTF: heat transfer fluid

$i, initial$: initial, starting condition

$inlet$: inlet, entrance

isc: intrinsic

l: liquid phase

m : mean effective

$outlet, o$: outlet, output

p: particle

r: reaction

$react$: reaction

s: salt, sample

s_salt: sensible heat of the salt

s_Al: sensible heat of the Aluminium part

$s1$: salt in hydrated form

$s0$: salt in dehydrated form

$stored$: stored energy or power

t, th: thermal

v: vapour, steam

w: water vapour

ABBREVIATION

CCM:	Chemical change material
CHE:	Compact heat exchanger
CHP:	Combined heat and power
CPU:	Central processing unit
DHW:	Domestic hot water
DSC:	Differential scanning calorimetry
GHC:	Guarded hot cartridge
GHG:	Greenhouse gas
GWP:	Global warming potential
HX:	Heat exchanger
ICTAC:	International confederation for thermal analysis and calorimetry
ODP:	Ozone depletion potential
PCM:	Phase change material
RAM:	Random access memory
TESS:	Thermal energy storage system
THSS:	Thermochemical heat storage system
TGA:	Thermogravimetry analysis
ZEB:	Zero energy/emission buildings

1. GENERAL INTRODUCTION

Renewable energy helps to mitigate the tension between the energy demands and public concerns on environmental pollution (Al-Badi and Albadi, 2012). Renewable energy plays a critical role in achieving low carbon economy. However, in Germany almost 90% of energy consumption for private households is used for heating (Tzscheutschler et al., 2009). Various types of energy consumption in buildings, such as cooling, heating, hot water, lighting as well as household appliance energy consumption, can be supplied by renewable energy systems (Zhao and Magoulès, 2012). The limited reserves of conventional energy resources have gradually become the bottleneck for economic development while the greenhouse gas emission is another issue associated with conventional energy sources. There are also concerns on other types of alternative energy resources. For instance, the recent nuclear accident in Japan has triggered intensive public scrutiny on nuclear energy developments which has been slowed down. Germany will shut down all nuclear power plants by 2022 and Switzerland will abandon plans to build new nuclear reactors and phase out nuclear power in the future (Dempsey and Ewing, 2011). In addition, the government's decision to disconnect nuclear plants (representing 25% of energy production) from the German grid to preserve the environment and the fact that about 80% of gas consumption imported from Norway and Russia will seriously decrease domestic energy production due to the depletion of reserves (Bourgeois, 2001). On the other hand, the European Union has set ambitious energy and climate policy targets (European Parliament, 2004). They consist, of an increase of 20% in energy efficiency, a reduction of 20% in CO_2 emissions and cover 20% of energy needs from renewable sources by 2020 (calculation with year 1990 as basis). Another issue with energy supply is the consumer needs. The consumer needs that energy when it is not easily or not cost efficiently available. So, it is necessary to store the waste energy to optimise the energy supply. It should then be taken into account, what amount of heat and for what time it has to be stored (short- or long-term storage). Nowadays, most developing countries put more accents on industrialization processes which imply energy efficiency issues such as residential heat demand.

Under such background, the growing energy consumption in buildings has played a critical role to achieve the strategic goal of sustainable development. Renewable energy, such as solar thermal energy with no greenhouse gas emission during power generation process, can be utilised in buildings to provide a solution to the problem (Panwar et al., 2011). For instance, solar water heater can save 10–15% energy consumption and solar heating system can create 45% energy saving in buildings (Yuan et al., 2013). In 2014, 25.8% of the German electricity was provided by renewables (Lang and Lang, 2015). There is a great potential on using thermal energy systems in buildings and the technology is relatively mature. The utilisation of solar energy has received increasingly level of attention worldwide, with inexhaustible source and no greenhouse gas emission. Germany is one of the most industrialised countries in Europe. In a global rise of economy, Germany, to boost its technology drives to promote climate change protection, new energy technologies and energy efficiency. In his new integrated energy and climate program, combined heat and power (CHP), also known as cogeneration, tops the list of key elements. CHP which uses 90% of the input energy to produce both electricity and heat, may significantly reduce the peak demand (peak shaving) of electricity (Auer et al., 2008) and over 50% of the country's energy used in winter for heating of households water, cars and facilities could be provided through micro-CHP (WikiProject Energy, 2013). In the other hand, thermal energy (heat or cooling) produced by CHP can be easily stored and later delivered to meet demand, this, through an efficient energy storage system.

The concept of energy efficiency is indispensable in many engineering applications and in fact has a strong relationship with the per capita energy consumption and economic growth rate. The term energy efficiency refers to the amount of energy actually required to generate or produce the desired end products. In other words, energy efficiency is a feature that indicates the level of energy to perform an associated task and that largely depends on the state-of-the-art technological and production processes. Energy efficiency is highly valued in almost of all engineering and technological fields because of the workability of end-use product that consume less energy on long term basis (Parameshwaran et al., 2012). The storage of energy (waste, solar, electrical) is necessary today if greater energy efficiency is to be achieved and to use a large scale of this resource, in particular for the long-term storage.

1.1. EVOLUTION OF THERMOCHEMICAL HEAT STORAGE SYSTEMS

Whether controlling the flow of intermittent renewable energy or recover heat from industrial discharges, the energy storage appears to be a promising method for the introduction of low carbon energy and energy efficiency. Thermal energy storage is important since its application may improve the performance of energy systems. There has been active research in the application of thermal energy storage in space heating. In particular, thermal energy storage for one day or over several months is an attractive solution for the development of energy in buildings. A major cause of energy inefficiency is a result of the generation of waste heat and the lack of suitable technologies for cost-effective utilisation of low grade heat in particular. Talking about thermal energy storage in this thesis leads to the thermochemical heat storage, because of the involved chemical reactions. This terminology has been used in different manners by many authors in the past; however some authors (N'Tsoukpoe et al., 2009) clearly bring an answer to that. Beside the thermochemical, there is latent and sensible storage, for which research development and prototypes are well mastered (Garg et al., 1985). Thermal storage systems involve at least three steps: charging, storage and discharging. In sensible heat storage systems, during the charging step, external thermal energy is used to heat a fluid or a solid medium, thus, increasing its energy content. Then, the medium is stored at the charging step temperature. When this energy is released (discharging step), the medium temperature decreases. The sensible heat stored is associated with the increase or decrease of the temperature (strongly dependent on heat capacity of the medium). In latent heat storage, during the charging step, thermal energy can be used as the heat source that initiates a phase change. Then, the medium is stored at the charging step temperature in its new phase. When this energy is released (discharging step), the medium phase changes into the first state (strongly dependent on the latent enthalpy of the medium). The latent heat stored is associated with this phase change; the used materials are called phase change materials (PCM). In thermochemical and/or sorption heat storage system the reactions involved are reversible:

$$A + \Delta H_r \leftrightarrows B + C \qquad (1.1)$$

Heat is stored during the endothermic reaction step and released during the exothermic one. The thermochemical heat stored is linked to the reaction enthalpy. During the charging step, thermal energy is used to dissociate a chemical reactant (A), into products (B) and (C). This reac-

tion is endothermic. During the releasing step, the products of the endothermic reaction (B and C) are mixed together and react to form the initial reactant (A). This reaction is exothermic and releases heat. The products of both reactions can be stored either at ambient temperature or at operating temperature. Researchs on thermochemical energy storage systems have been investigated four decades ago. It was initially called chemical change material (CCM) (Maru et al., 1976), due to chemical reactions involved.

Before showing the evolution of the thermochemical energy storage, let us remind why it is chosen among the others. A comparison of the benefits and drawbacks of latent, sensible, and thermochemical storage is given in Table 1.1. Thermochemical storage is mainly based on chemical reaction. The reason of selecting thermochemical method is developed in the following. Although there are different ways (latent, sorption, chemical) to store thermal energy, thermal performance of an energy system depends on thermodynamic properties of the used energy media. Higher energy storage density and reversibility are required for the materials for thermal energy storage. Figure 1.1 shows relative relationship of energy densities of physical and chemical changes (Kato, 2007). The energy density of chemical changes is relatively higher than one of physical changes. Sensible heat and physical phase changes are popular system for conventional energy storage technologies, such as steam engines, because of well reversibility of their changes. On the other hand, chemical changes such as oxidation are irreversible and hard to apply for repetitive heat storage operation.

Table 1.1. A comparison of properties of different types of thermal energy storage (adapted from (Kilkis and Kakac, 1989) and (Kousksou et al., 2014)).

	Thermochemical	Latent	Sensible
Storage density	High ($0.4 - 3$ GJ/m^3)	Moderate, increase at high temperature ($0.3 - 0.5$ GJ/m^3)	Low, unless large temperature interval (0.2 GJ/m^3)
Need for insulation	No	Yes	Yes
Operating temperature	Variable: low ($30 - 70$ °C), high ($100 - 500$ °C), higher if considering redox reaction	Constant	variable
Technology	Prototype available	Available for some temperature ranges	Available
Lifetime	Depends on degradation, and possible side reactions, frequent problem	Often limited by cycling ability of the material	Long, indefinitely!
Transport ability	Long distances possible	Short distances possible	Normally not
Heat losses	Losses through need for product cooling, long-term storage possible without additional losses	Depend on degree of insulation, long-term storage possible only with large scale storage.	Depend on degree of insulation, long-term storage possible only with large scale storage.

Regarding the above table, Pardo et al. (Pardo et al., 2014) added that the transport ability and the storage period can be unlimited, and heat can be stored at ambient temperature for thermochemical storage system. Then, reversible chemical reaction is expected to have potential for energy storage process nowadays because of its higher energy density and reversibility. A merit of chemical energy conversion is the capacity of efficient energy storage performance. Physical thermal storage gradually loses thermal energy by heat conduction and radiation; however, chemical storage can store energy in term of reactants with a small energy loss that can be neglected.
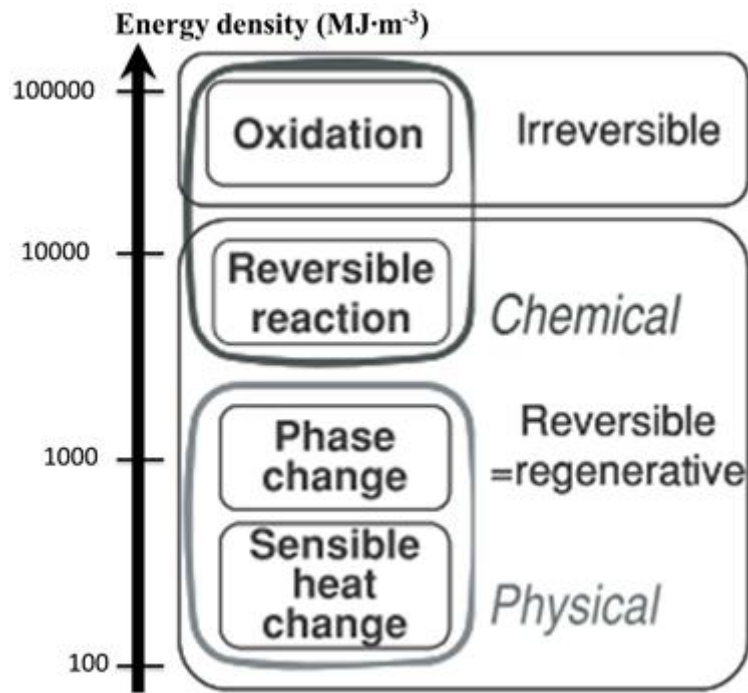
Figure 1.1: Energy density of physical and chemical changes, adapted from (Paksoy, 2005).

One of the major issue of heat storage for space heating is its compactness. Its use in the residential sector requires indeed the minimisation of the space occupied by this type of system. Given the large amount of energy to be stored, it is essential to develop a method for a system with high energy capacity. Moreover, as the heat storage is being performed over extended periods according to short or long-term, it is necessary to minimise the heat losses during that time, to maximise the compactness of the system and its effectiveness. Basic advantages are the possibility of keeping high storage densities and being able to increase the length of the storage period without incurring additional losses.

In terms of storage media (material), a wide variety of choices exists depending on the temperature range and application. For sensible heat storage, water is a common choice because, among its other positive attributes, it has one of the highest specific heats of any liquid at ambient temperatures. While the specific heat of water is not as high as that for many solids, it has the advantage of being a liquid that can easily be pumped to transport thermal energy. Being a liquid, water also allows good heat-transfer rates (Commandré et al., 2007; Shi et al., 2002). Solids have the advantage of higher specific heat capacities, which allow for more compact storage units. When higher temperatures are involved, such as preheating furnace air supplies, solids become the preferred sensible heat storage material. For latent heat storage, heat changes have received a great deal of attention. The most common example of latent heat storage is the

conversion of water to ice. Thermochemical heat storage can be classified in three types due to storage medium: chemical adsorption materials like zeolites, chemical absorption in hygroscopic solutions such as NaOH solution and chemical without sorption in salts such as salt hydrates. Salt hydrates have been selected because of their high energy density (see Figure 1.2) and low cost, while the main disadvantage is their lower stability and relatively slow kinetics (Zondag et al., 2013). The thermochemical heat storage system for energy storage based on salt hydrates use a reversible chemical reaction:

$$Salt \cdot \varsigma H_2O_{(s)} + Heat \leftrightharpoons Salt \cdot (\varsigma - \chi)H_2O_{(s)} + \chi H_2O_{(g)} \tag{1.2}$$
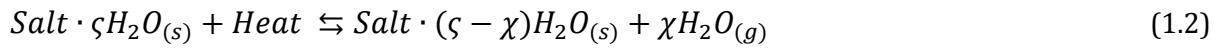
consisting of dehydration (charging mode; forward reaction) and hydration (discharging mode; backward reaction) of the material, through a decomposition/synthesis process. The performance of the system is then realised with the exothermic synthesis reaction and the endothermic decomposition reaction.
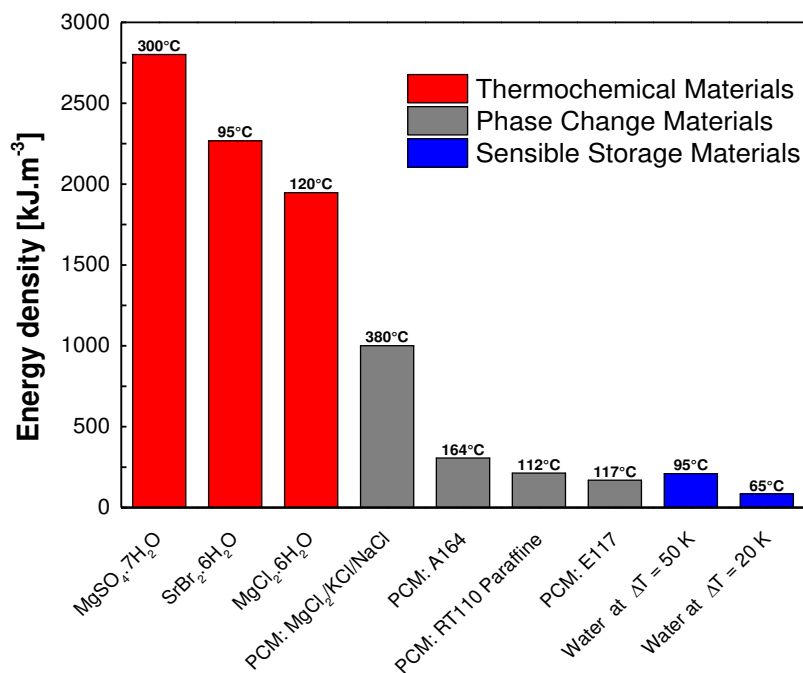
Figure 1.2: Theoretical energy storage density of materials for the main three thermal energy storage systems.

1.2. EMERGENCE OF THERMAL ISSUES

The drawback of energy consumption is related to environmental issues. Burning of conventional energy sources emits a lot of greenhouse gases (GHG) particularly carbon dioxide (CO_2). The CO_2 emission is increasing every year which mostly comes from the developing region . That increase is due to the massive economic development in these regions. Also, in the developing

countries, population is tremendously increasing which results in higher energy consumption (Enteria and Mizutani, 2011). In addition, as economic development progresses, massive usage and application of gadgets, devices and equipment contribute to the environmental problems. Hence, many of these contribute to greenhouse gases and ozone layer depleting substances. In fact, heating equipment and devices contribute a lot of these greenhouse gases (Enteria and Mizutani, 2011). CO_2 emissions can be reduced through technology development and application. Hence, for example, combined systems such as micro combined heating and power (CHP) and combined cooling, heating and power (CCHP) systems can reduce energy consumption and greenhouse gas emissions. Building sector represents 26% of CO_2 emissions in Germany (Tzscheutschler et al., 2009). Heating, accounting for almost 90% of the energy consumption of buildings is the main CO_2 emissions source in the sector. Therefore, the building sector appears as a significant energy saving potential deposit and can be a decisive asset in the division of greenhouse gas emissions by a factor of 4 by 2050 (Hongois, 2011).

In contrast to conventional power stations where the waste heat is not used, in combined heat and power plants, the waste heat can be re-used at its normal temperature. Re-using that waste heat could improve the production of industrial process steam or the heating of domestic premises (Rüdig, 1986). It has been observed that, the installation of a device for storing heat in micro-CHP plant can be desirable on economic grounds (Fragaki et al., 2008). This stored heat is typically called thermal store or heat accumulator, and when the process is led by chemical reaction, it is also called thermochemical heat.

In thermochemical storage, the products may in many cases be stored at ambient temperature, eliminating the need for insulating. However, an amount of heat used to charge the system is released when the products are cooled down to storage temperature. It is therefore important to design a system that uses almost 100% of available heat and does not allow heat loss or at least significantly reduce it.

1.3. MOTIVATION OF THIS THESIS

Thermal energy storage provides a flexible heating and/or cooling tool to fight climate change through conserving energy and increasing energy efficiency. Using local and renewable sources can be greatly improved and be more productive when coupled with thermal energy storage systems. Thermal energy storage can also be used to level out both diurnal and seasonal peaks occurring in energy demand curves. This work aims to give as much as possible design parameters and performances analysis in order to build a prototype to be coupled with micro-CHP.

In order to achieve ambitious targets for energy efficiency and zero energy/emission buildings (ZEB), technologies for heat recovery have been highly recommended. Heat recovery in buildings can involve different strategies, among others, moving heat from one zone to another, integrated solutions, and using waste heat. Implementation of these strategies could imply the use of thermochemical heat storage systems. To face this situation, it is important to find a way to store heat (generated by electricity production, gas plants, heating devices) that is supposed to be lost to a high extent (such as exhaust gas). This way of renewable energy could replace/save the fossil fuels in several years. So the development of a heat storage device in combination with CHP (Figure 1.4) to compensate electricity fluctuations or upgrade heat

production would be a solution to this problem in buildings. This implies new insights through thermal energy systems.

As seen on Figure 1.3, space and water heating represent 43% of the world energy demand. Hence, there is an interest of finding or working on energy systems, that might fulfil that demand is necessary. This thesis is a first step toward this achievement. It is focused on numerical and experimental study so that the results will help to avoid some prototype trials, and will help optimise the system. The system in this thesis is a "thermal battery" with objective to improve of the efficiency of micro-CHP using thermochemical heat storage system.
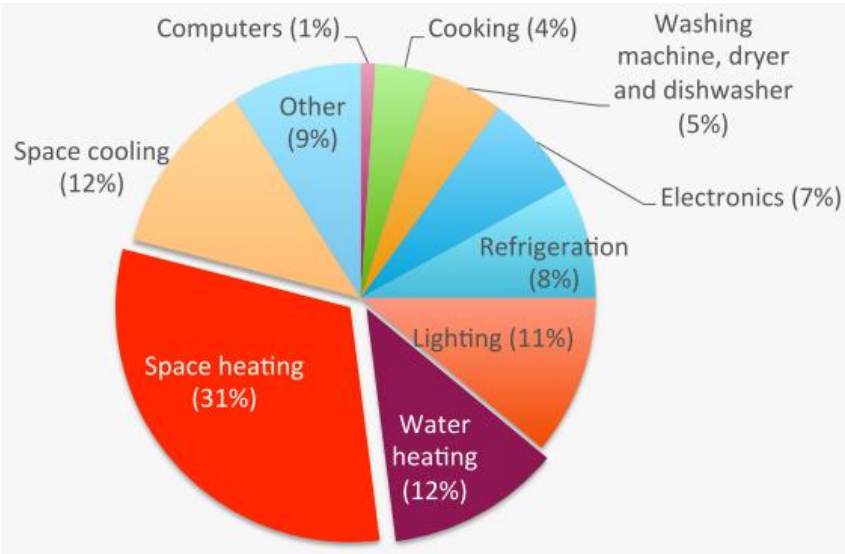
Source: IEA Electricity/Heat in the world from 2009 to 2012.

Figure 1.3: Energy consumption in the world during 2009-2012. (Lindburg, 2014).

Thermal energy is produced by micro-CHP during supplying electricity and heat is lost during the process. Anyway, micro-CHP does not have a storage unit. The difficulty to transfer useful heat over long distances is a serious constraint, which may limit the use of simultaneous generation of CHP when the heat load is highly variable or limited to excessively short time intervals. This is, for instance, in the case of space heating in many buildings in the tertiary sector, where the heating load is limited to the daily time on working days. In a thermal load following operation, time variation of the heating load would cause the micro-CHP unit to be switched on and off very frequently. Therefore, a transient behaviour is generated that may have a negative effect on both energy efficiency and system lifetime. While in an electric power, time variation of the heating load may cause an excessive amount of waste heat, resulting in a decrease of the energy saving. Because of the difficulty to match the generated heat with the existing requirements, cogeneration systems may operate efficiently, if the production of electricity and heat are uncoupled by using a thermal energy storage (TES) facility where heat, that is not needed during the production period can be stored.

The idea to combine such a storage unit to a home-device micro-CHP is the basis of this thesis (Figure 1.4). However, during the use of the micro-CHP there is a heat estimated between 9%

and 13% (Nowak et al., 2010) released to the environment. The Vattenfal Company© (industrial partner of the project "Thermal Battery") says their unit could provide a waste heat in a temperature range of 95 – 115 °C. This waste heat is left unused due to its relatively low grade.
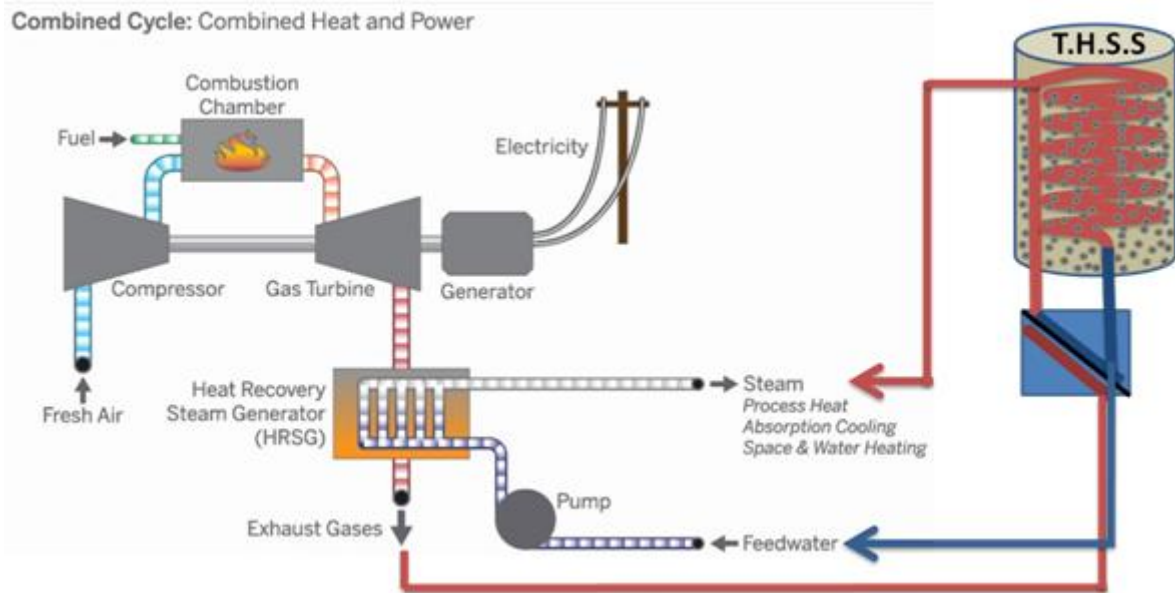
Figure 1.4: Schematic idea of micro-CHP with a compact thermal energy storage system (compact-TESS) Picture from (Webber, 2013).

In that case, thermal energy storage systems (TESS) will not only allow the waste heat to be re-used, but also to be upgraded by means of chemical heat pump or heat storage as enlightened by several authors (Cot-Gores et al., 2012; Fopah Lele et al., 2012; D. Wang et al., 2012; Wong-suwan et al., 2001). Thermal energy or heat storage systems using chemical reaction to store and release energy operate in charging and discharging phases, hence the name thermal battery. The aim is to understand those phases in which chemical reaction with heat and mass transfer are coupled, so that prediction and optimisation can be made. As thermochemical storage systems are still at a very early stage of development, most of the studies are limited to laboratory scale. Considerable amount of time, money and efforts are required before a commercially viable system becomes operational. To achieve the fixed objective, a numerical model coupling reaction kinetics with heat and mass transfer and main parameter characterization will be performed. To develop such a system, technical expertise from multi-disciplines is required (Figure 1.5). Usually, the first step to develop a thermochemical energy storage system is the selection of the reaction and the study of its chemical characteristics such as the reversibility, the rate of reaction, the operating conditions (p and T) and the kinetic properties. Some authors (N'Tsoukpoe et al., 2009; Pardo et al., 2014) reported the most important criteria to be respected for choosing the most suitable chemical reaction for TESS.

This thesis is performed within the Innovations-Incubator Project named "Thermal Battery", funded by the European Fonds for Regional Development (EFRE), the Lower-Saxony state and the Leuphana Universität Lüneburg. The main scientific objective is the realisation of a compact thermochemical heat storage prototype with energy storage density of about 80 kWh of waste heat from the micro-CHP in a box of 1 m³, including all other components and fulfilling sustainability requirements, where 60 kWh·m⁻³ is the state-of-art (Lahmidi et al., 2006; Mauran

et al., 2008). Through numerical and experimental investigations, a sensitivity and performance analysis of the system is done, in order to establish the feasibility of such thermochemical system.
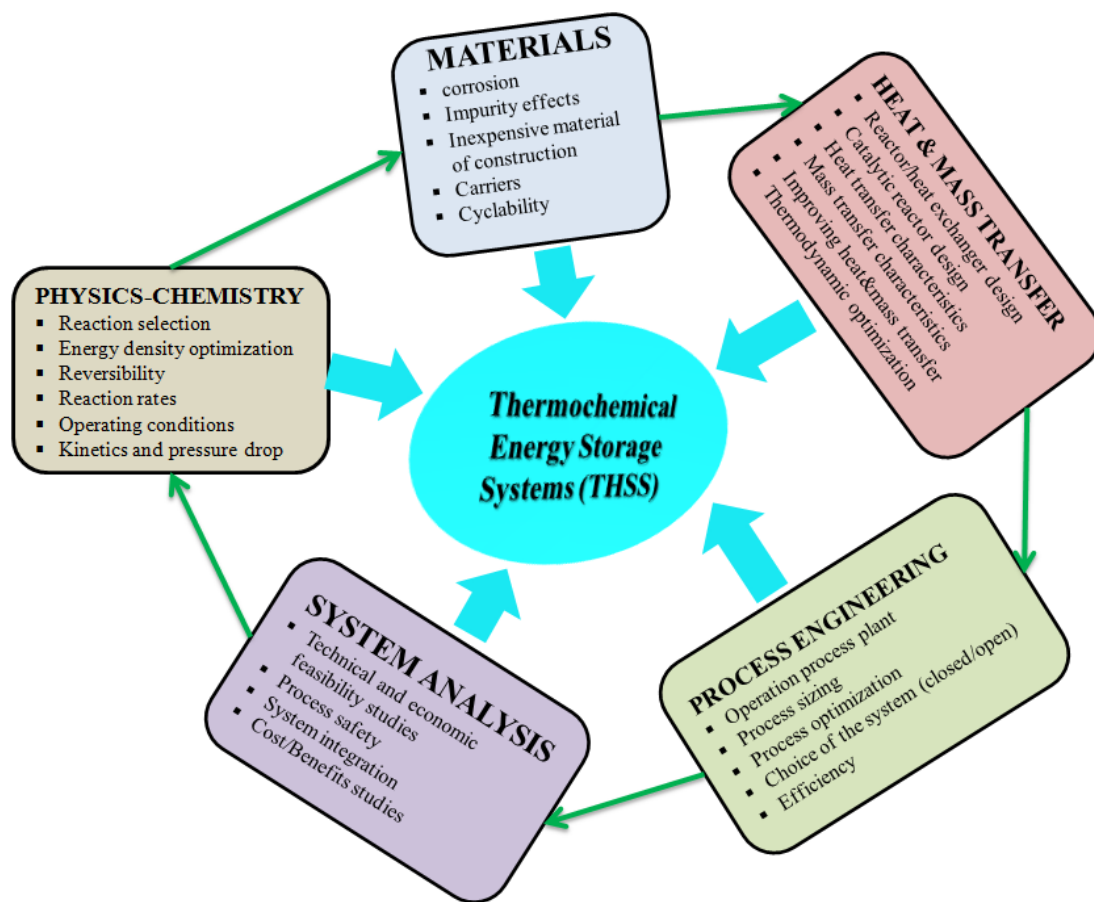
Figure 1.5: Necessary multidisciplinary field to the development of a TESS based on chemical reactions (adapted from Pardo et al., 2014).

In the second chapter, mainly based on reviewing, accent is put on showing how storage systems are coupled to existing power or thermal machines to upgrade their efficiency. So the review shows the feasibility of thermal energy storage system with some cogenerations. Then, different storage systems are reviewed and the reason of selecting thermochemical system is highlighted. Finally, some examples of systems are shown and thermodynamic study performed, followed by brief overview of heat and mass transfer with sorption and chemical reaction. The third chapter shows first, a short comparative study between different reactors for such thermochemical storage system. The storage system is then described and the accent is put on one of the most important element of the reactor, namely the heat exchanger. Therefore, three types of heat exchanger are numerically compared in order to come out with the appropriate one in terms of performance. Once the heat exchanger is selected, modelling of chemical kinetics, heat and mass transfers are described along with the relevant hypothesis. This chapter ends with the presentation of the commercial software, Comsol Multiphysics, which will serve to simulate the established models. Chapter four is mainly based on experimental characterisation. Chemical kinetics, heat and mass transfer are experimentally represented by the reaction conversion (and chemical rate), thermal conductivity (and heat capacity) and permeability,

28

respectively. So, experimentations were designed and tested. Available commercial devices were also used. For thermal conductivity measurement, two apparatus are used, one under steady state conditions, built in the laboratory and the other under transient state condition using differential scanning calorimeter (DSC) from Mettler Toledo, Gießen in Germany. This latter device is used for heat capacity measurement, but also coupled to a thermogravimetric analysis (TGA) device for chemical kinetic characterization. Permeability experiments are also built in the laboratory based on the simple principle of fluid mechanics through porous media. These experimentally obtained parameters are therefore used as input for process simulation. The fifth chapter presents the numerical investigation results on the reactor geometry (macro-scale) and into the bed (micro-scale) along with a lab-scale experiment of the thermochemical heat storage system under vacuum. Results are discussed in terms of performance analysis of the process. A comparison between the experiment and the simulation is then performed in order to validate the numerical modelling. A general conclusion is therefore drawn, followed by suggested work perspectives.

REFERENCES CHAPTER

Al-Badi, A.H., Albadi, M.H., 2012. Domestic solar water heating system in Oman: Current status and future prospects. Renew. Sustain. Energy Rev. 16, 5727–5731. doi:http://dx.doi.org/10.1016/j.rser.2012.06.007

Auer, J., Berger, S., Just, T., 2008. Combined heat and power. A pillar of Germanys integrated energy and climate program (Research No. Current issue), Energy and Climate Change. Deutsche Bank Research, Germany.

Bourgeois, I., 2001. Allemagne 2001: Regards sur une économie en mutation, 1st ed, 1. Copyright CIRAC, rue Anatole France - 92300 Levallois-Perrret, France. ISBN 2-905518-30-8.

Commandré, J.-M., Salvador, S., Nzihou, A., 2007. Reactivity of Laboratory and Industrial Limes. Chem. Eng. Res. Des. 85, 473–480. doi:10.1205/cherd06200

Cot-Gores, J., Castell, A., Cabeza, L.F., 2012. Thermochemical energy storage and conversion: A-state-of-the-art review of the experimental research under practical conditions. Renew. Sustain. Energy Rev. 16, 5207–5224. doi:10.1016/j.rser.2012.04.007

Dempsey, J., Ewing, J., 2011. Germany, in reversal, will close nuclear plants by 2022. N. Y. Times (online):http://www.nytimes.com/2011/05/31/world/europe/31germany.html?_r=2&.

Enteria, N., Mizutani, K., 2011. The role of the thermally activated desiccant cooling technologies in the issue of energy and environment. Renew. Sustain. Energy Rev. 15, 2095–2122. doi:10.1016/j.rser.2011.01.013

Euopean Parliament Council, 2004. DIRECTIVE 2004/8/EC OF THE EUROPEAN PARLIAMENT AND OF THE COUNCIL of 11 February 2004 on the promotion of cogeneration based on a useful heat demand in the internal energy market and amending Directive 92/42/EEC. http://eurlex.europa.eu/LexUriServ/LexUriServ.do?uri=CELEX:32004L0008:EN:HTML.

Fopah Lele, A., Rönnebeck, T., Rohde, C., N'Tsoukpoe, K.E., Schmidt, T., Ruck, W.K.L., 2012. Process engineering of a new thermochemical heat storage system, in: 7th International Renewable Energy Storage Conference and Exhibition". Presented at the IRES 2012, Eurosolar, November 0-12, 2012, Berlin-Germany, p. CD–ROM at page 1872.

Fragaki, A., Andersen, A.N., Toke, D., 2008. Exploration of economical sizing of gas engine and thermal store for combined heat and power plants in the UK. Energy 33, 1659–1670. doi:10.1016/j.energy.2008.05.011

Garg, H.P., Mullick, S.C., Bhargava, A.K., 1985. Solar thermal energy storage, library of Congress Cataloging in Publication Data. D. Reidel; Kluwer Academic Publishers, Dordrecht; Boston; Hingham, MA, USA.

Hongois, S., 2011. Stockage de chaleur inter-saisonnier par voie thermochimique pour le chauffage solaire de la maison individuelle (Doctorate/Ph.D). INSA de Lyon, France.

Kato, Y., 2007. Chemical Energy Conversion Technologies for Efficient Energy Use, in: Paksoy, H.Ö. (Ed.), Thermal Energy Storage for Sustainable Energy Consumption, NATO Science Series. Springer Netherlands, pp. 377–391.

Kilkis, B., Kakac, S., 1989. Energy Storage Systems, Proceedings of the NATO Advanced Study Institute, Çesme, Izmir, Turkey, 27 June-8 July, 1988, Nato Science Series E: Vol. 167. ISBN 978-0-7923-0209-4.

Kousksou, T., Bruel, P., Jamil, A., El Rhafiki, T., Zeraouli, Y., 2014. Energy storage: Applications and challenges. Sol. Energy Mater. Sol. Cells 120, Part A, 59–80. doi:10.1016/j.solmat.2013.08.015

Lahmidi, H., Mauran, S., Goetz, V., 2006. Definition, test and simulation of a thermochemical storage process adapted to solar thermal systems. Sol. Energy 80, 883–893. doi:10.1016/j.solener.2005.01.014

Lang, M., Lang, A., 2015. BDEW 2014 German Electricity Mix: Renewables Highest at 25.8%, Followed by Lignite (25.6%), Hard Coal (18%), Nuclear (15.9%) and Gas (9.6%). Ger. Blog.

Lindburg, A., 2014. Net Zero: Opportunities for Neighborhood Development [WWW Document]. Blogspot. URL http://streets.mn/2014/06/12/net-zero-opportunities-for-neighborhood-development/ (accessed 7.23.14).

Maru, H.C., Dullea, J.F., Huang, V.S., 1976. Molten Salt Thermal Energy Storage Systems: Salt Selection (Project 8981/ United States energy research No. COO-2888-1). Institute of Gas Technology, Chicago, Illinois, USA.

Mauran, S., Lahmidi, H., Goetz, V., 2008. Solar heating and cooling by a thermochemical process. First experiments of a prototype storing 60kWh by a solid/gas reaction. Sol. Energy 82, 623–636. doi:10.1016/j.solener.2008.01.002

Nowak, W., Arthkamp, J., Weddeling, K., 2010. BHKW - Grundlagen, seite 11. Publishe: ASUE-Arbeitgemeinschaft für Sparsamen und Umweltfreundlichen Energieverbrauch e.V (http://asue.de/cms/upload/broschueren/2011/bhkw-grundlagen-kurz/asue-bhkw-grundlagen-kurz-0411.pdf). Accessed 22 october 2013.

N'Tsoukpoe, K.E., Liu, H., Le Pierrès, N., Luo, L., 2009. A review on long-term sorption solar energy storage. Renew. Sustain. Energy Rev. 13, 2385–2396. doi:10.1016/j.rser.2009.05.008.

Paksoy, H.Ö., 2005. Thermal Energy Storage for Sustainable Energy Consumption - Fundamentals, Case Studies and Design, Proceedings of the NATO Advanced Study Institute on Thermal Energy Storage for Sustainable Energy Consumption—Fundamentals, Case Studies and Design Izmir, Turkey. ed, NATO Science Series II. Springer, Dordrecht, The Netherlands.

Panwar, N.L., Kaushik, S.C., Kothari, S., 2011. Role of renewable energy sources in environmental protection: A review. Renew. Sustain. Energy Rev. 15, 1513–1524. doi:http://dx.doi.org/10.1016/j.rser.2010.11.037

Parameshwaran, R., Kalaiselvam, S., Harikrishnan, S., Elayaperumal, A., 2012. Sustainable thermal energy storage technologies for buildings: A review. Renew. Sustain. Energy Rev. 16, 2394–2433. doi:10.1016/j.rser.2012.01.058

Pardo, P., Deydier, A., Anxionnaz-Minvielle, Z., Rougé, S., Cabassud, M., Cognet, P., 2014. A review on high temperature thermochemical heat energy storage. Renew. Sustain. Energy Rev. 32, 591–610. doi:10.1016/j.rser.2013.12.014

Rüdig, W., 1986. Energy conservation and electricity utilities: A comparative analysis of organizational obstacles to CHP/DH. Energy Policy, Vol. 14, pp. 104–116. doi:10.1016/0301-4215(86)90122-9

Shi, H., Zhao, Y., Li, W., 2002. Effects of temperature on the hydration characteristics of free lime. Cem. Concr. Res. 32, 789–793. doi:10.1016/S0008-8846(02)00714-7

Tzscheutschler, P., Nickel, M., Wernicke, I., Buttermann, H.G., 2009. Energy Consumption in Germany. BWK 61, 6 – 14.

Wang, D., Zhang, J., Xia, Y., Han, Y., Wang, S., 2012. Investigation of adsorption performance deterioration in silica gel–water adsorption refrigeration. Energy Convers. Manag. 58, 157–162. doi:10.1016/j.enconman.2012.01.013

Webber, Michael, 2013. online course UT.1.01x Energy 101: Energy technology and Policy, from the University of texas, Austin, USA. https://courses.edx.org/courses/UTAustinX/UT.1.01x/2013_Sept/info. Accessed on 19 september 2013.

WikiProject Energy, 2013. District heating. a wikipedia article. http://en.wikipedia.org/wiki/District_heating. Accessed on september 7th, 2013.

Wongsuwan, W., Kumar, S., Neveu, P., Meunier, F., 2001. A review of chemical heat pump technology and applications. Appl. Therm. Eng. 21, 1489–1519. doi:http://dx.doi.org/10.1016/S1359-4311(01)00022-9

Yuan, X., Wang, X., Zua, J., 2013. Renewable energy in buildings in China—A review. Renew. Sustain. Energy Rev. 24, 1–8. doi:http://dx.doi.org/10.1016/j.rser.2013.03.022

Zhao, H.X., Magoulès, F., 2012. A review on the prediction of building energy consumption. Renew. Sustain. Energy Rev. 16, 3586–3592.

Zondag, H., Kikkert, B., Smeding, S., Boer, R. de, Bakker, M., 2013. Prototype thermochemical heat storage with open reactor system. Appl. Energy 109, 360–365. doi:10.1016/j.apenergy.2013.01.082

2. STATE-OF-ART OF THERMOCHEMICAL HEAT STORAGE SYSTEMS

2.1. SHORT REVIEW OF THERMAL ENERGY STORAGE SYSTEM WITH COGENERATION SYSTEM

A combined heat and power (CHP) or cogeneration plant simultaneously produces thermal and electrical energy, primarily to meet industry and household demand. As we focus on household's application, we talk about a residential micro-CHP. Micro-CHP plants have a higher energy efficiency than conventional (without coupling thermal and power) thermal power systems, leading to a decreased environmental impact, in other words, reduced greenhouse gas emission (CO_2, N_2O, CH_4) and a significant increase of economic profitability (Yusta et al., 2008). They can also decrease fuel consumption by 30% compared with decoupled production in conventional power plants (Lund et al., 2005). The use of micro-CHP plants has been recognised as crucial by the European Parliament for the achievement of the Kyoto Protocol objectives, and consequently, legislation to encourage the use of cogeneration has been approved. These regulations dictate the parameters that define a plant as a cogeneration power plant (Tina and Passarello, 2012). Installation of thermal energy storage systems, particularly thermochemical heat storage systems (THSS) allow heat accumulation, which increases the flexibility of heat and electricity production in the power plant (Katulić et al., 2014). In a micro-CHP with regulated steam extraction turbines, at constant load, an increase in thermal energy production reduces the amount of electrical energy production. The main objective of THSS in a micro-CHP system is to support the simultaneous of thermal and electrical energy production. A THSS can store thermal energy during phases when it can be produced in excess for use when it cannot be produced to meet the heat demand or when its production is not a priority. Figure 2.1 shows an example of such system.
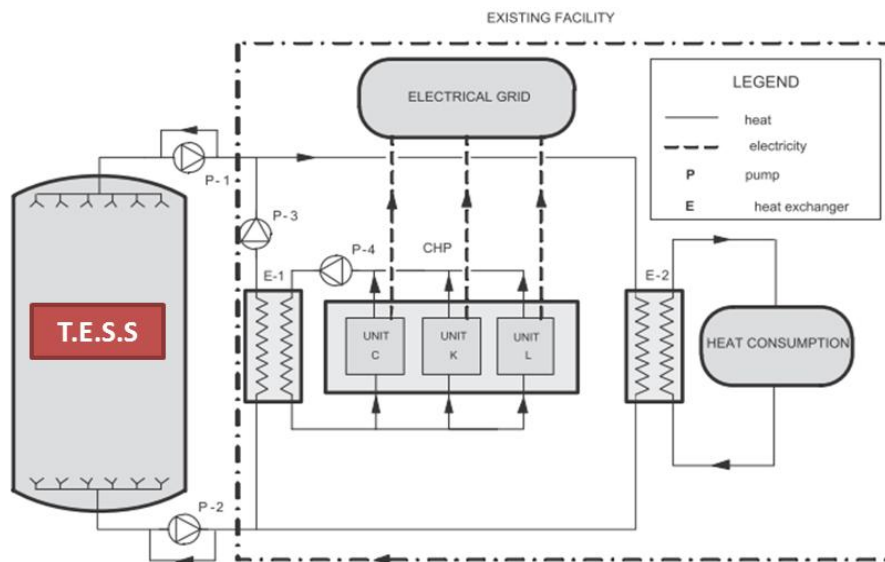
Figure 2.1: Scheme of a combined heat and power plant with a thermal energy storage system (TESS) where C, K and L are steam turbines (adapted from (Katulić et al., 2014)).

Using THSS, thermal energy can be accumulated while electricity market prices are low and discharged while prices are high (i.e., when it is more profitable to produce and sell larger quantities of electrical energy) (Katulić et al., 2014) via a conversion chain-like electricity→heat→chemical→heat→electricity. Heat storage system also makes it possible to

operate production units at more efficient loads. There are three mechanisms of heat accumulation in THSS: (a) increasing the temperature of a working fluid (heat carrier) within the THSS (sensible heat accumulation), (b) changing phase of a working fluid (latent heat accumulation) and (c) thermochemical heat accumulation (Paksoy, 2005). The latter is the most appropriate, though not yet commercialized. It is important to note that the design of market regulations play a major role in defining the optimal performance of a micro-CHP plant when maximizing the income from electricity sales. Optimising the operation mode of a micro-CHP plant coupled with a THSS can lead to significant financial savings and more stable and secure thermal energy supply. The benefits of THSS systems are recognised in large scale residential micro-CHP systems (Arteconi et al., 2013).

Since 2006, there are some studies considering energy storage system and cogeneration plant, but mostly on optimisation process. However, using THSS and closed systems (will be explained in section §2.2) with a micro-CHP for household's application is quite new. Though on CHP plant, some studies focusing on modelling approaches show considerable results. Some authors (Bogdan and Kopjar, 2006), while considering CHP plant and hot water tank for district heating and steam for industry and electric power (trigeneration), noted both, the economic and environmental benefits of using an energy storage system in a CHP plant.
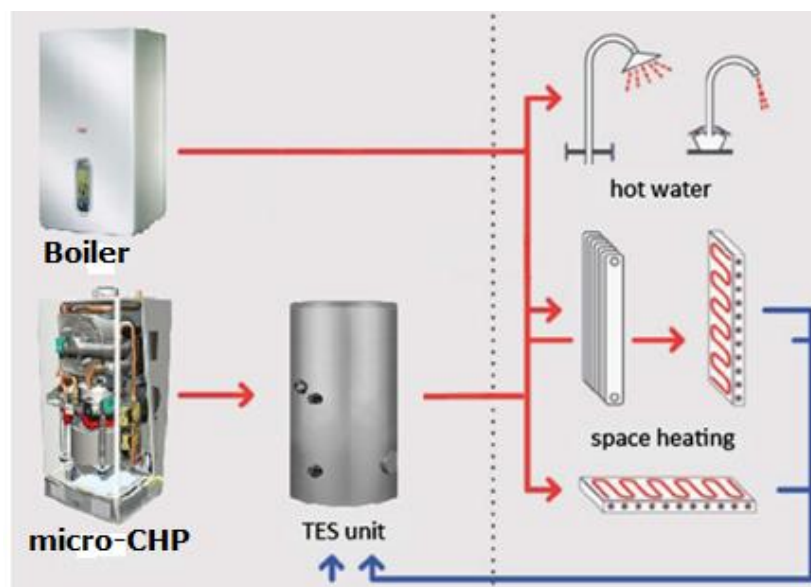
Figure 2.2: Energy system sketch of micro-CHP with a TES unit (Barbieri et al., 2012).

Khan et al. (Khan et al., 2007) presented a feasibility study, both technical and economical, of cogeneration coupled with a THSS intended for energy conservation in institutional buildings. They conclude that the use of THSS can provide a 23% reduction in peak demand and 21% savings in energy consumption. Some authors (Haeseldonckx et al., 2007) analysed the environmental impact of micro-CHP facilities and concluded that using a small or compact THSS device causes a net reduction of CO_2 almost three times higher than a cogeneration plant without a THSS. Barbieri et al presented a model (Barbieri et al., 2012) for the calculation of the profitability of micro-scale combined heat and power systems consisting of a CHP unit, heat boiler and thermal energy storage (TES) unit for residential building applications (Figure 2.2).

Siddiqui et al. (Siddiqui et al., 2007) demonstrated the effects of using a thermal energy storage system by analysing five commercial buildings in San Francisco, California. Pagliarini and Rainieri (Pagliarini and Rainieri, 2010) presented an analysis of a CHP system coupled with a TES which matched the heating load of the campus of the University of Parma. These authors concluded that a TES facility can effectively reduce the auxiliary boiler contribution, leading to a proportional decrease of CO_2 emission. (Chesi et al., 2013) showed that to allow high energy efficiencies, smart systems like small-size combined heating and power units should be coupled with thermal energy storage devices instead of the conventional energy supply from boilers. The authors focused on the effect of different volumes of the storage device when coupling to a micro-CHP. They concluded that a thermal storage system of 10.7 m^3 reduces the heater (own thermal system of the micro-CHP) contribution to a third and allows a year-round reduction in fuel consumption of approximately 12%, which is a big step towards reducing use of fossil energies. Making the TES system, compact, reduces the space but it remains the challenge to keep the performances.
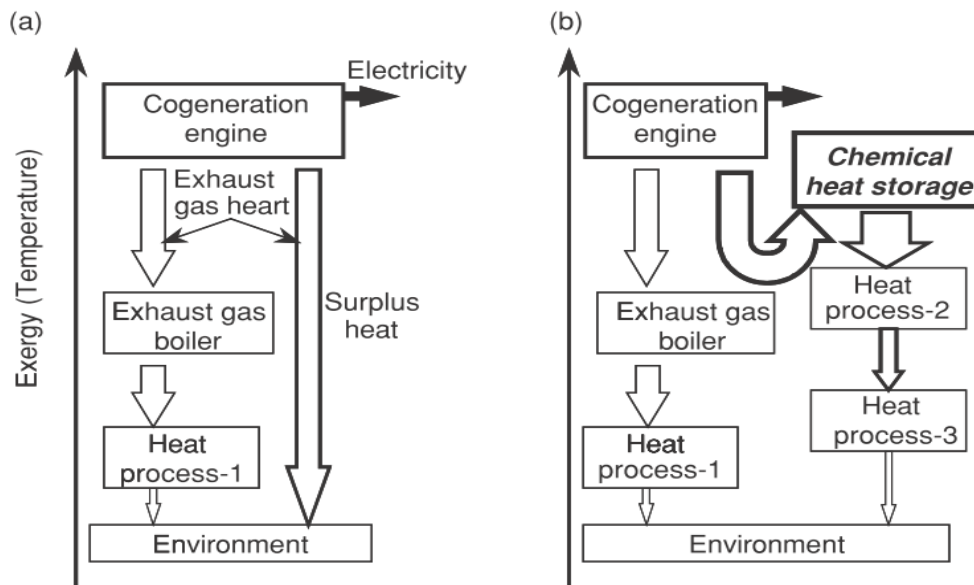
Figure 2.3: Contribution of chemical heat storage on cogeneration; a) conventional cogeneration system, b) combined system with chemical heat storage system (Paksoy, 2005).

Few and al. (Few et al., 1997; Smith and Few, 2001) introduced the innovative concept of heat pump incorporation into a domestic scale cogeneration plant (called the CHP/HP plant). Further works were led by them, using computer modelling, to demonstrate the potential of such systems and how heat pump incorporation overcomes many problems associated with domestic-scale cogeneration (micro-CHP). Their results show an energy upgrade of the combined system. However, their heat pump was water-based with a lower energy density. Years ago, (Kato, 2000) has shown the contribution of chemical heat storage process to a cogeneration system. Kato first analyses a conventional cogeneration system (Figure 2.3a) from a shaft work and an exhaust heat of a gas, then, a diesel engine or micro gas turbine for electrical and heat output, respectively. The exhaust gas of the engine is generally used to generate steam at an exhaust gas boiler. However, since demand for electrical output is generally inconsistent with that of the heat output, a large amount of surplus heat output is occasionally discharged into the atmosphere as shown in Figure 2.3a. Chemical heat storage has a possibility to enhance

the energy use efficiency of a cogeneration. Kato proposed then a system as shown in Figure 2.3b. The system consists of a cogeneration engine and a chemical heat storage system. With this system, the exhaust heat at 70°C was reheated to 200°C, showing an impressive heat upgrade. (Streckienė et al., 2009) study the feasibility of a coupled CHP with a thermal energy storage system in the German energy market. The drawn conclusions from their work was that coupling a TES with a CHP could reduce the CHP-plant investment and reduce the simple payback time from 9 to 10 years down to 5 years.

The notion of incorporating or associating a thermal energy storage system to an existing micro-CHP or CHP to upgrade the energy efficiency existed decades ago. Some attempts on the size reduction of the storage system were performed, but not enough to have a compact device. The research goal of the project "Thermal Battery" in which this thesis is performed, is to minimize the thermal heat storage component through an optimised integration into the micro-CHP system, as well as the targeted optimisation of the process and appropriate storage materials to reduce costs. However, the previous authors were not focusing on the idea to have a more compact and powerful storage system oriented to micro-CHP upgrading. Energy storage has been identified as an important solution for decentralized energy systems. Storage is particularly crucial for thermal energy systems based on renewable energy, which often offer their highest potential during low demand periods. On the other hand, energy storage helps improving the performance of combined heat and power (CHP), which is considered as a fundamental principle or practice of decentralized energy. Indeed, during off-peak electricity periods, the CHP can switch off while heat is supplied by the storage, and provide the energy demand mainly in periods of high market price. However, there is not always a sufficiently space when the thermal storage has to be installed in family houses or urban areas where the space may be restricted or expensive (Ibrahim et al., 2008). That is why a compact TESS should be constructed. In addition, Raine et al. (Raine et al., 2014) mentioned three main advantages such as increase of running time of a CHP, reduction of payback period of the system and reduction of carbon dioxide emissions, of using heat storage in a classic CHP as summarized above by previous authors. Furthermore, volume of an energy storage unit affects the cost of such a project when considering for instance the containers (which may have to be maintained under vacuum or insulated) and the size of heat exchanger. Thermochemical heat storage appears to be relevant towards these problems because they promise high energy density (specific thermal storage capacity) and an negligible heat loss (Ding and Riffat, 2012; Tatsidjodoung et al., 2013). Thermochemical heat storage review is presented in the following section.

2.2. Review of thermochemical heat storage systems

Talking about thermochemical always refer to sorption and chemical reaction phenomena (Tatsidjodoung et al., 2013). Large amounts of heat can be stored in reversible chemical reactions and sorption processes. In a sorption process, heat is stored by breaking the binding force between the sorbent and the sorbate in terms of chemical potential. The term "Sorption" was first proposed by McBain in 1909 (McBain, 1909) as a general expression covering both adsorption and absorption. He reported that the uptake of hydrogen by carbon appeared to occur in two stages: a rapid process of adsorption appeared to be followed by a slow process of absorption into the interior of the solid. Sorption of molecules on a surface is a prerequisite to any surface mediated chemical process. The expressions "chemical", "thermochemical",

"thermochemical sorption", "compact" and "sorption" have all been used in different contexts by many authors regarding thermal energy storage (Chan et al., 2013; Cot-Gores et al., 2012; Ding and Riffat, 2012; Li et al., 2013; Meunier, 2013; Neveu and Castaing-Lasvignottes, 1997). Each term carries its own connotation and scope concerning which kind of phenomenon it encompasses and it seems difficult to distinguish clear boundaries between these terms. In most cases, these expressions are employed without special statements. Some attempts have been made in the literature to elucidate their definitions (Cot-Gores et al., 2012; Ding and Riffat, 2012; N'Tsoukpoe et al., 2009). Research works regarding sorption thermal energy storage in which chemical reaction coexists are well mentioned in Refs. (Abedin and Rosen, 2011; Chan et al., 2013; Cot-Gores et al., 2012b; Ding and Riffat, 2012; Mette et al., 2012; Tatsidjodoung et al., 2013).

The sorption thermal storage method is as follows:

1. Desorption (charging) process, which requires the supply of heat to remove the sorbate from the sorbent. The heat required is higher than that associated with the evaporation (or condensation) heat of pure sorbate (such as water). Large integral heat of desorption involved during the desorption (or sorption) process causes high energy densities of sorption materials in theory, only next to chemical reaction (see Figure 2.4). Thus a smaller volume is needed for a given storage capacity for sorption thermal storage. For example, only one third of the volume is required for sensible heat storage system with water (Yu et al., 2013).
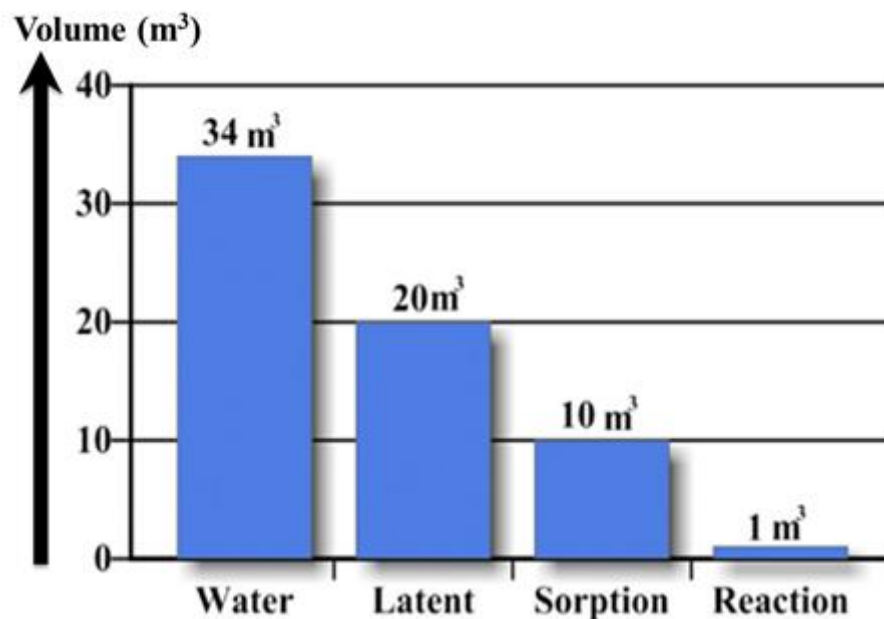
Figure 2.4: Volume to store 1850 kWh with 25% heat losses consideration (Yu et al., 2013).

2. Sorption (discharging) process, will not occur until the sorbent contacts with the sorbate, so the binding energy can be stored, independent of the time span between the desorption process and the sorption process. The sorption can be of adsorption or absorption depending on the process. Thus, sorption storage is also called an "indirect" thermal storage approach from the view of thermodynamics, distinguished from other "direct" sensible and latent methods (Gil et al., 2010). The heat and entropy is not stored in the storage vessels but released to the

environment for the indirect storage. This feature makes sorption thermal storage a promising solution for long-term energy storage applications, where solar energy is stored in summer to meet with heating demands in winter (N'Tsoukpoe et al., 2009). The discharging process could be operated to provide a cooling effect from the evaporator in summer or heating effect from the reactor in winter, exhibiting some extent of flexibility. Although sorption thermal storage systems offer some benefits, there are still critical drawbacks. Among them, are the great complexity in the system configuration (for closed systems), expensive investment, poor heat and mass transfer ability (for chemical reaction) and low heat storage density in actual systems. To overcome these barriers, extensive academic efforts are now being carried out worldwide.
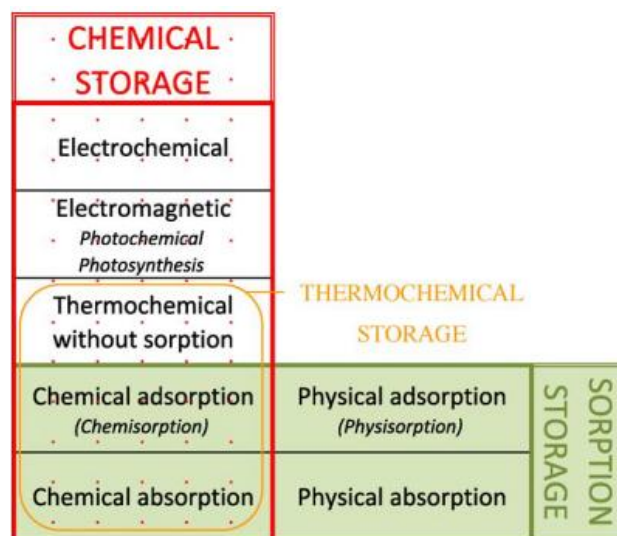
Figure 2.5: Chemical storage and sorption storage classification (N'Tsoukpoe et al., 2009).

N'Tsoukpoe et al. (N'Tsoukpoe et al., 2009) identified thermochemical storage as a part of chemical storage disregarding electrochemical and electromagnetic storage (see Figure 2.5). Thermochemical storage was further classified into chemical adsorption, chemical absorption and thermochemical without sorption. The first two also belonged to sorption storage and the exact definition of "thermochemical without sorption" was not given by the authors. This was corrected by Yu et al. (Yu et al., 2013). They suggested sorption thermal storage to be distributed into four categories:

1. liquid absorption,

2. solid adsorption,

3. chemical reaction,

4. and composite materials as illustrated in Figure 2.6.

Thus, the term "sorption thermal energy storage" in this thesis will refer to these four categories. It can be only one or two of them processing simultaneous.
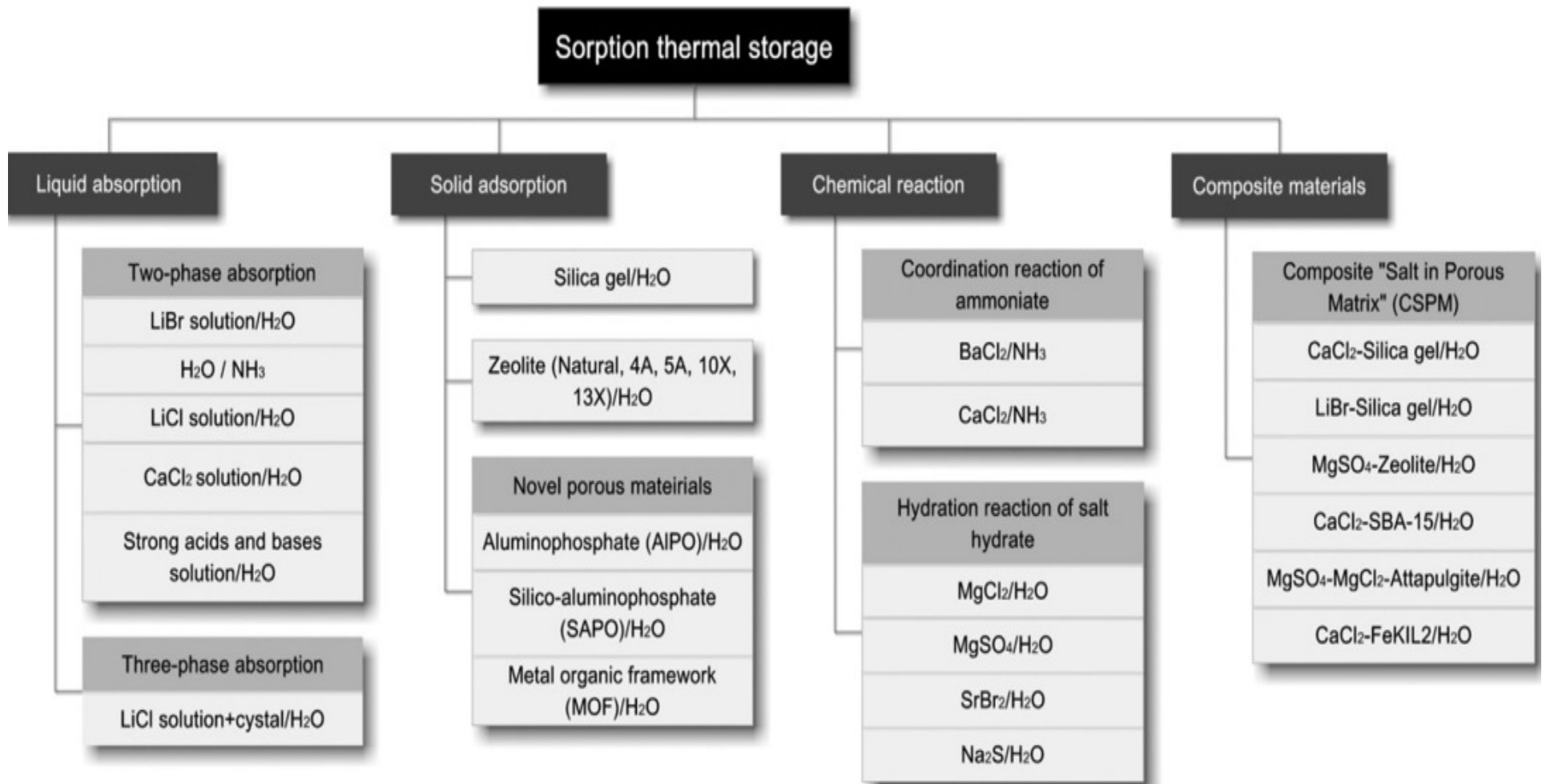
Figure 2.6: New sorption thermal storage classification (Yu et al., 2013).

The term adsorption is universally understood (Rouquerol et al., 1999) as the enrichment of one or more of the components in the region between two bulk phases (i.e. the interfacial layer), in which cohesive forces including Van der Waals and hydrogen bonding act between the molecules of phase substances. If the solid is ionic, we will also have cation-water and anion-water interactions. In the present context, one of these phases is necessarily a solid or liquid (called sorbent) and the other a fluid (i.e. gas called sorbate, see Table 2.1). With a certain system (like some salt hydrates exposed to water vapour), the adsorption process is accompanied by absorption, i.e. the penetration of the fluid into the solid phase. The International Union of Pure and Applied Chemistry (IUPAC) also gives some definitions in the same way (Robert and Burwell, 1976; Sing, 1985). Depending on the interface between sorbent and sorbate, adsorption can be divided into four types: solid/gas, solid/liquid, liquid/liquid, and liquid/gas. The solid/gas adsorption has been widely used and studied, playing a pivotal role in interface chemistry. As a rule in this chapter, when talking about adsorption or solid adsorption, it is referred in particular to solid/gas adsorption.

Based on the cohesive force between the two phases, adsorption is further divided into two types: physical adsorption (physisorption) and chemical adsorption (chemisorption) (Wang et al., 2010, 2009). Physical adsorption is a general phenomenon whenever an adsorbate is brought into contact with the surface of the adsorbent. The forces involved are intermolecular forces (Van der Waals forces) of the same kind as those responsible for the imperfection of real gases and the condensation of vapours. Chemical adsorption is due to covalent forces of the same kind as those operating in the formation of chemical compounds. There are certain differences in the properties of the two kinds of adsorption, which can be used as experimental criteria for deciding the adsorption type. The best single criterion is the magnitude of the heat of adsorption (Bolis et al., 2006, 2003). Because chemical forces are normally stronger than physical forces, the released heat of chemical adsorption should therefore be larger than the heat of physical adsorption. In addition, as a chemical reaction, chemical adsorption requires appreciable activation energy, resulting that it can only proceed at a reasonable rate above a certain minimum temperature. In contrast, physical adsorption needs no activation energy, leading to a rapid adsorption speed. Though these features will help to recognise physical adsorption and chemical adsorption, there are many cases where it is uncertain which kind of adsorption is operating or both of them may are taking place at different moments and sites. Chemisorption processes provide high energy of sorption than physisorption, but may be irreversible. Silica gel and zeolite are widely studied and applied as common adsorbents using water as working fluid. Some new classes of materials (Duquesne, 2013), including aluminophosphates (AlPOs), selective water sorbents (SWS), salts in porous matrix (CSPM) (Gordeeva and Aristov, 2012; Tanashev and Aristov, 2000), silico-aluminophosphates (SAPOs) and metal-organic frameworks (MOFs), have recently emerged as promising porous materials for thermal energy storage. More description on those porous materials will be presented later.

The term absorption is used when the molecules of the adsorbate penetrate the surface layer and enter the structure of the bulk solid/liquid, causing the change of the composition of one or both bulk phases (Robert and Burwell, 1976). If the absorbent is a liquid and the absorbate is a gas, the process can be named liquid-gas absorption or liquid absorption. As the liquid-gas absorption process has been applied in refrigeration industry for a long time, sometimes absorption is specially referred to liquid/gas absorption. The most familiar liquid absorption working pairs encompass $LiBr/H_2O$ (N'Tsoukpoe et al., 2013) and H_2O/ammonia, which have been successfully applied in commercial absorption chillers and heat pumps.

Table 2.1. Definition of different adsorption terms (Rouquerol et al., 1999).

Term	Definition
Adsorption	Enrichment of one or more components in an interfacial layer
Adsorbate	Substance in the adsorbed state
Adsorptive	Adsorbate substance in the fluid phase
Adsorbent	Solid material on which adsorption occurs
Chemisorption	Adsorption involving chemical bonding
Physisorption	Adsorption without chemical bonding

Conventionally, liquid absorption is referred to as two-phase absorption. Another innovative kind of absorption thermal storage process, using lithium chloride crystals to increase energy density, is called "three-phase absorption" (Yu et al., 2013).

A chemical reaction corresponding to sorption mainly consists of three kinds of reactions:

1- coordination reaction of ammoniate with ammonia,

2- hydration reaction of salt hydrate with water,

3- hydration reaction of salt hydrate with alcohol (Douss and Meunier, 1989; Li et al., 2004).

Strictly speaking, the three reactions can be regarded as coordination reactions. Molecules of ammonia, water vapour or alcohol are attracted by metal ions to form coordinate bonds. There still exists a controversy about whether the coordination reaction should be classified into solid adsorption or solid absorption. In order to homogenize the appellation, all are called chemical reactions. Unlike a chemical reaction, there is no change in molecular configuration of the compound in the sorption process. The term composite materials enclose sites where chemical reaction and ad/absorption takes place.

Among the three reaction partners mentioned in the above paragraph, water has been chosen since the storage is suitable for building application. Not only for this reason, water has presented many valuable assets for this application. Besides the fact that water vapour transport does not need electrical energy, it is a non-corrosive and chemically inert component, it is non-flammable, and has the thermodynamic requirements: high specific enthalpy of vaporization (Radermacher and Hwang, 2005) and high polarity for its use in a sorption system (Dinçer and Rosen, 2002). Compared with other adsorbates such as ammonia or methanol, water achieves highest energy densities. Besides the high enthalpy of vaporization, water provides the following benefits: it is chemically stable, it is ecologically and physiologically harmless, it is available and it is economical. However due to the low vapour pressure of water, desorption and particularly the lower pressure adsorption processes can be limited by mass transfer.

According to the system configurations, thermochemical and sorption systems dedicated to storage can be sorted as open and closed systems (Bales, 2008; Hauer, 2007). Whether close or open, the system can have separate or integrate (compact) reactors (Zondag et al., 2008). The

authors suggested that separate reactors are most appropriate for seasonal storage (Figure 2.7). However, the authors clearly stated that integrated reactors are for solid sorption material because the transport of the solid material is not necessary although they exhibit heat loss to the ambient during and after discharging. Which is what we are aiming for in the present application: that means this heat lost to the ambient, here the space to be heated. Furthermore, the reactor can be easily insulated. By contrast, only little amounts of sorbent and sorbate are to be heated up in a separate reactor, according to the desired reactor power so that the system is more efficient (N'Tsoukpoe et al., 2009). The Table 2.2 shows a few comparisons.

Table 2.2. Short comparison between open and closed systems.

Type	+	-
Closed systems (Vacuum conditions)	Small and compact design. Low pressure. Higher reaction power.	Presence of non-condensable gases. Tightness. Good heat transfer, mass transfer need to be worked out.
Open systems (Atmospheric conditions)	Non-compact and easy design. Better heat and mass transfer.	High pressure. Low reaction power. Additional humidifier to wet enough air. Limitation of pressure drop.

Closed sorption systems have long time been studied for refrigeration, heat pump and energy storage applications (Wongsuwan et al., 2001). They are able to supply higher output temperatures for heating applications than open systems (Hauer and Avemann, 2007; Michel, 2012; Michel et al., 2014). In closed systems, not the sorbate itself but the energy is released/absorbed to/from the environment via a heat exchanger (Bales, 2008). The process is alike chemical heat pumps with a major difference. The purpose of a heat pump is to absorb heat in one place where it is plentiful, then to transport and release it in another location where it can be used in a continuous process. The need of a condenser and an evaporator is therefore required. Additionally to the desorber and the ab/adsorber, a heat storage system is a batch process and the desorber might be used as an ab/adsorber and the condenser also as an evaporator (N'Tsoukpoe et al., 2009).

The operating principle of a closed sorption thermal storage system is presented in Figure 2.8. The system is mainly composed by two vessels: a reactor where the reactive sorbent is located and a condenser/evaporator where water is collected or condensed and later evaporated. The vessels are connected by a conduct or a pipe as a passage for vapour. The charging process consists of a desorption reaction in the reactor and a gas-liquid phase change reaction in the condenser. Once the collected waste heat (from the micro-CHP) is added to the reactor, the sorbate which cleaves to the solid sorbent, starts to break loose from the binding force between the sorbate and the sorbent. Through the pipe, the vapour turns into its liquid state in a condenser at a low temperature level. The heat of condensation is taken away and released to the heat sink (here the water in the condenser). Besides, the heat of condensation is also absorbed by the thermal mass of the reactor (reactor metal, heat exchanger metal). After the charging process is finished, the reactor and the condenser are separated from each other.
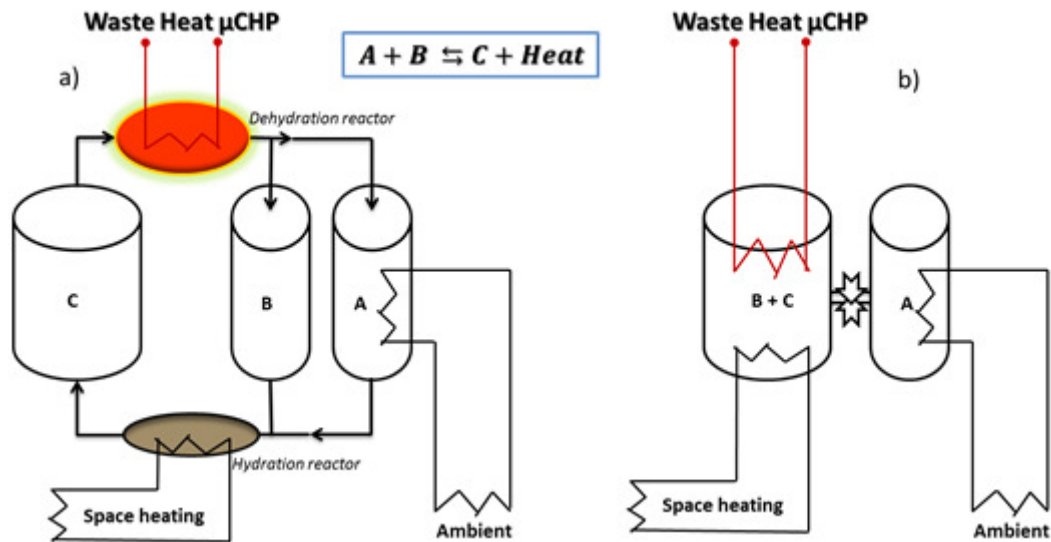
Figure 2.7: Modes of closed systems (a) Separate reactor and (b) Integrated reactor (adapted from (Zondag et al., 2008))

Separation here, means close the connecting valve. If heating or cooling demands are needed, the reactor and the condenser/evaporator are connected again. The discharging process works in a reverse direction: it includes a sorption reaction in the reactor and a liquid-gas phase change reaction in the evaporator. Depending on the practical requirement, a cooling effect can be produced by the evaporator or a heating effect can be created by the reactor. This feature makes the sorption thermal storage processes able to offer "cold storage" function in summer and "heat storage" function in winter. Discharging of closed sorption systems requires an additional heat source to provide the heat of evaporation, making the choice of heat sources a critical issue. Yu et al. (Yu et al., 2013) showed that by designing an efficient heat exchanger, air can be an additional heat source. He also suggested geothermal source heat exchangers which are unfortunately time-consuming and costly. However, for houses or buildings with an already existing solar system, the heat of evaporation would not be a problem. A connection from the solar panel can be made to provide the low temperature heat source.

Open systems operate at the atmospheric pressure to allow the release and sorption of the sorbate. Thus, only water can be used in those systems to preserve or not to harm the environment. The operation principle of open sorption thermal storage system is shown in Figure 2.9. In charging process, a dry air stream, after heating by an external heat source, becomes a dry hot stream and enters a reactor filled with sorbent. Water adsorbed/absorbed by the sorbent is extracted by the hot air and leaves the bed. The air then becomes wetter and cooler. During discharging, a humid, cool air stream goes into the previously desorbed reactor. Part of the water vapour in the air is pulled in by the sorbent. The released heat of sorption warms up the air so that it could be used for heating. The lower cost of investment, coupled with better heat and mass transfer conditions (compared with closed systems), provide compelling reasons for practical projects employing open sorption systems to store thermal energy (Paksoy, 2005). Moreover, strategy need to be considered to reduce or to limit the pressure drop when blowing humid air through the reaction system, to keep the electricity demand for the blower on a low level.
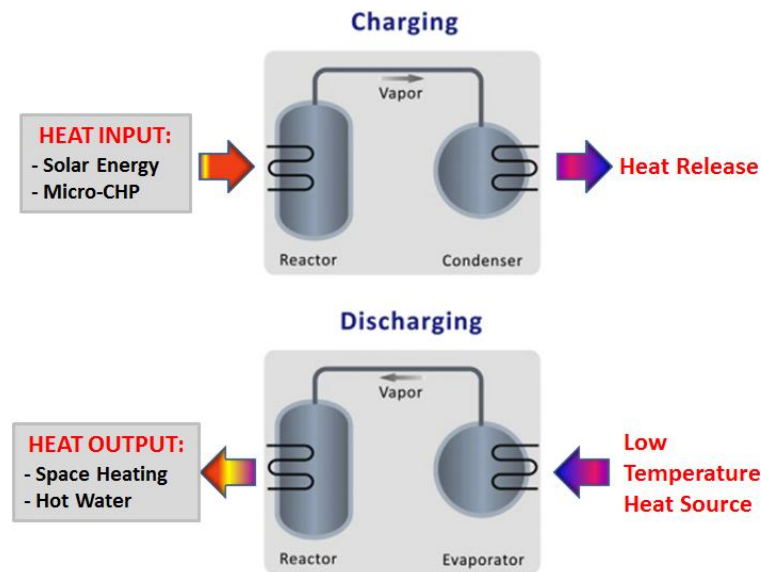
Figure 2.8: Operating principle of closed sorption thermal storage system (adapted from (Yu et al., 2013)).
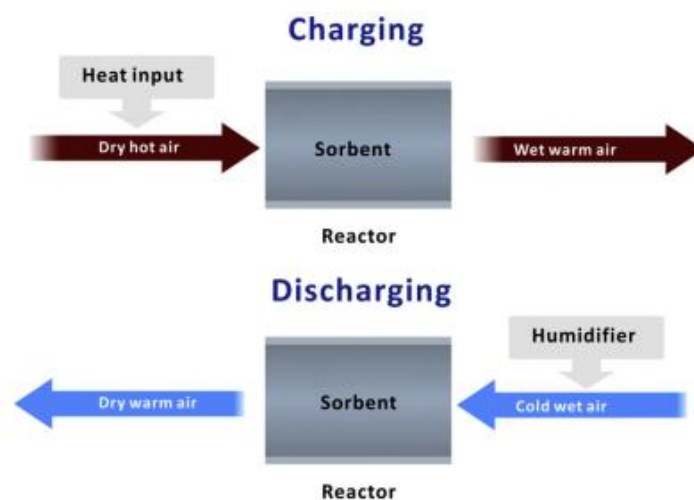
Figure 2.9: Operating principle of open sorption thermal storage system (Yu et al., 2013)

Once a system classification, a reactor configuration and a design are known or decided, the material selection fulfilling the required operating conditions should be processed. The storage material strongly affects the performance and cost of such a heat storage system according to some economical studies for various applications (typically, about 30% of the total investment cost) (Hauer, 2007; Kerkes and Drück, 2011; Krönauer et al., 2012). Therefore, the material selection is a critical point in an energy storage unit development. Material selection for a given application is often conflicting when it is not simply profoundly antagonistic (Kokouvi Edem N'Tsoukpoe et al., 2014c). The Figure 2.12 shows what we face when considering material selection for thermal energy storage systems. However a few investigations (Courbon et al., 2011; Visscher and Veldhuis, 2005) have considered a comparison of several materials under operating conditions but most of them were theoretically conducted.

Numerous salt hydrates have been reviewed for thermochemical storage in the literature (N'Tsoukpoe et al., 2009; Tatsidjodoung et al., 2013; Yu et al., 2013). However, almost all of these salt hydrates fail to meet the great expectations to cover both space heating and DHW.

44

Therefore, in the framework of the large-scale EU-funded project "Thermal Battery", devoted to micro-CHPs efficiency improvement (mainly economic savings) using thermochemical storage (Schmidt et al., 2012), a systematic evaluation of the potential of salt hydrates for low temperature thermochemical heat storage have been considered. N'Tsoukpoe et al. (N'Tsoukpoe et al., 2014b) performed a rough evaluation of the suitability of salt hydrates for a low temperature thermochemical heat storage application below 105 °C based on theoretical and experimental approaches. The authors concluded that $SrBr_2 \cdot 6H_2O$, $MgSO_4 \cdot 6H_2O$ and $LaCl_3 \cdot 7H_2O$ are the most promising materials for this application, disregarding an economic analysis.

Besides the shown criteria in Figure 2.10, a first condition "thermodynamically reasonable" for material selection should be always met. This is linked to finding a reaction which changes direction at a desired temperature so that energy is stored at higher temperatures and given off at lower temperatures. For a general thermodynamic screening of suitable processes, it has been found advantageous to use the concept of turning temperature T_t (Wentworth and Chen, 1976). T_t is the temperature at which the reaction changes its direction so that at $T > T_t$ the products dominate while at $T < T_t$ the reactants dominate. A first approximation $T_t = \Delta H_r / \Delta S_r$, where ΔH_r and ΔS_r are the reaction enthalpy and the reaction entropy respectively, results from setting the equilibrium constant as unity and assuming that the heat capacity is constant during the chemical reaction. However, where only one type of gas molecule is formed, the Clausius-Clapeyron equation defines the turning temperature.
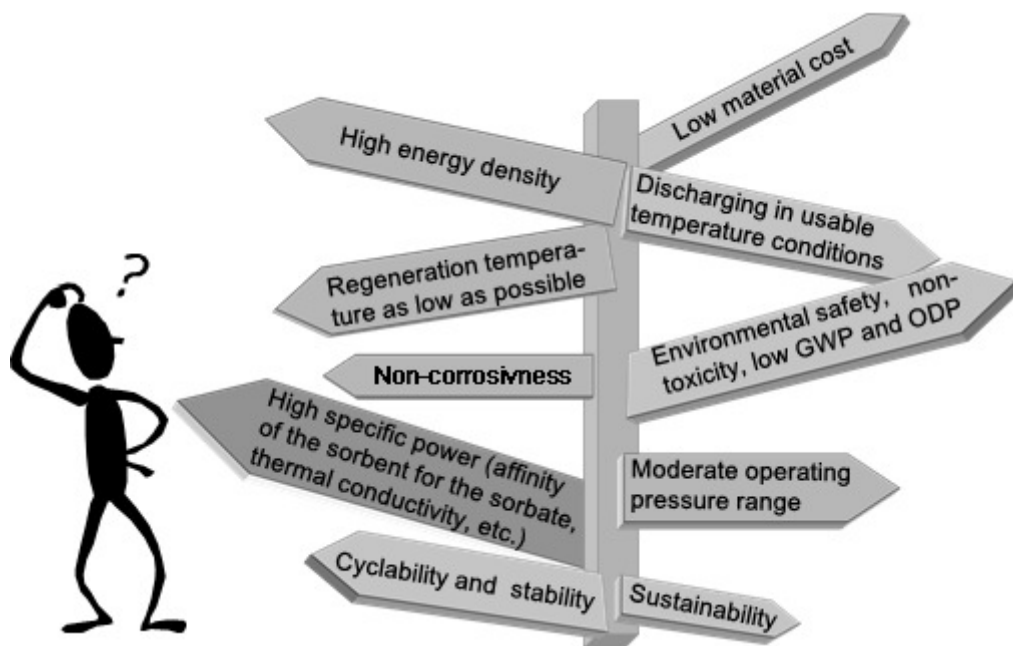
Figure 2.10: Dilemma around material selection for thermochemical heat storage system (N'Tsoukpoe et al., 2014b). GWP: Global warming potential; ODP: Ozone depletion potential.

Let comeback on the criterion energy storage density which brings controversy in some storage material discussion. It is most valuable characteristic of a thermal energy storage system. In the following different used terms of energy density are clarified:

1- the *theoretical energy density (kJ·kg⁻¹)*, widely used for sorption systems, is the maximal energy density of the material considering the porosity;

2- The *mass energy density (kJ·kg^{-1})*, which is the ratio between the reaction enthalpy and the molecular mass;

3- The *volume energy density (kJ·m^{-3})*, depending on the highest involved hydrates in the reaction (initial salt to be dehydrated), is calculated as the product of the mass energy density and the density of the salt particles (it is not the bulk density and therefore, the required porosity is not considered here);

4- The *lean energy density (kJ·m^{-3})*, which takes into account the stored heat and the evaporation energy, corresponds to the actual and real energy storage potential (N'Tsoukpoe et al., 2014b).

In the following, different systems (open and close) are presented where sorption and/or thermochemical phenomenon is/are involved. Technically spoken, each system is classified by the storage material. So the systems will be discussed with respect to the storage material. The aim is to show their operating conditions and performances, to address the encountered issues followed by their overcomings if possible.

2.2.1. ABSORPTION SYSTEMS

Also called liquid-gas systems, absorption systems are promising storage option because they can be pumped and used as the working heat transfer fluid in solar collectors and heat exchangers. However, it can be defined as a process in which the sorbate diffuses into the liquid or solid sorbent accompanying a phase change and/or a chemical reaction. Faster heat and mass transfer rates are possible with liquid absorption. Materials recently investigated include aqueous solutions of Calcium Chloride (CaCl$_2$), Lithium Chloride (LiCl), Lithium Bromide (LiBr), Sodieum Hydroxide (NaOH), Potassium Hydroxide (KOH) and Amonia as shown in Table 2.3. Hui et al. (Hui et al., 2011) compared absorption materials for the use in low pressure (1.2 – 4.2 kPa) absorption cycles and have reported theoretical material energy densities up to 476 kWh·m^{-3}. CaCl$_2$ with a desorption temperature of 44 °C, has an energy density of 263 kWh·m^{-3} and a limited absorption temperature range of 20 to 23 °C.

LiCl with desorption temperature of 66 °C, has the highest storage density of 476 kWh·m^{-3}, but also has a high absorption temperature range, 20 to 35 °C (Davidson et al., 2013). NaOH with a desorption temperature of 50°C, has an energy density of 233 kWh·m^{-3} and the highest absorption temperature of 45°C (Weber and Dorer, 2008). LiBr presenting an absorption temperature between 25 – 35 °C with a desorption at 72 °C (prototype value is 40 °C), can store 8 kWh heat and produce 1 kW (N'Tsoukpoe, 2012) and has an energy density of 400 kWh·m^{-3}. KOH with a desorption temperature of 63 °C, has an energy density of 400 kWh·m^{-3} and an absorption temperature of 35 °C. Figure 2.11 illustrates a closed- and an open-cycle absorption system. The system comprises of multiple storage vessels, two reactors (for absorption/desorption), a condenser and evaporator, and heat exchangers. The concept with separated storage and reactor, in this case, consist of physical transport of the sorbent and heat and mass transfer in the reactors. Three and two storage vessels respectively, one each for water, diluted (discharged), and concentrated (charged) solutions, are shown in this illustration to emphasize the necessity of preventing mixing prior to discharging.
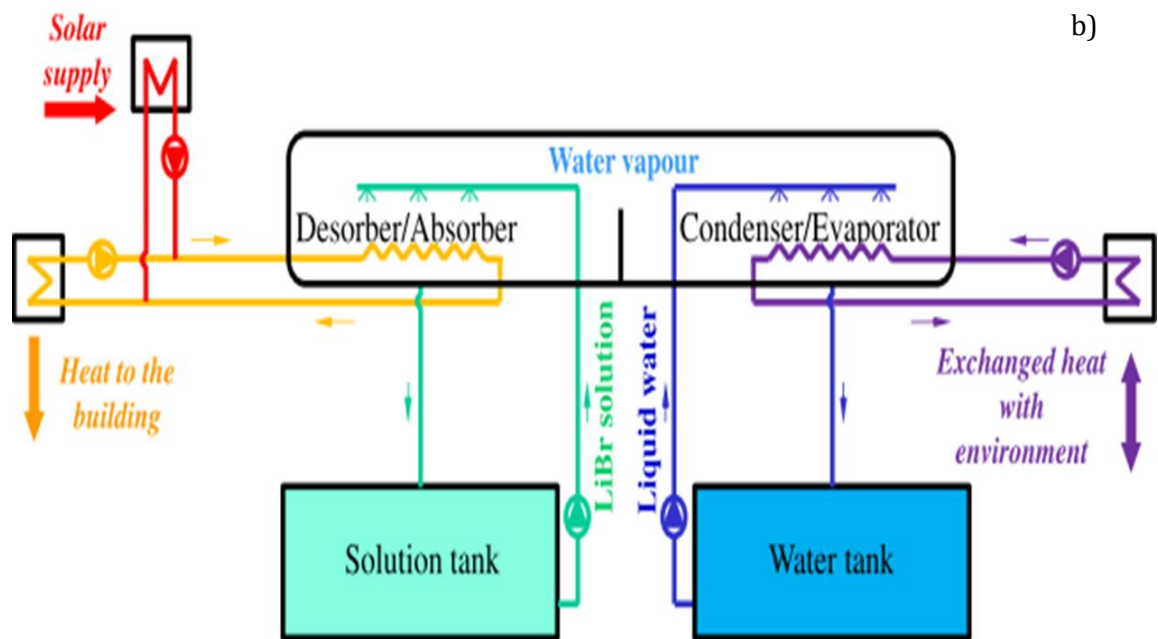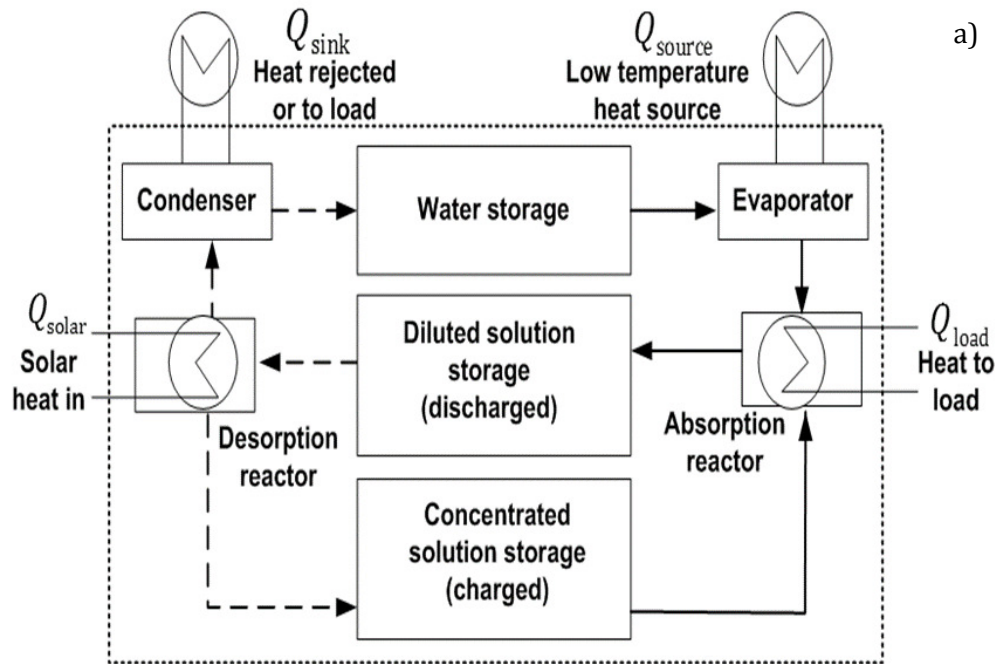
Figure 2.11: Scheme of a closed (Quinnell and Davidson, 2012) (a) and an open (N'Tsoukpoe et al., 2013) separate absorption storage system (b).

Table 2.3. Absorption systems for household application.

Working pair	Characteristics	Projects	Scale level	References
H_2O/NH_3	Charge: 93 °C; Discharge: 43°C. Heat: 900 MJ·m^{-3} of NaOH (with single stage reactor). Theoretical energy density: 119 kWh·m^{-3} of anhydrous. Storage capacity: 40 kWh. Discharging time: 12 hours for 5 kW power	Delft University of Technology – Netherlands	Reactor scale, Numerical scale and Prototype	(Ruiter, 1987)
$NaOH/H_2O$	Charge: 100-150 °C; Discharge: 40-65 °C. Heat: 900 MJ·m^{-3} of NaOH (with single stage reactor). Theoretical energy density: 250 kWh·m^{-3} of anhydrous. Storage capacity: 8.9 kWh. Discharging time: 8.9 hours for 1 kW power	EMPA, COMTES	Reactor scale, Prototype, commercial	(Fumey et al., 2014a, 2014b; Weber and Dorer, 2008)
$LiCl/H_2O$	Charge: 46-87 °C; Discharge: 30 °C. Heat: 910.8 MJ·m^{-3} of LiCl (with crystallization in the storage tank). Theoretical energy density: 253 kWh·m^{-3} of anhydrous. Storage capacity: 35 kWh. Discharging time: 4.4 hours for 8 kW power	SERC	Reactor scale, Prototype	(Bales, 2008; Bales and Nordlander, 2005)
$LiBr/H_2O$	Charge: 40-90 °C; Discharge: 30-33 °C. Heat: 907.2 MJ·m^{-3} of solution. Theoretical energy density: 251 kWh·m^{-3} of solution. Storage capacity: 8 kWh. Discharging time: 8 hours for 1 kW power	LOCIE, LRHPT-China	Reactor scale, Prototype, commercial	(Kokouvi Edem N'Tsoukpoe et al., 2014a; N'Tsoukpoe et al., 2013; Xu et al., 2011)
$CaCl_2/H_2O$	Charge: 70-80 °C; Discharge: 21 °C. Heat: 428 MJ·m^{-3}. Simulated energy density: 200 kWh·m^{-3} of anhydrous. Prototype energy density: 116 kWh·m^{-3}. Storage capacity: 15 kWh. Discharging time: 27 to 500 hours for 560 W power	LOCIE, SOLVAY, BEMS	Reactor scale, Numerical scale, Prototype	(Courbon et al., 2011; Hui et al., 2011)
Expanded Vermiculite + $LiNO_3$	Discharge: 33-36 °C. Heat: 450 MJ·m^{-3} of reactor.	-		(Tatsidjodoung et al., 2013)

Mixing of the diluted and concentrated solutions releases the stored binding energy and converts the chemical potential into sensible energy, which is subject to thermal loss to the ambient. The use of multiple storage vessels ensures long-term storage of chemical potential but decreases the system-level energy density and increases the cost.

In an absorption system, there is one loop for concentrated solutions and diluted solutions (after the sorbate is diluted in the base solution) and another loop solely for sorbate. The strong solution becomes a weak solution after it absorbs the sorbate from the evaporator. The weak solution becomes a strong solution after it evaporates the sorbate from the base solution and condenses in the condenser after being heated up in a generator (Pang et al., 2013). These systems are very well developed and proof-tested and already on the market.

2.2.2. ADSORPTION SYSTEMS

The field of solid adsorption started as historical curiosity and the first scientific and quantitative work was performed in 1773, by Scheele and Fontana (Critoph and Zhong, 2005). It is a process where the sorbate does not diffuse into the sorbent but changes phase on the surface of the sorbent. Depending on adsorbent and adsorbate phases, adsorption systems may be classified as solid/gas, liquid/gas, solid/liquid, and liquid/liquid (Srivastava and Eames, 1998). As it is a surface phenomenon, surface polarity corresponds to strong affinity with polar substances such as water in this case. Polar adsorbents are thus called 'hydrophilic' and aluminosilicates such as zeolites, porous alumina, silica gel or silica–alumina are examples of adsorbents of this type. On the other hand, non-polar adsorbents are generally 'hydrophobic'. Carbonaceous adsorbents, polymer adsorbents and silicalite are typical non-polar adsorbents. In the following, talking about adsorption systems refers only to gas-solid adsorption system. These materials are the most widespread sorbents for water vapour adsorption. Their sorption behaviour is based on the presence of regular or irregular pore systems within their molecular structure. Silica gels are widely studied as hydrophilic materials due to their large water sorption capacity at low humidity, low cost, and easy regeneration (Chua et al., 2002). Surprisingly, this compound presents hydrophilic limitations for adsorption condition at 35 °C and 12 mbar and desorption condition at 150 °C and 56 mbar (Henninger et al., 2012). In the same order, several materials have been used for heat storage purpose such as: - zeolites (natural and synthetics as types 4A, 5A, 13X, Y), more hydrophilic than silica gel with the major inconvenient of higher desorption temperature (> 200 °C precisely in close system) although some experiment results show possibility at 120 °C (Steiger et al., 2008). - Aluminophosphates (AlPO$_4$-34 or AlPO-Tric) (the most promising) and silica-aluminophosphates (SAPO-34). - Metal-organic-frameworks (MOFs) but still with hydro-thermal instability (Henninger et al., 2012; van Helden and Hauer, 2013a), materials with crystalline open porous structure. - Salts and composites (Hongois et al., 2011; Lahmidi et al., 2006; Mauran et al., 2008; Mette et al., 2013; Zondag et al., 2013). These materials have been theoretically and experimentally studied, and some were prototyped and commercialized as resume in Table 2.4. Composites based on those materials have also been developed in order to behave as shape-stabilized material at macroscopic scale and Tatsidjodoung et al. emphasized them in his review (Tatsidjodoung et al., 2013).

These systems can be designed in the open or closed mode. In the closed mode (under vacuum), the principle is similar to absorption system with the difference that the sorbate

diffuses only at the surface of the solid sorbent and the solution tank and water tank are the same. However, the inconvenient of the closed system remains the low pressure for water. In the open mode, water is of course the perfect sorbate candidate and air plays the role of heat transfer fluid. So, partial pressures are taking into account and there is not need a condenser and a water tank any more.

Table 2.4. Adsorption systems for household application.

Materials	Characteristics	Projects	Scale level	References
Silica gel/H_2O (Close system)	Charge: 88 °C at 1.5 kW; Discharge: 32-42 °C at 1-2.87 kW for 9.5 hours. Theoretical energy density: 50 kWh·m^{-3} of anhydrous. Experimental energy density: 300 kWh·m^{-3} of material. Prototype energy density: 33.3 kWh·m^{-3}. Storage capacity: 13 kWh.	AEE-INTEC, Austria	Reactor scale, Numerical scale and Prototype	(Bales, 2008; Ng and Mintova, 2008)
Zeolites 13X/H_2O (Open system)	Charge: 130-180 °C; Discharge: 55-65 °C at 1.8 kW. Experiemental energy density: 124-180 kWh·m^{-3} of material. Prototype energy density: 57.8 kWh·m^{-3}.	ZAE-Bayern, Germany. SPF, Switzerland	Reactor scale, Prototype	(Bales, 2008; Hauer, 2007)
Zeolites 13X/ H_2O (Close system)	Charge: 350°C; Discharge: 15 °C at 4.1 kW (cold storage). Theoretical energy density: 167 kWh·m^{-3} of material. Storage capacity: 5.5 kWh.	SJTU, China	Reactor scale	(Lu et al., 2003)
Zeolites 4A/H_2O (Open system)	Charge: 180 °C at 2.5 kW; Discharge: 35 °C at 1.5 kW. Experimental energy density: 160 kWh·m^{-3} of material. Prototype energy density: 120 kWh·m^{-3} Storage capacity: 12 kWh.	ITW, Germany	Reactor scale, Prototype	(Bales, 2008; Kerkes, 2006)
Metal-organic-framework (MOFs)	Charge: 45-50 °C; Discharge: 15 °C for cooling. Very low affinity to water. Up to 1.4 g·g^{-1} as sorption capacity.	USA, NJNU, China. BIC, Russia	-	(Aristov, 2013; Li and Xu, 2013; Ng and Mintova, 2008; Rowsell and Yaghi, 2004)

2.2.3. Thermochemical systems

As mentioned before, thermochemical storage is in general, a simultaneous chemical reaction and sorption. Yu et al. argue that there is no clear boundary between them anyway (Yu et al., 2013). Although it can be noticed that chemical materials present higher heat capacities than sorption materials. In this section we focus only on hydration reaction (disregarding coordination reaction with ammonia) at low-temperature application for environmental reasons (Introduction, section 1.1).

For thermochemical energy storage units, the choice of the storage material is critical (Figure 2.10). A complete couple of the material properties and working conditions could allow significant improvements in the thermal performances of the system. According to Gordeerva and Aristov (Gordeeva and Aristov, 2012), the common way to select the best adsorbent for a given application is to screen the properties of available adsorbents in order to select which meet the application demands. The previous authors argued that this method is difficult and time-consuming and usually results in a compromise choice rather than in the ultimate one. One smart and more precise method, namely the target-oriented design, was proposed and Gordeeva et al. (Gordeeva and Aristov, 2012) describes it as follows: (1) determining the demand (based on thermodynamic analysis of the cycle efficiency) of the application for the required storage material properties, (2) choice of the candidate material (based on equilibrium sorbent-sorbate), whose properties precisely or nearly fit these demands. Based on a similar method, Ma et al. (Ma et al., 2009) investigated more than two hundred salt hydrates (for adsorption) and recently N'Tsoukpoe et al. (N'Tsoukpoe et al., 2014) screened 125 hygroscopic salts leading to 17 possible candidates for low temperature thermochemical energy storage (Table 2.5) and from which prototype a maximal energy density of 60 kWh could be obtained.

Among the 17 materials for heat storage application, only magnesium chloride ($MgCl_2$), sodium sulfide (Na_2S), strontium bromide ($SrBr_2$) and magnesium sulphate ($MgSO_4$) are of great interest and were applied in many works and research projects (Table 2.6). The products of hydration reactions of these salts are generally assumed to be hydrates with a high number of crystal water molecules. However, in some cases, the relative humidity/pressure is so high that the product of the hydration is a saturated salt solution, rather than a salt hydrate. This process is called deliquescence, which is an important solid/water interaction phenomenon. Deliquescence is defined as a process by which a substance sorbs water vapour from the environment and gradually dissolves in the sorbed water to form a solution at a critical relative humidity (RH) value, namely, the deliquescence relative humidity (DRH) (Mauer and Taylor, 2010). The water intake or uptake strongly depended on the deliquescence relative humidity (DRH) and this latter on the properties of the salt and the temperatures. If the relative humidity (RH) of the environment exceeded the DRH, the salt absorbs water and dissolved until reaching the equilibrium, i.e. until the water activity of the solution equaled the relative humidity. At relative humidity below the DRH, the salt lifts up water vapour forming a higher hydrated state but no solution. Both cases are shown in the following equations (Posern and Kaps, 2010):

$$Salt_{(s)} + \chi H_2O_{(g)} \leftrightarrows Salt \cdot \chi H_2O_{(s)} \quad \text{for RH < DRH} \tag{2.1}$$

$$Salt_{(s)} + \chi H_2O_{(g)} \leftrightarrows Salt \cdot \chi H_2O_{(l)} \quad \text{for RH > DRH} \tag{2.2}$$

The deliquescence phenomenon favours some issues such as chemical instability. The forming of a liquid film on the surface of salt crystal will not only forbid the occurring hydration reaction, but also cause corrosion problems due to the dripping of solution to other metal components (in case of the LiCl, LiBr, $CaCl_2$, showing why it was used in absorption systems).

Thermodynamically spoken, thermochemical systems are based on reversible reaction between a solid and a gas (here water vapour) as shown in Eq. (2.3), where ΔH_r is the reaction enthalpy, standing for every specie enthalpy in the reaction and strongly depends on the melting temperature of phase transition ($J \cdot mol^{-1}$ of water) and x, y the stoichiometric coefficients.

$$Salt \cdot \varsigma H_2O_{(s1)} + \Delta H_r \leftrightarrows Salt \cdot (\varsigma - \chi)H_2O_{(s0)} + \chi H_2O_{(g)} \qquad (2.3)$$
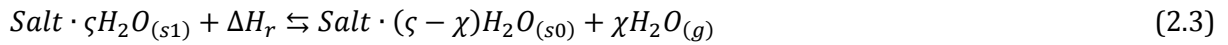
In contrast to absorption and adsorption equilibria, the thermodynamic equilibrium of thermochemical reactions is monovariant (Stitou, 2013) and therefore follows the Clausius-Clapeyron relationship. This relationship is obtained by using the fact that, for this transformation, the Gibbs free energy is equal to zero at the thermodynamic equilibrium (Levine, 2002). Assuming constant heat of reaction ΔH_r and pure ideal gas phase, the thermodynamic equilibrium results in the Van't Hoff equation (Raldow and Wentworth, 1979) since vapour is far from ideal:

$$ln\left(\frac{p_{eq}}{p^0}\right) = \frac{-\Delta H_r^0}{R \cdot T_{eq}} + \frac{\Delta S_r^0}{R} \qquad (2.4)$$

with p_{eq}: equilibrium pressure (Pa). ΔS_r^0: formation entropy ($J \cdot K^{-1} \cdot mol^{-1}$ of water) of reaction at reference pressure p^0 (Pa) and R: ideal gas constant ($J \cdot K^{-1} \cdot mol^{-1}$). Eq. (2.4) ordinarily stands for pure vapour system and for a corresponding pressure; the equilibrium temperature can be deduced. That equilibrium temperature allows to evaluate the temperature in the reactor during the whole cycle and consequently to perform the energy and exergy analysis of the process (Hongois et al., 2011). Energy analysis is related to the first law of thermodynamics through energy balances and energy efficiencies. Additionally, energy analysis is the evaluation method on how energy is used in a process, involving the physical or chemical processing of materials and the transfer or conversion of energy. However, it is not sufficient to evaluate all the aspects of energy utilisation in the process. So, the exergy analysis method, which is based on the first and second laws of thermodynamics, is a supplement for full understanding and is used to improve the real efficiencies of the system. Exergy is also defined as potential or quality of energy. With exergy analysis it is possible to make a sustainable quality assessment of energy for any thermodynamic system (Caliskan et al., 2012).

In the Clausius-Clapeyron diagram, the thermodynamic equilibrium of the reaction in Eq. (2.3) is plotted as a nearly straight line, by neglecting the enthalpy and entropy variation of the process with the temperature (Figure 2.12). This is due to the fact that reaction enthalpy varies slightly when temperature interval is not large. Below the equilibrium line of the solid/gas reaction, the salt is in its desorbed solid form or less hydrate form (s0). Conversely, above the equilibrium line, the salt is in its solid form (s1).

Initially, in the state (s1) (in the reactor), the material in the reactor is heated up through a heat exchanger (in case of a closed system) via heat loss from the micro-CHP. The desorbed water is then condensed at condensation conditions (p_{cond} and T_{cond}) followed by an endothermic heat release (Q_{cond}).

This is called the charging phase or charge mode. The endothermic heat release or energy of condensation can be used in the existing DHW (domestic hot water) system or stored elsewhere. In the discharging phase, water in the house system is heated up via a low energy source, so that water can evaporate and flow through the salt bed in the reactor. The transport is favoured by a pressure difference in the reactor and in the evaporator (p_{evap} and T_{evap}). The occurring exothermic reaction releases a higher heat (Q_{react}) that can be used for both space heating and DHW again.
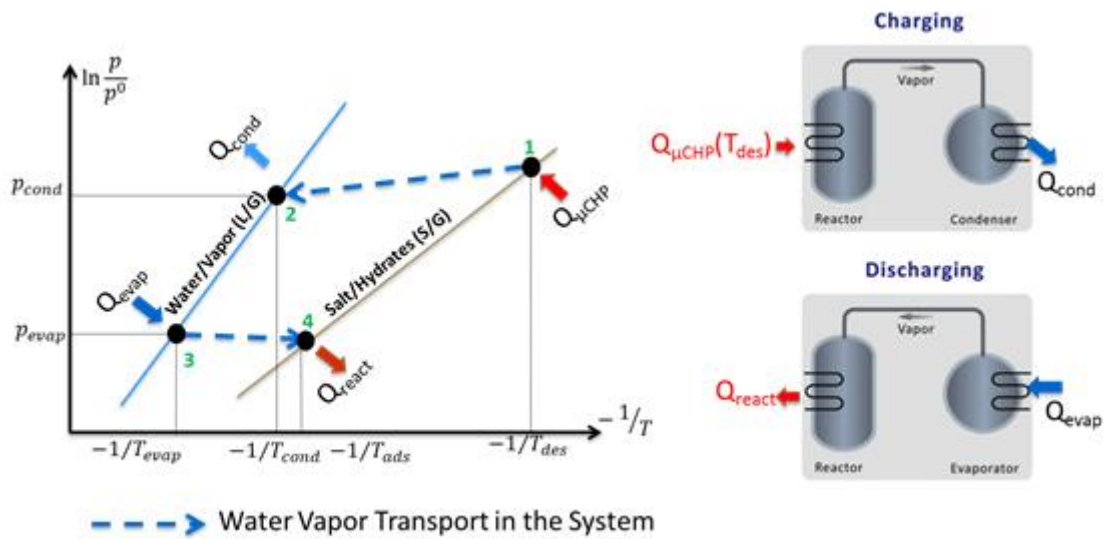
Figure 2.12: Theoretical thermodynamic equilibrium of a thermochemical system in the Clausius-Clapeyron diagram. 1: decomposition; 2: condensation; 3: evaporation; 4: synthesis.

In practise, Figure 2.12 does not proceed as shown, since it is ideal. Though Sharanov et al. showed and confirmed that the efficiency equal to the Carnot efficiency can, in principle, be obtained for a chemical heat pump that results from a monovariant equilibrium of a gas–solid reaction (Sharonov and Aristov, 2008). However, according to the principle of Le Chatelier's, by increasing or decreasing the temperature during the thermal decomposition or synthesis, the process shifts towards vapour formation or absorption and an increase or decrease of the vapour pressure. This shifts of the equilibrium to the formation of the anhydrous salt by imposing a deviation from the thermodynamic equilibrium as shown in Figure 2.13. In addition, a synthesis or decomposition reaction can only take place if the reagent equilibrium is deviated to allow a reaction kinetic (Stitou, 2013). This deviation is defined for the decomposition as the difference between the temperature T_{des} imposed to the reactor and the solid/gas equilibrium temperature $T_{eq}(p_{cond})$ at the reactor pressure. For the synthesis, it is the difference between the temperature T_{ads} imposed to the reactor and the solid/gas equilibrium temperature $T_{eq}(p_{evap})$ at the reactor pressure. Figure 2.13 explained the shifted equilibrium. Such of studies have been performed by many authors (Castets and Mazet, 2001, 2000; Mazet et al., 1991; Stitou, 2013) and they showed that there is an important effect on the reaction kinetics due to

those deviations. However, in a closed system, the system pressure is imposed by the evapo-condenser pressure (Michel, 2012). So the shifted equilibrium (pressure and temperature) for decomposition and synthesis respectively are defined as:

$$\Delta T_{eq,des} = T_{des} - T_{eq}(P_{cond}) \text{ and } \Delta P_{eq,des} = P_{eq}(T_{des}) - P_{cond} \tag{2.5}$$

$$\Delta T_{eq,ads} = T_{ads} - T_{eq}(P_{evap}) \text{ and } \Delta P_{eq,ads} = P_{eq}(T_{ads}) - P_{evap} \tag{2.6}$$

Returning to these salts of great interest, $MgCl_2 \cdot 6H_2O$ was identified at the Energy research Centre of the Netherlands (ECN) (C. J. Ferchaud et al., 2012; Zondag et al., 2013) as the promising material for a heat storage application in a 50 W power prototype. This material was also investigated in our Lab. To reach a tetra-hydrate form of $MgCl_2$, a 120 °C source was needed depending on the water vapour pressure which would have been difficult to obtain from the micro-CHP heat losses. Other studies (C. Ferchaud et al., 2012; C. J. Ferchaud et al., 2012; Opel et al., 2011; van Essen et al., 2009a) showed that a quasi-complete dehydration was possible for a temperature higher than 125 °C but cycle stability was not very good. Complete dehydration is not possible since it leads to the formation of hydrochloric acid and magnesium oxide (Sugimoto et al., 2007). Hongois (Hongois et al., 2011) has clearly demonstrated that $MgSO_4 \cdot 7H_2O$ also was worthy using for heating purpose. At the ECN, they identified $MgSO_4 \cdot 7H_2O$ as one of the most interesting salt hydrates for compact seasonal heat storage. van Essen et al. stated that first experiments performed in a closed system at low pressure indicate that a small amount of heat can be released at 50 °C with a water vapour pressure of 1300 Pa. If a heat storage system has to operate at atmospheric pressure, then the application of $MgSO_4 \cdot 7H_2O$ for seasonal heat storage is possible for space heating operating at 25 °C, a water vapour pressure of 2100 Pa and a dehydration temperature of 150 °C which is difficult to reach with micro-CHP heat losses. However, this salt is corrosive, has a bad kinetic, and is expensive. Additionally, the release power is small when considering an evaporation temperature of 10 °C (the power for evaporation should be less to be provided naturally or economically).
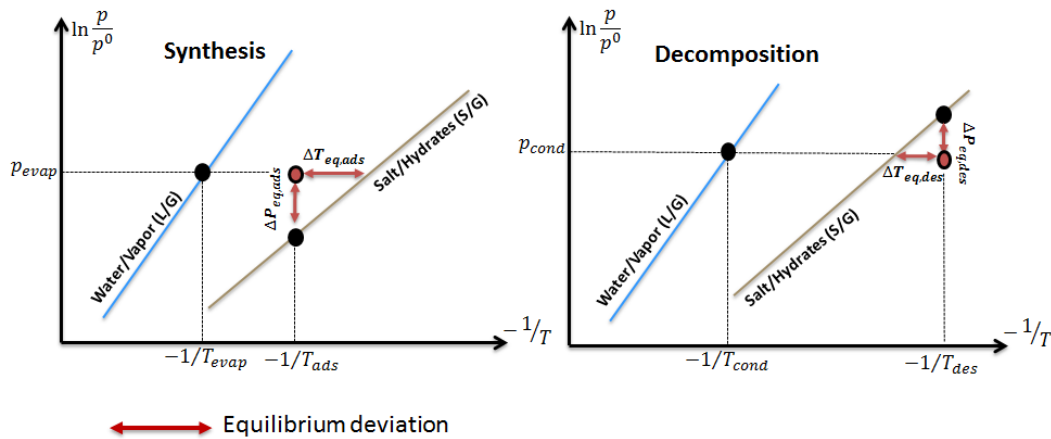
Figure 2.13: Shifted thermodynamic equilibrium of a thermochemical system in the (left) synthesis and (right) decomposition phase.

The couple Na_2S/H_2O (with 9-, 5-, 2-hydrates) has also attracted the ECN interest, but the kinetic is relatively slow and during decomposition, the structure pattern is modified showing simultaneous region of higher and slower hydration (Boer et al., 2004; De Boer et al., 2002). However this salt can not allow sufficient release temperature for heating purpose and has a low melting temperature of 49 °C. The salt which seems to fit our need is $SrBr_2 \cdot 6H_2O$ according to the Table 5. At the Institute of Science and Materials Processing (PROMES) in France, this well investigated salt, showed good results followed by a 1 m^3 prototype development which can store 60 kWh in heating capacity and a water flow rate of 0.1 l·s^{-1} (Mauran et al., 2008). The only inconvenient is the irritation and the price which is around 195€/kg for 95% purity (http://www.alfa.com/). It however shows good cycle stability over >20 cycles.

Once the above-mentioned salts have been identified, the first tests in a close heat storage system (pure salts in powder form), always presented, transfer problems such as agglomeration, swelling, expansion and phase change. During the hydration, to bring the water vapour in contact with the salt, it was sometimes difficult. Small deliquescence can be noticed, in fact a skin of hydrated salt is sometimes formed on the surface of the bulk powder and strongly limits the diffusivity of the water vapour within the unreacted part of the sorbent (Tatsidjodoung et al., 2013). Since the performance of the system depends on heat and mass transfer, this had to be improved within the reactive bed, and therefore composites have been developed over the past two decades. They combine the heat storage capacity of the salt and the heat storage capacity of the host. This hybrid character of composites provides to the material some physical and chemical properties (large sorption area, hydrophobic character) between the salt and the host. The hosts (Aristov, 2013; Critoph and Zhong, 2005) can be in porous sorbent materials such as silica gel (Aristov et al., 2000; Fopah Lele et al., 2013; Gordeeva and Aristov, 2012), vermiculite (Fopah Lele et al., 2013; Michel et al., 2012) and zeolites (Hongois et al., 2011). Furthermore, they can be in nonreactive host materials, such as expanded natural graphite (Jiang et al., 2014; S. L. Li et al., 2011; Oliveira and Wang, 2007; Wang et al., 2006), metal foam (Guilleminot et al., 1993; Haije et al., 2007; Thapa et al., 2014), carbon fiber (Fukai et al., 2000; Wu and Chou, 2012), or activated carbon (Tamainot-Telto and Critoph, 2001; L. W. Wang et al., 2012; Ye et al., 2013) to improve the heat and mass transfer performance of the composites. The host/carrier matrix fulfils different functions: it defines the stability, the shape and the size of the material, which can be specially adapted for the application (van Helden and Hauer, 2013b). The use of composite materials as well as the reactor design has been found to considerably improve the heat and mass transfer within thermochemical processes, though the use of a host matrix strongly affects the sorption equilibrium of the salt with the sorbate (Gordeeva et al., 2013). So a compromise has to be found when performing synthesis of composites.

Azoumah et al. showed that an optimum value can be obtained by playing on the bulk density (Azoumah et al., 2004). Porosity of the composite or the bed is also an optimum parameter to overcome the heat and mass transfer issue (Dawoud and Aristov, 2003). The previous both authors show that water vapour sorption in the composite is quicker (reducing the hydration time) than in pure salt due to the host sorption properties. The composite materials are obtained using different methods: mixture based salts (Rammelberg et al., 2013) and minerals (Druske et al., 2013), salt impregnation or a mixing/impregnation and consolidation (Wang et al., 2009), synthesizing (Gordeeva et al., 1999).

2.3. THERMAL MANAGEMENT AND CHEMICAL REACTION IN HEAT STORAGE SYSTEMS

Thermochemical heat storage system based on the heat of reversible reactions between a solid and a gas allows efficient energy management. The first results of laboratory research, the performance of early prototypes and the versatility of their uses promise significant developments. However, the knowledge and understanding of transport phenomena, the nature of the media exchange is not yet complete. General literature (Azoumah et al., 2004; Ghommem et al., 2011; Ishitobi et al., 2013; Lahmidi et al., 2006; Lu et al., 1996; Mazet et al., 1991; Neveu et al., 2013) on the study of solid-gas reaction media revealed a great interest of research: mastering and transport optimisation via the use of a solid-gas reaction to store energy and recover it through the reaction enthalpy. This implies heat and mass exchange in the system, as it is related to transport phenomena.

Whether the chosen process (chemical or/and sorption) or the sorbent material state (liquid or solid), researchers and engineers face the heat and mass transfer issues at different scales: the material itself, the reactor and the whole system. In general and especially in a solid-gas thermochemical system, the solid is under porous media. Because, its structure will receive or reject a gas in order to fulfil the thermochemical reaction. As a first requirement, the solid should possess a higher energy density, since this is well reduced when putting together with all the reactor components (observation from Table 2.5). Among others, the material density is another requirement which needs to be high. Unfortunately, when the material desnity is high, porosity is reduced and favours mass transfer limitation for the thermochemical reaction. Heat transfer can laso be the transfer limitation since heat exchanged involves different phenomena depending on operating conditions. The presence of heat exchanger in the reactor, which represents thermal mass, thermal contact, can be a heat transfer limitation. The fact that the gas is pure (water vapour) or mixed (air), the material configuration (size, particle size of the solid, presence of the binder, compaction, texture, etc.) are among many things that influence heat and mass transfer and must be therefore handled in order to optimise the transport phenomena. In the following a short bibliography is given at the material or reactive bed level.

2.3.1. HEAT TRANSFER IN THE MATERIAL/REACTIVE BED PROCESS

A porous material is a body consisting of a solid matrix having pores with irregular shape, different size and random distribution that are filled with one or more fluids. Usually, some pores are interconnected and another disconnected. The interconnection of the pores allows the heat and mass transfer and fluid flow through itself that is accompanied with heat transfer into the solid matrix (Delgado, 2012). Depending on the physical problem, the following phenomena may mainly occur between the phases into the solid at the pore and bed level: heat transfer by convection, diffusion (conduction) and radiation. As already mentioned, the fluid for synthesis reaction here is the water vapour. Water vapour (no air) is the reactive gas and the salt hydrate the reactive solid. Both are considered as pseudo-homogeneous media at the same temperature and only the solid heat capacity will be assumed in the energy balance.
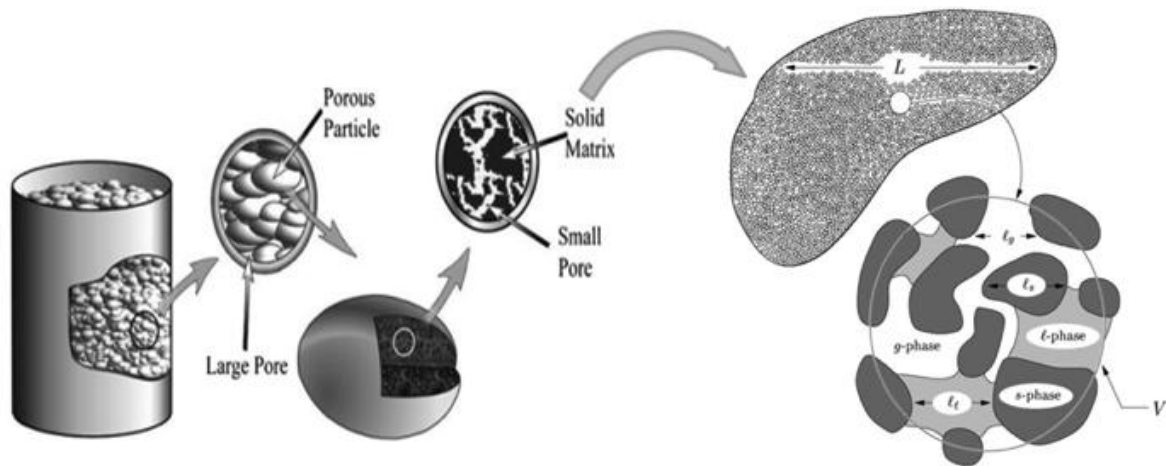
Figure 2.14: Schematic description from the packed bed to the solid matrix where process (sorption and chemical reaction) is performed (adapted from (Delgado, 2012) and (Duval et al., 2004)). g: gas; l: liquid; s: solid.

Olives et al. (Olives and Mauran, 2001) showed that the thermal radiation is neglected since the working temperature range of a thermochemical heat storage system is between 10 °C and 90 °C. Michel (Michel, 2012) mentioned in his thesis that, for a system with water vapour, the prevailing heat transfer is the conduction (convection is very small to be considered, hence neglected). Therefore, heat in a porous medium with water vapour is transferred by conduction according to Fourier's law. One of the heat transport problems in the reactive bed or material lies in the fluid phases, there is always non-condensable water which remains at the pore-level (Figure 2.14). This has been confirmed on silica gel for a specific pore (2-50 mm) (G. Zhang et al., 2014). That is why the introduction of the local-equilibrium (will be developed later) is one important assumption to reduce the complexity of the model development (avoiding three phases problem) to understand and/or optimise the lab-scale experiments.

The mastering of problems of heat transfer (and mass transfer) in these porous reactants bed or material is done through mathematical models knowledge. Three approach levels can be considered to achieve these models as raised decades ago by (Ajzoul, 1993): molecular, microscopic and macroscopic. The molecular approach has no practical value, because it is difficult to describe the movement of molecules, properly. The microscopic approach allows developing the general equations of transfers, but at this level of analysis, it is impossible to set the boundaries conditions of these equations. However, the results obtained in this approach are the starting point for the macroscopic approach, which allows to achieve the desired model. Then, resolution of the model equations is then possible after the introduction of simplifying assumptions that experiments can justify. This is the adopted strategy in this thesis to go forward on thermal management of the TESS.

Here, important points to mention in thermal management are the thermal properties related to heat transfer such as thermal conductivity and specific heat capacity of the material (defining the suitability of a material for TESS). The storage capacity need to be known and the thermal conductivity imposes charging and discharging rates and affects the complexity and cost of the heat exchanger design (Maru et al., 1976). Therefore these properties will be determined in chapter 4, and in the chapter 3 the adopted model for theoretical effective (accounting for bed porosity) thermal conductivity will be presented (actually, reminded).

2.3.2. Mass transfer in the material/reactive bed process

In the storage and release of energy process, two main phenomena are involved: chemical reaction and sorption. During desorption/dehydration or sorption/hydration, mass transfers of gas-solid phase occur in different ways according to many parameters. For example, in a fixed-bed sorption, the concentration of the gas phase and of the solid phase change with time as well as with position in the bed. Most of the time, mass transfer takes place near the inlet of the bed, where the gas contacts immediately the sorbent. If the solid contains no solute at the start, the concentration of the gas drops exponentially with distance essentially to zero before the end of the bed is reached. After some time, the solid situated at the inlet becomes slightly saturated, and most of the mass transfer takes place farther from the inlet (Benitez, 2009). In short, this explains the reaction front procedure and highlights how mass transfer can be limited.

In his thesis, Michel (Michel, 2012) principally studied mass transfer as a limiting factor for thermal efficiency by using modelling approach and experiments with the focus on the permeability of the salt hydrate. In fact the permeability (Sun et al., 1995) is one of the most important parameters to study mass transfer (diffusion, transport) by accounting to the material (salt hydrate) structure (texture, tortuosity, porosity, vapour flow regime, etc.). Hence the use of correlations in modelling is mandatory. (Mauran et al., 2001) used such a permeability correlation in his work, showing the porosity effect on the gas flow.

The diffusion of gases through consolidated media is viewed as a three-step process: (1) At a high-pressure interface, gas dissolves or condenses in the solid matrix. (2) Following dissolution or condensation, gas diffuses along a solid-phase concentration gradient in accordance with Fick's law to the low-pressure interface. (3) On arrival at the low-pressure gas - solid boundary, the dissolved gas is desorbed or released to the gaseous medium.

One important feature of chemical and sorption processes is the strong relation between mass and heat transfer characteristics. Low temperature boots the sorption/hydration while high temperature promotes desorption/dehydration (called adsorbent regeneration). Thermochemical reactors are characterised by a strong coupling between kinetics and thermal transfers. Anyway, simultaneous heat and mass transfer occur in a natural way whenever the transport of mass is accompanied by the evolution or consumption of heat. As an example of strong dependence, the way to fill the salt in the reactor bed, may have a profound impact on thermal performances of the system (Mauran et al., 1993). The resistance at the salt surface (Figure 2.15) is a limiting factor. In a heat exchanger, the number of plates and distance between them, can be limited. Numerical studies help to determine with configuration could be of interest. The knowledge at which reaction rate the mass transfer occurs is a hint of starting overcoming thermal transfers limitations in the system (Sieres and Fernández-Seara, 2007). In the following chapters 3 and 5, numerical studies are performed to attempt understanding of such phenomena and optimise them as possible as it can.
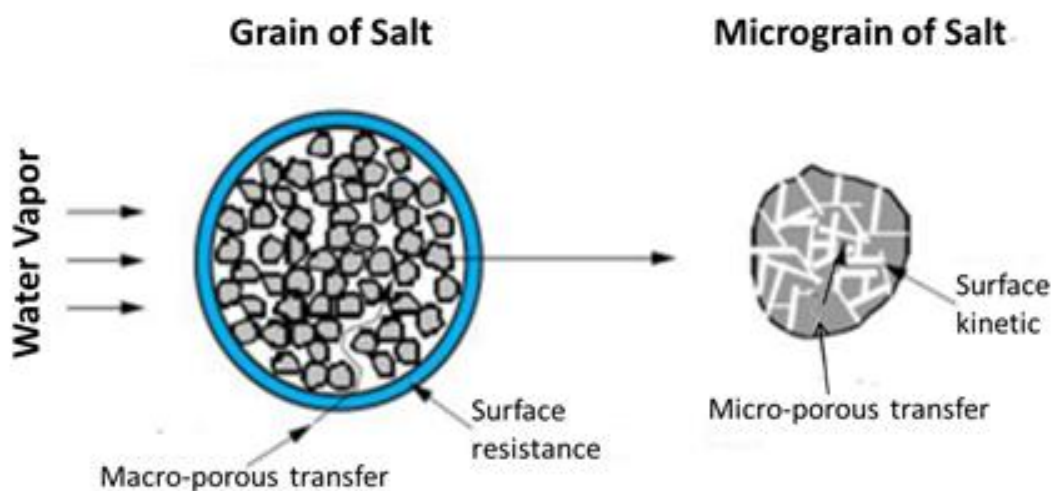
Figure 2.15: Mass transfer mechanisms in salt hydrates with porosity (adapted from (Duquesne, 2013)).

2.3.3. REACTION/SORPTION KINETICS

Reaction kinetics refers to chemical reaction mechanism and its evolution in terms of reaction rate (meaning the changes in concentration of reactants and products with time), reaction advancement/conversion. Reaction kinetics deals to a large extent with the factors which influence the reaction velocity. Those effects are concentration, temperature, reaction order, phase and surface area, solvents and catalysts. In this thesis solvent and catalyst effects will not be evocated or taken into consideration. One of the important reasons of studying chemical reaction rate is for practical reasons. The aim is to determine at which rate the solid-gas reaction approaches the equilibrium state. Due to the complexity (Frost and Pearson, 1961) of chemical phenomena (every elementary reactions has its own reaction mechanism), Asperger (Asperger, 2003) affirmed that complete knowledge of a reaction mechanism is rarely attained. Most of the time, modelling based on experimental data helps for rate determination. Another way of studying kinetics is through reaction advancement, which characterises the rate of the reacted salt during the decomposition or synthesis to the total salt hydrate (initial salt state).

Several models concerning the sorption kinetics have been developed over the past decades such as linear drive force (LDF), solid diffusion and equilibrium models (Chahbani et al., 2002; Ilis et al., 2010). These previous authors compared the three models. From their analysis, the equilibrium model uses the assumption where mass transfer is not a limiting factor due the slowness of intra-particles diffusion through micro- and macropores. It is however recommended when pore-diffusion are higher. The solid diffusion model has been extensively used (Chan et al., 1981; Inaba et al., 2004; Yong and Sumathy, 2002) and is the more accurate, but more cumbrous one. Concerning the LDF model (Sircar and Hufton, 2000), it is derived from the solid diffusion model adopting a simplifying mathematical assumption and this latter model tends to underevaluate the system performances as demonstrated by (Chahbani et al., 2002). Figure 2.16 (a) shows that an instantaneous equilibrium model is preferred for a low-pressure system. Concerning that pressure, it does not increase much. Figure 2.16 (b) reveals an overestimation when using the equilibrium model, leading to an surestimation of system

performance. However results are acceptable over a long time process and recommended for chemical processes having an adsorbate dimensionless concentration below 0.2.

a) Bed pressure evolution, one cycle   b) Average adsorbate concentration over time
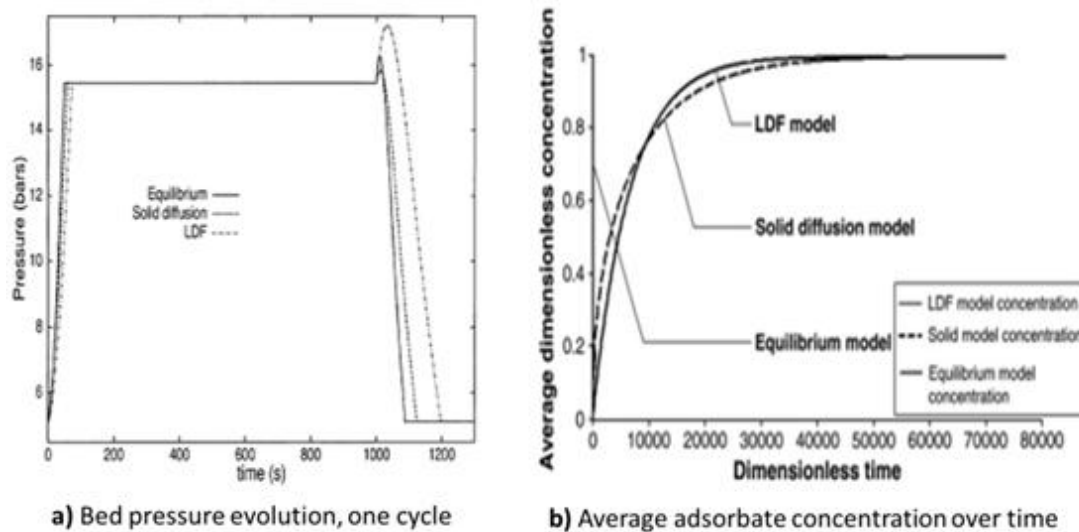
Figure 2.16: Dynamic comparison of (a) bed pressure (Chahbani et al., 2002) and (b) adsorbate concentration on the process time (Ilis et al., 2010).

On thermochemical kinetics, a phenomenological modelling requires good knowledge of the structure of the mixture and especially the mechanisms of ab/adsorption and desorption together with chemical reaction. This knowledge is still imperfect and insufficient to build a sufficiently representative model of the phenomenon. As ideal is only hypothetic, a semi-empirical law identified from measurements performed on a calorimeter combined to the equilibrium model is proposed. The equilibrium model has been chosen among the above reasons for thermochemical and sorption processes due to the low energy source needed such as solar energy (Duquesne, 2013) or micro-cogeneration. This model seems sufficient to describe the sorption kinetics. In the following chapter 3, the model is developed.

2.4. CONCLUSION OF THE CHAPTER

This chapter reviews the technology concept around the thermal energy storage systems. It allows drawing up an inventory of different storage systems, highlighting the thermochemical system as the better one. The idea of coupling or integrating thermal energy storage systems with existing power and/or thermal systems is not new and has proved an effective feasibility through different studies. This concerns mainly the latent and sensible energy storage. The first part of the chapter gave some detailed and practical examples. However, the idea of coupling thermochemical energy storage systems due to their high energy storage density with a combined heating and power system is rather new and challenging. How a reactor should be designed has been covered, showing why an integrated and closed (favoured vapour transport into the bed) reactor is preferred, although technical handling may offer more complexity (heat exchanger) and techmological constraints (vacuum control).

From a flourished literature on material selection, each of the researchers or institutes/universities have defined what they found as best thermochemical material for their

application. It appears that the strontium bromide has particularly drawn attraction due to the fact, it can reach or be closed to the target of the project: high prototype energy density of 80 kW·m^{-3} if possible, compatible charging temperature from the micro-CHP heat loss, environmentally safe, discharging temperature of 50 °C sufficient for heating and DHW. It can be for the moment, the best material for the low-temperature THSS. However, like most of pure salt, it presents kinetic issues leading to low system power. So composites are developed with larger surface in which chemical reaction can proceed and may overcome this issue. Hence, a high amount of heat release via the combined phenomena of sorption and chemical reaction.

The review also reveals the well-known heat and mass transfer issue into the reactive bed and in the whole system. It is mandatory to understand these coupled phenomena and characterise them, at least the main parameters. Numerical studies are used to bring some responses and solutions to that issue. Pinel et al. found that numerical studies on heat and mass transfer are very basis and do not try to be more real (such as 3D or 2D per example), but instead of that, too many assumptions are drawn to replace the reality of such system (Pinel et al., 2011). An emphasis is placed on heat transport, mass transport and kinetic in order to described the involved phenomena so that it will be modelled in the next chapter. For these transport/transfer phenomena, thermal conductivity, permeability and reaction advancement describe or represent them completely well. The next chapter will therefore present numerical modelling of the reactive bed under pure water vapour in the close system, after a brief description of the practical system.

Table 2.5. Suitable thermochemical materials for household applications at low temperature (from (N'Tsoukpoe et al., 2014b)).

Hydrated salt	$Al_2(SO_4)_3 \cdot 18H_2O$	$CaBr_2 \cdot 4H_2O$	$Ce(SO_4)_2 \cdot 4H_2O$	$K_2CO_3 \cdot 1.5H_2O$	$LaCl_3 \cdot 7H_2O$	$La(NO_3)_3 \cdot 4H_2O$
Dehydrated salt	$Al_2(SO_4)_3 \cdot 8.5H_2O$	$CaBr_2 \cdot 3H_2O$	$Ce(SO_4)_2 \cdot 2H_2O$	$K_2CO_3 \cdot 0.8H_2O$	$LaCl_3 \cdot H_2O$	$La(NO_3)_3 \cdot 1.5H_2O$
$T_{melting}$ [°C]	88	80-110	180	> 80	91	86-95
d_s [t·m^{-3}]	1.69	2.2	3.91	2.15	2.223	2.459
N	9.5	1	2	0.7	6	2.5
ΔH_r [kJ·mol^{-1}]	526.8	59.7	58.0*	44.6	355.5	158.6
$\Delta H_{r,m}$ [kWh·kg^{-1}]	0.220	0.061	0.040	0.075	0.266	0.111
$\Delta H_{r,V}$ [kWh·m^{-3}]	371	134	156	161	591	273
ΔH_{lean} [kJ·mol^{-1}]	103.1	15.1		13.4	88.0	47.1
$\Delta H_{lean,V}$ [kWh·m^{-3}]	73	34		48	146	81
η [%]	19.6	25.3		30.0	24.7	29.7
$\Delta H_{r,V*}$ [kWh·m^{-3}]	259	117		138	359	213
$\Delta H_{lean,V*}$ [kWh·m^{-3}]	51	30		41	89	63
Hydrated salt	$LiCl \cdot H_2O$	$MgCl_2 \cdot 6H_2O$	$MgSO_4 \cdot 6H_2O$	$Na_2S_2O_3 \cdot 2H_2O$	$\mathbf{SrBr_2 \cdot 6H_2O}$	$SrCl_2 \cdot 2H_2O$
Dehydrated salt	$LiCl$	$MgCl_2 \cdot 4.7H_2O$	$MgSO_4 \cdot 2H_2O$ [a]	$Na_2S_2O_3$	$\mathbf{SrBr_2 \cdot H_2O}$	$SrCl_2 \cdot H_2O$
$T_{melting}$ [°C]	99	117-118	88.5-93 [a]	-	**88**	100
d [t·m^{-3}]	1.7	1.569	2.04	1.69 [b]	**2.386**	2.672
N	1	1.3	4	2	**5**	1
ΔH_r [kJ·mol^{-1}]	62.2	71.5	225.1	110.3	**337.0**	59.0
$\Delta H_{r,m}$ [kWh·kg^{-1}]	0.286	0.098	0.274	0.158	**0.263**	0.061
$\Delta H_{r,V}$ [kWh·m^{-3}]	486	153	558	267	**628**	164
ΔH_{lean} [kJ·mol^{-1}]	17.6	13.5	46.8	21.2	**114.0**	14.4
$\Delta H_{lean,V}$ [kWh·m^{-3}]	137	29	116	51	**213**	40
η [%]	28.3	18.9	20.8	19.2	**33.8**	24.4
$\Delta H_{r,V*}$ [kWh·m^{-3}]	322	130	340	203	**392**	139
$\Delta H_{lean,V*}$ [kWh·m^{-3}]	91	25	71	39	**133**	34

[a] The $MgSO_4 \cdot 2H_2O$ is metastable according to (Grevel and Majzlan, 2009). 88.5-93 °C correspond to the phase transition point for crystalline modification of the $MgSO_4 \cdot 6H_2O$ (Kandiner, 1970). [b] This is the density of the $Na_2S_2O_3 \cdot 5H_2O$.

Table 2.6. Most used thermochemical materials in projects followed with some prototypes.

Material (TCM)	Characteristics	Research level	Projects/Institutions	References
$SrBr_2 \cdot 6H_2O \leftrightarrow SrBr_2 \cdot H_2O + 5H_2O$ (Additive: Expanded Natural Graphite in proportion 6% and 8%)	Charge: 70-80 °C at 4.4 kWh of HX for 840 min; Discharge: 35 °C at 2.2 kWh of HX for heating and evaporator at 12 °C, during 15-24h. Theoretical energy density: 628 kWh·m^{-3}of salt. Prototype energy density: 60 kWh·m^{-3}. Storage capacity: 60 kWh.	Reactor scale, Numerical scale and prototype.	PROMES, CEA-INES/LITEN: SOLUX prototype 170 kg of $SrBr_2 \cdot H_2O$. IEC-Leuphana.	(Lahmidi et al., 2006; Mauran et al., 2008; Tanguy et al., 2010)(Marias et al., 2014)
$MgSO_4 \cdot 7H_2O \leftrightarrow MgSO_4 + 7H_2O$ (Pure and Zeolite 13X impregnated with 15wt%)	Charge: 122-150 °C; Discharge: 30 °C. Theoretical energy density: 0.76-1.5 GJ·m^{-3} of salt. Total hydration energy density: 476 kWh·m^{-3}.	Reactor scale, Numerical scale (Balasubramanian et al., 2010) and prototype.	ECN-Netherlands, IWT-Bremen, INSA-Lyon, Bauhaus-Universität Weimar-Germany.	(Bales, 2008; C. J. Ferchaud et al., 2012; Hongois et al., 2011; Steiger et al., 2008; van Essen et al., 2009a, 2009b)(Posern, 2012)
$MgCl_2 \cdot 6H_2O \leftrightarrow MgCl_2 \cdot 2H_2O + 4H_2O$	Charge: 117 °C; Discharge: 35 °C. Theoretical energy density: 2.17 GJ·m^{-3} of $MgCl_2 \cdot 2H_2O$.	Reactor scale (labscale experiment).	ECN-Netherlands, IEC-Leuphana.	(C. J. Ferchaud et al., 2012; Opel et al., 2011)
$MgCl_2 \cdot 6H_2O \leftrightarrow MgCl_2 \cdot H_2O + 5H_2O$	Charge: 150 °C; Discharge: 60 °C at 50 W. Prototype density: 0.5 GJ·m^{-3}. Thermal power: 150 W after 25h.	Reactor scale, prototype (17 l of salt).	ECN-Netherlands.	(Zondag et al., 2013)
$CaCl_2 \cdot 2H_2O \leftrightarrow CaCl_2 \cdot H_2O + H_2O$	Charge: 95 °C; Discharge: 35 °C. Theoretical energy density: 0.72 GJ/m^3 of $CaCl_2$. Prototype energy	Reactor scale, (theoretical study).	SOLAUTARK project (BEMS-Liège, Belgium)	(Courbon et al., 2011; Hennaut et al., 2014)

	density: 60 kWh·m^{-3} (40 m^3).			
$Na_2S·5H_2O \leftrightarrow Na_2S·1.5H_2O + 3.5H_2O$ (ECN)	Charge: 72-83 °C and at 180 °C at 2.5 kW; Discharge: 35 °C at 0.7 – 1.5 kW for 4.6 h. Theoretical energy density: 2.8 GJ·m^{-3} of $Na_2S·5H_2O$. Experimental energy density: 780 kWh·m^{-3} of $Na2S·5H2O$. Storage energy density: 990 kWh·m^{-3}.	Reactor scale, SWEAT-prototype (3 kg of salt).	ECN-Netherlands. Chiang University, MCES Project)	(Boer et al., 2006, 2004; De Boer et al., 2002) (Wongsuwan, 2004)
$Na_2S·5H_2O \leftrightarrow Na_2S·1H_2O + 4H_2O$ (MCES Project)				
$Al_2(SO_4)_3·18H_2O \leftrightarrow Al_2(SO_4)_3·5H_2O + 13H_2O$	Charge: 150 °C; Discharge with temperature lift at a variation of 9.8 °C, reactor and evaporator both at 25.1 °C.	Reactor scale (40 g of salt).	ECN-Netherlands.	(van Essen et al., 2009a)
$KAl(SO_4)_2·12H_2O \leftrightarrow Al_2(SO_4)_3·3H_2O + 9H_2O$	Charge: 60 °C during 18 h; Discharge: 15 °C during 81 h. Experimental energy density: 0.86 GJ·m^{-3} of $KAl(SO_4)_2·3H_2O$.	Reactor scale, prototype (25 kg of $KAl(SO_4)_2·12H_2O$).	PROMES, CEA-INES-project (ANR-08-STOCK-E-04 ESSI).	(Marias et al., 2014)

All those performances stand for the heating only.

REFERENCES CHAPTER

Abedin, A.H., Rosen, M.A., 2011. A Critical Review of Thermochemical Energy Storage Systems. The Open Renewable Energy Journal 4, 42–46.

Ajzoul, T., 1993. Analyse et Optimisation des Transferts Thermiques dans les Réacteurs Solide-Gaz (Doctorate/Ph.D). University Abdelmalek Essaadji, Morocco.

Aristov, Y.I., 2013. Challenging offers of material science for adsorption heat transformation: A review. Applied Thermal Engineering 50, 1610–1618. doi:10.1016/j.applthermaleng.2011.09.003

Aristov, Y.I., Restuccia, G., Tokarev, M.M., Cacciola, G., 2000. Selective Water Sorbents for Multiple Applications, 10. Energy Storage Ability. Reaction Kinetics and Catalysis Letters 69, 345–353. doi:10.1023/A:1005616420331

Arteconi, A., Hewitt, N.J., Polonara, F., 2013. Domestic demand-side management (DSM): Role of heat pumps and thermal energy storage (TES) systems. Applied Thermal Engineering 51, 155–165. doi:10.1016/j.applthermaleng.2012.09.023

Asperger, S., 2003. Chemical Kinetics and Inorganic Reaction Mechanisms, 2nd ed, Inorganic Chemistry. sp, Zagreb, Croatia. http://www.springer.com/chemistry/organic+chemistry/book/978-0-306-47747-8.

Azoumah, Y., Mazet, N., Neveu, P., 2004. Constructal network for heat and mass transfer in a solid–gas reactive porous medium. International Journal of Heat and Mass Transfer 47, 2961–2970. doi:10.1016/j.ijheatmasstransfer.2004.03.022

Balasubramanian, G., Ghommem, M., Hajj, M.R., Wong, W.P., Tomlin, J.A., Puri, I.K., 2010. Modeling of thermochemical energy storage by salt hydrates. International Journal of Heat and Mass Transfer 53, 5700–5706. doi:10.1016/j.ijheatmasstransfer.2010.08.012

Bales, C., 2008. Final report of IEA-SHC task 32 subtask B "Chemical and sorption storage" The overview (A Report of IEA Solar Heating and Cooling programme - Task 32 Advanced storage concepts for solar and low energy buildings No. B7 of subtash B), Advanced storage concepts for solar and low energy buildings. BASE Consultants SA - Geneva, Swiss.

Bales, C., Nordlander, S., 2005. TCA Evaluation : Lab Measurements, Modelling and System Simulations (Research and Engineering No. SHA-512). Dalarna University, School of Technology and Business Studies, Environmental Engineering, Falun, Sweden.

Barbieri, E.S., Melino, F., Morini, M., 2012. Influence of the thermal energy storage on the profitability of micro-CHP systems for residential building applications. Applied Energy 97, 714–722. doi:10.1016/j.apenergy.2012.01.001

Benitez, J., 2009. Principles and Modern Applications of Mass Transfer Operations, 2 edition. ed, Environmental Chemistry / General Environmental Chemistry. Wiley-Interscience, Hoboken, N.J.

Boer, R. de, Haije, W.G., Veldhuis, J.B.J., Smeding, S.F., 2004. Solid-sorption cooling with integrated thermal storage: The SWEAT prototype, in: 3rd International Heat Powered Cycles Conference - HPC 2004, Larnaca, Cyprus, 11-13 Oktober 2004., ECN-RX--04-080. Presented at the International Heat Powered Cycles Conference (HPC-2004), ECN Energy Efficiency in Industry, Larnaca, Cyprus, p. 10.

Boer, R. de, Smeding, S.F., Bach, P.W., 2006. HEAT STORAGE SYSTEMS FOR USE IN AN INDUSTRIAL BATCH PROCESS: (Results of) a case study, in: ECOSTOCK 2006 Conference, Phase Change Materials/Thermochemical Storage/Solar. Presented at the The Tenth International Conference on Thermal Energy Storage, Richard Stockton College, Richard Stockton College of New Jersey, USA, p. 7.

Bogdan, Ž., Kopjar, D., 2006. Improvement of the cogeneration plant economy by using heat accumulator. Energy 31, 2285–2292. doi:10.1016/j.energy.2006.01.012

Bolis, V., Broyer, M., Barbaglia, A., Busco, C., Foddanu, G.M., Ugliengo, P., 2003. Van der Waals interactions on acidic centres localized in zeolites nanocavities: a calorimetric and computer modeling study. Journal of Molecular Catalysis A: Chemical 204–205, 561–569. doi:10.1016/S1381-1169(03)00339-X

Bolis, V., Busco, C., Ugliengo, P., 2006. Thermodynamic study of water adsorption in high-silica zeolites. Journal of Physical Chemistry B 110, 14849–14859. doi:10.1021/jp061078q

Caliskan, H., Dincer, I., Hepbasli, A., 2012. Thermodynamic analyses and assessments of various thermal energy storage systems for buildings. Energy Conversion and Management 62, 109–122. doi:10.1016/j.enconman.2012.03.024

Castets, K., Mazet, N., 2000. Analysis and optimisation of the cyclic working mode of thermochemical transformers. Applied Thermal Engineering 20, 1649–1666. doi:10.1016/S1359-4311(99)00083-6

Castets, K., Mazet, N., 2001. Optimisation of the reactor configuration on the performance of the cyclic working mode of thermochemical transformers: Reactor miniaturization. Energy 26, 271–286. doi:10.1016/S0360-5442(00)00065-7

Chahbani, M.H., Labidi, J., Paris, J., 2002. Effect of mass transfer kinetics on the performance of adsorptive heat pump systems. Applied Thermal Engineering 22, 23–40. doi:10.1016/S1359-4311(01)00067-9

Chan, C.W., Ling-Chin, J., Roskilly, A.P., 2013. A review of chemical heat pumps, thermodynamic cycles and thermal energy storage technologies for low grade heat utilisation. Applied Thermal Engineering 50, 1257–1273. doi:10.1016/j.applthermaleng.2012.06.041

Chan, Y.N.I., Hill, F.B., Wong, Y.W., 1981. Equilibrium theory of a pressure swing adsorption process. Chemical Engineering Science 36, 243–251. doi:10.1016/0009-2509(81)85002-6

Chesi, A., Ferrara, G., Ferrari, L., Magnani, S., Tarani, F., 2013. Influence of the heat storage size on the plant performance in a smart user case study. Applied Energy 112, 1454–1465. doi:10.1016/j.apenergy.2013.01.089

Chua, H.T., Ng, K.C., Chakraborty, A., Oo, N.M., Othman, M.A., 2002. Adsorption Characteristics of Silica Gel + Water Systems. J. Chem. Eng. Data 47, 1177–1181. doi:10.1021/je0255067

Cot-Gores, J., Castell, A., Cabeza, L.F., 2012. Thermochemical energy storage and conversion: A-state-of-the-art review of the experimental research under practical conditions. Renewable and Sustainable Energy Reviews 16, 5207–5224. doi:10.1016/j.rser.2012.04.007

Courbon, E., Skrylnyk, A., Hennaut, S., Andre, P., Frere, M., 2011. Simple procedure to evaluate thermal energy storage densities of solid- gas systems: Application to solar energy storage in buildings. Récents Progrès en Génie des Procédés, Ed. SFGP, Paris, France 6. doi:- ISBN 2-910239-75-6

Critoph, R.E., Zhong, Y., 2005. Review of trends in solid sorption refrigeration and heat pumping technology. Proceedings of the Institution of Mechanical Engineers, Part E: Journal of Process Mechanical Engineering 219, 285–300. doi:10.1243/095440805X6982

Davidson, J.H., Quinnell, J., Bursh, J., 2013. Development of Space Heating and Domestic Hot Water Systems with Compact Thermal Energy Storage - Report of the Working Group WB2 for the period February 2009 to December 2012 (A report of the IEA Solar Heating and Cooling / Energy Conservation through Energy Storage programme – Task 42/Annex 24: No. IEA SHC/ECES – Task 42/24 – Compact Thermal Energy Storage).

Dawoud, B., Aristov, Y., 2003. Experimental study on the kinetics of water vapor sorption on selective water sorbents, silica gel and alumina under typical operating conditions of sorption heat pumps. International Journal of Heat and Mass Transfer 46, 273–281. doi:10.1016/S0017-9310(02)00288-0

De Boer, R., Haije, W.G., Veldhuis, J.B.J., 2002. Determination of structural, thermodynamic and phase properties in the Na_2S–H_2O system for application in a chemical heat pump. Thermochimica acta 395, 3–19.

Delgado, J.M.P.Q., 2012. Heat and Mass Transfer in Porous Media, 1st ed, Advanced Structured Materials,. Springer-Berlin, Germany. ISBN 978-3-642-21966-5.

Dinçer, I., Rosen, M., 2002. Thermal energy storage systems and applications. Wiley, New York. USA. ISBN 0-471-49573-5 978-0-471-49573-4.

Ding, Y., Riffat, S.B., 2012. Thermochemical energy storage technologies for building applications: A state-of-the-art review. Int. J. Low-Carbon Tech. Voö. 0, pp. 1-11, cts004. doi:10.1093/ijlct/cts004

Douss, N., Meunier, F., 1989. Experimental study of cascading adsorption cycles. Chemical Engineering Science 44, 225–235. doi:10.1016/0009-2509(89)85060-2

Druske, M.-M., N'Tsoukpoe, K.E., Wickenheisser, M., Rammelberg, H.U., Schmidt, T., Ruck, W., 2013. Mineralogical Approach on the Selection of Candidates for Thermochemical Heat Storage, in: 8th International Renewable Energy Storage Conference and Exhibition. Presented at the IRES 2013, Eurosolar, Berlin, Germany, p. 1.

Duquesne, M., 2013. Résolution et réduction d'un modèle non-linéaire de stockage d'énergie par adsorption sur des zéolithes (Doctorate/Ph.D). Université Sciences et Technologies - Bordeaux I, France.

Duval, F., Fichot, F., Quintard, M., 2004. A local thermal non-equilibrium model for two-phase flows with phase-change in porous media. International Journal of Heat and Mass Transfer 47, 613–639. doi:10.1016/j.ijheatmasstransfer.2003.07.005

Ferchaud, C., Zondag, H., De Boer, R., Rindt, C.C.M., 2012. "Characterization of the sorption process in thermochemical materials for seasonal solar heat storage application., in: The 12th International Conference on Energy Storage, INNO-ST-08. Presented at the Innostock 2012, Lleida, Spain, p. 4.

Ferchaud, C.J., Zondag, H.A., Veldhuis, J.B.J., Boer, R. de, 2012. Study of the reversible water vapour sorption process of $MgSO_4.7H_2O$ and $MgCl_2.6H_2O$ under the conditions of seasonal solar heat storage. J. Phys.: Conf. Ser. 395, 012069. doi:10.1088/1742-6596/395/1/012069

Few, P.C., Smith, M.A., Twidell, J.W., 1997. Modelling of a combined heat and power (CHP) plant incorporating a heat pump for domestic use. Energy 22, 651–659. doi:10.1016/S0360-5442(96)00171-5

Fopah Lele, A., Korhammer, K., Wegscheider, N., Rammelberg, H.U., Schmidt, T., Ruck, W.K.L., 2013. Thermal Conductivity of Salt Hydrates as Porous Material using Calorimetric (DSC) Method, in: 8th World Conference on Experimental Heat Transfer, Fluid Mechanics, and Thermodynamics. Presented at the ExHFT-8, A. Faria - Edicao Electronica Lda., Lisbon, Portugal, p. 5.

Frost, A., Pearson, R., 1961. Kinetics and Mechanism, Second Edition. J. Phys. Chem. 65, 384–384. doi:10.1021/j100820a601

Fukai, J., Kanou, M., Kodama, Y., Miyatake, O., 2000. Thermal conductivity enhancement of energy storage media using carbon fibers. Energy Conversion and Management 41, 1543–1556. doi:10.1016/S0196-8904(99)00166-1

Fumey, B., Weber, R., Gantenbein, P., Daguenet-Frick, X., Williamson, T., Dorer, V., 2014a. Closed Sorption Heat Storage based on Aqueous Sodium Hydroxide. Energy Procedia, Proceedings of the 2nd International Conference on Solar Heating and Cooling for Buildings and Industry (SHC 2013) 48, 337–346. doi:10.1016/j.egypro.2014.02.039

Fumey, B., Weber, R., Gantenbein, P., Daguenet-Frick, X., Williamson, T., Dorer, V., 2014b. Development of a Closed Sorption Heat Storage Prototype. Energy Procedia 46, 134–141. doi:10.1016/j.egypro.2014.01.166

Ghommem, M., Balasubramanian, G., Hajj, M.R., Wong, W.P., Tomlin, J.A., Puri, I.K., 2011. Release of stored thermochemical energy from dehydrated salts. International Journal of Heat and Mass Transfer 54, 4856–4863. doi:10.1016/j.ijheatmasstransfer.2011.06.041

Gil, A., Medrano, M., Martorell, I., Lázaro, A., Dolado, P., Zalba, B., Cabeza, L.F., 2010. State of the art on high temperature thermal energy storage for power generation. Part 1—Concepts, materials and modelisation. Renewable and Sustainable Energy Reviews 14, 31–55. doi:10.1016/j.rser.2009.07.035

Gordeeva, L., Grekova, A., Krieger, T., Aristov, Y., 2013. Composites "binary salts in porous matrix" for adsorption heat transformation. Applied Thermal Engineering 50, 1633–1638. doi:10.1016/j.applthermaleng.2011.07.040

Gordeeva, L.G., Aristov, Y.I., 2012. Composites "salt inside porous matrix" for adsorption heat transformation: a current state-of-the-art and new trends. International Journal of Low-Carbon Technologies 0, 1–15. doi:10.1093/ijlct/cts050

Gordeeva, L.G., Mrowiec-Bialon, J., Jarzebski, A.B., Lachowski, A.I., Malinowski, J.J., Aristov, Y.I., 1999. Selective water sorbents for multiple applications, 8. sorption properties of CaCl2−SiO2 sol-gel composites. React Kinet Catal Lett 66, 113–120. doi:10.1007/BF02475749

Grevel, K.-D., Majzlan, J., 2009. Internally consistent thermodynamic data for magnesium sulfate hydrates. Geochimica et Cosmochimica Acta 73, 6805–6815. doi:10.1016/j.gca.2009.08.005

Guilleminot, J.J., Choisier, A., Chalfen, J.B., Nicolas, S., Reymoney, J.L., 1993. Heat transfer intensification in fixed bed adsorbers. Heat Recovery Systems and CHP 13, 297–300. doi:10.1016/0890-4332(93)90052-W

Haeseldonckx, D., Peeters, L., Helsen, L., D'haeseleer, W., 2007. The impact of thermal storage on the operational behaviour of residential CHP facilities and the overall CO_2 emissions. Renewable and Sustainable Energy Reviews 11, 1227–1243. doi:10.1016/j.rser.2005.09.004

Haije, W.G., Veldhuis, J.B.J., Smeding, S.F., Grisel, R.J.H., 2007. Solid/vapour sorption heat transformer: Design and performance. Applied Thermal Engineering 27, 1371–1376. doi:10.1016/j.applthermaleng.2006.10.022

Hauer, A., 2007. Evaluation of adsorbent materials for heat pump and thermal energy storage applications in open systems. Adsorption 13, 399–405. doi:10.1007/s10450-007-9054-0

Hauer, A., Avemann, E.L., 2007. Open absorption systems for air conditioning and thermal energy storage, in: Paksoy, H.Ö. (Ed.), Thermal Energy Storage for Sustainable Energy Consumption, NATO Science Series. Springer, Dordrecht, Netherlands, pp. 429–444.

Hennaut, S., Thomas, S., Davin, E., Skrylnyk, A., Frère, M., André, P., 2014. Simulation of a Vertical Ground Heat Exchanger as Low Temperature Heat Source for a Closed Adsorption Seasonal Storage of Solar Heat. Energy Procedia, Proceedings of the 2nd International Conference on Solar Heating and Cooling for Buildings and Industry (SHC 2013) 48, 370–379. doi:10.1016/j.egypro.2014.02.043

Henninger, S.K., Jeremias, F., Kummer, H., Schossig, P., Henning, H.-M., 2012. Novel Sorption Materials for Solar Heating and Cooling. Energy Procedia 30, 279–288. doi:10.1016/j.egypro.2012.11.033

Hongois, S., Kuznik, F., Stevens, P., Roux, J.-J., 2011. Development and characterisation of a new MgSO4−zeolite composite for long-term thermal energy storage. Solar Energy Materials and Solar Cells 95, 1831–1837. doi:10.1016/j.solmat.2011.01.050

Hui, L., N'Tsoukpoe, E.K., Nolwenn, L.P., Lingai, L., 2011. Evaluation of a seasonal storage system of solar energy for house heating using different absorption couples. Energy Conversion and Management 52, 2427–2436. doi:10.1016/j.enconman.2010.12.049

Ibrahim, H., Ilinca, A., Perron, J., 2008. Energy storage systems—Characteristics and comparisons. Renewable and Sustainable Energy Reviews 12, 1221–1250. doi:10.1016/j.rser.2007.01.023

Ilis, G.G., Mobedi, M., Ülkü, S., 2010. A parametric study on isobaric adsorption process in a closed adsorbent bed. International Communications in Heat and Mass Transfer 37, 540–547. doi:10.1016/j.icheatmasstransfer.2010.01.003

Inaba, H., Seo, J.K., Horibe, A., 2004. Numerical study on adsorption enhancement of rectangular adsorption bed. Heat Mass Transfer 41, 133–146. doi:10.1007/s00231-004-0512-x

Ishitobi, H., Uruma, K., Takeuchi, M., Ryu, J., Kato, Y., 2013. Dehydration and hydration behavior of metal-salt-modified materials for chemical heat pumps. Applied Thermal Engineering 50, 1639–1644. doi:10.1016/j.applthermaleng.2011.07.020

Jiang, L., Wang, L.W., Wang, R.Z., 2014. Investigation on thermal conductive consolidated composite CaCl2 for adsorption refrigeration. International Journal of Thermal Sciences 81, 68–75. doi:10.1016/j.ijthermalsci.2014.03.003

Kandiner, H.J., 1970. Die Legierungen des Magnesiums, in: Magnesium, Gmelin Handbook of Inorganic and Organometallic Chemistry - 8th edition. Springer Berlin Heidelberg, pp. 373–482.

Kato, Y., 2000. Low exergy reactor for decentralized energy utilisation. Progress in Nuclear Energy 37, 405–410. doi:10.1016/S0149-1970(00)00079-2

Katulić, S., Čehil, M., Bogdan, Ž., 2014. A novel method for finding the optimal heat storage tank capacity for a cogeneration power plant. Applied Thermal Engineering 65, 530–538. doi:10.1016/j.applthermaleng.2014.01.051

Kerkes, H., 2006. Seasonal sorption heat storage, in: DANVAK Seminar. Presented at the Solar heating systems-Combisystems-heat storage, DTU Lyngby.

Kerkes, H., Drück, H., 2011. Energetic and economic aspects of seasonal heat storage in single and multifamily houses, in: ESTEC 2011. Presented at the 5th European Solar Thermal Energy Conference, ESTEC, Marseille, France, p. 6.

Khan, M.Z.I., Alam, K.C.A., Saha, B.B., Akisawa, A., Kashiwagi, T., 2007. Study on a re-heat two-stage adsorption chiller – The influence of thermal capacitance ratio, overall thermal conductance ratio and adsorbent mass on system performance. Applied Thermal Engineering 27, 1677–1685. doi:10.1016/j.applthermaleng.2006.07.005

Krönauer, A., Lävemann, E., Hauer, A., 2012. MobS II – Mobile Sorption Heat Storage in Industrial Waste Heat Recovery.

Lahmidi, H., Mauran, S., Goetz, V., 2006. Definition, test and simulation of a thermochemical storage process adapted to solar thermal systems. Solar Energy 80, 883–893. doi:10.1016/j.solener.2005.01.014

Levine, I.N., 2002. Physical Chemistry - McGraw-Hill Companies 9780072318081 5th Edition - Better World Books [WWW Document]. URL http://www.abebooks.com/servlet/BookDetailsPL?bi=12041960887&searchurl=an%3DIra%2BN.%2BLevine%26amp%3Bsts%3Dt%26amp%3Btn%3DPhysical%2BChemistry (accessed 3.24.14).

Li, M., Sun, C.J., Wang, R.Z., Cai, W.D., 2004. Development of no valve solar ice maker. Applied Thermal Engineering 24, 865–872. doi:10.1016/j.applthermaleng.2003.10.002

Li, S.L., Wu, J.Y., Xia, Z.Z., Wang, R.Z., 2011. Study on the adsorption isosteres of the composite adsorbent CaCl2 and expanded graphite. Energy Conversion and Management 52, 1501–1506. doi:10.1016/j.enconman.2010.10.015

Li, S.-L., Xu, Q., 2013. Metal–organic frameworks as platforms for clean energy. Energy & Environmental Science 6, 1656. doi:10.1039/c3ee40507a

Li, T., Wang, R., Kiplagat, J.K., 2013. A target-oriented solid-gas thermochemical sorption heat transformer for integrated energy storage and energy upgrade. AIChE Journal 59, 1334–1347. doi:10.1002/aic.13899

Lindburg, A., 2014. Net Zero: Opportunities for Neighborhood Development [WWW Document]. Blogspot. URL http://streets.mn/2014/06/12/net-zero-opportunities-for-neighborhood-development/ (accessed 7.23.14).

Lu, H.-B., Mazet, N., Spinner, B., 1996. Modelling of gas-solid reaction—Coupling of heat and mass transfer with chemical reaction. Chemical Engineering Science 51, 3829–3845.

Lu, Y.Z., Wang, R.Z., Zhang, M., Jiangzhou, S., 2003. Adsorption cold storage system with zeolite–water working pair used for locomotive air conditioning. Energy Conversion and Management 44, 1733–1743. doi:10.1016/S0196-8904(02)00169-3

Lund, H., Šiupšinskas, G., Martinaitis, V., 2005. Implementation strategy for small CHP-plants in a competitive market: The case of Lithuania. Applied Energy 82, 214–227. doi:10.1016/j.apenergy.2004.10.013

Ma, Q., Luo, L., Wang, R.Z., Sauce, G., 2009. A review on transportation of heat energy over long distance: Exploratory development. Renewable and Sustainable Energy Reviews 13, 1532–1540. doi:10.1016/j.rser.2008.10.004

Marias, F., Neveu, P., Tanguy, G., Papillon, P., 2014. Thermodynamic analysis and experimental study of solid/gas reactor operating in open mode. Energy 66, 757–765. doi:10.1016/j.energy.2014.01.101

Maru, H.C., Dullea, J.F., Huang, V.S., 1976. Molten Salt Thermal Energy Storage Systems: Salt Selection (Project 8981/ United states energy research No. COO-2888-1). Institute of Gas Technology, Chicago, Illinois. (USA).

Mauer, L.J., Taylor, L.S., 2010. Water-Solids Interactions: Deliquescence. Annual Review of Food Science and Technology 1, 41–63. doi:10.1146/annurev.food.080708.100915

Mauran, S., Lahmidi, H., Goetz, V., 2008. Solar heating and cooling by a thermochemical process. First experiments of a prototype storing 60kWh by a solid/gas reaction. Solar Energy 82, 623–636. doi:10.1016/j.solener.2008.01.002

Mauran, S., Prades, P., L'Haridon, F., 1993. Heat and mass transfer in consolidated reacting beds for thermochemical systems. Heat Recovery Systems and CHP, Special Issue Solid Sorption Refrigeration and Heat Pumps 13, 315–319. doi:10.1016/0890-4332(93)90055-Z

Mauran, S., Rigaud, L., Coudevylle, O., 2001. Application of the Carman–Kozeny Correlation to a High-Porosity and Anisotropic Consolidated Medium: The Compressed Expanded Natural Graphite. Transport in Porous Media 43, 355–376. doi:10.1023/A:1010735118136

Mazet, N., Amouroux, M., Spinner, B., 1991. ANALYSIS AND EXPERIMENTAL STUDY OF THE TRANSFORMATION OF A NON-ISOTHERMAL SOLID/GAS REACTING MEDIUM. Chemical Engineering Communications 99, 155–174. doi:10.1080/00986449108911585

McBain, J.W., 1909. XCIX. The mechanism of the adsorption ("sorption") of hydrogen by carbon. Philosophical Magazine Series 6 18, 916–935. doi:10.1080/14786441208636769

Mette, B., Kerskes, H., Drück, H., 2012. Concepts of long-term thermochemical energy storage for solar thermal applications – Selected examples. Energy Procedia 30, 321–330. doi:10.1016/j.egypro.2012.11.038

Mette, B., Kerskes, H., Drück, H., Müller-Steinhagen, H., 2013. New highly efficient regeneration process for thermochemical energy storage. Applied Energy 109, 352–359. doi:10.1016/j.apenergy.2013.01.087

Meunier, F., 2013. Adsorption heat powered heat pumps. Applied Thermal Engineering 61, 830–836. doi:10.1016/j.applthermaleng.2013.04.050

Michel, B., 2012. Procédé thermochimique pour le stockage intersaisonnier de l'énergie solaire : modélisation multi-échelles et expérimentation d'un prototype sous air humide (Doctorate/Ph.D). Université de Perpignan, Perpignan - France.

Michel, B., Mazet, N., Mauran, S., Stitou, D., Xu, J., 2012. Thermochemical process for seasonal storage of solar energy: Characterization and modeling of a high density reactive bed. Energy 47, 553–563. doi:10.1016/j.energy.2012.09.029

Michel, B., Neveu, P., Mazet, N., 2014. Comparison of closed and open thermochemical processes, for long-term thermal energy storage applications. Energy 72, 702–716. doi:10.1016/j.energy.2014.05.097

N'Tsoukpoe, K., 2012. Etude du stockage à long terme de l'énergie solaire thermique par procédé d'absorption LiBr-H2O pour le chauffage de l'habitat (Doctorate/Ph.D). Université de Grenoble, France.

N'Tsoukpoe, K.E., Le Pierrès, N., Luo, L., 2013. Experimentation of a LiBr–H2O absorption process for long-term solar thermal storage: Prototype design and first results. Energy 53, 179–198. doi:10.1016/j.energy.2013.02.023

N'Tsoukpoe, K.E., Liu, H., Le Pierrès, N., Luo, L., 2009. A review on long-term sorption solar energy storage. Renewable and Sustainable Energy Reviews 13, 2385–2396. doi:10.1016/j.rser.2009.05.008

N'Tsoukpoe, K.E., Perier-Muzet, M., Le Pierrès, N., Luo, L., Mangin, D., 2014a. Thermodynamic study of a LiBr–H2O absorption process for solar heat storage with crystallisation of the solution. Solar Energy, Solar heating and cooling 104, 2–15. doi:10.1016/j.solener.2013.07.024

N'Tsoukpoe, K.E., Schmidt, T., Rammelberg, H.U., Watts, B.A., Ruck, W.K.L., 2014b. A systematic multi-step screening of numerous salt hydrates for low temperature thermochemical energy storage. Applied Energy 124, 1–16. doi:10.1016/j.apenergy.2014.02.053

Neveu, P., Castaing-Lasvignottes, J., 1997. Development of a numerical sizing tool for a solid-gas thermochemical transformer—I. Impact of the microscopic process on the dynamic behaviour of a solid-gas reactor. Applied Thermal Engineering 17, 501–518. doi:10.1016/S1359-4311(96)00065-8

Neveu, P., Tescari, S., Aussel, D., Mazet, N., 2013. Combined constructal and exergy optimisation of thermochemical reactors for high temperature heat storage. Energy Conversion and Management 71, 186–198. doi:10.1016/j.enconman.2013.03.035

Ng, E.-P., Mintova, S., 2008. Nanoporous materials with enhanced hydrophilicity and high water sorption capacity. Microporous and Mesoporous Materials 114, 1–26. doi:10.1016/j.micromeso.2007.12.022

Oliveira, R.G., Wang, R.Z., 2007. A consolidated calcium chloride-expanded graphite compound for use in sorption refrigeration systems. Carbon 45, 390–396. doi:10.1016/j.carbon.2006.09.007

Olives, R., Mauran, S., 2001. A highly conductive porous medium for solid–gas reactions: effect of the dispersed phase on the thermal tortuosity. Transport in porous media 43, 377–394.

Opel, O., Rammelberg, H.U., Gérard, M., Ruck, W.K.L., 2011. Thermochemical storage materials research - TGA/DSC-hydration studies, in: International Conference on Sustainable Energy Storage. Presented at the ICSES, Belfast 2011, Belfast, Ireland, p. 7.

Pagliarini, G., Rainieri, S., 2010. Modeling of a thermal energy storage system coupled with combined heat and power generation for the heating requirements of a University Campus. Applied Thermal Engineering 30, 1255–1261. doi:10.1016/j.applthermaleng.2010.02.008

Paksoy, H.Ö., 2005. Thermal Energy Storage for Sustainable Energy Consumption - Fundamentals, Case Studies and Design, Proceedings of the NATO Advanced Study Institute on Thermal Energy Storage for Sustainable Energy Consumption— Fundamentals, Case Studies and Design Izmir, Turkey. ed, NATO Science Series II: (closed). Springer, Dordrecht, The Netherlands.

Pang, S.C., Masjuki, H.H., Kalam, M.A., Hazrat, M.A., 2013. Liquid absorption and solid adsorption system for household, industrial and automobile applications: A review. Renewable and Sustainable Energy Reviews 28, 836–847. doi:10.1016/j.rser.2013.08.029

Pinel, P., Cruickshank, C.A., Beausoleil-Morrison, I., Wills, A., 2011. A review of available methods for seasonal storage of solar thermal energy in residential applications. Renewable and Sustainable Energy Reviews 15, 3341–3359. doi:10.1016/j.rser.2011.04.013

Posern, K., 2012. Untersuchungen von Magnesiumsulfat-Hydraten und Sulfat/Chlorid-Mischungen für die Eignung als Aktivstoff in Kompositmaterialien für die thermochemische Wärmespeicherung (Doctorate/Ph.D). Bauhaus-Universität Weimar, Fakultät Bauingenieurwesen, Weimar, Germany.

Posern, K., Kaps, C., 2010. Calorimetric studies of thermochemical heat storage materials based on mixtures of MgSO4 and MgCl2. Thermochimica Acta 502, 73–76. doi:10.1016/j.tca.2010.02.009

Quinnell, J.A., Davidson, J.H., 2012. Distributed Solar Thermal: Innovations in Thermal Storage," Annual Reviews in Heat Transfer. Annual Review in Heat Transfer 15, 11.

Radermacher, R., Hwang, Y., 2005. Vapor Compression Heat Pumps with Refrigerant Mixtures, 1st ed, CRC Press. Taylor & Francis Group, 6000 Broken Sound Parkway NW, USA.

Raine, R.D., Sharifi, V.N., Swithenbank, J., 2014. Optimisation of combined heat and power production for buildings using heat storage. Energy Conversion and Management 87, 164–174. doi:10.1016/j.enconman.2014.07.022

Raldow, W.M., Wentworth, W.E., 1979. Chemical heat pumps—A basic thermodynamic analysis. Solar Energy 23, 75–79. doi:10.1016/0038-092X(79)90046-X

Rammelberg, H.U., Myrau, M., Schmidt, T., Ruck, W.K.L., 2013. An Optimisation of Salt Hydrates for Thermochemical Heat Storage, in: IMPRES-2013, Paper No. IMPRES2013-117. Presented at the International Symposium on Innovative Materials for Processes in Energy Systems, Chemical Science & Engineering Series: Innovative Materials for Processes in Energy Systems, Fukuoka, Japan, p. 6.

Robert, L., Burwell, J., 1976. Manual of Symbols and Terminology for Physicochemical Quantities and Units - Appendix II. Definitions, Terminology and Symbols in Colloid and Surface Chemistry. Part II: Heterogeneous Catalysis. Pure and Applied Chemistry 46, 71–90. doi:10.1351/pac197646010071

Rouquerol, F., Rouquerol,, J., Sing, K. S. W., 1999. Adsorption by powders and porous solids. Academic Press, San Diego. Vakuum in Forschung und Praxis 11, 191–191. doi:10.1002/vipr.19990110317

Rowsell, J.L.C., Yaghi, O.M., 2004. Metal–organic frameworks: A new class of porous materials. Microporous and Mesoporous Materials 73, 3–14. doi:10.1016/j.micromeso.2004.03.034

Ruiter, J.P., 1987. Thermal energy storage by means of an absorption cycle, Ph.D Thesis, TU-Delft University of Technology, Delft, Netherlands.

Schmidt, T., Rammelberg, H.U., Rönnebeck, T., N'Tsoukpoe, K.E., Fopah Lele, A., Rohde, C., Ruck, W., 2012. Conception of a heat storage system for household applications, in: 7th International Renewable Energy Storage Conference and Exhibition. Presented at the IRES-2012, Eurosolar, Berlin, Germany, pp. 429–433.

Sharonov, V.E., Aristov, Y.I., 2008. Chemical and adsorption heat pumps: Comments on the second law efficiency. Chemical Engineering Journal 136, 419–424. doi:10.1016/j.cej.2007.07.026

Siddiqui, A., Marnay, C., Firestone, R., Zhou, N., 2007. Distributed generation with heat recovery and storage. Journal of Energy Engineering 133, 181–210. doi:10.1061/(ASCE)0733-9402(2007)133:3(181)

Sieres, J., Fernández-Seara, J., 2007. Mass transfer characteristics of a structured packing for ammonia rectification in ammonia–water absorption refrigeration systems. International Journal of Refrigeration 30, 58–67. doi:10.1016/j.ijrefrig.2006.04.009

Sing, K.S.W., 1985. Reporting physisorption data for gas/solid systems with special reference to the determination of surface area and porosity (Recommendations 1984). Pure and Applied Chemistry 57, 603–619. doi:10.1351/pac198557040603

Sircar, S., Hufton, J.R., 2000. Why Does the Linear Driving Force Model for Adsorption Kinetics Work? Adsorption 6, 137–147.

Smith, M.A., Few, P.C., 2001. Modelling of a domestic-scale co-generation plant thermal capacitance considerations. Applied Energy 68, 69–82. doi:10.1016/S0306-2619(00)00042-8

Srivastava, N.C., Eames, I.W., 1998. A review of adsorbents and adsorbates in solid–vapour adsorption heat pump systems. Applied Thermal Engineering 18, 707–714. doi:10.1016/S1359-4311(97)00106-3

Steiger, M., Linnow, K., Juling, H., Gülker, G., Jarad, A.E., Brüggerhoff, S., Kirchner, D., 2008. Hydration of MgSO4·H2O and Generation of Stress in Porous Materials. Crystal Growth & Design 8, 336–343. doi:10.1021/cg060688c

Stitou, D., 2013. Transformation, Conversion, Stockage, Transport de l'Énergie Thermique par Procédés Thermochimiques et Thermo-hydrauliques (HDR). Université de Perpignan, Perpignan, France.

Streckienė, G., Martinaitis, V., Andersen, A.N., Katz, J., 2009. Feasibility of CHP-plants with thermal stores in the German spot market. Applied Energy 86, 2308–2316. doi:10.1016/j.apenergy.2009.03.023

Sugimoto, K., Dinnebier, R.E., Hanson, J.C., 2007. Structures of three dehydration products of bischofite from *in situ* synchrotron powder diffraction data ($MgCl_2 \cdot n H_2O$; n = 1, 2, 4). Acta Crystallographica, Section B - Structural Science 63, 235–242. doi:10.1107/S0108768107002558

Sun, L.M., Ben Amar, N., Meunier, F., 1995. Numerical study on coupled heat and mass transfers in an absorber with external fluid heating. Heat Recovery Systems and CHP 15, 19–29. doi:10.1016/0890-4332(95)90034-9

Tamainot-Telto, Z., Critoph, R.E., 2001. Monolithic carbon for sorption refrigeration and heat pump applications. Applied Thermal Engineering 21, 37–52. doi:10.1016/S1359-4311(00)00030-2

Tanashev, Y.Y., Aristov, Y.I., 2000. Thermal conductivity of a silica gel + calcium chloride system: The effect of adsorbed water. J Eng Phys Thermophys 73, 876–883. doi:10.1007/BF02681573

Tanguy, G., Papillon, P., Paulus, C., 2010. Seasonal storage coupled to solar combisystem : dynamic simulations for process dimensioning, in: EuroSun_international Conference on Solar Heating, Cooling and Buildings. Presented at the EuroSun, ISES-EuroSun, Graz, Austria, p. 8.

Tatsidjodoung, P., Le Pierrès, N., Luo, L., 2013. A review of potential materials for thermal energy storage in building applications. Renewable and Sustainable Energy Reviews 18, 327–349. doi:10.1016/j.rser.2012.10.025

Thapa, S., Chukwu, S., Khaliq, A., Weiss, L., 2014. Fabrication and analysis of small-scale thermal energy storage with conductivity enhancement. Energy Conversion and Management 79, 161–170. doi:10.1016/j.enconman.2013.12.019

Tina, G.M., Passarello, G., 2012. Short-term scheduling of industrial cogeneration systems for annual revenue maximisation. Energy 42, 46–56. doi:10.1016/j.energy.2011.10.025

Van Essen, V.M., Cot Gores, J., Bleijendaal, L.P.J., Zondag, H.A., Schuitema, R., Bakker, M., van Helden, W.G.J., 2009a. Characterization of Salt Hydrates for Compact Seasonal Thermochemical Storage, in: ASME 2009 3rd International Conference on Energy Sustainability. Presented at the ASME 2009 3rd International Conference on Energy Sustainability, ASME, San Francisco, California, USA, pp. 825–830. doi:10.1115/ES2009-90289

Van Essen, V.M., He, Z., Rindt, C.C.M., Zondag, H.A., Gores, J.C., Bleijendaal, L.P.J., Bakker, M., Schuitema, R., van Helden, W.G.J., 2009b. Characterization of $MgSO_4$ Hydrate for Thermochemical Seasonal Heat Storage. J. Sol. Energy Eng. 131, 041014–041014. doi:10.1115/1.4000275

Van Helden, W., Hauer, A., 2013a. Task 42 - Annex 24, Compact Thermal Energy Storage: Material Development for System Integration - Final Report (Research and Engineering No. IEA SHC/ECES Task 42/24 Final Report), IEA SHC/ECES Task 42/24. International Energy Agency, Europe.

Van Helden, W., Hauer, A., 2013b. 2012 Annual report-Feature article on advances in compact thermal energy storage - material development (Research and Engineering No. IEA Solar Heating & Cooling Programme), IEA Solar Heating and Cooling Programme. International Energy Agency, Europe.

Visscher, K., Veldhuis, J., 2005. Comparison of candidate materials for seasonal storage of solar heat through dynamic simulation of building and renewable energy system, in: Buildings Simulations 2005 (The Ninth International Building Performance Simulation Association). Presented at the ECN-RX--06-017, ECN-RX--06-017, Montréal, Canada, pp. 1285 – 1292.

Wang, D.C., Li, Y.H., Li, D., Xia, Y.Z., Zhang, J.P., 2010. A review on adsorption refrigeration technology and adsorption deterioration in physical adsorption systems. Renewable and Sustainable Energy Reviews 14, 344–353. doi:10.1016/j.rser.2009.08.001

Wang, K., Wu, J.Y., Wang, R.Z., Wang, L.W., 2006. Effective thermal conductivity of expanded graphite–CaCl2 composite adsorbent for chemical adsorption chillers. Energy Conversion and Management 47, 1902–1912. doi:10.1016/j.enconman.2005.09.005

Wang, L.W., Metcalf, S.J., Critoph, R.E., Thorpe, R., Tamainot-Telto, Z., 2012. Development of thermal conductive consolidated activated carbon for adsorption refrigeration. Carbon 50, 977–986. doi:10.1016/j.carbon.2011.09.061

Wang, L.W., Wang, R.Z., Oliveira, R.G., 2009. A review on adsorption working pairs for refrigeration. Renewable and Sustainable Energy Reviews 13, 518–534. doi:10.1016/j.rser.2007.12.002

Weber, R., Dorer, V., 2008. Long-term heat storage with NaOH. Vacuum 82, 708–716. doi:10.1016/j.vacuum.2007.10.018

Wentworth, W.E., Chen, E., 1976. Simple thermal decomposition reactions for storage of solar thermal energy. Solar Energy 18, 205–214. doi:10.1016/0038-092X(76)90019-0

Wongsuwan, W., 2004. A performance study on a chemical energy storage system using sodium sulphide-water as the working pair, in: 6th IIR Gustav Lorentzen Natural Working Fluids Conference. Glaskow, UK.

Wongsuwan, W., Kumar, S., Neveu, P., Meunier, F., 2001. A review of chemical heat pump technology and applications. Applied Thermal Engineering 21, 1489–1519. doi:http://dx.doi.org/10.1016/S1359-4311(01)00022-9

Wu, A.S., Chou, T.-W., 2012. Carbon nanotube fibers for advanced composites. Materials Today 15, 302–310. doi:10.1016/S1369-7021(12)70135-9

Xu, S.M., Huang, X.D., Du, R., 2011. An investigation of the solar powered absorption refrigeration system with advanced energy storage technology. Solar Energy 85, 1794–1804. doi:10.1016/j.solener.2011.04.022

Ye, H., Yuan, Z., Li, S., Zhang, L., 2013. Activated Carbon Fiber Cloth and CaCl2 Composite Sorbents for a Water Vapor Sorption Cooling System. Applied Thermal Engineering. doi:10.1016/j.applthermaleng.2013.10.035

Yong, L., Sumathy, K., 2002. Review of mathematical investigation on the closed adsorption heat pump and cooling systems. Renewable and Sustainable Energy Reviews 6, 305–338. doi:10.1016/S1364-0321(02)00010-2

Yu, N., Wang, R.Z., Wang, L.W., 2013. Sorption thermal storage for solar energy. Progress in Energy and Combustion Science 39, 489–514. doi:10.1016/j.pecs.2013.05.004

Yusta, J.M., De Oliveira-De Jesus, P.M., Khodr, H.M., 2008. Optimal energy exchange of an industrial cogeneration in a day-ahead electricity market. Electric Power Systems Research 78, 1764–1772. doi:10.1016/j.epsr.2008.03.012

Zhang, G., Tian, C., Shao, S., 2014. Experimental investigation on adsorption and electro-osmosis regeneration of macroporous silica gel desiccant. Applied Energy 8. doi:10.1016/j.apenergy.2014.04.087

Zondag, A., Kalbasenka, A., van Essen, M., 2008. First studies in reactor concepts for Thermochemical Storage., in: 1st International Conference on Solar Heating, Cooling and Buildings. Presented at the EUROSUN 2008, Proceedings of Eurosun 2008, Lisbon, Portugal, p. 6.

Zondag, H., Kikkert, B., Smeding, S., Boer, R. de, Bakker, M., 2013. Prototype thermochemical heat storage with open reactor system. Applied Energy 109, 360–365. doi:10.1016/j.apenergy.2013.01.082

3. THERMAL MANAGEMENT MODELLING IN THERMO-CHEMICAL HEAT STORAGE SYSTEMS

3.1. DIFFERENT TYPES OF CHEMICAL REACTORS

In thermal and chemical engineering, chemical reactors are designed vessels where chemical reactions can take place. The design of a chemical reactor deals with multiple aspects of chemical engineering. Chemical engineers design reactors to maximize net present value for the given reaction. Designers ensure that the reaction proceeds with the highest efficiency towards the desired output product, producing the highest yield of product while requiring the least amount of money to purchase and operate. Normal operating expenses include energy input, energy removal, raw material costs, labor stuffs, etc.

Energy changes can come in the form of heating or cooling, pumping to increase or reduce pressure (under vacuum), frictional pressure loss (such as pressure drop across a 90 °C elbow or an orifice plate), agitation, etc. As described in the previous chapter, the reaction involves hydration and dehydration always followed by thermal exchanges, so the selected reactor should correspond to that need. The number of types of reactors in this field of application is not very large; we denote the packed or fixed bed and the fluidized bed reactors. Small benchtop reactor designs are intended for use in labs (McMahon and Wallace, 2003), for example, while large tanks can be used to synthetise chemicals on an industrial scale. The design also includes a variety of features which can be used to control conditions inside the reactor such as evapo-condenser. A quick review on reactor type is described in the following paragraphs. The advantages and disadvantages (Table 3.1) are highlighted, so that a selective comparison becomes easier.

In thermochemical processing, a fixed bed is a hollow tube, pipe, or other vessel that is filled with a packing material. The packing can be randomly filled with small objects or else it can be a specifically designed structured packing. Fixed beds may also contain adsorbents such as powders, pellets, granular activated carbon, etc. forming a system of solid particles in contact, surrounded by a fluid (gas or liquid) phase. Therefore it is called packed bed reactor. This type of reactor has a high reaction conversion per unit of mass conversion, low operating cost and is known as a continuous operation. However, an undesired thermal gradient may exist in the reactor, the temperature control is poor, channelling may occur, and units may be difficult to maintain and to clean.

Several aspects of fluidized beds are not yet fully understood and therefore a lot of research is dedicated to these reactors (Froment et al., 2011). A fluidized bed reactor is a type of reactor device that can be used to carry out a variety of multiphase chemical reactions. In this type of reactor, a fluid (gas or liquid) is passed through a granular solid material (usually a catalyst possibly shaped as tiny spheres) at high enough velocities to suspend the solid and cause it to behave as though it were a fluid. The solid substrate material in the fluidized bed reactor is typi-cally supported by a porous plate, known as a distributor. The fluid is then forced through the distributor up through the solid material. At lower fluid velocities, the solids remain in place as the fluid passes through the voids in the material. In this state (lower fluid velocity), it is known as a packed bed reactor. Anyway, from the comparison in Table 3.1, it comes out that the packed bed reactor should be the best for our application since the focus is on characteristics such as good salt conversion, efficient process, low particle attrition or grinding (Zhang et al., 2014) and reactor compactness. In addition, this reactor type has been widely used in thermal engineering with proof-efficiency (Cascetta et al., 2014; Ishitobi et al., 2013; Kato, 2007; Kato et al., 2000; Wen and Ding, 2006; Zondag et al., 2013).

Table 3.1. Comparison between possible reactors for solid-gas thermochemical energy storage.

Reactor type	Variance	Advantage	Inconvenient	References
Packed or fixed bed	Packed or fixed bed reactor	- High effectiveness and low pressure drop. Easier for modelling. - Efficient thermal behaviour and enhance the solid conversion. - Large amount of heat transfer surface can be contained in a small volume.	- Agglomeration or sintering. - Low heat and mass transfer. - Undesired thermal gradients. - Channelling and difficulty of cleaning. - Non-uniformity in bed temperature.	(Cascetta et al., 2014; Elsarrag et al., 2005; Oró et al., 2013; S. Zhang et al., 2014)
Fluidized bed	Plug flow reactor	- Good for irreversible reactions in first or two order reaction. - Idealistic contact behaviour between the gas and the solid can be achieved. - Long-term stable operation.	-Continuous flowing requiring constant additional power. Particle attrition. - For most chemical reactions, it is impossible for the reaction to proceed to 100% completion or conversion. - Materials erosion.	(Pardo et al., 2014a; S. Zhang et al., 2014)
	Extruder reactor	- Transports the material and additionally causes stirring, thereby improving vapour and heat transport. - Minimum effective heat transfer to the wall of about 300 W·m^{-2}·K^{-1}.	- Risk of the material sticking to the screw. - Uniformity of the bed temperature	(Zondag et al., 2008)
	A"gravity-assisted" bulk flow reactor	- Material flows by means of gravity along a number of vertical plate heat exchangers. High heat transfer.	- Special provisions are required for the vapour transport and there is some risk of the material sticking to the heat exchanger plates. - Need of active means to transport the material to the top of the reactor.	(Zondag et al., 2008)

After selecting the reactor type, another issue is its geometry of this latter. Here, applied process involves thermal (heat and mass) exchanges, heat exchanger and diffuser. How would the reactor be designed (cylindrical or parallelepiped geometry)? Answering this question is not in the scope of this thesis. However, there is a reactor geometry impact on heat and mass transfer and hence on system power (Azoumah, 2005). Several authors (Azoumah et al., 2007; Bejan, 1998; Neveu et al., 2013) worked on parallelepiped geometry using constructal approach and form optimisation based on entropy production without accounting for cylindrical geometry which is widely used. Azoumah (Azoumah, 2005) raised that pertinent question: why a preferred use of cylindrical reactor for such an application? He proposed a criterion for future optimisation study to later compare with the parallelepiped geometry in order to justify this choice made by many researchers and engineers. The present choice made for the reactor is the cylindrical one due to the ease of designing and the integrated heat exchanger and its shape.

3.2. STORAGE SYSTEM DESCRIPTION

The thermal energy storage research in the project "Thermal Battery" at the Institute for Sustainable and Environmental Chemistry focused on a compact and close thermochemical system (Figure 3.1). In the dehydration or desorption mode, the thermochemical material (TCM) was energetically being charged. In this mode, the principle was as follows: desorption heat came from the Unistat, representing here the connected system to the heat loss of the micro-CHP. A by-pass was used in order to obtain the required temperature of the fluid for decomposition before opening the valve at the inlet of the heat exchanger and the sufficient heat provided by the heating fluid (here the thermo-oil) is then transported in the bed through heat exchanger ($T_{HTF\_inlet} > T_{HTF\_outlet}$). This setup simulates the required heat recovered from the micro-CHP. Subsequently, the decomposition reaction in term of kinetic, mass and heat will be analysed. According to Le Chatelier's principle in the thermal decomposition, increasing the temperature shifts the process toward water vapour formation and an increase of the vapour pressure. The gases formed during this process were carried away through the pipe at the bottom of the reactor and condensed to liquid water in the evapo-condenser. The condenser was then set at the thermodynamic condition as shown in Figure 3.2. The condensation of the water shifted the equilibrium toward formation of the less hydrated or the anhydrous salt. The gas transport was improved by the vacuum generated in the evapo-condenser, because of the lower resistance compared to normal pressure where additional gas molecules are hindering the vapour transport. The water released from the salt was then stored in the tank or evapo-condenser and will be re-used during the hydration or discharging mode. - In the hydration or/and ab-/ad- sorption mode, the water in the evapo-condenser was evaporated at 10 °C which corresponded to a pressure of around 1230 Pa (12.3 mbar) according to the equilibrium curve. Since there was a vacuum in the reactor, the pressure difference and the hygroscopic character of the salt favoured the vapour flow into the salt bed for a synthesis reaction. The water vapour (reactive gas) entered from the bottom and flowed to the bed, and the exothermic reaction of hydration proceeds with a higher heat release, removing the previous stored heat plus the sensible heat. That released heat at an output temperature of 52 °C is transferred to the heat transfer fluid ($T_{HT\_Finlet} < T_{HTF\_outlet}$) for purpose such as DHW and space heating.
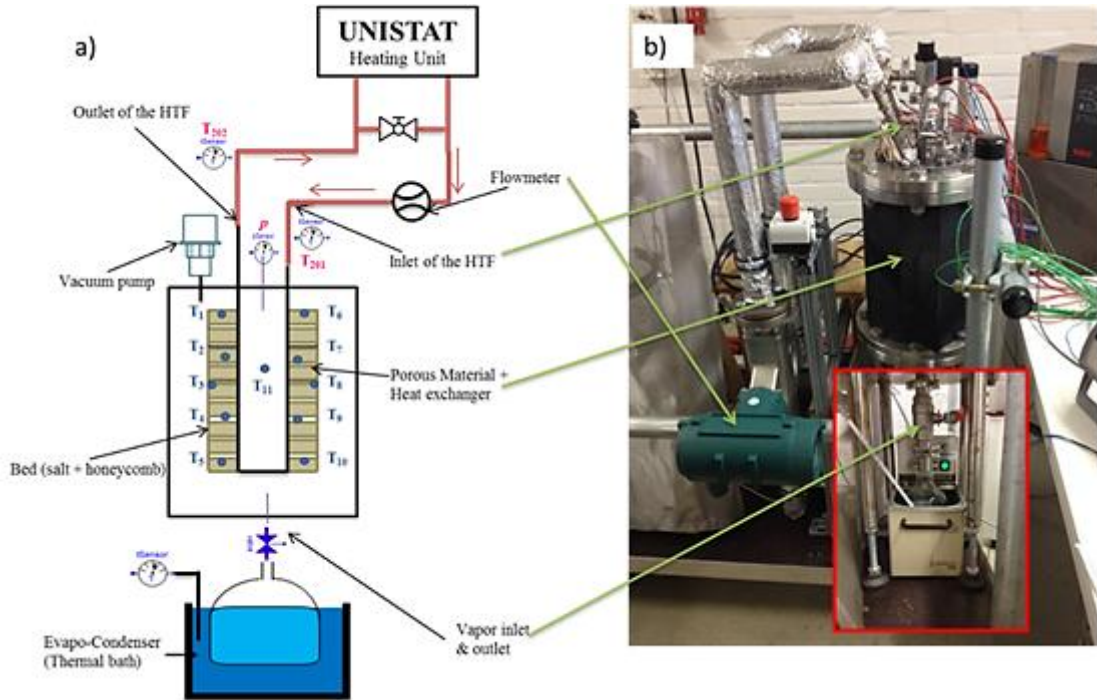
Figure 3.1: (a) The corresponding 2D schematic system with honeycomb heat exchanger and (b) the experimental lab-scale thermochemical energy storage system.

A storage system description also implies thermodynamic from the material side which is the heart of the system. The reactive couple $SrBr_2/(1\text{-}6)H_2O$ had already been theoretically and experimentally performed with success in previous works (Lahmidi et al., 2006; Mauran et al., 2008; Michel et al., 2014a). Its ideal energy storage density was very high: 628 kWh·m⁻³ (referring to the bulk density of 2390 kg·m⁻³ and the molar mass of non-porous hydrated salt of 0.3555 kg·mol⁻¹) but could be 400 kWh·m⁻³ with additional components in a prototype (Michel et al., 2014a). As for example, a micro-CHP delivering heat loss in the range of 80 - 90 °C is sufficient to insure the complete dehydration from the hexahydrate to the monohydrate without incongruent dissolution of water vapour in the solid phase, as the solubility curve shows in Figure 3.2. The solubility line informs about the approximate limit of saturated solution of the $SrBr_2·6H_2O$. An evaporator pressure above 12 mbar (~10 °C) was required to reach around 50 °C output in the reactor, direct use for desired application. Note that in those conditions, the energy required to afford 10 °C at the evaporator can be done with geothermal source energy. The retained solid-gas thermochemical reaction in the system related to the two following monovariant equilibriums:

$$H_2O_{(l)} + \Delta H_{l/g} \leftrightarrows H_2O_{(g)} \qquad (3.1)$$

$$SrBr_2 \cdot 6H_2O_{(s1)} + 5\Delta H_r^0 \leftrightarrows SrBr_2 \cdot 1H_2O_{(s2)} + 5H_2O_{(g)} \qquad (3.2)$$
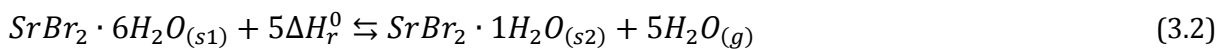
with $\Delta H_{l/g} = 2519$ kJ·kg⁻¹ H_2O (at 10 °C) the enthalpy of evaporation and $\Delta H_r^0 = 3744$ kJ·kg⁻¹ H_2O, the reaction enthalpy.

79

The heat loss from the micro-CHP is stored and then released via a heat exchanger which needed to be investigated in order to use the efficient one in terms of conversion rate, output temperature, heat transfer coefficient, pressure drop, and handling (cleaning, material change, cycle effect). Three types of integrated heat exchanger in cylindrical reactor are most used in thermal engineering: the helical coil, the plate-fin and the honeycomb. Numerical investigations were performed to select between these heat exchangers, the efficient one in terms of good thermal performances and handling.
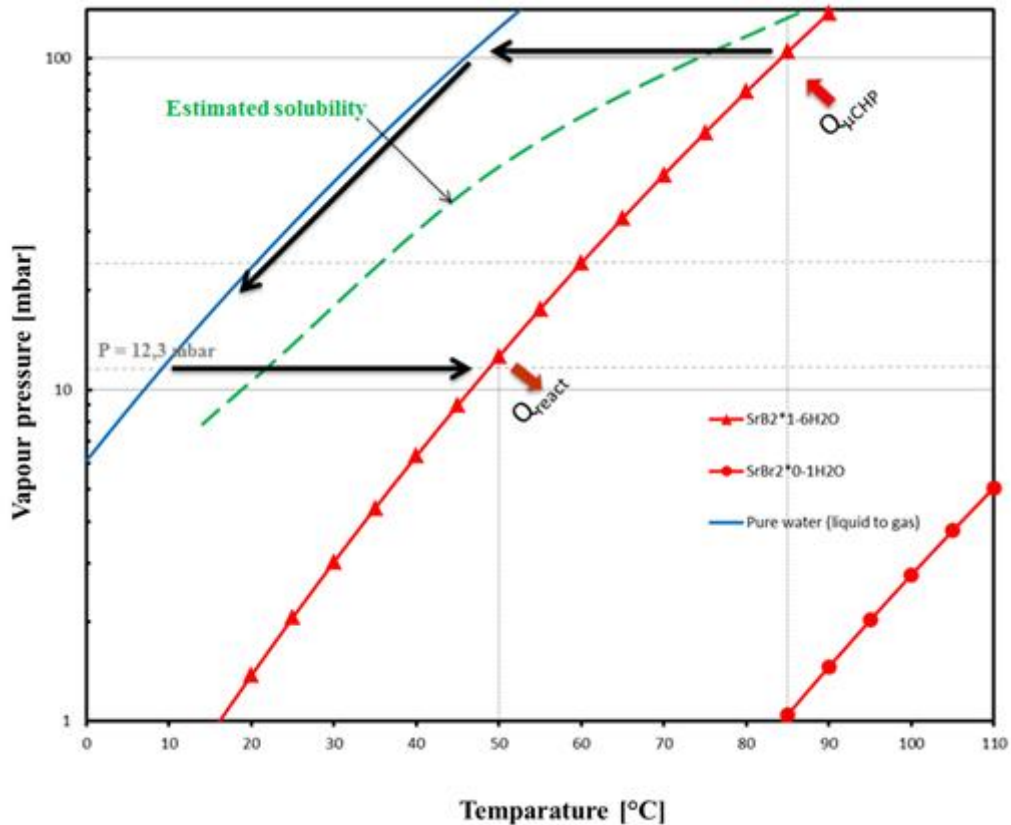
Figure 3.2: Equilibrium curve and thermodynamics of the $SrBr_2 \cdot 6H_2O$ for direct heating supply application (Wagman et al., 1982).

3.3. HEAT EXCHANGER INVESTIGATIONS

A decade ago, it has been shown that helical coil and plate-fin heat exchanger increase the heat transfer coefficient and that the temperature rise of the fluid for a helically coiled exchanger depends on the tube geometry and the flow rate (Prabhanjan et al., 2002). A honeycomb exchanger exhibits a high storage capacity and wall thermal conductivity (Luo et al., 2014). So, to develop a long or short term thermochemical heat storage using solid-gas reaction, just like the development of thermal energy storage systems, a heat exchanger is an absolute requirement, especially in closed processes. In that field of thermal energy storage, various research projects (Li et al., 2011; Luo et al., 2014; Schaube et al., 2011) where different heat exchangers were used, recommend that, the heat exchanger should be as compact as possible. Compact, because of large area density which leads to a high heat transfer surface per volume. For compact heat exchangers (CHEs), the ratio of heat transfer surface to heat exchange volume, was determined to be over 700 $m^2 \cdot m^{-3}$ (Luo, 2013). This large area density indicated small hydraulic diameter for

fluid flow and lead to high heat transfer coefficient (Li et al., 2011). A good heat exchanger performance includes small temperature differences across the heat exchanger to maximize the heat transfer coefficient. The heat exchanger therefore has to be designed in a compact way (heat exchange surface-to-mass ration, small volume, allowing good vapour transport), but also has to work with a high heat transfer coefficient (Li et al., 2011). That is the reason the focus was on these three heat exchangers. Helical coil tubes and plate-fin are feasible passive enhancement methods of compact heat exchanger. No identified experimental work or detailed modelling using a helical coil tube as heat exchanger in gas-solid thermochemical heat storage process has been yet found in the literature, except in condenser/evaporator and hydrogen storage applications where interaction was involved (Raju and Kumar, 2010). However plate fins were quite broadly used due to their large heat transfer surface area (Jacobi and Shah, 1995; Li et al., 2011; Zhang et al., 2010). The honeycomb heat exchanger was also widely used but in high temperature application (Cadavid et al., 2013; Zheng et al., 2013). The attempt in low temperature application is presented here.

3.3.1. NUMERICAL DESIGN AND MODELLING

The three heat exchangers were 3D-modeled and numerically solved using the commercial software Comsol Multiphysics 4.3b© (Figure 3.3). The focus was only on the charging process (decomposition) because of heat amount exchanged in this phase, meaning dehydration step, in order to evaluate the thermal performances. The model construction was based on real values (Appendices - A1) as it was designed by the manufacturer. The investigations on each heat exchanger were proceeded with the strontium bromide hexahydrate. As a notice, the heat exchangers here were indirect contact type (heat transfer fluid and the solid are separated by a wall), meaning a higher global heat transfer coefficient, a large interfacial area virtually free. They can be modified within a certain range, the risk of corrosion and furring up, a low pressure drop, the disappearance of differential expansion and a potential reduction in capital cost due to the simplicity of the exchanger (Techniques de l'ingénieur, 1999).

The numerical method used here tried to improve the accuracy of the calculation by decomposing the physical phenomena involved and took into account the nature of the flow. It was based on the logarithmic mean temperature difference (LMTD). Many criteria were considered in heat exchanger design but thermal power was the most important, although for a definitive choice other parameters like pressure drop, thermal mass, cluttering or clogging had to be taken into account. Basically, the thermal power is strongly linked to the overall heat transfer, so in order to evaluate it for each exchanger, mathematic modelling had to be set.

For calculation purposes, heat exchangers presented in Figure 3.3 were inserted in a cylindrical reactor. The bed was considered immobile and the initial bed pressure was assumed to be constant through the bed and equal to pressure imposed at the inlet of the bed. The heat capacities were assumed constants due to their small temperature variation. The gas phase (vapour released) and the bed temperature were assumed to be identical since the temperature difference was small to have a significant influence and it is an adiabatic system. The radiative heat transfer and the work done by pressure changes were not taken into account here because of the minor effect under vacuum and relatively low temperature.
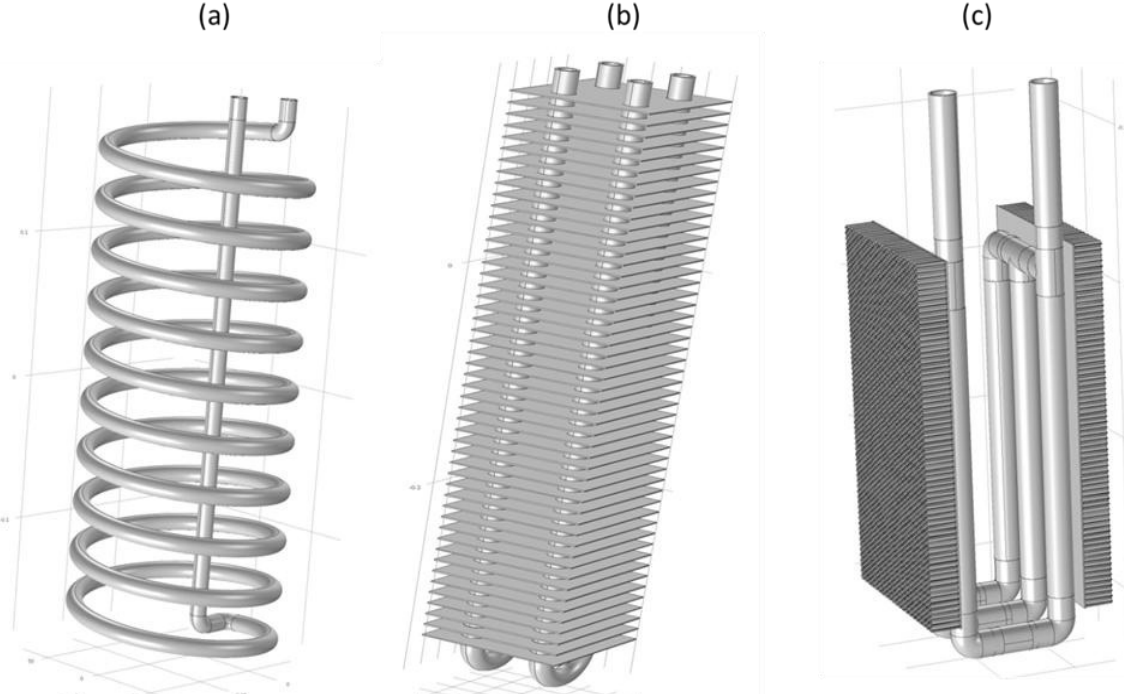
Figure 3.3: Schematic of the three investigated heat exchanger types: (a) helical coil, (b) plate-fin and (c) honeycomb.

The tube side heat transfer coefficient was assumed to be constant, and was evaluated base on the heating flow rate. Also thermal resistance of walls was neglected due to the fact that model idealize the contact heat exchanger/material bed. Most of these previous assumptions also found their justification to the fact that we performed a stationary study. This choice is for a rough comparative study and time-saving for rapid selection. In fact, stationary study in heat transfer was mostly used to compute the temperature field at thermal equilibrium.

As already mentioned, this study focused only on charging phase. The heat from the heat transfer fluid (HTF) was supplied to the material bed via conduction (convection is not neglected even though the conducted wall is a metal) and leaved the latter via advection (water vapour) after the phase change of water (inside the material) from liquid to gas leading to a small pressure drop in the reactor. The energy source in the bed (Q_{stored}) is the stored energy from the micro-CHP ($Q_{\mu CHP}$) plus the generated sensible heat (Q_{sen}). The stationary energy balance in the bed and in the fluid can be respectively written by the following equation:

$$(\rho C_p)_{bed} \cdot \boldsymbol{u_v} \cdot \nabla T = \nabla \cdot \left(\lambda_{eff} \nabla T\right) + Q_{stored} \tag{3.3}$$

Where $(\rho C_p)_{bed} = (1 - \varepsilon)\left(\rho C_p\right)_s + \varepsilon(\rho C_p)_v$ and $\lambda_{eff} = \lambda_s \cdot (1 - \varepsilon)^\xi$

$$\left(\rho C_p\right)_{HTF} \cdot \boldsymbol{u_f} \cdot \nabla T = \nabla \cdot (\lambda_{HTF} \nabla T) - Q_{\mu CHP} \tag{3.4}$$

Adiabatic conditions were assumed at the outer surface of the cylindrical shell. Convective heat transfer boundary condition $\vec{q} \cdot \vec{n} = h \cdot A_0 \cdot (T_{bed} - T_{ext})$ was applied at the surface of the heat exchanger which was in contact with the bed. The flow inside a heat exchanger always undergoes pressure drop in different ways such as contraction or expansion (Cadavid et al., 2013). Which is expressed by the so called Forchheimer-Darcy equation for the heat transfer fluid:

$$\frac{\Delta P}{z} = \frac{\mu}{k_D} \cdot \boldsymbol{u}_f + \frac{\rho}{k_E} \cdot \boldsymbol{u}_f^2 \tag{3.5}$$

The pressure drop across a hexagonal duct (Appendix – A1-3) of length L_{du} (height of the honeycomb element) had been numerically obtained by Yutaka et al. (Yutaka et al., 1988) as follows:

$$\Delta P = \frac{L_{du}}{a} \cdot 2f \cdot \rho_v \cdot \boldsymbol{u}_v^2 \tag{3.6}$$

where the small entrance/outlet effects have been ignored and $f = 15.065 Re^{-1}$ is the friction factor developed for Darcy flow type. Eq. (3.6) was valid for a honeycomb heat sink of length L_{du} where the average vapour velocity was linked to the free stream velocity $\boldsymbol{u}_0$ as follows:

$$\boldsymbol{u}_v = \boldsymbol{u}_0 \cdot \left(1 + {}^{t}\!/_{2a}\right)^2 \tag{3.7}$$

Since the heat exchanged involves a solid and a fluid, the heat exchanger analysis is not common as usual. In Figure 3.4 (the heat exchanged analysis), the operation of a fluid-solid heat exchanger is presented along with the electrical analogy in order to determine the equation parameters. It can be seen that the heat is transferred in three processes as follows:

- Convective heat transfer from the fluid to the inner wall of the tube,
- Conductive heat transfer through the tube wall itself,
- Conductive heat transfer from the outer tube wall to the bed, the vapour is then released and heat stored in the bed.

As the system is adiabatic, these heats are equal between them. Using an electrical analogy like the Ohm law, the different thermal resistances can be determined as follows (Legay, 2012):

$$R_{cht} = \frac{1}{h_f \cdot A_f}; \quad R_{tc2} = \frac{e_{wall}}{\lambda_{wall} \cdot A_{wall}}; \quad R_{tc1} = \frac{\ln(d_o/d_i)}{2\pi\lambda_{bed} \cdot L_{bed}} \tag{3.8}$$
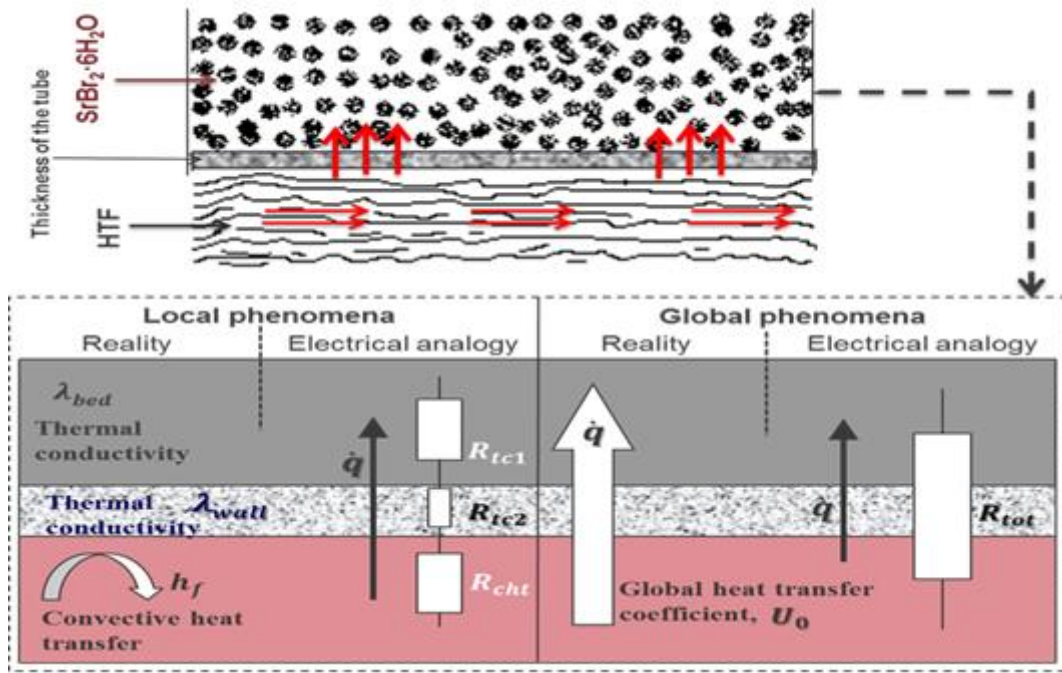
Figure 3.4: Operation principle of a fluid-solid heat exchanger with simplifications and analogies.

As the analogy shows a series disposition, the total thermal resistance is directly the sum of each thermal resistance. This addition highlights the overall heat transfer coefficient as follows:

$$R_{tot} = R_{cht} + R_{tc2} + R_{tc1} <=> \frac{1}{U_0 \cdot A_0} = \frac{1}{h_f \cdot A_f} + \frac{e_{wall}}{\lambda_{wall} \cdot A_{wall}} + \frac{\ln(d_o/d_i)}{2\pi\lambda_b \cdot L_b} \tag{3.9}$$

The overall heat transfer coefficient, U_o, was directly calculated from the temperature data and the flow rates (Jamshidi et al., 2013) or the total heat transferred during the charging using the following equations, where A_0 (m²) is the total heat transfer surface of coiled tube, plate fin or honeycomb, $\dot{q}$ is the heat transfer rate (thermal power) and ΔT_{LM} is the log mean temperature difference, based on inlet temperature difference, ΔT_1, and the outlet temperature difference, ΔT_2, using the following equation:

$$U_o = \frac{\dot{q}}{A_0 \cdot \Delta T_{LM}} \text{ with } \Delta T_{LM} = \frac{(\Delta T_1 - \Delta T_2)}{\ln(\Delta T_1/\Delta T_2)} \tag{3.10}$$

In this case of solid-gas heat transfer, which differs from co-flow and counter flow systems, the used temperature in the solid is an average at different positions of the solid.

3.3.2. NUMERICAL INVESTIGATION RESULTS

The material bed initially at 20 °C was heated up to 100 °C corresponding to the temperature supply by heat losses from the micro-CHP. This variation was in agreement with the temperature need to charge the heat storage system since the salt bed required around 88 °C to

be charged. The waste energy for charging can be also supplied from other sources like solar collector, electricity losses, and extra wind energy production. Figure 3.5 exhibits the temperature distribution of a layer between the tube or the plate and the bed, along the z-axis for the three heat exchangers. It can be seen that the honeycomb heat exchanger transfers the exact heat input to the bed, while the two others show some differences of about 1 °C.

To highlight the temperature that each exchanger exhibits, an arc length is defined in the middle of the bed along the z-axis. Arc length, known as irregular arc segment and also called rectification of a curve, is the integrated surface element value along an edge. It is a function given in Comsol Multiphysics, meaning that for a cut line on the geometry, it move along the contour of the line for a selected direction or axis. Figure 3.6 shows the bed temperature and the values observed are 89.7 °C, 89.9 °C and 90.3 °C for the helical coil, the plate-fin and the honeycomb heat exchangers respectively. Temperature fluctuation less than 1 °C which was in the range of the acceptable thermocouple uncertainty was observed. These fluctuations had no influence on the results. The plate-fin with 50 plates had a bigger heat transfer surface than of the helical coil and of honeycomb. The reason of temperature difference could be that the flow is affected by secondary flow caused by centrifugal forces in the helical coil, which caused a delay on the heat transfer to the bed. The system with a honeycomb heat exchanger exhibits a higher temperature variation than one with the helical coil and the plate heat exchanger (see Table 3.2).
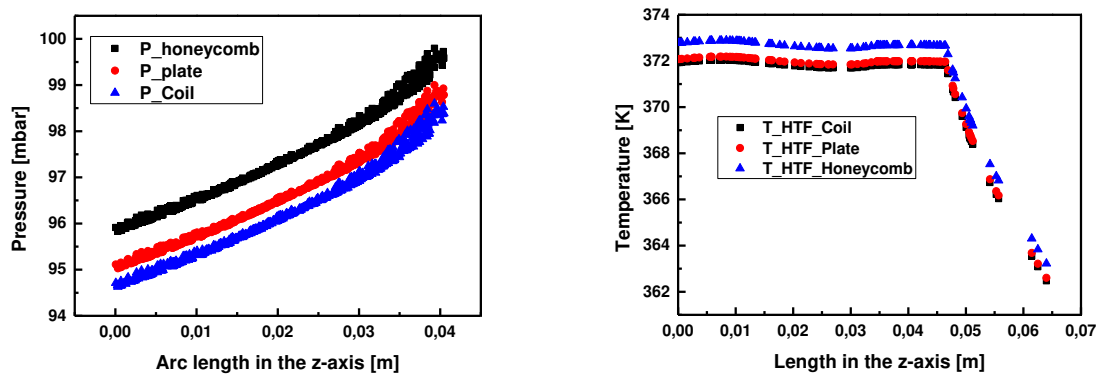
Figure 3.5: Pressure drop (left) and temperature distribution heat transfer fluid (right) of the layer between the plate/tube and the bed.

The used logarithmic mean temperature method was a sizing tool for characterizing the heat recovery (Cadavid et al., 2013). In fact, the heat transfer coefficient allowed the evaluation of the power store in the thermochemical material. To achieve great thermal performances in order to supply heat for space and DHW, this coefficient should be around 200 $W \cdot m^{-2} \cdot K^{-1}$ (Rambaud, 2009). The honeycomb exhibited higher heat transfer coefficient despite the lower heat transfer area. This can be explained by its compactness. Indeed, the area density of the honeycomb structure was about 3876 $m^2 \cdot m^{-3}$ which was much greater than 700 $m^2 \cdot m^{-3}$ the value of the solid-liquid heat exchanger (Q. Li et al., 2011). This area density refers to the present Aluminium honeycomb as a typical micro-cell honeycomb (Lu, 1999). The high value of the area density favoured a corresponding high volumetric heat transfer power (heat flux density, $W \cdot m^{-3}$). The numerical results show that a higher overall heat transfer capacity of three times compared to the plate-fin or helical coil with the same reactor geometry was obtained. The high value of the coefficient for the honeycomb heat exchanger represented his good effectiveness and could be

up to 200 W·m⁻²·K⁻¹ if the power loss from the micro-CHP is higher than what we used for calculation.
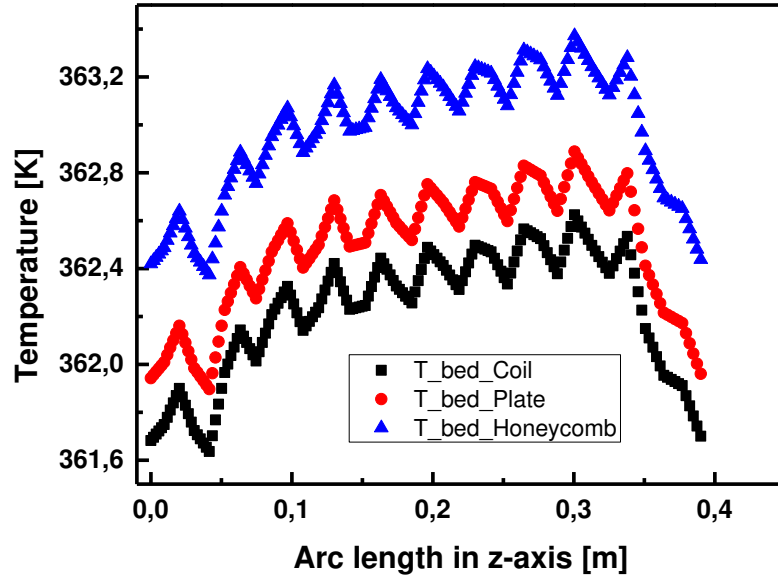
Figure 3.6: Bed temperature distribution along an arc length defined in the middle of the bed for the three heat exchangers: a) the helical coil, b) the plate-fin and c) the honeycomb.

Table 3.2. Parameters for the evaluation of the heat transfer coefficient of heat exchangers.

	Helical coil	Plate-fin	Honeycomb
$\dot{q} = Q_{\mu CHP}$ (W)	454.2	454.2	454.2
T_{HTF_in} (K)	373.15	373.15	373.15
T_{HTF_out} (K)	372.05	371.35	371.85
T_{bed_i} (K)	293.15	293.15	293.15
T_{bed_f} (K)	371.2	371.3	372.2
A_0 (m^2)	0.49	0.62	0.17
ΔT_{HTF} (K)	1.1	1.8	1.3
ΔT_1 (K)	80	80	80
ΔT_2 (K)	0.85	0.02	0.35
$\Delta T_1 / \Delta T_2$	94.12	4000	228.57
ΔT_{LM}	17.42	9.64	14.66
U_o $(W/m^2 \cdot K)$	**53.2**	**75.9**	**182.2**

The left picture on Figure 3.5 shows the change of pressure drop of the three heat exchangers at different positions of the layer between the plate/tube and the bed without considering phase

change of the bed side. According to the theory when charging the salt bed, the pressure dropped from 100 mbar to around 98 mbar. In Figure 3.5, this is not the case due to the non-considering of the phase change in the simulations. This figure also reveals a pressure drop of 4 mbar, 4.4 mbar and 4.1 mbar for honeycomb, plate-fin and helical coil heat exchangers, respectively. This difference was due to the heat exchanger geometry which strongly affected the pressure drop in a heat exchanger (Mao et al., 2014). This small pressure drop was in the acceptable range when looking at the theoretical value from Figure 3.2. However, a high pressure drop is a negative factor since it needs higher mechanic power as well as constraints on system accessories such as valves and pumps.

Once the optimal heat exchanger (good heat transfer coefficient and small pressure drop) had been selected, thermal management modelling of the storage system was performed. This consisted of heat and mass transfer plus chemical kinetics modelling.

3.4. KINETICS MODELLING

The principal experimental approach to the study of the reaction process involves the measurement of the rate at which a reaction proceeds and the determination of the dependence of this reaction rate on the concentrations of the reacting species and on the temperature. Thermal analysis is concerned with thermally stimulated processes, meaning the processes that can be initiated by a change in temperature. These factors are grouped together in the term reaction kinetics and the results for a given reaction are formulated in a rate equation which is of the general form:

$$Rate = k(T) * f(C_i) \tag{3.11}$$

The quantity $k(T)$ is called the rate constant and is a function only of the temperature if the term involving the reactant concentrations correctly expresses the rate dependence on concentration. Thus the experimental information on the reaction process is summarized in the rate equation by the nature of the concentration function and temperature dependence of the rate constant.

The use of Eq. (3.11) in computational methods can limit or reduce the quality of the results in the area of thermal characterization or analysis. The International Confederation for Thermal Analysis and Calorimetry (ICTAC) mentioned that the ignorance of the pressure dependence can be the reason since the pressure may had a profound effect on the kinetics of processes, whose reactants and/or products are gases (Vyazovkin et al., 2011). Numerically, rate constants were used instead of equilibrium constant. Fortunately, the van't Hoff's differential equation helped determining the reaction equilibrium constant, which was equal to the ratio of forward and reverse rate constants.

Since kinetics deals with measurement and parameterisation of the process rates, the rate can be parameterised using three major variables: the temperature T, the chemical conversion α and the pressure p. Systematic studies had been performed about the different expressions of

the kinetic rates (Ajzoul, 1993; Neveu and Castaing-Lasvignottes, 1997) in heterogeneous kinetics and the global form of that rate can be presented as follows:

$$\frac{\partial \alpha}{\partial t} = k(T) \cdot f(\alpha) \cdot h(p) \tag{3.12}$$

The value of the conversion α in time-dependence reflects typically the progress of the overall transformation of a reactant to products, meaning the advancement of the reaction. The overall transformation in this study involved multiple reaction steps each with specific extent of conversion. The rate of overall transformation process that involved N subsequent reactions can be described by the following equation:

$$\frac{\partial \alpha}{\partial t} = \sum_{i=1}^{N} k_i(T) \cdot f_i(\alpha_i) \cdot h_i(p_i) \tag{3.13}$$

Pressure dependence was generally ignored in most kinetic computational methods, but used in the area of thermal analysis. It was the case of TGA-DSC measurements (Jörimann and Riesen, 2009). According to the ICTAC, for reversible solid-state decomposition, the pressure dependence of their rate can be presented as:

$$h(p) = 1 - \frac{p}{p_{eq}} \tag{3.14}$$

For reversible solid-gas synthesis, the Institute of Science and Materials Processing at the University of Perpignan in France worked on that for several decades. Lu et al. (Lu et al., 1996; Mazet et al., 1991) had shown that the pressure dependence can be expressed as:

$$h(p) = 1 - \frac{p_{eq}}{p} \tag{3.15}$$

Where p and p_{eq} were the partial and equilibrium pressures of the gas product respectively (here the water vapour). Assuming that mass transfer and chemical reaction are sufficiently rapid so that equilibrium values of concentrations always exist at prevailing temperature, the equation linking the equilibrium pressure to the temperature for the decomposition is given by the Clausius-Clapeyron relationship:

$$\ln(p_{eq}) = -\frac{\Delta H_r^0}{\mathcal{R} T_{eq}} + \frac{\Delta S_r^0}{\mathcal{R}} \tag{3.16}$$

In the numerical determination of reaction rate, the term $h(p)$ function of the pressure is obtained with water equilibrium curve and the partial water vapour pressure from the ideal gas equation function of temperature. Using the experimental results of Longuet et al. (Longuet and Gillard, 2009) based on a generalized expression of the Prout-Tompkins equation mentioned by the ICTAC; the overall rate of decomposition/synthesis reaction was described as:

$$\frac{\partial \alpha}{\partial t} = A_f \exp\left(-\frac{E_a}{\mathcal{R}T}\right) \cdot \alpha^b (1-\alpha)^c \cdot (1 - \frac{p_{eq}}{p}) \text{ (Dehydration)} \tag{3.17}$$

$$\frac{\partial \alpha}{\partial t} = A_f \exp\left(-\frac{E_a}{\mathcal{R}T}\right) \cdot \alpha^b (1-\alpha)^c \cdot (1 - \frac{p_{eq}}{p}) \text{ (Hydration)} \tag{3.18}$$

where b and c were two constants parameters depending on the experiment, A_f was the pre-exponential Arrhenius factor taking into account the kinetic effect, E_a the Arrhenius activation energy. The term α represented the extent conversion degree or number of molecules per unit volume processed at time t, was defined by (Janković et al., 2008) as follows:

$$\alpha(t) = \frac{m_0 - m(t)}{m_0 - m_f} \text{ (Experiment) and } \alpha(t) = \frac{C_0 - C(t)}{C_0 - C_f} \text{ (Numerical)} \tag{3.19}$$

Here, m_0 and m_f were the initial and final mass of the salt hydrate, respectively. Concerning the kinetic equation for this type of reaction, some authors (Lu et al., 1996; Mazet et al., 1991; Michel et al., 2014b) had demonstrated that the parameters in the first equation could be taken as b = 1; c = 0 for the dehydration and b = 0; c = 1 for the hydration.

The salt hydrate mass evolution during the process time can be determined. Eqs. (2.17), (2.18) were chosen because they fitted better with Avrami-Erfoveev and normal Prout-Tompkins equation for kinetic description (Longuet et al., 2006) than classical model without pressure of gaseous product (Vyazovkin, 2002). It took into account the reaction interface (Huang, 2004; Neveu and Castaing-Lasvignottes, 1997). The above reaction rate is for a constant heating rate at non-isothermal conditions. Considering the lifetime prediction by the E698 method (Vyazovkin et al., 2011) based on the assumption of the first-order kinetics (Vyazovkin et al., 2011), the pre-exponential factor can be determined as:

$$A_f = \frac{\beta E_{a,w}}{\mathcal{R}T_p^2} \exp\left(\frac{E_{a,w}}{\mathcal{R}T_p}\right) \tag{3.20}$$

where T_p, the peak temperature was obtained in the thermal analysis experiment, $E_{a,w}$ was the activation energy for desorption-the minimum energy a water molecule needs to be desorbed and β the heating rate (dT/dt)[1].

3.5. HEAT AND MASS TRANSFER MODELLING

This section highlights the development of the thermochemical heat storage reactor model at a macroscopic scale. Thus, the dimensions of the modelled system are assumed large compared to the size of the thermochemical material (salt hydrate), which allowed to assume the material bed as a homogeneous porous storage medium described by equivalent characteristics, such as the heat capacity and the thermal conductivity. Beforehand, the modelling required the definition of a representative system of the actual reactor storage system. For this reason, a construction was performed in 3D in order to have all the real aspects. Relevant assumptions were made to simplify the resolution of the problem, while ensuring their justification and validity. The expected results aiming to predicting profiles of temperature, pressure and power of the system will be compared with experimental results for model validation.

3.5.1. HYPOTHESIS AND ASSUMPTIONS

As phases mentioned in the storage system description section, the macroscopic description of heat transfer in a porous medium subjected to a two-phase flow with phase change is often investigated by the use of a single temperature equation. One-equation models had been proposed a decade ago based on this assumption (Duval et al., 2004). Here, local thermal equilibrium meant that the macroscopic temperatures of the three phases (liquid water in the salt, water vapour the reactive gas and the solid salt itself) were close enough so that a single temperature was sufficient to describe the heat transport process. Duval et al. (Duval et al., 2004) added that though the assumption of local thermal equilibrium was acceptable in many cases of unsaturated porous media with liquid–vapour phase change, particularly for most thermal decomposition processes. The great simplicity of the one-equation model regarding the effective transport coefficients motivated its use when the particles or pores are small enough, or when the thermal properties did not differ widely. Olives et al. (Olives and Mauran, 2001) showed that thermal radiation was neglected since the working temperature range of a thermochemical heat storage system is between 10 °C and 90 °C. They also showed that, for a system with water vapour, the prevailing heat transfer was conduction (Michel, 2012). Therefore, heat in porous medium with water vapour is transferred by conduction according to Fourier law. Under water vapour system, total pressures were all assumed to be water vapour pressures.

Mass transfer and chemical reaction are assumed sufficiently rapid so that equilibrium values of concentrations always exist at prevailing temperature, so that the equation linking the equilibrium pressure to the temperature for the decomposition is given by Clausius-Clapeyron equation. In the synthesis, mass transfer can be of Knudsen, Darcy or inertial flow type since it depends on vapour pressure and velocity of this latter in the porous media. In this case, the fluid flows through a bed of approximately spherical particles with constant porosity. Water vapour is considered as an ideal gas, due to the low concentration and partial pressure.

---

[1] This parameter is often given in pressure versus temperature desorption curves analysis.

3.5.2. Geometry design

Here, the 3D model consisted of a cylindrical reactor in which a honeycomb heat exchanger was inserted. The honeycomb plates made of aluminium held the salt in an amount of about 1 kg. The cylinder with a height of 400 mm and a diameter of 200 mm represented the reactive gas domain.
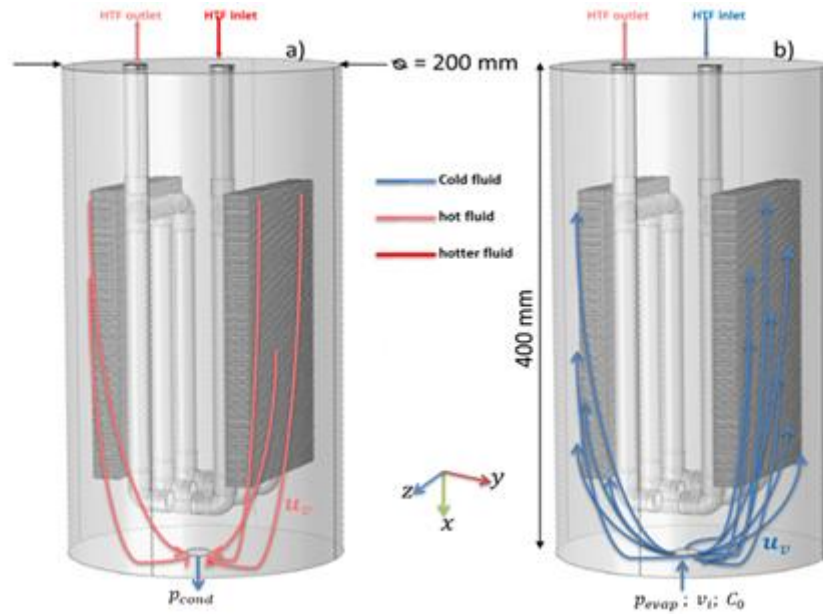
Figure 3.7: Reactor geometry model in (a) charging phase and (b) discharging phase for simulations. p_{cond}: represents the water vapour at which vapour condenses into the condenser; p_{evap}: represents the water vapour at which vapour is evaporated from the evaporator at a given concentration (v_i) and velocity (C_0).

The casing plate on which honeycomb was deposed had the dimension of 130 x 235 x 19 mm³ and a 1 mm thickness plate was glued below to insure the thermal conduction. The tube through which the heat transfer fluid circulates had a height of 245 mm and a diameter of 18 mm. The honeycomb structure consisted of regular hexagonal cells of cell size $a = \sqrt{3}l$, cell wall length l and thickness t (Appendix A1-3).
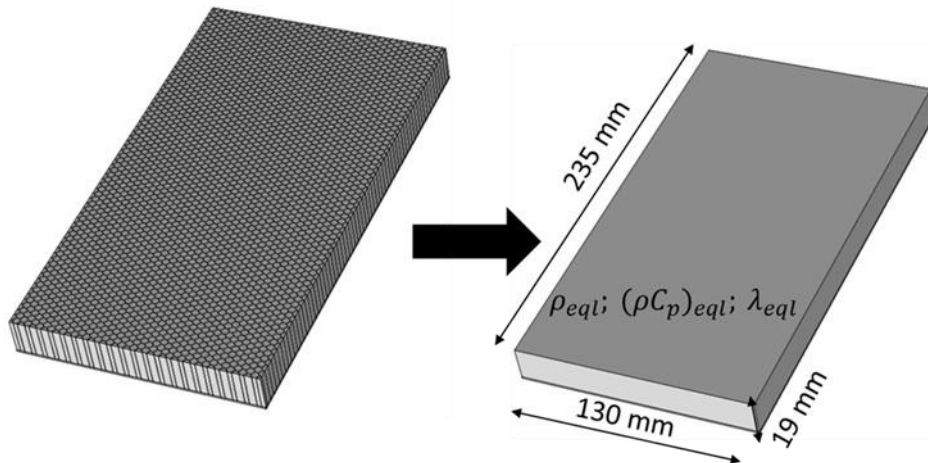
Figure 3.8: Analogy of the honeycomb salt bed in order to simulate the bed as homogeneous.

The bed corresponded to the domain occupied by each honeycomb. Since the numerical objective is to be close to the reality (Figure 3.7), honeycomb structure had been introduced. However, the structure itself had more than two million of domain and boundaries elements, requiring a powerful computer (than what it is available for the moment). In order to keep the properties of the honeycomb structure, an analogy of the beds (Figure 3.8) is then defined. The honeycomb bed was modelled as porous material made of salt bed (solid salt and bounded water + porosity) and the aluminium fins. In terms of volume fraction the followings equivalences holds, as follows:

$$\rho_{eql} = \rho_{Al} \cdot \gamma_{Al} + \rho_{bed} \cdot \gamma_{bed} \qquad (3.21)$$

where $\gamma_{bed} + \gamma_{Al} = 1$, represents the volume fraction relationship.

$$\left(\rho \cdot C_p\right)_{eql} = \left(\rho \cdot C_p\right)_{Al} \cdot \gamma_{Al} + \left(\rho \cdot C_p\right)_{bed} \cdot \gamma_{bed} \qquad (3.22)$$

where $C_{p\_bed} = \varepsilon C_{p\_v} + (1 - \varepsilon) \cdot C_{p\_s}$, represents the specific heat capacity of the salt.

$$\lambda_{eql} = \lambda_{Al} \cdot \gamma_{Al} + \lambda_{bed} \cdot \gamma_{bed} \qquad (3.23)$$

Using these equivalent parameters mimic the real bed with salt and the honeycomb structure. During the experimentation, the honeycomb made of aluminium is weighted and so the volumes are determined. A honeycomb plate weight 118.42 g (without salt inside) and by knowing the density of the aluminium, the aluminium volume is hence determined as of $4.39 \cdot 10^{-5}$ m³. The volume of the salt was then obtained as of the difference between the total volume and the aluminium volume with a volume density of 3480 kg·m³ (Michel, 2012). The total volume was then of $5.81 \cdot 10^{-4}$ m³. The fractions were then determined using the volume fraction relationship. Except thermal conductivity, these equivalent parameters are about 98% of the bed parameters (Appendix A4, Table A4.4).

3.5.3. MATHEMATICAL MODELLING

The objective was to translate a real situation into a mathematical form with the purpose of solving the mathematics (to provide useful answers to a real situation). In order to understand the thermochemical heat storage process, mathematical modelling was required for sensitivity analysis and pointed out where optimisation was needed. In the following, modelling of the storage and release of heat is presented along with an analytical model which allows determining the reaction time for a quasi-complete hydration.

A set of partial differential equations controlling the kinetic, conservations of mass, momentum and energy in the reactor bed were organized to simulate the heat storage and release process by desorption and sorption. The appropriate parameters of these governing equations

were important for simulating the process. Therefore, the effect of the parameters was considered here. In addition, a Prout-Tompkins model developed in the previous section, was used to describe desorption's kinetic phenomena in thermochemical material.

3.5.3.1.   Dehydration phase (storage of heat)

During this phase, the movement of water vapour release from the salt hydrate was not taken into account. Balasubramanian et al (Balasubramanian et al., 2010) justified this neglecting of convective heat and mass transfer, with the fact that salt hydrates are generally porous and contain voids in their structure so that hydrated salt does not occupy the entire volume of the system. The Eq. (3.17) was used here for chemical rate.

3.5.3.1.1.   Mass balance and mass transfer

Since the system is closed and isolated, there is no mass exchange with its surroundings. Thus a decrease in hydrate mass density results in an increase in the mass density of the anhydrous and water vapour and the bed, respectively. Taking into account the porosity of the bed, the mass conservation equation of water desorption system can be expressed as follows:

$$\varepsilon \frac{\partial \rho_g}{\partial t} = -\nabla \cdot \left(\rho_g \cdot \boldsymbol{u_v} \right) + D_g \cdot \Delta \rho_g + \chi \cdot \rho_g \cdot \frac{\partial \alpha}{\partial t} \cdot \frac{M_g}{M_{s1}} \tag{3.24}$$

Where ε is the total porosity of the bed, ρ_g is the gas phase mass density of the salt hydrate bed, $\boldsymbol{u_v}$ is the water vapour velocity, D_g is the diffusion coefficient of water vapour, χ stoichiometric coefficient of water and the last term of right hand side of Eq. (3.24) is the mass source term, which accounts for the decomposition rate of salt hydrate from the solid phase to the desorbed phase. $\frac{M_g}{M_{s1}}$ is the ratio of the molecular mass of water vapour on molecular mass of solid phase. Eq. (3.24) is also known as the CDR (convective-diffusion-reaction) equation.

The gas produced during the reaction of decomposition is supposed to be able to diffuse into and out of the bed. By considering and modifying Arnold method, Gilliland method, Hirschfelder et al. method, Slattery-bird method, (Chen and Othmer, 1962) established a new generalized equation for gas diffusion coefficient for a binary system. This led us to effective gas diffusivity in solid (porous media) and was defined as:

$$D_g = \left(\frac{0.43 \left(\frac{T}{100} \right)^{1.81} \left(\frac{1}{M_g} + \frac{1}{M_s} \right)^{0.5}}{p_{eq} \left(\frac{T_{cg} T_{cs}}{10000} \right)^{0.1406} \left[\left(\frac{V_g}{100} \right)^{0.4} + \left(\frac{V_s}{100} \right)^{0.4} \right]^2} \right) \frac{\varepsilon \cdot \delta}{\tau} \tag{3.25}$$

Where δ is the constrictivity (this parameter is viewed to depend on the ratio of the diameter of the diffusing particle to the pore diameter). Its value is always less than 1. It was defined not for a single pore, but as the parameter of the entire pore space considered. τ was the tortuosity (a quantity which characterises the convoluted nature of the porous pathways followed by diffusing species). T_{cg} and T_{cs} were gas and solid phase temperatures at the critical point respectively, and V_g and V_s gas and solid atomic volume, respectively.

3.5.3.1.2. Flow regime in the bed

The potential flow types are Knudsen, Darcy or inertial flow type. Assuming the porous reactive bed is of salt particles with a diameter of 100 µm, it is possible to evaluate the Knudsen flow number (Appendix A2-1). The flowing gas in our case was water vapour (molecular diameter of 10.05 Å) which had a free mean path of 0.6 µm. Applying the Knudsen formula, a Knudsen number of 0.006 is obtained. Consequently, the flow could be of Darcy or inertial. The flow was considered as Darcy type for Reynolds number lower than 0.1, otherwise it was of inertial type. Using the general definition of the Reynolds number and replacing the gas velocity by the pressure gradient as driving force (Lu et al., 1996), we obtained $Re = 0.003$. Therefore Darcy's law was used. By heating the salt hydrate, the water vapour finds a way to get out through diffusion. The mass transfer at a gas phase occurs not only from diffusion, but also from advection, where a difference in pressure causes bulk motion of the gas. The velocity of the gas leaving the bed is generally expressed as follows:

$$u_v = -\frac{k}{\mu}\left(\nabla p_{bed} - \rho_v g\right) \tag{3.26}$$

Where k is the intrinsic permeability of the salt hydrate medium, μ is the viscosity of water vapour, g is the acceleration of gravity, and ρ_v is the water vapour density. ∇p_b is the pressure difference across the bed. The intrinsic permeability is a function of the particle radius r_p (value of 0.001 m assuming that particles are regarded as uniform sphere granules) and can be calculated by the following semi-empirical Blade-Kozeny equation (Carman, 1956) for granular medium (with a total porosity < 0.83):

$$k = \frac{\varepsilon^3 \cdot d_p^2}{36 \cdot \tau^2 \cdot f_{CK} \cdot (1-\varepsilon)^2} \tag{3.27}$$

where f_{CK} is the pore shape factor. It is unity when assuming a spherical shape and more than unity for any other shape.

According to the usual range value of particle radius and porosity, the permeability $k \ll 0,1$ this is the condition for Darcy flow in fluid flow engineering. Combining Darcy's law with mass conservation equation, it gave the equation for both mass and momentum conservations and subsequently the Eq. (3.24) becomes as follows:

$$\varepsilon \frac{\partial \rho_g}{\partial t} = -\nabla \cdot \left(\rho_g \cdot \frac{k}{\mu}\left(\nabla p - \rho_g g\right)\right) + D_g \cdot \Delta \rho_g + \chi \cdot \rho_g \cdot \frac{\partial \alpha}{\partial t} \cdot \frac{M_g}{M_{s1}} \tag{3.28}$$

Where the acceleration of gravity is taking into account and the gas phase is assumed to be ideal, i.e. partial pressure $p = \rho_g \mathcal{R} T / M_{H2O}$. In Eq. (3.28), the first term represents the water vapour accumulation in the pores of the salt bed, the second term the transport out of the salt bed, the third term is the vapour diffusion through the salt bed, and the fourth term the mass desorption rate of water from the solid salt to the gaseous phase.

3.5.3.1.3.　　Energy balance

The heat recovered from cogeneration or micro-CHP is supplied to the salt hydrate bed through a heat exchanger as shown in system concept in Figure 3.1. During the decomposition reaction, the heat of reaction was transferred by convection and conduction through in thermochemical material media (Mbaye et al., 1998). The radiation is neglected. It was not necessary in this mode to solve the heat equation for both solid and gas phase because during the decomposition the different phase temperatures were roughly equal ($T_s \approx T_g \equiv T$). For the solid phase, a source term of internal heat generation by chemical reactions was considered. The energy balance equation was written as follows:

$$(\rho \cdot C_p)_{eql} \cdot \frac{\partial T}{\partial t} = \nabla \cdot \left(\lambda_{eql}\nabla T\right) - C_{pg} \cdot \rho_g \, \boldsymbol{u_v} \cdot \nabla T + \frac{\rho_{eql}}{M_{s1}} \cdot \frac{\partial \alpha}{\partial t} \cdot \Delta H_r \tag{3.29}$$

Heat accumulation = Heat conduction + Heat convection + Heat source term

The source term in the Eq. (3.29), a multiple of the reaction enthalpy which was assumed to be constant here, is the energy associated with desorption of water between the solid salt and the gas phase.

3.5.3.1.4.　　Boundaries and initial conditions

Temperature and pressure were investigated where $T = T\,(t, x, y, z)$ and $p = p\,(t, x, y, z)$. The temperature (salt hydrate), pressure, HTF velocity and extent conversion distributions in any direction inside the reactor were initially considered to be uniform.

$$T(0, x, y, z) = \, T_0 \, ; (0, x, y, z) = \, p_i \, ; u_v = 0 \text{ and } \alpha = 0 \tag{3.30}$$

Referring to the domain of Figure 3.7a, at $x = 0$ (at the bottom) boundary it was assumed that the vapour pressure is equal to the evapo-condenser pressure and temperature gradient is zero (i.e. adiabatic boundaries).

$$\lambda_{eff}\nabla T = 0 \, ; \, p(t, 0, y, z) = \, p_{cond} \, ; \text{and } \alpha \neq 0 \tag{3.31}$$

At the boundary $x = L$ (top) the pressure gradient was zero since the walls are airtight and a convective heat transfer boundary condition exists for the solid phase.

$$\lambda_{eff} \frac{\partial T(t, L)}{\partial x} = 0 \, ; p(t, L, y, z) = 0 \, ; \text{and } \alpha \neq 0 \tag{3.32}$$

$$\boldsymbol{n} \cdot \left(-\lambda_{eql}\nabla T\right) = h(T - T_{ext}) \tag{3.33}$$

3.5.3.2. Hydration phase (release of heat)

During this phase, the anhydrous salt gradually cools due to the flow of water vapour through it. This cooling, leading to the extraction of sensible heat, reduces the salt temperature until the thermochemical reaction temperature is reached. At this time, hydration is activated due to the combination of salt with vapour to produce the salt hydrate. The energy required for the process depends on the reaction rate and the enthalpy of the hydration. Eq. (3.18) is used here for chemical rate.

3.5.3.2.1. Mass balance and mass transfer

In the gas diffuser, the continuity equation describes the vapour transport and in the salt there is a mass source due to the reaction. Therefore, the equations are expressed as follows:

$$\frac{\partial(\varepsilon \cdot \rho_g)}{\partial t} = \dot{m} - \nabla \cdot (\rho_g \boldsymbol{u_v}) + D_g \cdot \Delta \rho_g \tag{3.34}$$

Solving the momentum equation is very difficult in a porous medium. Indeed, given the complexity of the geometry of the porous medium, the local distribution of the fluid velocity flow in the pores is generally not accessible. The fluid (water vapour) is driven by the diffusion and by pressure gradient along the porous bed, but the diffusion coefficient ($\approx 10^{-9}$) is very low compare to the pressure gradient. In addition the flow is of Darcy as demonstrated in the previous section. It is usual to substitute the equation of conservation of momentum by a phenomenological law connecting the velocity to the force behind the flow of material, the pressure gradient in the case of water vapour. This phenomenological law takes into account many parameters, such as porosity, pore size of the porous medium, the medium pressure, the gas velocity or the size of the molecules of fluid. The mass transfer at a gas phase occurs not only from diffusion, which describes the relative motion of gases, but also from advection, where a difference in pressure causes bulk motion of the gas. This led to a viscous flow with a vapour velocity as expressed in Eq. (3.26). The dynamic viscosity (μ) of a fluid is a function of its temperature and generally known in the literature. The Sutherland law or the viscosity-temperature relation (Shapiro, 1953) is often used to determine the viscosity of a gas in the range of 117.15 K to 2060.15 K as follows:

$$\frac{\mu}{\mu_0} = \left(\frac{T}{T_0}\right)^{1/2} \left\{ \frac{1 + S/T_0}{1 + \frac{S/T_0}{T/T_0}} \right\} \tag{3.35}$$

where μ_0 is the dynamic viscosity at the temperature of the porous media surface T_0, S the Sutherland temperature, the ratio S/T_0 is empirically taken as 0.505 (Shapiro, 1953).

In order to avoid the direct measurement of the permeability, many authors have attempted to correlate this parameter with the texture of the porous medium. Most of the time, the correlations are function of the porosity of the porous medium, its tortuosity and the average pore diameter. The tortuosity factor (τ) is the ratio between the distance travelled by the fluid (L_f) and the length of the sample (x_s):

$$\tau^2 = \left({L_f}/{x_s}\right)^2 \tag{3.36}$$

The mass source term is the water vapour mass due to the reaction and is a function of the reaction advancement (α):

$$\dot{m} = -M_v \cdot \frac{\partial \dot{n}_v}{\partial t} = -\chi \cdot \frac{\partial \alpha}{\partial t} \cdot \frac{M_v}{M_{s0}} \cdot \rho_{eql} \quad \text{(kg.m^{-3}.s^{-1})} \tag{3.37}$$

where χ is the stoichiometric coefficient of water molecules in the salt, $\frac{\partial \alpha}{\partial t}$ the reaction rate expressing the kinetic of the reaction. With this rate, the mass transfer equation can be written as follow:

$$\frac{\partial(\varepsilon \rho_g)}{\partial t} = D_g \cdot \Delta \rho_g - \nabla \cdot \left(\rho_g \frac{k}{\mu} \left(\nabla p - \rho_v \cdot g\right)\right) - \chi \frac{\partial \alpha}{\partial t} \frac{M_v}{M_{s0}} \rho_{eql} \tag{3.38}$$

3.5.3.2.2. Energy balance

In the reactive medium, the internal energy variation is due to the conductive and convective fluxes of water vapour. Therefore, the energy balance can be written as follows:

$$\left(\rho \cdot C_p\right)_{eql} \frac{\partial T}{\partial t} = \nabla \cdot \left(\lambda_{eql} \nabla T\right) - \rho_g C_{p\_v} \, \boldsymbol{u_v} \, \nabla T + \dot{q} \tag{3.39}$$

where $\dot{q}$ the energy source term due to the hydration reaction is as follows: $\dot{q} = -\Delta H_r^0 * \frac{\partial \alpha}{\partial t} * \frac{\rho_{eql}}{M_{s0}}$

In summary, the energy balance of the system using water vapour as the reactive salt and the heat exchanger is written respectively, as follows:

$$\left(\rho \cdot C_p\right)_{eql} \frac{\partial T}{\partial t} + \rho_g C_{p\_g} \, \boldsymbol{u_v} \, \nabla T = \nabla \cdot \left(\lambda_{eql} \nabla T\right) - \Delta H_r^0 * \frac{\partial \alpha}{\partial t} * \frac{\rho_{eql}}{M_{s0}} \tag{3.40}$$

3.5.3.2.3. Boundaries and initial conditions

The reactor wall is cooled by a convective heat flux. Thus the boundary condition as follows:

$$-\mathbf{n} \cdot \left(\lambda_{eql} \nabla T\right) = h \cdot \left(T_{ext} - T\right) \tag{3.41}$$

Where h is the convective heat transfer coefficient. The top and the bottom of the reactor are considered thermally insulated:

$$-\mathbf{n} \cdot \left(\lambda_{eql} \nabla T \right) = 0 \tag{3.42}$$

For the fluid mechanics:

Reactor wall: $-\boldsymbol{n} \cdot \nabla u = 0$ \hfill (3.43)

Inlet: $-\boldsymbol{n} \cdot \nabla u = v_i$ \hfill (3.44)

Outlet: $p = 0$ \hfill (3.45)

For the species transport:

No flux on the reactor wall: $-\boldsymbol{n} \cdot N = 0$ \hfill (3.46)

Inflow: $c = c_0$ \hfill (3.47)

Outflow: $-\boldsymbol{n} \cdot D \nabla c = 0$ \hfill (3.48)

where v_i is the inlet velocity of the vapour steam m·s⁻¹. c_0 is the inlet concentration of steam in *mol/m³.* The utilisation of concentration is required for Comsol simulation. For this purpose, the density equation is turned into concentration equation using the conversion $\rho_g = M \cdot c$.

3.5.3.3.   Reaction front model

This 1D model assumes mass transfer as limiting transfer and hence, reaction happens at sharp front level, which moves at a given time, throughout the bed separating the reacted parts from those not yet reacted. The reaction ends when the front join the boundary closed to the heat exchanger. This model will permit to find out, the reaction rate and the needed reaction time to hydrate or dehydrate a reactive bed, taking into account its characteristics (energy density, bed thickness, permeability) and operating conditions (temperature, water vapour pressure). This model is based on the same geometry of the previous 3D model under water vapour, with additional hypothesis. Its simplicity leads to an analytical resolution of the reaction time.

3.5.3.3.1.   Model hypothesis

The principal hypothesis is the existence of a sharp front reaction moving through the bed. The thermodynamic constraints apply to the boundaries and the transfer properties of the bed mark out by the front impose the front movement. Below are the used hypothesis in this model:

- The heat and mass transfer are unidirectional.
- Steady-state mode, therefore no accumulation (transient) term in the mass equation.
- During the reaction (i.e. between reaction rate and reaction rate + delta (reaction rate)), all physic parameters are constants.
- As the mass transfer is assumed to be the limiting transfer, heat transfer is non-limiting and the bed temperature is supposed constant and equal to the constraint temperature ($T = T_{HX}$) defined by the heat exchanger.
- The reaction kinetics is supposed non-limiting, hence at the front level, thermodynamic equilibrium are performed ($p_f = p_{eq}(T_{HX})$), with expression obtained via Eq. (3.16).

- The water vapour pressure between the front and the outlet is kept constant ($p_o = p_f$) moving to the boundary closed to the heat exchanger.
- The inlet water vapour pressure is known. It is defined from the evaporation temperature of the water in the evaporator ($p_i = p_{eq}(T_{evap})$).
- The pressure at the outlet of the bed (at the frontier with the heat exchanger) is nil.

These defined principles are similar in hydration and dehydration mode. Here, we will develop detailed model for the hydration. The water vapour flux passes through a bed of thickness X_b, submitted to a pressure difference Δp at his boundaries. The salt reacts with the water vapour at the front level, at X_f, separating the bed in two parts. Between 0 and X_f the salt is hydrated and between X_f and X_b the salt is dehydrated (Figure 3.9). Therefore, during the reaction, the front (X_f) moves from 0 to X_b. The reaction advancement (conversion) can be defined as follows:

$$\alpha = 1 - {X_f}/{X_b} \tag{3.49}$$
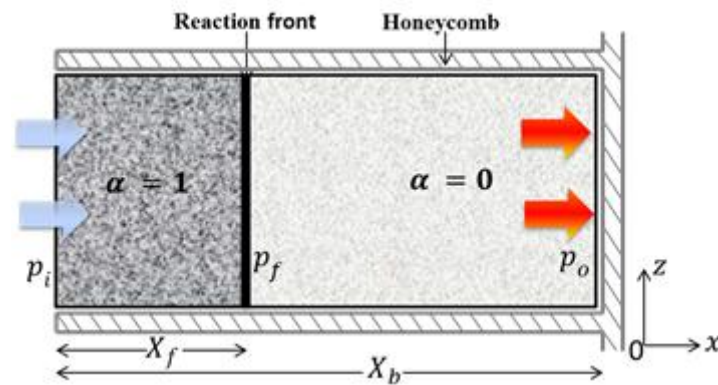
Figure 3.9: Schematic sharp front reaction model of the thermochemical reactor functioning in hydration mode. The reaction occurs at the front level.

3.5.3.3.2.   Model equations

Mass conservation and reaction rate

The main equation of this model, the reaction rate depends on the mass transfer through the bed. This equation is adapted from the previous model and the above hypothesis. Using the first two hypotheses in the x-direction, Eq. (3.34) can be re-written as follows:

$$\frac{d}{dx} \cdot (\rho_v \, \boldsymbol{u}) = \frac{d}{dx} \cdot \left(\rho_v \, \frac{k_s}{\mu} \left(\frac{dp}{dx} \right) \right) = \chi \frac{\partial \alpha}{\partial t} \frac{M_v}{M_s} \rho_s \tag{3.50}$$

The mass flux (kg·m^{-2}·s^{-1}) of water vapour can be defined as follows: $\boldsymbol{j_w} = \rho_w \boldsymbol{u}$. The integration of Eq. (3.50) between the inlet and the outlet of the salt bed, leads to the reaction rate as follows:

$$\int_i^o \frac{d}{dx} \cdot (\boldsymbol{j_w}) = \int_i^o \chi \frac{\partial \alpha}{\partial t} \frac{M_v}{M_s} \rho_s \equiv \frac{j_{wi} - j_{wo}}{\chi \frac{M_v}{M_s} \rho_s} = \frac{\partial \alpha}{\partial t} \cdot X_b \equiv \frac{\partial \alpha}{\partial t} = \frac{j_{wi} - j_{wo}}{\chi \frac{M_v}{M_s} \rho_s X_b} \tag{3.51}$$

Hence, to determine the reaction time, it is mandatory to know the mass flux of water vapour at the inlet and the outlet of the bed. This can be obtained for two constraints: at fixed pressures at the boundaries of the bed, or mass flux imposed and the outlet pressure fixed.

a) *Fixed pressures at the bed boundaries*

According to the sharp front model hypotheses, the bed is divided in two layers, one hydrated and the other one dehydrated (Figure 3.9); each layer having a different water vapour velocity (due to the permeability difference). For this type of diffusion, i.e. pure steam through a porous solid, the driving force is the gas pressure gradient and the pure steam or water vapour is assumed incompressible. Therefore Darcy's law is used and can be re-written for steam through a hydrated salt layer (between X_f and X_b) as follows:

$$u_x = \frac{\dot{V}_f}{A} = \frac{k_1}{\mu} \frac{p_i - p_f}{X_b - X_f} \tag{3.52}$$

Where $\dot{V}_f$ the volume flow rate and A is the cross section perpendicular to u_x. Assuming the water vapour to an ideal gas, we obtain the following expression:

$$\dot{V}_f = A \frac{j_{wi}}{M_{s1} \cdot p_i} RT \tag{3.53}$$

Using Eqs. (3.52) and (3.53), the inlet mass flux of water vapour trough the layer of hydrated salt can be re-written as follows:

$$j_{wi} = \frac{M_{s1} \cdot k_1 \cdot p_i}{\mu \cdot R \cdot T_{HX}} \frac{(p_i - p_f)}{\alpha \cdot X_b} \tag{3.54}$$

This equation is also similar, when water vapour passes through the layer of dehydrated salt layer (between 0 and X_f) until it encountered the external boundary of the heat exchanger.

$$j_{wo} = \frac{M_{s0} \cdot k_0 \cdot p_o}{\mu \cdot R \cdot T_{HX}} \frac{(p_f - p_o)}{(1-\alpha) \cdot X_b} \tag{3.55}$$

These two previous equations for the determination of the reaction rate involve another un-known parameter, p_f, which have to be determined using the Eq. (3.16) at the heat exchanger temperature. Integrating the Eq. (3.51) of the reaction rate between advancement $\alpha = 0$

and $\alpha = \alpha(t)$, and keeping the pressure gradient constant at the bed boundaries, we can obtain the necessary time to hydrate the bed at $\alpha(t)$ as follows:

$$t_\alpha = \left[\alpha \cdot \frac{M_v}{M_s} \cdot \chi \cdot \rho_s \cdot \mu \cdot R \cdot T_{HX}\right] \bigg/ \left[\frac{M_{s1}k_1 p_i}{(X_b - X_f)X_b} \cdot (p_i - p_f) - \left(\frac{M_{s0}k_0 p_o}{X_f X_b}\right) \cdot (p_f - p_o)\right] \tag{3.56}$$

Knowing that the energy density of the reactive bed is expressed as the reaction enthalpy and the salt moles involve during the process, the hydration time can be re-written as:

$$t_\alpha = \frac{\alpha \cdot E_d \, [M_v \cdot \chi \cdot \mu \cdot R \cdot T_{HX}]}{\Delta H_r^0 \left[\frac{M_{s1}k_1 p_i}{\alpha X_b{}^2} \cdot (p_i - p_f) - \left(\frac{M_{s0}k_0 p_o}{(1-\alpha)X_b{}^2}\right) \cdot (p_f - p_o)\right]} \tag{3.57}$$

Proceeding with the same method, the dehydration time where the conversion varies from 1 to 0 can be written as follows:

$$t_{\alpha'} = \frac{(\alpha - 1) \cdot E_d \, [M_v \cdot \chi \cdot \mu \cdot R \cdot T_{HX}]}{\Delta H_r^0 \left[\frac{M_{s1}k_{s1}p_f}{(\alpha-1)X_b{}^2} \cdot (p_i - p_f) + \left(\frac{M_{s0}k_{s0}p_o}{\alpha X_b{}^2}\right) \cdot (p_f - p_o)\right]} \tag{3.58}$$

3.6. Comsol Multiphysics and meshing

Numerical modelling is the process of obtaining approximate solutions to problems of scientific and/or engineering interest. It therefore needs software tools to achieve such of objectives.

The COMSOL Multiphysics® software is a powerful finite element (FEM), partial differential equation (PDE) solution engine for engineering purpose. The basic COMSOL Multiphysics software has about twenty five add-on modules (Comsol, 2014) that expand the capabilities of the basic software into the following application areas. Among them, the Chemical Reaction Engineering and Heat Transfer modules were used for the present work. The first one helps for simulating mass transport and chemical kinetics, while the other helps computing heat transfer. The COMSOL Multiphysics software also has other supporting software, such as the CAD Import Module (in association with Inventor and SolidWorks) and the Material Library. According to the phase (charging or discharging) different nodes are used for the purpose.

To solve the above mathematical model in the discharging, two physics are used and coupled in Comsol. The Reacting flow diluted species (rfds) and Heat transfer in Porous media (ht) from the both modules mentioned earlier. The Reacting flow diluted species node solves mass transfer via the Navier-Stokes equations and the kinetic reaction as well. Its outputs are the concentration, the velocity vector and the pressure. The Heat transfer in porous media node includes the two heat transfer modes: conduction and convection in porous, in solid and in fluid. The only output for this node is the temperature. Both physics are coupled and solved in a transient study on a time-scale of 5 hours with a time step of 20 s.

For the charging phase, the non-isothermal flow (*nitf*) combined of fluid and solid heat transfer was used. As Figure 3.10 shows, the implementation of the numerical study started with the

geometry, the allocation of the materials to the respective domains and the physics to the corresponding domains and boundaries. Then the meshing was performed before the study is launched.

3.6.1. REACTING FLOW IN POROUS MEDIA (RFDS)

This physic concerns the whole domain except the honeycomb and the tubes (where the fluid does not flow in) in the discharging. One important thing is to consider the domain as steam only, to solve the fluid mechanics.

The porous medium is created by setting the porosity and the permeability of the salt bed in the "porous matrix properties" sub-node. Thus the sub-node "transport properties" was attributed to the water steam. The calculated diffusion coefficient is around 10^{-9} m²·s⁻¹. That very small value showed why diffusion is neglected. The reaction is simulated by using Eq. (3.37). It was applied on the salt strips. Every output parameter is initially set to zero, unless the pressure sets to the final water vapour (steam) pressure.
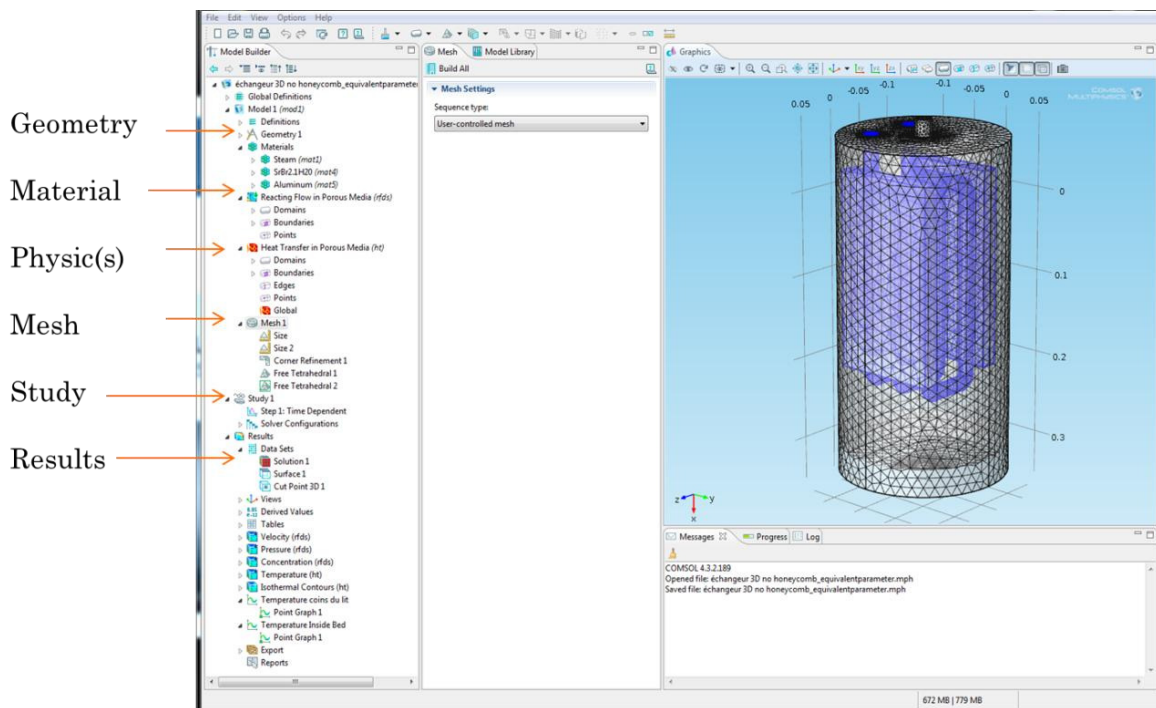
Figure 3.10: Comsol Multiphysics overview of the workspace showing a geometry meshing.

Concerning the boundary conditions, there were an inlet and an inflow set on the lowest boundary of the reactor. The outlet and outflow were not set on the same boundary for different models. The most realistic case was to set them on the border between the salt and the aluminum: here the steam is supposed to react with the salt and was absorbed. However in the first model, the honeycomb was not used. Hence the outlet and outflow are set on the higher boundary of the reactor for this case. Other boundaries were "wall" for the fluid mechanics point of view and "no flux" for the species concentration.

3.6.2. HEAT TRANSFER IN POROUS MEDIA (HT)

This physic concerns the whole domain including solid parts. "Heat transfer in fluids" was used where the steams flows out of the porous, "heat transfer in solids" was used for the

honeycomb and the tubes, the rest is solved with "heat transfer in porous medium" by default. In terms of heat transfer, the reaction creates a "heat source". This latter uses the source term expression in Eq. (3.39) as the general source in W·m⁻³. The initial temperature was 293.15 K all over the domain.

Concerning the boundary conditions, a conductive heat flux was set on the reactor side wall. The inlet temperature of the steam is 283.15 K. These two first conditions were the cooling effect sources and were studied in the chapter 4. An outflow was set on the highest boundary of the geometry. Otherwise every boundary was insulated.

3.6.3. NON-ISOTHERMAL FLOW (NITF)

This physics solve simultaneously the flow dynamic and the heat transfer from the fluid to the solid. The heating fluid and the bed are concerned by the two nodes. The movement of the fluid is defined by the inlet velocity and the inlet temperature and the low Reynolds number $k - \varepsilon$ is used here through the Reynolds-Average Navier-Stokes (RANS) equations adapted to the above model. The heat source for the fluid is the 9-11% of the micro-CHP waste heat (Nowak et al., 2010). Considering a micro-CHP with a power of 237 kW, a heat source to heat the bed was estimated to 21 kW. Heat fluxes are imposed on the layers between the fluid and the heat exchanger, and between the heat exchanger and the bed. Although the shell is insulated, a convective heat transfer to the ambient is imposed.

3.6.4. MESHING

The mesh quality is very important for the accuracy and stability of numerical computation. Structured or unstructured grid generation approaches can be used for producing a discretized representation of the geometries. Structured grids are well suited for simplistic geometries. The complex ones pose significant challenges and are in general time consuming and cumbersome. Unstructured grid generation or what is more commonly, referred to as "auto- meshing", is a viable alternative to the difficulty-to-generate structured grid. To recall that, grid independence is achieved via successive levels of adaptive remeshing. Adaptive remeshing is performed in an automated manner and is based upon normalized undivided differences in field variables in Comsol Multiphysics.

The geometries have been drawn in Inventor and SolidWorks©, then exported to the Comsol Multiphysics software for purpose. However, difficulties were encountered during the meshing phase due to the complexity of the geometry itself. Despite the fact that it was not useful to have a high accuracy for the calculations in the aluminum casing, Comsol needed a minimum number of elements in every corner to not crash. To avoid a too high number of elements and thus a long numerical time, different sizes were used for the heat exchanger and the rest of the reactor. Triangular mesh was directly preferred to the tetrahedral mesh on shape boundaries, though both are isotropic. This latter is not well-suited when there are different element sizes: coarse on the reactor edges, fine in the heat exchanger. Thereby it needed that the whole mesh is rather fine or extra fine. On the shape of the plates and ducts, sweeping mesh was applied. It is an economical way for meshing by creating a surface of mesh on a boundary and then sweeps it from source boundaries to destination boundaries. This gives the advantage to control the number of elements layers and their distribution. This tool is available in the mesh node on Comsol.

Our results had been improved by using successively smaller cell sizes for the calculations. In order to examine the effect of mesh quality, four cases attempted to search for the optimum cell number: (1) fine mesh: 96038 tetrahedral and triangular elements, (2) finer mesh: 126157 tetrahedral and triangular elements, (3) extra fine mesh: 224684 tetrahedral and triangular elements, (4) extremely fine mesh: 398483 tetrahedral and triangular elements. The effects of the cells size on the accuracy of the simulation of fluid velocity and simulation of the material temperature were studied, respectively. When extremely fine mesh was adopted, the accuracy had no significant increase but it tripleed the computation time. Using the fine or finer mesh decreased the stability of computations. Therefore, the extra fine mesh was adopted. The CPU time for solving this model was 17 hours 48 min 30 s on an i7 Dell computer with an Intel Xeon core duo 2.5 GHz processor and RAM of 128 GB).

3.7. Conclusion of the chapter

In this chapter, accent was put on thermal management modelling. After a careful theoretical investigation (pros and cons), the current reactor choice has been justified for the ongoing application. Then, the real system and thermodynamics were described for the direct heat supply mode of the thermochemical sorption heat storage. Finally as important reactor component, the choice of the heat exchanger has been performed using stationary numerical investigations based on the overall heat transfer coefficient, the pressure and temperature drop. It can be seen that a cylinder reactor with a honeycomb heat exchanger exhibit better performances.

As a resume, two transient models adapted to thermochemical reactors under pure water vapour were established. The 3D model concerned the heat and mass transfers coupled to chemical reaction in the salt bed. This model was developed in order to understand and analyze the thermal process of a thermochemical reactor under pure vapour and was used in the last chapter to compare experimental results and if possible explain the observed phenomena. The second model was a 1D model developed here in the only purpose of hydration reaction time determination since mass transfer is not the limiting transfer phenomenon in closed system. However a consolidation of the bed should be checked because in the case of a consolidated bed, it might be the limiting transfer (N'Tsoukpoe et al., 2014b). It helped designing the storage prototype.

Heat and mass transfer coupled to chemical reaction in closed thermochemical storage system are of great importance. Therefore their characterization is necessary in order to determine the corresponding parameters:

1- the thermal conductivity and the specific heat capacity of the bed for the heat transfer and

2- the permeability for the mass transfer.

Then, through thermal analysis the chemical kinetics are performed. The different experiments design and measurements along with results are presented in the next chapter. These results will be used for the simulations.

REFERENCES CHAPTER

Ajzoul, T., 1993. Analyse et optimisation des transferts thermiques dans les réacteurs solide-gaz (Doctorate/Ph.D). University Abdelmalek Essaadji, Morocco.

Azoumah, Y.K., 2005. Conception optimale, par approche constructal, de reseaux arborescents de transferts couplés pour reacteurs thermochimiques (Doctorate/Ph.D). Université de Perpignan, France.

Azoumah, Y., Neveu, P., Mazet, N., 2007. Optimal design of thermochemical reactors based on constructal approach. AIChE J. 53, 1257–1266. doi:10.1002/aic.11152

Balasubramanian, G., Ghommem, M., Hajj, M.R., Wong, W.P., Tomlin, J.A., Puri, I.K., 2010. Modeling of thermochemical energy storage by salt hydrates. Int. J. Heat Mass Transf. 53, 5700–5706. doi:10.1016/j.ijheatmasstransfer.2010.08.012

Bejan, A., 1998. Constructal theory: from thermodynamic and geometric optimisation to predicting shape in nature. Energy Convers. Manag. 39, 1705–1718. doi:10.1016/S0196-8904(98)00054-5

Cadavid, Y., Amell, A., Cadavid, F., 2013. Heat transfer model in recuperative compact heat exchanger type honeycomb: Experimental and numerical analysis. Appl. Therm. Eng. 57, 50–56. doi:10.1016/j.applthermaleng.2013.03.034

Carman, P.C., 1956. Flow of gases through porous media. Academic Press, New-York, USA.

Cascetta, M., Cau, G., Puddu, P., Serra, F., 2014. Numerical Investigation of a Packed Bed Thermal Energy Storage System with Different Heat Transfer Fluids. Energy Procedia 45, 598–607. doi:10.1016/j.egypro.2014.01.064

Chen, N.H., Othmer, D.F., 1962. New generalized equation for gas diffusion coefficient. J. Chem. Eng. Data 7, 37–41.

Comsol, 2014. COMSOL Multiphysics. COMSOL (http://www.comsol.de/release/4.4), Göttingen, Germany.

Duval, F., Fichot, F., Quintard, M., 2004. A local thermal non-equilibrium model for two-phase flows with phase-change in porous media. Int. J. Heat Mass Transf. 47, 613–639. doi:10.1016/j.ijheatmasstransfer.2003.07.005

Elsarrag, E., M. Ali, E.E., Jain, S., 2005. Design guidelines and performance study on a structured packed liquid desiccant air-conditioning system. HVACR Res. 11, 319–337. doi:10.1080/10789669.2005.10391140

Froment, G.F., Bischoff, K., De Wilde, J., 2011. Chemical reactor analysis and design 3rd Ed - G. Froment, Et Al., (Wiley, 2011) BBS crekjkdijfiu [WWW Document]. Scribd. URL http://www.scribd.com/doc/138537099/Chemical-Reactor-Analysis-and-Design-3rd-Ed-G-Froment-Et-Al-Wiley-2011-BBS (accessed 1.29.14).

Huang, H., 2004. Modeling of gas–solid chemisorption in chemical heat pumps. Sep. Purif. Technol. 34, 191–200. doi:10.1016/S1383-5866(03)00192-8

Ishitobi, H., Uruma, K., Takeuchi, M., Ryu, J., Kato, Y., 2013. Dehydration and hydration behavior of metal-salt-modified materials for chemical heat pumps. Appl. Therm. Eng. 50, 1639–1644. doi:10.1016/j.applthermaleng.2011.07.020

Jacobi, A.M., Shah, R.K., 1995. Heat transfer surface enhancement through the use of longitudinal vortices: A review of recent progress. Exp. Therm. Fluid Sci., Generation and Structure of Vortical Flows for Heat Transfer Enhancement 11, 295–309. doi:10.1016/0894-1777(95)00066-U

Jamshidi, N., Farhadi, M., Ganji, D.D., Sedighi, K., 2013. Experimental analysis of heat transfer enhancement in shell and helical tube heat exchangers. Appl. Therm. Eng. 51, 644–652. doi:10.1016/j.applthermaleng.2012.10.008

Janković, B., Mentus, S., Janković, M., 2008. A kinetic study of the thermal decomposition process of potassium metabisulfite: Estimation of distributed reactivity model. J. Phys. Chem. Solids 69, 1923–1933. doi:10.1016/j.jpcs.2008.01.013

Jörimann, U., Riesen, R., 2009. Kinetics - A versatile method for predicting reaction behavior. Webinar - Mettler Toledo, Germany.

Kato, Y., 2007. Chemical Energy Conversion Technologies for Efficient Energy Use, in: Paksoy, H.Ö. (Ed.), Thermal Energy Storage for Sustainable Energy Consumption, NATO Science Series. Springer Netherlands, pp. 377–391.

Kato, Y., Takahashi, F., Watanabe, A., Yoshizawa, Y., 2000. Thermal performance of a packed bed reactor of a chemical heat pump for cogeneration. Chem. Eng. Res. Des. 78, 745–748. doi:10.1205/026387600527743

Lahmidi, H., Mauran, S., Goetz, V., 2006. Definition, test and simulation of a thermochemical storage process adapted to solar thermal systems. Sol. Energy 80, 883–893. doi:10.1016/j.solener.2005.01.014

Legay, M., 2012. Intensification des processus de transfert de chaleur par ultrasons, vers un nouveau type d'échangeur de chaleur : l'échangeur vibrant (Doctorate/Ph.D). Université de Grenoble, Grenoble, France.

Li, Q., Flamant, G., Yuan, X., Neveu, P., Luo, L., 2011. Compact heat exchangers: A review and future applications for a new generation of high temperature solar receivers. Renew. Sustain. Energy Rev. 15, 4855–4875. doi:10.1016/j.rser.2011.07.066

Longuet, B., Gillard, P., 2009. Experimental investigation on the heterogeneous kinetic process of the low thermal decomposition of ammonium perchlorate particles. Propellants Explos. Pyrotech. 34, 59–71. doi:10.1002/prep.200700203

Longuet, B., Pascaud, J.M., Gillard, P., 2006. Chemical reactions thermal transfers and gas diffusion in an energetic material, in: Excerpt from the Proceedings of the COMSOL Users Conference. Presented at the COMSOL Users Conference, Paris - France, p. 5.

Lu, H.-B., Mazet, N., Spinner, B., 1996. Modelling of gas-solid reaction—Coupling of heat and mass transfer with chemical reaction. Chem. Eng. Sci. 51, 3829–3845.

Luo, L., 2013. Heat and mass transfer intensification and shape optimisation - A Multi-scale Approach, 1st ed. Springer London, Nantes, France.

Luo, Z., Wang, C., Xiao, G., Ni, M., Cen, K., 2014. Simulation and experimental study on honeycomb-ceramic thermal energy storage for solar thermal systems. Appl. Therm. Eng. doi:10.1016/j.applthermaleng.2014.07.053

Lu, T.J., 1999. Heat transfer efficiency of metal honeycombs. Int. J. Heat Mass Transf. 42, 2031–2040. doi:10.1016/S0017-9310(98)00306-8

Mao, S., Love, N., Leanos, A., Rodriguez-Melo, G., 2014. Correlation studies of hydrodynamics and heat transfer in metal foam heat exchangers. Appl. Therm. Eng. 71, 104–118. doi:10.1016/j.applthermaleng.2014.06.035

Mauran, S., Lahmidi, H., Goetz, V., 2008. Solar heating and cooling by a thermochemical process. First experiments of a prototype storing 60kWh by a solid/gas reaction. Sol. Energy 82, 623–636. doi:10.1016/j.solener.2008.01.002

Mazet, N., Amouroux, M., Spinner, B., 1991. Analysis and experimental study of the transformation of a non-isothermal solid/gas reacting medium. Chem. Eng. Commun. 99, 155–174. doi:10.1080/00986449108911585

Mbaye, M., Aidoun, Z., Valkov, V., Legault, A., 1998. Analysis of chemical heat pumps (CHPS): basic concepts and numerical model description. Appl. Therm. Eng. 18, 131–146.

McMahon, M., Wallace, O., 2003. What Is a Chemical Reactor? [WWW Document]. wiseGEEK. URL http://www.wisegeek.com/what-is-a-chemical-reactor.htm (accessed 1.29.14).

Michel, B., 2012. Procédé thermochimique pour le stockage intersaisonnier de l'énergie solaire : modélisation multi-échelles et expérimentation d'un prototype sous air humide (Doctorate/Ph.D). Université de Perpignan, Perpignan - France.

Michel, B., Mazet, N., Neveu, P., 2014a. Experimental investigation of an innovative thermochemical process operating with a hydrate salt and moist air for thermal storage of solar energy: Global performance. Appl. Energy 129, 177–186. doi:10.1016/j.apenergy.2014.04.073

Michel, B., Neveu, P., Mazet, N., 2014b. Comparison of closed and open thermochemical processes, for long-term thermal energy storage applications. Energy 72, 702–716. doi:10.1016/j.energy.2014.05.097

Neveu, P., Castaing-Lasvignottes, J., 1997. Development of a numerical sizing tool for a solid-gas thermochemical transformer—I. Impact of the microscopic process on the dynamic behaviour of a solid-gas reactor. Appl. Therm. Eng. 17, 501–518. doi:10.1016/S1359-4311(96)00065-8

Neveu, P., Tescari, S., Aussel, D., Mazet, N., 2013. Combined constructal and exergy optimisation of thermochemical reactors for high temperature heat storage. Energy Convers. Manag. 71, 186–198. doi:10.1016/j.enconman.2013.03.035

Nowak, W., Arthkamp, J., Weddeling, K., 2010. BHKW - Grundlagen, seite 11.

N'Tsoukpoe, K.E., Restuccia, G., Schmidt, T., Py, X., 2014. The size of sorbents in low pressure sorption or thermochemical energy storage processes. Energy 77, 983–998. doi:10.1016/j.energy.2014.10.013

Olives, R., Mauran, S., 2001. A highly conductive porous medium for solid–gas reactions: effect of the dispersed phase on the thermal tortuosity. Transp. Porous Media 43, 377–394.

Oró, E., Chiu, J., Martin, V., Cabeza, L.F., 2013. Comparative study of different numerical models of packed bed thermal energy storage systems. Appl. Therm. Eng. 50, 384–392. doi:10.1016/j.applthermaleng.2012.07.020

Pardo, P., Anxionnaz-Minvielle, Z., Rougé, S., Cognet, P., Cabassud, M., 2014. Ca(OH)2/CaO reversible reaction in a fluidized bed reactor for thermochemical heat storage. Sol. Energy 107, 605–616. doi:10.1016/j.solener.2014.06.010

Prabhanjan, D.G., Raghavan, G.S.V., Rennie, T.J., 2002. Comparison of heat transfer rates between a straight tube heat exchanger and a helically coiled heat exchanger. Int. Commun. Heat Mass Transf. 29, 185–191. doi:10.1016/S0735-1933(02)00309-3

Raju, M., Kumar, S., 2010. Modeling of a helical coil heat exchanger for sodium alanate based on-board hydrogen storage system, in: Excerpt from the Proceedings of the Comsol Confernce. Presented at the COMSOL Multiphysics Conference, Boston, USA, p. 8.

Rambaud, G., 2009. Problématique des transferts en milieu poreux réactif déformable pour procédés de rafraîchissement solaire (Doctorate/Ph.D). Université de Perpignan, France.

Schaube, F., Wörner, A., Tamme, R., 2011. High Temperature Thermochemical Heat Storage for Concentrated Solar Power Using Gas–Solid Reactions. J. Sol. Energy Eng. 133, 031006–031006. doi:10.1115/1.4004245

Shapiro, A.H., 1953. The dynamics and thermodynamics of compressible fluid flow, Ronald Press Co. ed. Ronald Press Co., USA.

Techniques de l'ingénieur, 1999. Echangeurs de chaleur à contact direct, © Techniques de l'Ingénieur, traité Génie énergétique. Techniques de l'ingénieur, France.

Vyazovkin, S., 2002. Thermal Analysis. Anal. Chem. 74, 2749–2762. doi:10.1021/ac020219r

Vyazovkin, S., Burnham, A.K., Criado, J.M., Pérez-Maqueda, L.A., Popescu, C., Sbirrazzuoli, N., 2011. ICTAC Kinetics Committee recommendations for performing kinetic computations on thermal analysis data. Thermochim. Acta 520, 1–19. doi:10.1016/j.tca.2011.03.034

Wagman, D.D., Evans, W.H., Parker, V.B., Schumm, R.H., Halow, I., 1982. The NBS Tables of Chemical Thermodynamic Properties. Selected Values for Inorganic and C1 and C2 Organic Substances in SI Units,.

Wen, D., Ding, Y., 2006. Heat transfer of gas flow through a packed bed. Chem. Eng. Sci. 61, 3532–3542. doi:10.1016/j.ces.2005.12.027

Yutaka, A., Hiroshi, N., Faghri, M., 1988. Developing laminar flow and heat transfer in the entrance region of regular polygonal ducts. Int. J. Heat Mass Transf. 31, 2590–2593. doi:10.1016/0017-9310(88)90186-X

Zhang, L., Hihara, E., Matsuoka, F., Dang, C., 2010. Experimental analysis of mass transfer in adiabatic structured packing dehumidifier/regenerator with liquid desiccant. Int. J. Heat Mass Transf. 53, 2856–2863. doi:10.1016/j.ijheatmasstransfer.2010.02.012

Zhang, S., Xiao, R., Zheng, W., 2014. Comparative study between fluidized-bed and fixed-bed operation modes in pressurized chemical looping combustion of coal. Appl. Energy 130, 181–189. doi:10.1016/j.apenergy.2014.05.049

Zheng, L., Wu, D., Pan, B., Wang, Y., Sun, B., 2013. Experimental investigation and numerical simulation of heat-transfer properties of metallic honeycomb core structure up to 900 °C. Appl. Therm. Eng. 60, 379–386. doi:10.1016/j.applthermaleng.2013.07.014

Zondag, A., Kalbasenka, A., van Essen, M., 2008. First studies in reactor concepts for
    Thermochemical Storage., in: Of the Eurosun 2008, 1st Interna- Tional Conference on So-
    lar Heating, Cooling and Buildings. Presented at the EUROSUN 2008, Proceedings of Eu-
    rosun 2008, Lisbon, Portugal, p. 6.
Zondag, H., Kikkert, B., Smeding, S., Boer, R. de, Bakker, M., 2013. Prototype thermochemical heat
    storage with open reactor system. Appl. Energy 109, 360–365.
    doi:10.1016/j.apenergy.2013.01.082

4. CHARACTERIZATION OF THERMAL TRANSFERS AND CHEMICAL KINETICS

Transport phenomena in porous media have been the focus of many engineering and academic research investigations. Most of the applied studies dealt with low porosity media such as granular materials and packed beds. The widespread range of applications of thermochemical materials has led to an increase in the interest of modelling the heat and mass transfer phenomena coupled to chemical reaction in such porous media. It can be noticed that the precise determination of thermal conductivity, specific heat capacity, permeability and chemical kinetic is required for accurate modelling of the thermal transport through packed or granular beds of thermochemical storage systems.

4.1. Heat transfer characterization (thermal conductivity and specific heat capacity)

In thermal engineering where thermal transport is always involved, scientists or engineers have to manage or to know the thermal properties of the used materials in order to design or choose an appropriate system. In thermal energy storage application, particularly the thermochemical and sorption thermal storage (Yu et al., 2013), the material development plays an important role. Thermal energy storage operates in open or closed systems (Yu et al., 2013). For the closed one, heat transfer is responsible for the storage performance (van Helden and Hauer, 2013a). Therefore the material property for the three heat transfer mode has to be determined (Kaviany, 1999). There are three mechanisms whereby heat can be transported from one region of space to another under the influence of a temperature difference. One is by transmission in the form of electromagnetic waves (radiation); the second is the process of convection, in which a bulk or local motion of the material effects the transport; and the final process is that of thermal conduction, when energy is transported through a medium. In most practical situations, heat transport is accomplished by all three processes to some extent, but the relative importance of each contribution varies markedly. In the case of solid-gas interaction and low temperature application in a packed bed, conduction is prominent compared to convection and radiation (Wen and Ding, 2006). Among the three, that of thermal conduction is the simplest to describe in principle, since the empirical law of Fourier simply states that the heat transported by conduction per area unit in a particular direction is proportional to the gradient of the temperature in that direction. The coefficient of proportionality in this law is known as the thermal conductivity and denoted here by the symbol λ.

Thermal conductivity is not strictly a property of the material since it can often depend on a large number of parameters, including the origine of the material, its method of manufacture, and even the character of its surface. The fact that in most practical situations all three heat transfer mechanisms are present, complicates the process of measurement of the thermal conductivity. Thus, much early work in the field is substantially in error, and it has been really quite difficult to devise methods of measurement that unequivocally determine the thermal conductivity. For that reason, the instruments to be described in the following sections often seem to be rather far from the apparent simplicity implied by Fourier's Law.

Evaluating the thermal conductivity of the used material is a requirement for closed thermal energy storage systems. As for a material, thermal conductivity is a key factor as well as heat transfer of the apparatus which is depending on thermal conductivity of the container, heat exchanger and convectional heat transfer coefficients of the working fluid (van Helden and Hauer, 2013a). The test and characterization of storage materials is crucial for the development

and evaluation of novel material approaches. The task 42/24 (van Helden and Hauer, 2013a) of the joint international energy agency and the solar heating and cooling/energy conservation through energy storage program (IEA-SHC/ECES) has been working on material development for several years, trying to characterise them in order to proceed with optimisation. Laboratory techniques used to measure thermal conductivity of thermochemical materials as particle or packed bed can be classified into three main categories: steady-state, quasi-steady and non-steady-state (transient) methods (Degiovanni, 2012). The purpose of of measuring that thermal property is to know the material capacity to transfer heat, so it could be improved; and to be used in computer codes for large structures calculation. The quasi-steady proceeds by simultaneous measurement of the heat flow (usually constant) and the temperature (time-dependent) for which the parameters identification takes long time. Alrtimi et al. resumed the three classes of methods into two, where they mentioned that transient method procedures are simpler, but the steady state methods are considered more accurate (Alrtimi et al., 2014).

In a reactor for thermochemical storage based on salt hydrates, hydration reaction rate is strongly linked to the thermal conductivity of the salt bed. Reaction rate increases with the effective thermal conductivity of the salt (Michel, 2012). Knowing that salts in general have a low thermal conductivity, composites based on salts are generally synthesized in order to enhance the thermal conductivity. Composite materials are based on host porous carrier matrix and a salt. The host matrix fulfils different functions: it defines the stability, the shape, and the size of the material, which can be specially adapted for the application (van Helden and Hauer, 2013b). Literature on thermal conductivity measurement of salt hydrates is not broad and there are only few using calorimetric methods. Measurements of the thermal conductivity of salt hydrates are relatively rare and are scattered throughout the scientific and technological literature. Decades ago, Hakvoort evocated a possibility of porous media thermal conductivity measurement, using a differential scanning calorimetry (DSC) (Hakvoort et al., 1985). Guanghua and Zhi-ying have also performed some DSC measurements by concluding with uncertainties on results between 2 and 3% (Guanghua, 2004; Guanghua and Zhi-ying, 2002). Iverson et al. determined the thermal conductivity of molten nitrate salts using a DSC. The direct determination was closed to the regression data determination and results fitted to those described in the literature (Iverson et al., 2011). Some attempts have been performed on pure salts and composites (Fopah Lele et al., 2013). Concerning composites based salt hydrates or hosts, Freni et al. measured by means of quasi-steady method (hot wire) the thermal conductivity of silica gel/$CaCl_2$ under various conditions of pressure and temperature (Freni et al., 2002). They used the results (constant and temperature dependent thermal conductivity) for the simulation of a dynamic model. The drowned conclusion was that, the use of a constant value of thermal conductivity leads to 30% uncertainty in specific power of the thermal system. Transient thermal conductivity measurements were conducted on pure $CaCl_2$ and natural graphite soaked in sulphuric acid-calcium chloride, and the results highlighted an important enhancement of thermal conductivity with a magnitude of 2 (Jiang et al., 2014, 2012). Steady conductivity measurements were performed on silica gel by (Gurgel et al., 2001; Gurgel and Klüppel, 1996) with proper accuracy. Until now, the available thermal conductivity property of salts was revealed when working with in a specific field of application. Two different devices working on transient and steady state methods were used in this chapter to determine the thermal conductivity. In this work, thermal conductivity measurements of the most used salt hydrates in thermochemical energy storage and some composites are performed using these two different methods. A validation of the method, mainly for salt hydrates was performed through comparison with literature. The

presented results were also intended to be used on the heat and mass transfer modelling that occurs in thermochemical and sorption systems.

4.1.1. EXPERIMENTAL METHODS

Thermal conductivity characterises the ability of a material to conduct heat. Traditional methods for measuring the thermal conductivity of materials comprise imposing a temperature gradient upon a material of known geometry, and a measure of the heat flow through the material. There are a number of possible ways to measure thermal conductivity, each of them suitable for a limited range of materials, depending on the thermal properties and the medium temperature. In this section, the steady and the transient methods, respectively were used for the same material samples. Among several transient state methods (Lei et al., 2009; Zhang and Fujii, 2000), the flash method was considered as it was the main technique for thermal conductivity measurement of solids (Parker et al., 1961). The DSC was also chosen because it performed quick measurements using small samples and took into account the experimental time which modified the output signal in the calorimeter (differential power ∆P) and Hakvoort demonstrated its feasibility with solid materials (Hakvoort et al., 1985; Camirand, 2000). Besides, the samples were able to be easily and rapidly changed and the measurement was not restricted to a set of discrete temperatures. Among steady state methods, Xamán and co-workers stated that the guarded hot plate (GHP) was considered as the most accurate and precise technique for low thermal conductivity materials (Xamán et al., 2009; Degiovanni, 2012). However, the radial method which was a bit close to the GHP was able to yield an accurate measurement within ±4% and reached ±2% with a careful handling (Presley and Christensen, 1997). Now, the exact geometry of the GHP depends on the material state (powder, grains, plate, pellets). As thermochemical heat storage in our case was based on inorganic salts under powder form, a self-made device had been designed with a heating element guarded in the material. The all-in-one in a small-scale vessel was called guarded hot cartridge (GHC). The designed device was a radial flow apparatus with its principle described in (Presley and Christensen, 1997). Each used apparatus will be presented in details in the following.

4.1.1.1.   The differential scanning calorimeter (DSC)

The heat flux calorimeter TGA-DSC 1 (Figure 4.5) from Mettler Toledo©, which allows simultaneous weigth and heat flux measurements, was used for the measurements. The working principle of such calorimeter was well described in (N'Tsoukpoe et al., 2014). However, in this case, the main purpose was to analyse the heat fluxes and the temperature through the sample in order to evaluate the thermal resistance of this latter. In the DSC cell, both, temperature and heat flow were measured at the contact area between sample and sensor (Fopah Lele et al., 2013). The temperature at the opposite side of the sample could not be measured directly, but by applying a pure metal, placed on top of the sample, the temperature of that opposite side was known during the melting of the metal (Hakvoort et al., 1985). The thermal conductivity could be measured without modification of the DSC cell, using a method based on the assumption that the bottom side of the sample at the heat source follows an applied modulation (Marcus and Blaine, 1994), implying no thermal resistance between the sample and the furnace (Merzlyakov and Schick, 2001). The porous and host materials were measured at different heating rates with nitrogen flow rate of 50 ml·min⁻¹. The heating rate of 10 °C·m⁻¹ was adopted due to the consistency of results obtained. The amount of materials used is around 0.1 g. For the calibration, two sensor materials, Gallium and Indium, with known thermal conductivities, gave clear different melting peaks at 29.7 °C and 156.6 °C respectively (standard deviation of the used

device was 0.0006 W for the heat flow and of 0.03 °C for the temperature). However, Gomez et al. affirmed that DSC was able to perform thermal property measurements with low uncertainty, if the calibration was carefully performed (Gomez et al., 2012). In addition to the given resolution on DSC, the results could be meaningfully interpreted with up to four significant digits. For each sensor material, three measurements were made in order to find the accurate one to use it in the final measurements. Then an adjustment was made in order to scope the apparatus to the calibration sample parameters. Finally, a re-calibration was performed to validate the calibration process. At the first step of the DSC measurements, sensor material pellets (diameter = 1 mm) prepared under atmospheric pressure were placed in an aluminium pan and then the melting curves were determined (Figure 4.1a). At the second step, the sensor material was placed on top of the sample of material which was not compacted in the aluminium pan. The pan had an inner diameter of 5 mm and a specific height of 5.1 mm.
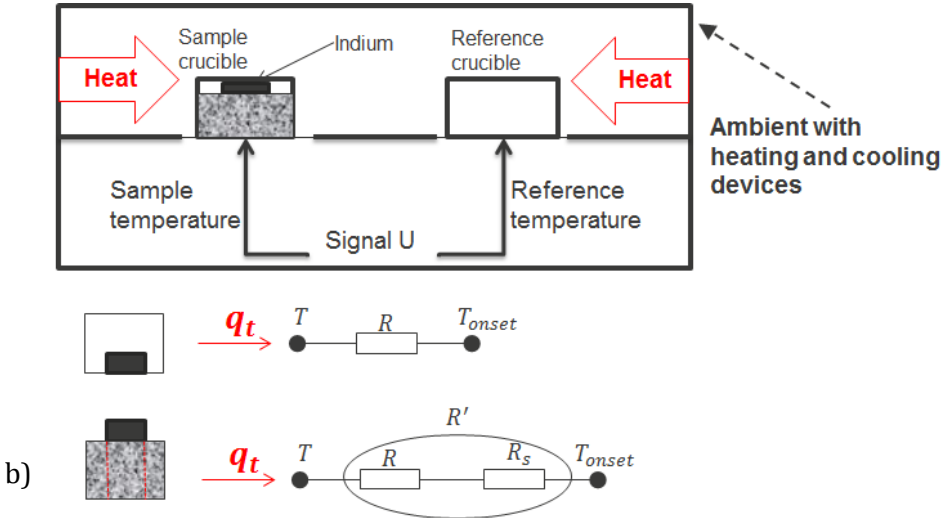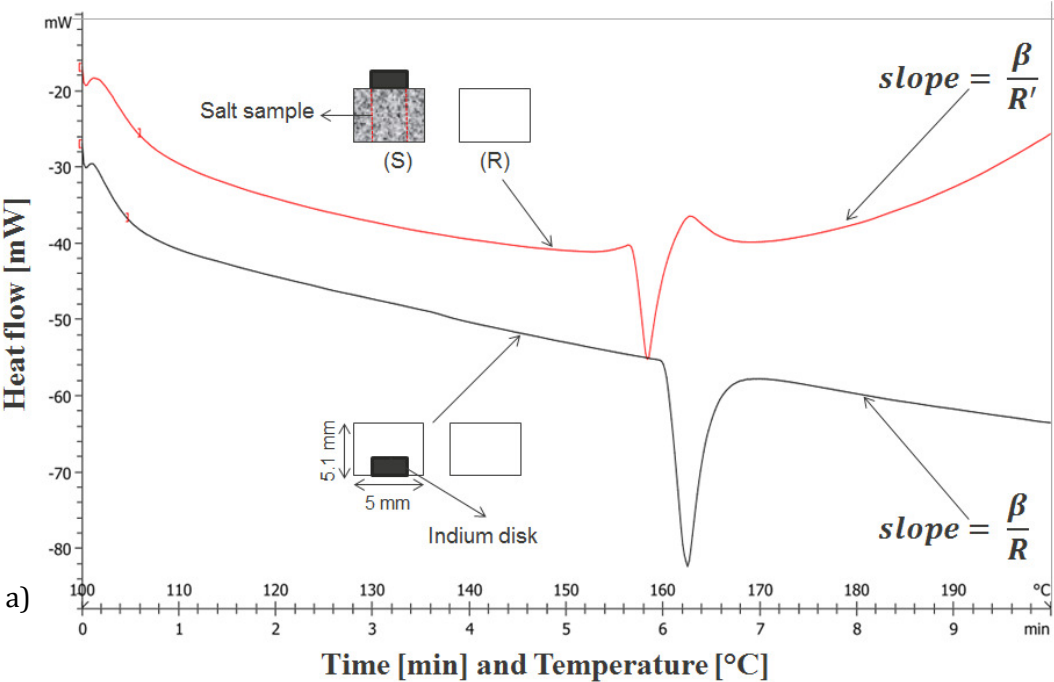
Figure 4.1. a) The schematic description of the measurement, showing aluminium pans, the reference (R) and the sample (S) with the corresponding melting curves of Indium on top of the sample and the Indium alone. b) The physical model of the DSC measurement.

However, the sample height in the pan was about 4.9 mm. The surface area ($A_s = 7.8 \times 10^{-7}\ m^2$) of the Indium corresponded to the exact surface area of the sample (delimited by red line in Figure 4.1a) where the thermal resistance was measured. Subsequently the DSC measurements were carried out again until the sensor material melted. Heat flux DSC determines the amount of heat absorbed or released by a sample upon a change of the sample temperature. For this, the temperature development of the sample crucible in a furnace was compared to the temperature of an empty reference crucible in a symmetric position, as shown in Figure 4.1b. The signal U of a DSC was the temperature difference or a thermocouple voltage.

This previous configuration, though results are quite satisfactory, allowed a heat loss. Therefore a wrong or not accurate thermal resistance evaluation might occured. Hakvoort obtained best results when the sensor totally covers the sample or having the same cylindrical diameter of the sample with a height not more than 3 mm (Hakvoort et al., 1985). Due to technical limitations, measurements with 1 mm diameter Indium pills were performed. The purpose of this measurement was to determine the thermal conductivity values from an adaptation to Camirand's method (Camirand, 2004) which is an improvement of the method presented by Flynn et al. (Flynn and Levin, 1988). The method used here, utilised the measurement of the rate of heat flow into a sensor material during its first order transition to obtain the thermal resistance of a material placed between the sensor material and the heater in DSC. Starting at low temperature, when the indium was solid, sample and reference pans were heated with a constant heating rate (1, 5 and 10 °C·m⁻¹) and the heating rate to be selected was the one for which melting of sample could be avoided instead of using a constant number as Camirand did. The sensor temperature and the DSC signal were recorded against time. During melting of the sensor (Indium), the temperature of the sensor had to be constant, so that the top of the sample remained at constant temperature, while the temperature of the lower side of the sample increased at a constant rate. A scan was performed to measure the differential power produced during the melting of the sensor substance. The obtained curve tended to decrease linear before the melting and decreased exponentially during melting (Figure 4.1).

The thermal resistance (R_{th}) to heat flow through a sample is a constant between the thermal power (q_t) and temperature difference between the heater and the melted sensor. The proportionality could be expressed as follows:

$$q_t = \frac{[T(t) - T_{onset}]}{R_{th}} \tag{4.1}$$

Taking up the slopes of the DSC curves at melting stage of the sensor material, the thermal resistance of the sample is determined by difference between the measurement with the Indium on top and without as follows:

$$R_s = R - R' \tag{4.2}$$

where, R is the thermal resistance between calorimeter and sensor material, R' is the thermal resistance between calorimeter and sensor material on top of the sample (see Figure 4.1).

Measurement of the slope of the decreasing part of the curve allowed the determination of the thermal conductivity of the sample. Taking into account all the thermal resistances, the slope could be defined from the linear side of the melting peak (Iverson et al., 2011). The slope calculation was based on the principle of Figure 4.2 with the aid of the STARe software from Mettler Toledo. The first derivative of the heating curve (meaning the thermal power against the time) gave a specific slope which is further divided by the heating rate. Therefore, the following expression could be obtained:

$$Slope = \beta \cdot \frac{q_t(t) - q_{t\_onset}}{T(t) - T_{onset}} = \frac{\beta}{R_{th}} \qquad (4.3)$$

where q_{t_onset} and T_{onset} were the heat flow and melt temperature of salt at the onset of melting. $q_t(t)$ was the thermal power at a given time, β the heating rate and R_{th} the thermal resistance (can be R or R' depending of what is measured). This correlation of temperature in the material to the thermal resistance is in principle similar to the resistance temperature detector (RTD) where only the thermal resistance was measured and correlated to the temperature.
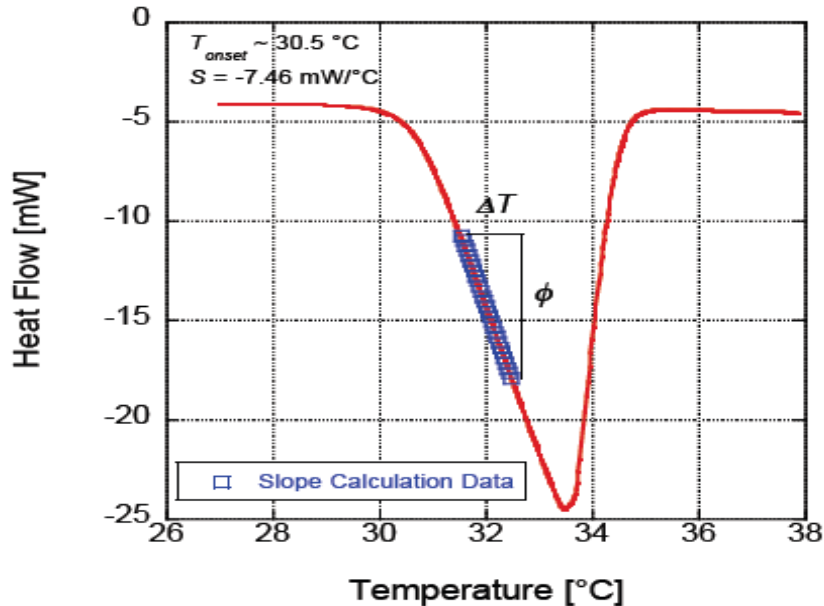
Figure 4.2. Slope calculation example from the "heat flow vs. temperature" curve for a salt sample (Iverson et al., 2011).

It clearly showed the heating rate dependence. The obtained total (crucible, sample and sensor) thermal resistance in comparison with the thermal resistance of the sensor and the crucible yielded directly to the thermal conductivity as follows:

$$\lambda_s \ = \ \frac{L_s}{A*R_s} = \ \frac{L_s}{A*(R-R')} \tag{4.4}$$

where, L_s was the sample height and A is the contact area between sample and sensor material.

The method used, requires an accurate measurement of the axial (middle central line of the crucible) temperature gradient to the sensor at the bottom. If not properly accounted for, some uncertainty may lead to inaccurate heat flow measurement. Some possible uncertainty sources may occured from thermal contact with the bottom of the pan, it is not good enough. Samples are not thin enough and no lid is used to cover the sample in order to maintain the contact.

4.1.1.2.   The guarded hot cartridge (GHC)

This test stand was based on radial heat conduction and the use of a cylindrical vessel designed to work under atmospheric pressure at steady state conditions (Figure 4.3). The sample of test material was packed as a powder or granular bed within a stainless steel tube limited at the upper and lower ends by stainless steel disks. An electrical cartridge heater, 8 mm in diameter, dissipated a heat flux in the radial direction of the cylinder. Four Pt 100 temperature sensors were radially located along the diameter of the cylinder (Figure 4.3).
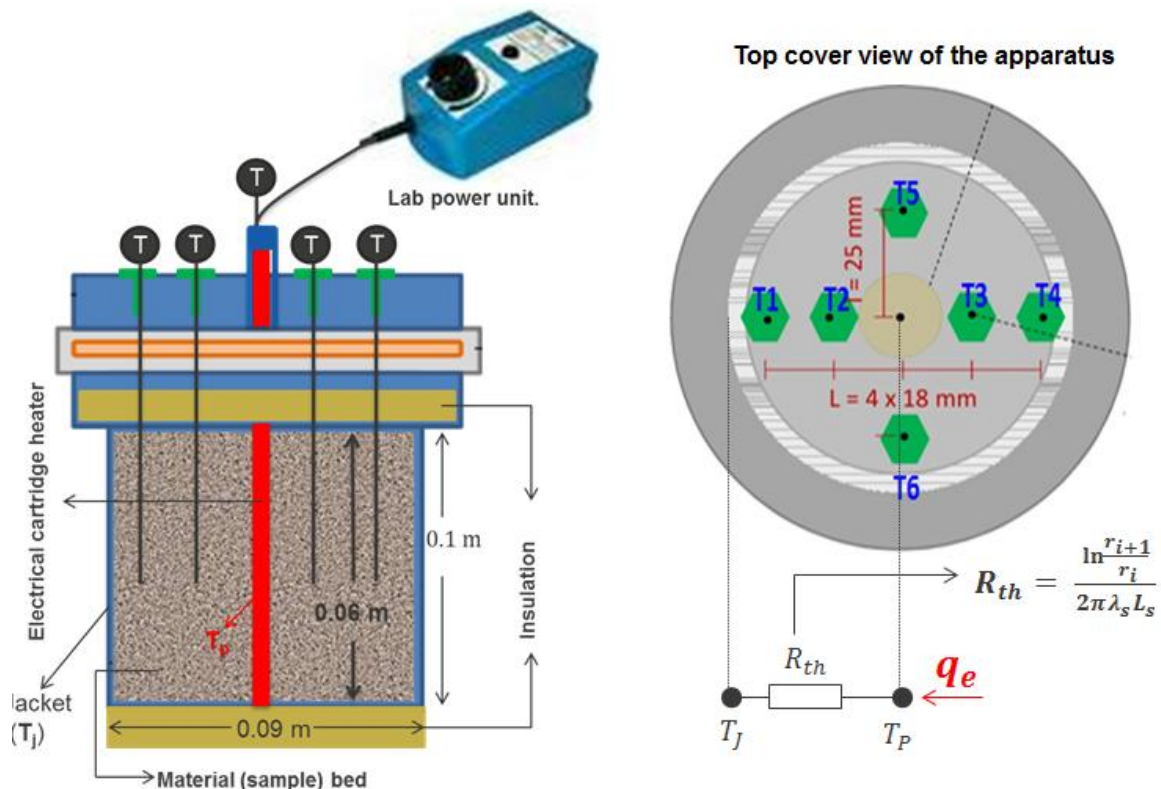
Figure 4.3. Intermediate Reactor as radial heat flow apparatus for thermal conductivity measurement (adapted from (Gurgel et al., 2001; Gurgel and Grenier, 1990)) along with model analogy.

The applied temperature sensors (precision of 0.3 °C) measured 1.5 mm in diameter and 57 mm in active length (the part embedded in the bed) of a sample. The top and the bottom were well insulated using an insulating paste (KAIMANN EPDM PL32-R, thickness 32 mm), in order to insure only radial temperature gradients.

The bed length is shown in Figure 4.3. The heat flow area was around 0.0169 m². The use of this apparatus required a calibration of the thermocouples. The validation experiment was performed using a fluid (dry air) and solid (glass) of known thermal conductivity filling the gap. The well known thermal conductivity of air was (as a function of temperature) and was available as tabulated data in (Lide, 2005). In an experiment conducted with dry air, heat transferred across the gap could be determined using Fourier law of heat conduction, assuming that the air in the reactor is not in motion. The heat input to the electrical heater was given by the power unit and the difference between the heater and the cylinder jacket represented the heat loss. The experiment was conducted with different amounts of electrical power input (and hence different temperature difference across the air layer). It was represented as a function of the temperature difference across the gap. So, the heater voltage (V), the current intensity (I) through the heater resistance (R_h) which delivers the plug-in temperature (Tp); and the jacket temperature (Tj) given as the room temperature, needed to be known.

Steady state conductivity measurements were performed by dissipating a constant heat power q in the axis of the sample bed, while the external cylinder wall was kept at room temperature of 21 °C ± 2°C. The temperatures $T(r_i, t)$, at the radial locations r_1 to r_4 were recorded until the steady state condition was reached. The conductivity of the sample bed was then calculated from the Fourier radial-dimensional heat conduction Eq. (4.5):

$$\lambda_s = \frac{q_e}{2\pi L_s} \cdot \frac{d(\ln\frac{r_{i+1}}{r_i})}{dT}$$

(4.5)

where $dT/d(\ln\frac{r_{i+1}}{r_i})$ represented the slope on the temperature fitting curve and L_s was the sample axial length. As stated by Presley and Christensen, inaccuracies in this method occured from longitudinal heat loss, convection currents, radiation losses, thermal expansion of the sample or core heater, perturbation of the heat flow by the thermocouples, and unsymmetrical heat flow (Presley and Christensen, 1997). The three first reasons were minimized using an insulating paste as shown in Figure 4.3.

The slope and the occurring uncertainty were both obtained with the LinearFit function using the software Origin 9.0. Eq. (4.4) was based on the following assumptions:

- unidirectional heat conduction,

- variations of temperature along the flow direction,

- temperature difference is very small compared to the mean temperature of the medium.

The uncertainty introduced by the assumption of one-directional heat conduction was verified by Gurgel et al. (Gurgel et al., 2001). The authors concluded that the axial heat losses will have a negligible influence (less than 1%) on the measurement of low thermal conductivity of material with a ratio of length to the diameter of the sample bed greater than 2.5. In the present case, this rapport was much lower than 2.5. Hence a calibration is performed with dry air as mentioned in the above section, to evaluate the useful heat transferred in the bed. Thermal conductivity of air is well known (as a function of temperature) and a mean value of 0.03 W·m⁻

[1]·K^{-1} for temperature range from 0 °C to 327 °C was used (Lide, 2005). An experiment was conducted with dry air; heat transferred across the bed is determined using Fourier law of heat conduction. Direct evaluation of the thermal conductivity based Eq. (4.5) was complex. Thus, for most practical applications, the parameters were obtained from the best fit to the experimental data.

In order to ensure the useful electrical power supplied in the bed, some blank measurements on empty cylinder were performed. The blank measurement was a process to eliminate the disturbance, some systematic uncertainties and buoyancy effect (in the case of DSC) in order to perform a differentiation and ensure the useful heat in the material. In the DSC, this measurement was automatized during the temperature program settings. In the GHC, the air-filled reactor was subjected to the heating and thermocouples recorded the temperature variation between the heating element and the outer jacket surface. It was considered as the heat calibration during the process.

The heat supplied by the electrical power device can be writing as follows:

$$P = V \cdot I \tag{4.6}$$
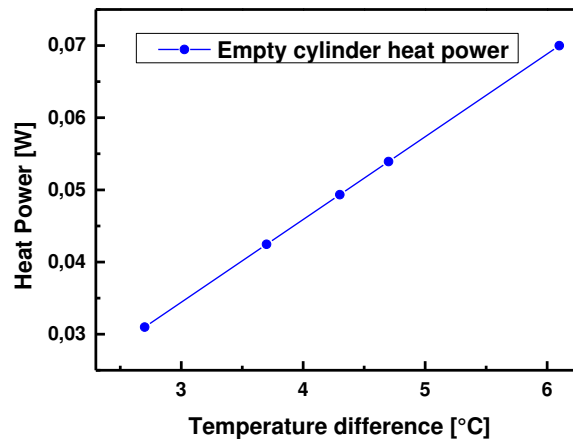
Figure 4.4. Heat evaluation of the empty (only air) GHC for thermal conductivity measurement.

The heat data from empty cylinder were measured in the experimental apparatus and was shown as a plot in Figure 4.4. The data showed linear behaviour. Hence the heat from empty cylinder was represented as a linear function of the temperature difference across the bed using regression analysis. The heat power from the empty cylinder was a function of temperature difference and was given by the following polynomial:

$$L = 0.0115 \cdot \left(T_p - T_j\right) \tag{4.7}$$

with $\Delta T = (T_p - T_j)$. The heat power calibration itself was estimated by the above formula with an uncertainty bar less than ± 1%.

4.1.1.3. Specific heat capacity

The specific heat capacity is an important, temperature-dependent material property and is often available in material data sheets. But when unavailable, it can be conveniently and reliably measured by DSC according to the DIN 51007. The specific heat capacity is a key property for the safety analysis of thermochemical processes and the design of thermochemical reactors. The developed method procedure was as follows:

From a typical DSC scan, explained in Figure 4.5, the specific heat capacity of the scanned material was calculated from the displacement in the baseline before and after the start of the transient, at the very start of the scan. In this work, in analogue to the starting transient, two isothermal steps were imposed at the temperatures (60 and 90°C), where heat capacity was required. With slow heating rate (2K·min⁻¹) and adequate isothermal step (5 min), equilibrium condition was reached: the heat continued to flow in an exponential decay until the difference between the sample pan and the empty pan diminished. Similar approach has been performed, but in a more dense technique, in the Temperature Modulated Differential Scanning Calorimetry (TMDSC), and by PerkinElmer Instruments in the StepScan™ DSC (SSDSC) (Schick, 2002). This is by applying continuous temperature steps, in time domain, covering the whole scanned range, as can be seen in Figure 4.6. Heat capacity was then calculated by two methods, either from the displacement or from the area of the generated isothermal step, highlighted in Figure 4.6.
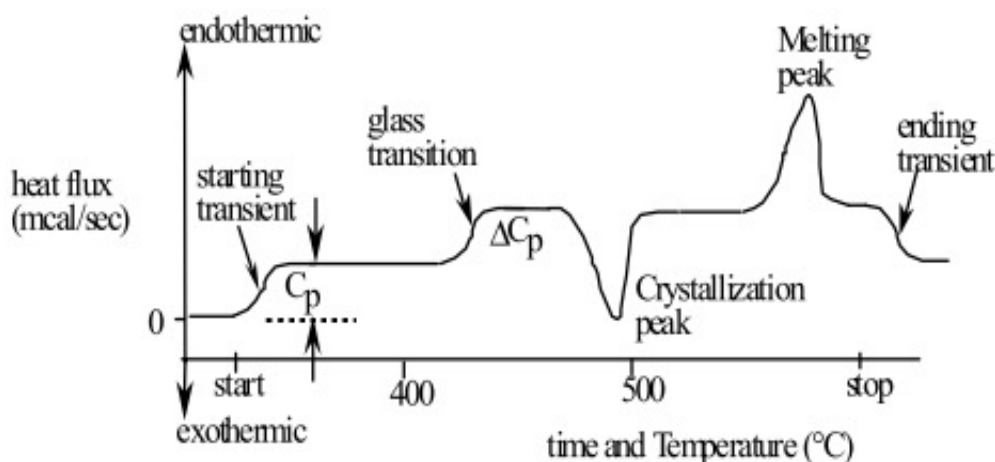
Figure 4.5. The classic DSC heat flow scan showing the shift in baseline at the starting transient where the heat capacity is calculated (Colby College, 2007).

From the displacement in heat flow (mW), heat capacity is calculated, as follows:

$$\frac{dq_t}{dt} = C_p \cdot \frac{dT}{dt} = C_p \cdot \beta \tag{4.8}$$

Where $\frac{dq_t}{dt}$ is the DSC heat flow signal or the displacement at the isothermal step (mW), C_p is the sample specific heat multiply by the sample weight and β the heating rate, here 2 °C·min⁻¹ = 0.03 °C·s⁻¹. Therefore the specific heat capacity of the material can be determined as follows:

$$c_p = \frac{dq_t}{dt} \cdot \frac{K_{cp}}{m \cdot \beta} \qquad (4.9)$$

where K_{cp} is the heat capacity calibration constant. It was determined from a third scan, of standard material (with known specific heat capacity like aluminum or sapphire). All were scanned at identical conditions of heating rate, and temperature range.
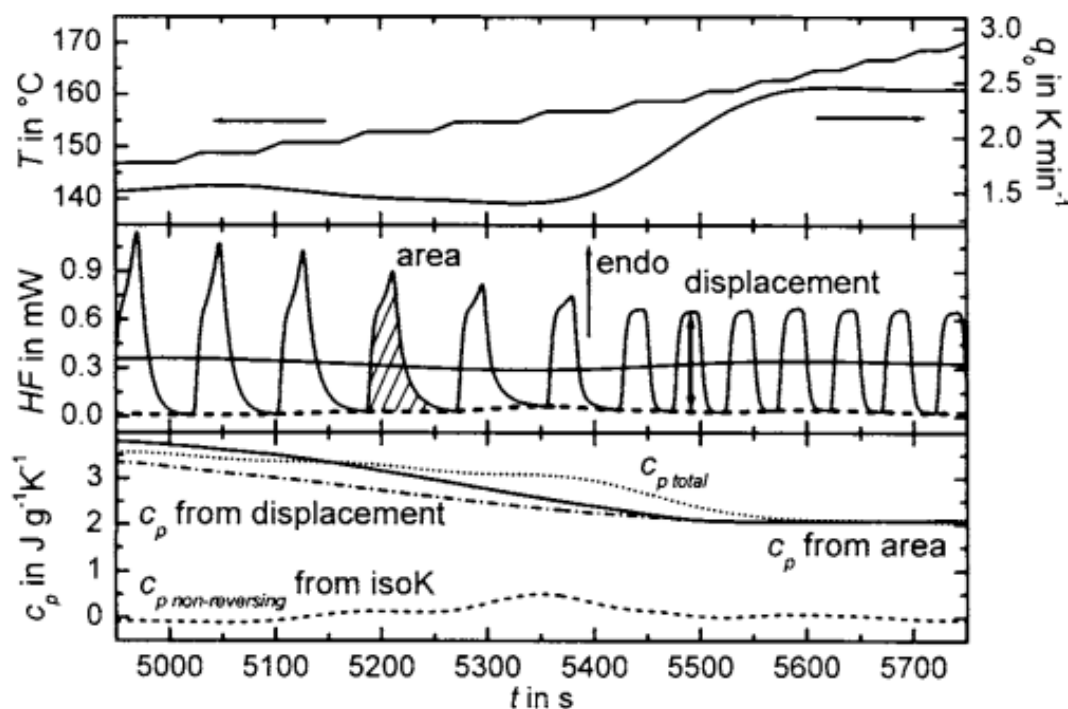
Figure 4.6. The approach used by PerkinElmer Instruments in the StepScan TM DSC (SSDSC) (Schick, 2002).

Eq. (4.9) stands for calculating heat capacity based on displacement at isothermal (**method one**) of the signal (mW). From a scan of standard material (Aluminum, in Figure 4.7), at identical scanning conditions, the calibration factor is calculated ($C_{p\_Al} \cdot m_{Al}/Al_{displacement}$). **Method two** is based on the area under the curve (J·g^{-1}) at the isothermal step, multiplied by a calibrating factor (C_{p_Al}/Al_{area}). Different weights of each material were scanned and the average value was used.

Repeated baseline scans for empty pans are strongly required to determine the zero line. On the other hand, ensuring zero baseline reproducibility was the most difficult step in this approach. This was due to natural changes in the background temperature of the machine and in the surrounding air temperature throughout the day. It was found that baseline shift causes an error of about 10% in the calculation process of heat capacity. That shift made baseline determination practically very difficult. Alternative methods that give indication about specific heat capacity directly from the DSC scan is a solution. In this work, two methods were developed, for direct heat capacity measurements from one scan only, with a potential of 1% precision, using the DSC.
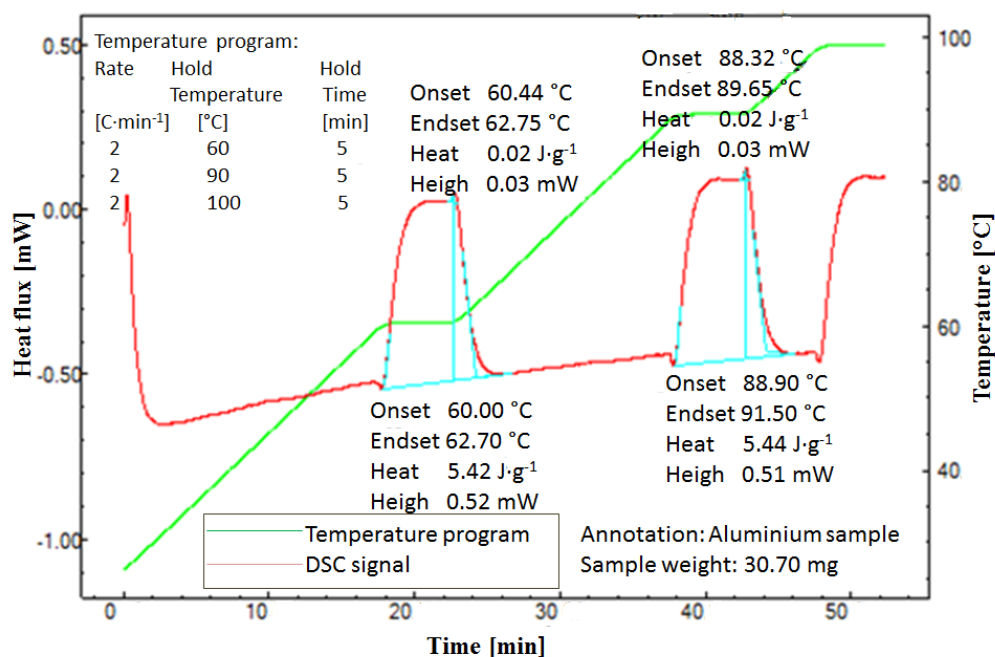
Figure 4.7. Aluminium DSC heat flow scan showing peak net heights (0.54 mW) and the area under the curve (5.4 J·g⁻¹) at two isothermal temperatures (60 and 90°C). Overshoots of height and area were subtracted (measurements, Dr. Haiam, Auckland University).

4.2. MASS TRANSFER CHARACTERIZATION (PERMEABILITY)

Fluid flow and transport processes through porous structures are topics of great interest in various scientific and technical fields, and the permeability and porosity are those parameters which decide whether the material can be used in a thermochemical/sorption reactor bed or not. Permeability in literature is defined as the ability of the fluid to flow through a material and its unit is "m^2". Whereas the porosity or void fraction is a measure of the void (i.e., "empty") spaces in a material, and is a fraction of the volume of voids over the total volume. Permeability is often related with porosity of a substance as they are interchangeable parameters since their permeability depends on the amount pore-space or porosity of the material. In order to determine the permeability of a material, many scientists and researchers have given many correlations some of which are discussed below. The major problem of reactive media bed (solid-gas) used in thermochemical process is their ability to transfer heat and reactive gas. For example, increasing the density of the reaction medium (and hence energy density) results to improve the transfer of heat thereto, but in parallel to reduce the transfer of mass. A development of porous matrix is primarily intended to increase the thermal conductivity of reactive media bed. In order to characterise the mass transfer during the reaction, transfers in a reactive porous medium with a high energy density, an experimental setup is needed using a gas with properties close to water vapour (nitrogen). In reality, the reactive gas to be used is pure water vapour. However precise mass or volumetric flowmeter to detect the vapour flow is very expensive and nearly not available. That is, why a gas with physical properties close to water vapour, Nitrogen was chosen to perform the measurements.

4.2.1. EXPERIMENTAL METHODS

There are many methods available in the literature to determine the permeability of a material bed, some of the methods will be covered here in this section. Vasques et al. designed and constructed a device called Permeameter to determine the permeability of the bed filled with a solid (Vasques et al., 1999). The bed was maintained inside the Permeameter and the pressure drop across the bed was determined using a pressure gauge. The flow and the inlet pressure were measured using some conventional flowmeters. This methodology was well established and had been widely used for non-consolidated materials that can be packed into a column or vessel along of which manometers could be placed. This is not appropriate, however, for thin-thickness samples due to the difficulty to handle or to measure the pressure at specific positions. Gascoin et al. developed a comparatively new and much more accurate than the pressure decay technique (Gascoin et al., 2012). In this technique, the residence time distribution (RTD) was used to find the permeability of the material bed. Firstly, the N_2 was allowed to flow through the bed of the porous media at a constant inlet pressure and a small amount of tracer- Methane (40 cm³) is periodically injected in the main flow with a fixed gauge pressure. To deliver the tracer, a manual valve was open and then closed rapidly (about 0.5 s of opening time). The infra-red signals were then read by the optical sensors to get the data between tracer concentration and time. Later this data are modified in terms of main flow rate of carrier gas, sampling line flow rate, nature of carrier gas and of tracer, injected quantity of tracer, permeation of material by analytical exploitation of the Forccheimer's and Darcy's equations which helped the permeability of the material bed to be determined. The used method in this work was the pressure decay in order to avoid high investment cost and time consuming. Beside, this technique was suitable for salt hydrates.

4.2.1.1. Description of the experimental bench

The experimental set-up was based on the difference of pressure taken in one point before and one after a nitrogen gas was inputted to the reactive bed. The holder's size fitted the sample amount by aid of metallic net, so that any mechanical pressure on the sample was minimized or not existed. The position of the sample bed was determined after optimal trials effect on the results (see section on permeability results). The metallic net having large pore size did not affect neither the entrance of the flow nor the porosity of the material and defined a fixed bed width. The holder was located in a middle distance between the pressure gauges that were fixed along the chamber (see Figure 4.8), allowing measurements independent of sample thickness. A long feeding tube from the pressurized nitrogen bottle, connected to the chamber attained the maintenance of a steady fluid flux condition during the measurements. That specific tube assured the reduction of the turbulence around the measuring points. The schematic representation of the experimental setup is shown in Figure 4.8.

As previously developed in the chapter 2, the regime of the gas flow was determined in order to know which law can be properly applied. Darcy's law was limited to low surface speeds. When the speed was high like in this case of nitrogen flow at 11 L·min⁻¹ inertial effects tend to oppose the flow. The flow is then called inertial flow. For this type of flow, the Austrian scientist Phillip Forchheimer (1901) in his work "Wasserbewegung durch Boden" investigated fluid flow through porous media for high velocity regime. During this study, he observed that as the flow velocity increases, the inertial effects started to dominate the flow. In order to account for these high velocity inertial effects, he suggested the inclusion of an inertial term representing the kinetic energy of the fluid to the Darcy equation (Teng and Zhao, 2000).
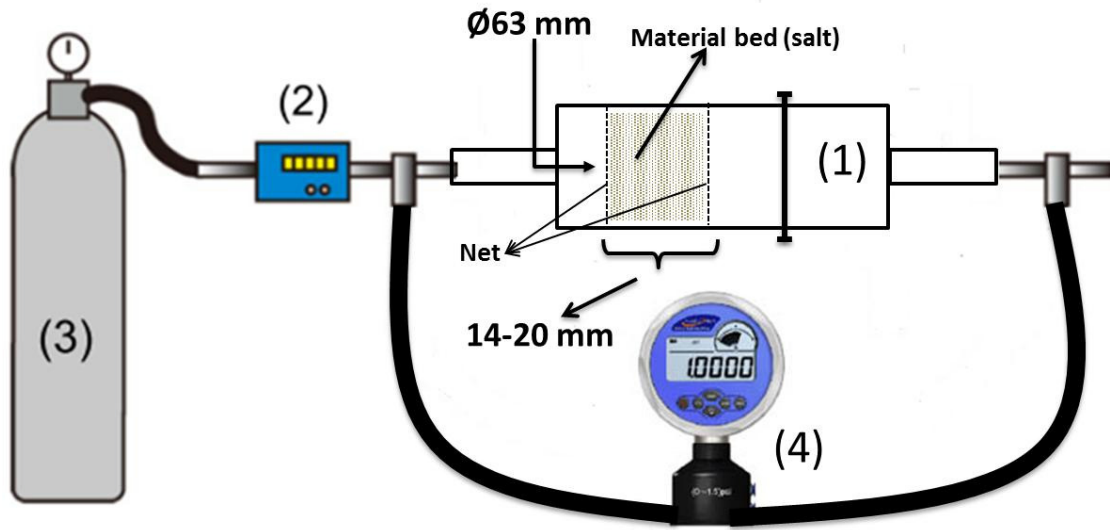
Figure 4.8. Sketch of the experimental bench set-up, out of scale for the permeability evaluation. (1) test vessel; (2) volumetric flow meter; (3) nitrogen gas-bottle; (4) differential pressure gauge (DPG).

The Forchheimer equation was the result of a model that was widely used to quantify the permeability of non-consolidated granular porous media. It was given as follows:

$$\nabla p = -\frac{\mu}{k_D} v_f + \frac{\rho}{k_E} v_f^2 \qquad (4.10)$$

Here, the parameter k_D was called the Darcian permeability and k_E stands for the Ergun permeability which contains the coefficient of inertial conductance. Theoretical evaluation of the Forchheimer coefficients was cumbersome. Thus, for most practical applications, the parameters were obtained from the best fit to the experimental data.

A general equation was given to calculate the theoretical Darcian permeability as follows (Kaviany, 1999):

$$k_D = \frac{\varepsilon^3}{(1-\varepsilon)^2 \, k_k \, A_0^2} \; (m^2) \qquad (4.11)$$

where $A_0 = \frac{solid\ surface}{solid\ volume} = \frac{A_S}{V_S}$ was the specific surface area based on the solid volume. ε is the porosity and k_k is the Kozeny constant. For a sphere shape grain, it is known that:

$$A_0 = \frac{A_S}{V_S} = \frac{4\,\pi\,r^2}{\frac{4}{3}\,\pi\,r^3} = \frac{3}{r}, \text{ therefore } r = \frac{3}{A_0} \text{ and } d_p = 2\,r = \frac{6}{A_0} = \frac{1.5(1-\varepsilon)}{\varepsilon} d_o \qquad (4.12)$$

The Kozeny constant k_k was taken to be equal to 5 for fixed or packed bed (Carman, 1956). With all these above modifications, the general equation now became (the *Carman-Kozeny equation*):

$$k_D = \frac{\varepsilon^3}{(1-\varepsilon)^2 \, 180} \, d_p^2 \; (m^2) \tag{4.13}$$

The theoretical or the non-Darcian permeability for fixed or packed bed was proposed by Ergun (Ergun and Orning, 1949) as follows:

$$k_E = \frac{\varepsilon^3}{(1-\varepsilon) \, 1.75} \, d_p \; (m^2) \tag{4.14}$$

d_p was the mean particle diameter of granular medium, but in this case it is the average pore diameter of the bed and d_o the medium pore size, generally obtained via scanning electron microscopy (SEM). The correlation between theoretical and experimental values of permeability will allow us to establish a strong validation and give good accuracy of the measurements.

The gas inertia effects are no longer negligible when the flow Reynolds number (Re_f) was greater than 0.1, which corresponds to a pressure drop due to the inertia representing 10% of the total pressure drop. Geertsma proposed a correlation of this number as follows:

$$Re_f = \frac{k_D \cdot \rho}{k_E \cdot \mu} \tag{4.15}$$

In the results section, this number is well higher than 0.1 confirming the turbulent flow and the presence of inertia effects during this measurement. So, reported results for a process (gas-solid thermochemical) was only an estimation because water vapor had a lower velocity and could not have a turbulent regime.

4.3. CHEMICAL KINETICS ANALYSIS (SORPTION AND REACTION RATE)

In this part of work, the suitability of $SrBr_2 \cdot 6H_2O$ to be used for thermochemical energy storage was evaluated by a simultaneous thermogravimetric analysis (TGA) and differential scanning calorimetry (DSC) device. Both hydration (discharging) and dehydration (charging) measurements were performed at atmospheric pressure to determine the water sorption rate and energy storage density of the pure salts and designed materials. The hydration levels of the used pure salts and composite materials were calculated from the mass loss analysed via TGA. This device (TGA/DSC 1 device from Mettler Toledo) determined simultaneously the change in sample mass (precision of mass determination is ±0.1 µg) as a function of time while the

specimen is subjected to a T scanning program in a controlled atmosphere and the heat flux (precision of heat power determination is ±1 mW) into the specimen compared to a reference. The experimental setup is shown in Figure 4.9.
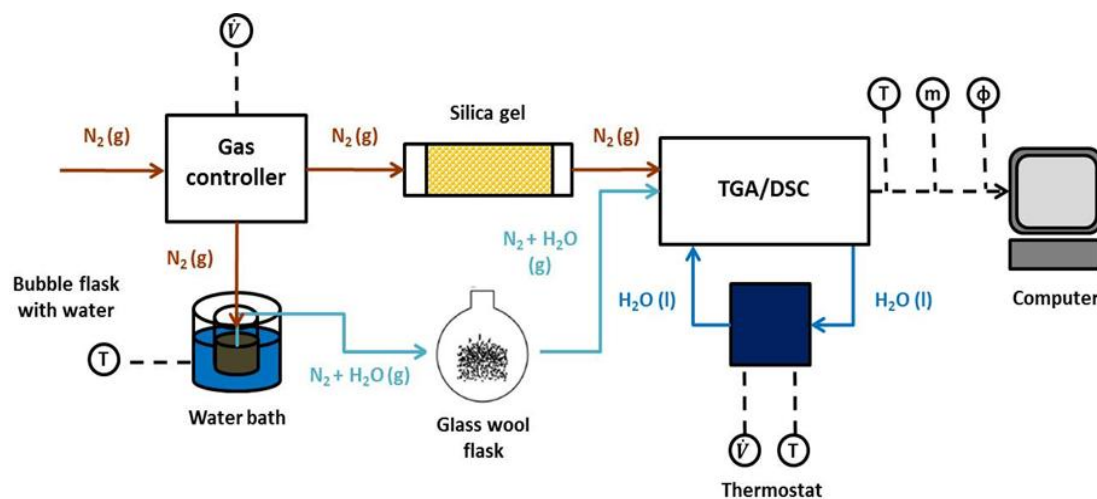
Figure 4.9. Schematic of the TGA/DSC experimental set-up for sorption and rate analysis. $\dot{V}$: nitrogen volume flow rate; T: temperature; m: mass change of the sample; ϕ: heat flux.

A gas box, providing two different mass flow controllers, connected to the TGA/DSC controlled the gas flow rate of the protective purge gas. Silica gel-dried nitrogen was used as purge gas at a flow rate of 50 mL/min. During hydration a reactive gas stream, which was humidified via a tempered gas bubbler flask, was used, in addition to the purge gas stream. By forcing this gas stream through a glass frit filled with glass wool the containing water droplets were homogenized and the gas is adapted to the ambient temperature in the laboratory.

Samples of 10 – 20 mg were tested in crucibles made of alumina with a volume of 70 µL under realistic conditions. All experiments were performed under realistic conditions of the developed closed thermochemical storage system. The equilibrium temperatures for the charging and discharging should meet the target applications source such as micro-CHP and usage temperature. Therefore, the following conditions were used:

- Dehydration at temperature of 95 °C under condenser temperature of about 25 °C (32 mbar) with the corresponding relative humidity. This temperature is taken according to micro-CHP with water as heat transfer fluid. It might be more if another fluid is used instead.
- Hydration at temperature of 60 °C under evaporator temperature of about 10 °C (12 mbar) with the corresponding relative humidity. This temperature could be sufficient for heating and domestic hot water.

The single-stage method used is described in the following Figure: heating up at a lower heating rate reduces the viscosity of the water and allow dehydration whereas isotherm allows time for the chemical reaction to take place.
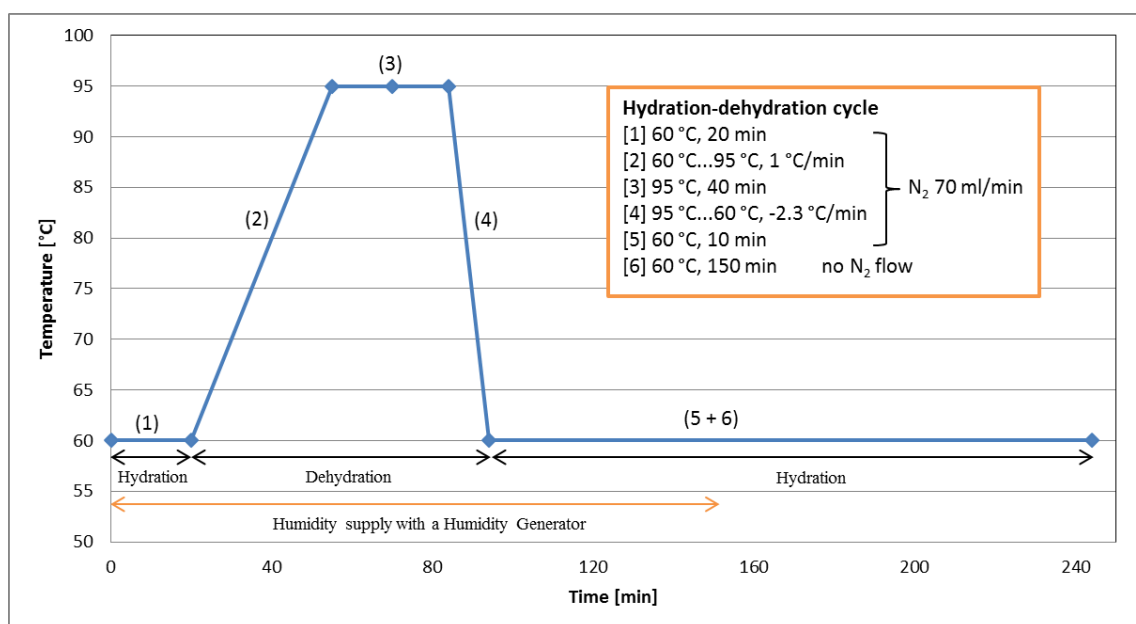
Figure 4.10. Basics TGA/DSC measurement method for the chemical kinetic analysis.

4.4. Material preparation

Samples were stored in a sealed container and placed in a dry area to protect them from moisture. The used materials in this thesis were pure salt hydrates and some host matrices (for later composites design). Their weight varied in the range of 0.003 to 0.098 g and in the range of 60 to 500 g for DSC and GHC, respectively. So, it concerned micro and macro scale measurements. The materials were neither subjected to any compression nor to compaction or modification. They were put into the crucible or in the GHC in the initial state as from the supplier storage. The following Table 4.5 gives the thermal conductivity results performed on both DSC and GHC.

For this work anhydrous calcium chloride ($CaCl_2$), hexahydrate calcium chloride ($CaCl_2 \cdot 6H_2O$), the magnesium chloride hexahydrate ($MgCl_2 \cdot 6H_2O$), the anhydrous (at 99%) magnesium chloride ($MgCl_2$) and the magnesium sulphate heptahydrate ($MgSO_4 \cdot 7H_2O$) all met the specifications of the US and European Pharmacopeia and were in pure form of solid state. Table 4.1 summarizes some properties. The anhydrous ($SrBr_2$) was obtained after heating at 270 °C during 4 hours the strontium bromide hexahydrate ($SrBr_2 \cdot 6H_2O$). The three host matrices: silica gel 60, expanded natural graphite (ENG-P/B) and the activated carbon (AC) were first preheated at 200 °C for 4 hours to remove residual water. The ENG-P was the expanded natural graphite thermophit GFG600. The samples were neither subjected to any structural modification nor to any compaction.

For the synthesis of the salt-porous-carrier composites two different procedures were applied (Druske et al., 2014): wet impregnation under vacuum (VI) and soaking (S). In the wet impregnation method, a saturated aqueous salt solution of $CaCl_2$, had a volume that exceeded the pore volume. Prior impregnation the carriers (AC and ENG-P/B) were dried in an oven at 200 °C and cooled down in a vacuum desiccator to remove any residual moisture. After drying they were immersed into the saturated aqueous solution or molten salt placed in a vacuum sealed

126

vessel which was evacuated with a membrane vacuum pump to 10 mbar. The impregnation time was set to several minutes. The wet $CaCl_2$-based composites were finally dried in an oven at 200 °C until the weight remained constant. All samples were stored in a sealed bottle in a dry area to protect them against moisture and exposure. In the latter method the ENG-P was soaked in a saturated aqueous solution of $MgCl_2$ and $CaCl_2$ respectively, with a $MgCl_2/CaCl_2$:ENG-P ratio of 2:1 and 1:1 while stirring. The excess solvent was removed by evaporation and drying at 200 °C.

The bulk density of materials was calculated by dividing mass of this latter with total occupied volume by the material. Void fraction and density of the bed, were respectively determined using the following formula:

$$Void\ fraction\ (\%) = \frac{V_s}{V_o} * 100\% = \frac{m_s}{d_s * V_o} * 100\% \tag{4.16}$$

$$bed\ density\ (d_b) = \frac{m_s}{V_o} \tag{4.17}$$

where V_s is the volume of the sample, V_o the volume occupied by the sample in the cylinder, m_s the sample weight in grams, d_s the theoretical density of the sample and d_b the bulk density of the bed. In the next section the results of performed measurements are shown and discussed.

Table 4.1. Thermochemical and host materials characteristics considered for this study.

Sample name	Shape	Grain size (mm)	Supplier company
Glass-GP	beads	0.3 – 0.4	Kuhmichel Abrasiv Ltd.
AC	Fine grain	0.315 – 0.580	Blücher GmbH
ENG-P/B	Powder worm	0.005 – 1.4	SGL Carbon Group
Silica Gel 60	Coarse grain	0.1 – 0.3	Roth
$CaCl_2·6H_2O$	Powder	~1.01	Applichem GmbH
$CaCl_2$	Powder	~1.01	Applichem GmbH
$MgCl_2·6H_2O$	Powder	~1.1	Applichem GmbH
$MgCl_2$	Powder	~1.01	Alfa Aesar GmbH
$SrBr_2·6H_2O$	Powder	~1.01	Chemos GmbH
$SrBr_2$	Powder	~1.01	Chemos GmbH
$MgSO_4·7H_2O$	Powder	~1.01	Honeywell Specialty Chemicals GmbH

The void fraction was calculated based on the theoretical value of the material density. However, this helped to understand the stand of the thermal conductivity of the measured samples. Some of the grain size was supplied and others with the symbol "~" were determined using a sieve consisting of holes with diameter around 1.01 mm.

4.5. RESULTS, ANALYSIS AND DISCUSSION

4.5.1. THERMAL CONDUCTIVITY RESULTS

After the blank measurement on GHC, the heat transferred through the material bed during the flux conduction was deduced and Eq. (4.5) re-written as follows:

$$q_e = P - L = \lambda_s \cdot 2\pi L_s \cdot \frac{dT}{d(\ln\frac{r_{i+1}}{r_i})} \tag{4.18}$$

Small uncertainty on the electrical power (Appendix A6-1) was due to the technical properties of the power supplier device and the cartridge. The absolute precision of the measured thermal conductivity value depended on the sensors measurements precision as well as on the uncertainty in their positioning. Repeated stationary measurement of air temperature in two different reactors was performed and the results showed a difference less than 1%. Additionally, Gurgel et al. concluded that the uncertainty in positioning the sensors is smaller than 1% (Gurgel et al., 2001). So only the accuracy of sensors is considered.

4.5.1.1. Experimental validation

In order to validate the experimental apparatus, the thermal conductivity of anhydrous glass was determined and compared with the literature and supplier data. The glass that is studied here was commercially known as "glass beads – GP", produced by Kuhmichel®. The chosen glass presented as spheroidal beads was in a homogeneous spherical form with the following properties:

Table 4.2. Glass beads physic-chemical properties and thermal conductivity (Kuhmichel, 2014).

Grain shape	Spherical
Melting temperature	Approx. 730 °C
Bulk density (*depending on granular size*)	Approx. 1.5 – 1.6 g·cm^{-3}
Average grain size	200 – 300 μm
Thermal conductivity according to the chemical analysis and temperature range	0.8 – 1.2 W·m^{-1}·K^{-1} for % SiO_2 < 96 and % Fe_2O_3 < 1 at T > 20 °C
Chemical analysis of the used glass beads	SiO_2 (70 – 75%) MgO (max. 5%) Na_2O (12 – 15%) Al_2O_3 (max. 2.5%) CaO (7 – 12%) K_2O (max. 1.5%) Fe_2O_3 (max. 0.5%) Others (max. 2%)

The measurements under stationary heat flow yielded the radial temperature gradient necessary to calculate the thermal conductivity of the packed bed, using Eq. (4.18); while under transient heat flow it was determined using Eq. (4.4). The results are shown in Table 3 and 4. The effective thermal conductivity of the bed as a function of parameters such as the thermal conductivity of the beads, bed porosity, dimensions of the grains was not determine here, since it required some model to be designed or adapted. It is developed in the following for the

samples. The average thermal conductivity of glass beads under dry air at 100 kPa was λ_s = 1.03 ± 0.09 W·m^{-1}·K^{-1} with the GHC (m$_{glass}$ ~ 700 g) and λ_s = 1.16 ± 0.02 W·m^{-1}·K^{-1} with the DSC (m$_{glass}$ ~ 139 mg). The uncertainties evaluation in this work were purely systematics and based on the guide to the expression of uncertainty in measurement (GUM) (Kristiansen, 2003) (Appendices A6-1 and A6-2). For DSC measurements, it was calculated from the Eq. (4.4) using the standard deviation on heat flow and temperature mentioned in section 4.1.1.1. For the GHC measurements, the uncertainties were evaluated based on Eq. (4.5) with the known uncertainties of voltage, current intensity (for electrical power uncertainty) and length.

Table 4.3. Experimental results for effective thermal conductivity of glass beads using GHC with a starting temperature of 17 °C.

Material	Power (W)	Bed length (m)	Void fraction (%)	Maximal temperature (°C)	Thermal conductivity (W·m^{-1}·K^{-1})	Uncertainty on Thermal conductivity (W·m^{-1}·K^{-1})
Glass beads	2.35	0.05	90	26	1.39	0.167
	3	0.05	90	28	0.76	0.061
	4.56	0.05	90	36	0.93	0.076
	5	0.05	90	36	1.02	0.066

Table 4.4. Experimental results for effective thermal conductivity of glass beads using DSC.

Material	Specific energy (J/g)	Bed length (m)	Void fraction (%)	Temperature range (°C)	Thermal conductivity (W·m^{-1}·K^{-1})	Uncertainty on Thermal conductivity (W·m^{-1}·K^{-1})
Glass beads	2.21	0.0051	89	100-200	1.29	0.019
	2.62	0.0051	89	100-200	1.12	0.020
	2.9	0.0051	89	100-200	1.07	0.016

The results both measured in the GHC and the DSC were in the range of literature value with relative uncertainty less than 10%, as shown in the Tables 4.3 and 4.4. That led to the validation of our measurement procedure.

4.5.1.2. Experimental results and discussion

When using a DSC for thermal conductivity evaluation implies a good compromise of the heating rate need to be found, in other terms, to select the appropriate heating rate in the slope formula (Eq. (4.3)). Some salts may partially or completely melted in the actual temperature range, depending on the heating rate, instead of simple heating when their melting temperature was exceeded. After the calibration experiments were completed and validated, the calculations showed consistent results with a heating rate of 10 °C·min^{-1}, so it has been adopted for the following. This thermophysical property of salts was investigated here with small discrepancies among the various data reported in the literature.

During the experiment on the GHC, the temperature evolution increased after a short time and tended to a linearity (nearly isotherm) for about 3 hours for each experiment. For each material, three or four measurements were performed and the average was taken as result. Figure 4.6 exhibited the steady state thermal conductivity results for a number of salts and host matrices and then comparison with literature values was highlighted. Although the results were closed to the literature values, slight discrepancies were noticed. However the phase change of hydrated salts was an influencing parameter and was part of the incontrollable phenomena (molecular level for instance) to handle during the measurement.

Literature values of thermal conductivity of salts are varying much and depend on different methods and of course on temperature. In this range of temperature (20-70 °C) the hydrates tend to decrease whereas the anhydrous tend to increase. For example, strontium bromide was selected for the regression. The best fit of the data distribution is achieved with a polynomial regression and it yields:

For $SrBr_2 \cdot 6H_2O$: $\lambda_s = -0.0016 \cdot T^2 + 0.15 \cdot T - 2.73$, with 20 °C < T < 70 °C $\hspace{1cm}$ (4.19)

For $SrBr_2$: $\lambda_s = -0.0039 \cdot T^2 - 0.32 \cdot T + 6.67$, with 20 °C < T < 70 °C $\hspace{1cm}$ (4.20)

The maximum standard deviation between the measured thermal conductivity and the regression polynomial was ± 3%. Another remark was that the thermal conductivity of hydrated was higher than the anhydrous or dehydrated. The reason was shown in the void fraction, implying larger porosity (which is, 1-void fraction) for anhydrous than hydrates. So, larger porosity exhibited small thermal conductivity, as demonstrated by Wang et al. (Wang et al., 2006) with $CaCl_2$.

Figure 4.11 shows solid thermal conductivity of different salts and the hydrates have high values as mentioned above, simply due to the fact that the presence of water molecules filled the space between the solid and facilitate the internal thermal contact. Tanashev et al. justified this by stating that the presence of the film enhanced the heat contact and, hence, the heat transfer between adjacent salt particles (Tanashev et al., 2013). Another remark was that those salt hydrates have a thermal conductivity in the range (0.3 – 1.3) $W \cdot m^{-1} \cdot K^{-1}$, hence for thermal energy applications, some improvement was taken such as composites design with highly conductive host matrices. This Figure 4.11 highlights the comparison between the two methods (DSC and GHC) and their closeness to the literature range values. Here, the DSC seemed to overestimate the thermal conductivity of the first four salts and underestimate the last three. The reason could be the closeness behaviour of $MgCl_2 \cdot 6H_2O$ and $CaCl_2 \cdot 6H_2O$ as thermochemical materials. However, the standard deviation between the two methods was less than 16%, except in the case of $MgSO_4 \cdot 7H_2O$ and ENG-P. Another remark is that measurements were performed at micro-scale on DSC and at macro-scale on GHC. Here, the scalability might affected the measurement.
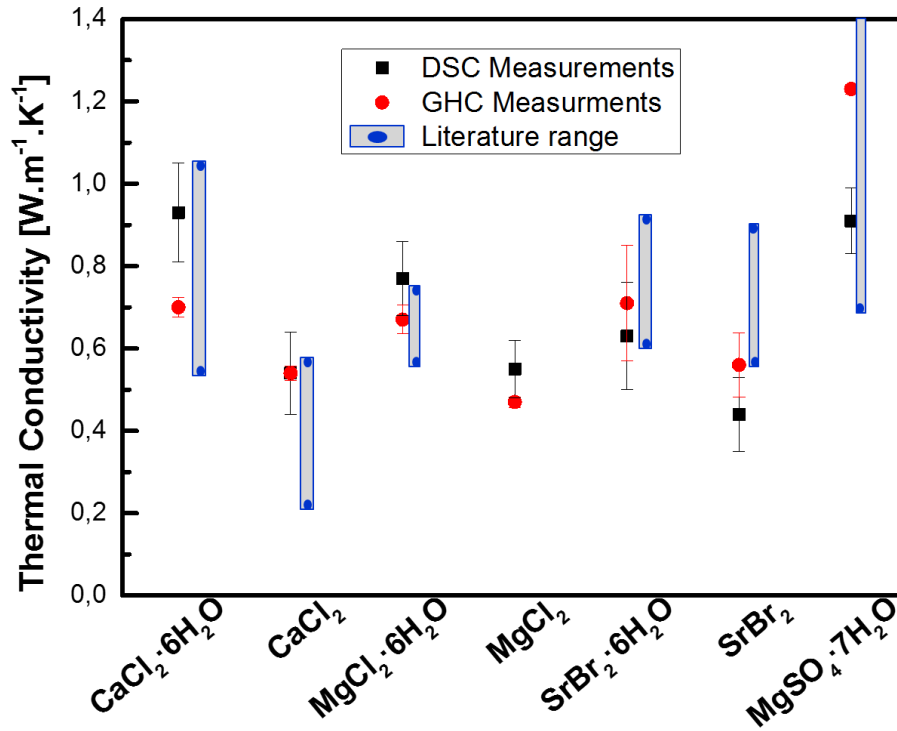
Figure 4.11. Thermal conductivity comparison of salt hydrates with uncertainty bars obtained on DSC and GHC.

It can be concluded that the GHC was more accurate than the DSC, due to the uncertainty bar observation. So in the following we mainly talk about GHC. However, knowing the exact intrinsic thermal conductivity of the entire solid bed (including porosity, tortuosity and texture) is a cumbersome task and required very accurate apparatus. Therefore theoretical means were used in order to evaluate it. Tsotsas et al. described it as a legitimate procedure (Tsotsas and Martin, 1987). In order to find the thermal conductivity of solid salt adsorbent, it was assumed that the solid part and the gas present in the microspores form parallel paths of heat conduction (Wang et al., 2006). Hence for the effective thermal conductivity (according to the salt bed in the Aluminium container for DSC and in the small cylinder reactor for GHC), a relationship commonly used in the case of porous media composed of a single component was the relationship of Archie (Archie, 1942). This correlation was validated for porous beds by Olivès (Olives and Mauran, 2001):

$$\lambda_s = S_w * \lambda_{isc} * (1 - \varepsilon)^\xi \tag{4.21}$$

where λ_{isc} was the intrinsic thermal conductivity of the solid salt (hydrate or anhydrous), S_w the pre-factor near 1 which contains information about structural geometry of the bed, ε the porosity of the porous medium and ξ the degree of consolidation (cementation factor), which reflects the mechanical strength of the material. This factor is generally between 1 and 4. For granular (1 – 3 mm) porous media, it was commonly accepted that the degree of consolidation is between 1.3 and 2.0 (Archie, 1942) and in this work an average value of 1.5 was used as mentioned by

Michel (Michel, 2012) for similar salt bed. The pre-factor was very important according to the material structure and should be accounted for effective thermal conductivity prediction.
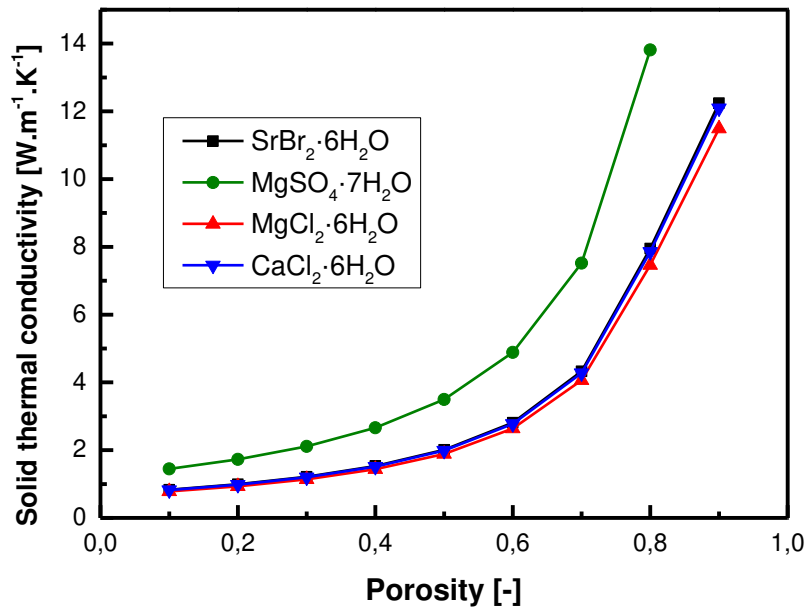
Figure 4.12. Solid thermal conductivity of salt hydrates on Guarded Hot Cartridge device.

The porosity of the dehydrated/hydrated salt bed should be a function of the energy density, the molar density of the material, and the reaction enthalpy, so the experimental sample parameters account for the texture, structure and tortuosity. Since no porosimetry was performed, results, presented as a function of porosity, ranged from 0 to 1. Only the hydrated salts were simulated on Figure 4.12 due to the fact that the variation of porosity is a function of the number of water molecules inside the salt. As the water is desorbed or absorbed, the porosity increase or decrease respectively.

From the Figure 4.12, the intrinsic thermal conductivity of the salt hydrate increased with the increase of porosity. Some conclusion from this figure can be drawn here: the magnesium sulphate heptahydrate is thermally the best material. Genceli et al. corroborated it via crystallization studies (Genceli et al., 2009). The effective thermal conductivity property of strontium bromide hexahydrate and calcium chloride hexahydrate behave in the same way with the bed porosity. The majority of salt beds had a porosity comprise between 0.6 and 0.7 and when looking at this range for those salts, their intrinsic solid thermal conductivity <5 W·m^{-1}·K^{-1}. Therefore the assertion of all salt hydrates having a very low thermal conductivity was demonstrated here, despite its high intrinsic conductivity which drastically drops when considering bed texture and structure. Hence the need of host matrices utilisation to improve this dominant heat transfers property in packed bed.

Evaluation of thermal conductivity of salt hydrates (respectively of the bed) is complex when wishing to account for all the characteristics and how it is use in a system, but for packed bed case, a model was develop to be a hint for researchers and engineers.

The evaluation of effective thermal conductivity of some salts and host matrices was performed through two different systems and methods. From these experiments, a conclusion that the heat flux type of DSC cell was a helpful instrument for measuring the thermal conductivity of salt hydrates was highlighted. Though care need to be undertaken to handle heat loss and good thermal contact.

However, the GHC under atmospheric conditions remains the more accurate method and is also more representative for a real storage system. The results obtained can be used for mathematical modelling of both open and closed thermal energy storage systems that utilise the salt hydrates involved as solid sorbents. For ease of numerical models, the temperature dependences are approximated by polynomial functions in the case of strontium bromide in Eqs. (4.19) and (4.20). For all hydrated salt samples studied the porosity dependence on the effective thermal conductivity is satisfactory and can be described by Archie's model. As a work perspective the undergoing composites designed should be subjected to thermal conductivity measurement using the steady state measurement (GHC).

Table 4.5. Experimental results for thermal conductivity using the heat flux DSC and the GHC.

Materials	Specific Energy (J·g⁻¹)	Average Elect. Power (W)	Bulk density (kg·m⁻³)	Void fraction (%)	Thermal conductivity (W·m⁻¹·K⁻¹)	Source
Activated Carbon	3.84	-	537	93	0.55	Own DSC
	-	3.80	449	78	0.40	Own GHC
	-	-	-	20~60 mesh	0.15 – 0.5	(Menard et al., 2007)
				Pore size 6.4$\mathring{A}$	0.36	(Tian et al., 2012)
ENG-P	93.8	-	23	48	4.78	Own DSC
	-	3.47	11	24	4.05	Own GHC
	-	-	-	-	3 – 10	(Smalc et al., 2007)
Silica-Gel 60	4.90	-	281	13	0.47	Own DSC
	-	5.00	353	16	0.58	Own GHC
	-	-	-	-	0.5–0.8	(Gurgel et al., 2001)
CaCl$_2$·6H$_2$O	3.14	-	643	38	0.93	Own DSC
	-	4.50	1097	64	0.70	Own GHC
	-	-	-	-	0.5–1.088	(Zalba et al., 2003)
CaCl$_2$	2.54	-	497	23	0.54	Own DSC

	-	3.64	751	35	0.54	Own GHC
	-	-	-	-	0.1 – 0.5 0.26 0.45	(Fopah Lele et al., 2013; Kiplagat et al., 2012; Wang et al., 2006). (Jiang et al., 2014). (El-Dessouky and Al-Juway-hel, 1997)
MgCl$_2$·6H$_2$O	2.31	-	854	54	0.77	Own DSC
	-	4.25	1053	67	0.67	Own GHC
	-	-	-	-	0.5–0.704	(Zalba et al., 2003)
MgCl$_2$	1.92	-	786	34	0.55	Own DSC
	-	3.33	1009	43	0.47	Own GHC
	-	-	-	-	-	n.a.
SrBr$_2$·6H$_2$O	3.67	-	976	41	0.63	Own DSC
	-	3.98	1606	67	0.71	Own GHC
	-	-	-	-	0.53–0.89	(Mauran et al., 2008)
SrBr$_2$	2.52	-	842	20	0.44	Own DSC
	-	3.51	1509	36	0.56	Own GHC
	-	-	-	-	0.2–0.4 0.47–0.93	(Lahmidi et al., 2006). (Mauran et al., 2008)
MgSO$_4$·7H$_2$O	2.3	-	764	46	0.91	Own DSC

	-	3.35	1231	73	1.23	Own GHC
	-	-	-	-	0.6 – 2.427	(Genceli et al., 2009; Melinder, 1997)
CaCl$_2$-AC-VI	2.7		649		1.03	Own DSC
CaCl$_2$-ENG-P-1:1	21.1		85		1.64	Own DSC
CaCl$_2$-ENG-P-1:2	35.7		46		0.74	Own DSC
MgCl$_2$-ENG-P-1:1	9.35		159		2.22	Own DSC
MgCl$_2$-ENG-P-1:2	12.1		150		1.51	Own DSC
CaCl$_2$-ENG-B-VI	4.3		462		0.73	Own DSC
MgCl$_2$-ENG-B-VI	6.7		291		0.8	Own DSC
MgSO$_4$-ENG-B-VI	5.8		378		1.82	Own DSC
MgSO$_4$-AC-VI	2.3		392		1.6	Own DSC

P: powder worm, B: compacted pellet

The last results based on composites, presented in the above table are not part of this work. It was just pointed out as additional measurements.

4.5.2. Heat capacity results

Specific heat capacities from the two methods are listed in Table 4.6. Good accuracy was achieved for most of the materials. No significant difference was found between the two methods, which supports the accuracy of our measurements. Calculating the area under the curve based on the displacement (mW) was similar to the area from the peak analysed based on the tangent lines from the DSC-TA software, as listed in Table 4.7. This indicates that any of the methods can be used to determine the values of specific heat capacity of any materials. In spite of that, averaging the two values is recommended to reduce associated errors.

For each material, fresh and heated (dried using hot air) samples were used in order to point out the moisture effect since they are all high hygroscopic materials. Repeated test were performed with considerable variation in the results due to the moisture loss during heating process. The fresh samples exhibited higher heat capacity because of the moisture content. The DSC scans for each material show large heat flow values equivalent to around three to four times the heat capacity of Aluminium in the temperature range from 60 °C to 100 °C. The Figure 4.13 and 4.14 show an example with strontium bromide.
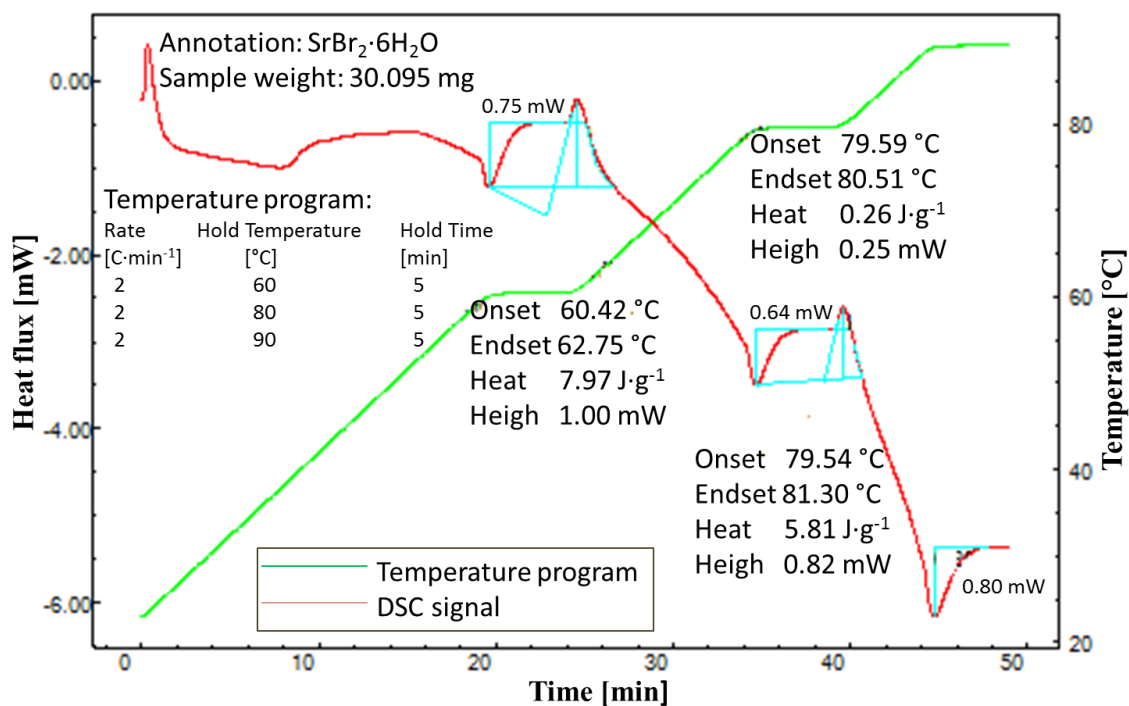
Figure 4.13. DSC scans of fresh powder sample of 30.095 mg and melting after 80 °C.

Table 4.6. Specific heat capacity of different materials based on the two applied methods: displacement method and area method at the isothermal steps (60 and 90°C).

Methods / Materials	Specific heat capacity ($J \cdot kg^{-1} \cdot K^{-1}$) at isothermal steps			Specific heat capacity ($J \cdot kg^{-1} \cdot K^{-1}$) at isothermal steps			Literature [2] (Barin et al., 1977; Chase et al., 1998)	
	Area method [60 °C]	Displacement method [60 °C]	Standard deviation [%]	Area method [90 °C]	Displacement method [90 °C]	Standard deviation [%]	60 °C	90 °C
$CaCl_2 \cdot 6H_2O$	3277	3391	3.36	2998	3354	10.61	1420	1420
$CaCl_2$	1015	1067	4.89	954	958	0.36	1049	1060
$MgCl_2 \cdot 6H_2O$	1686	1779	5.24	1779	1755	1.40	1490	1620
$MgCl_2 \cdot 2H2O$	980	984	0.42	989	1008	1.84	-	-
$SrBr_2 \cdot 6H_2O$	986	979	0.69	890	935	4.80	967	970
$SrBr_2 \cdot H2O$	457	434	5.35	498	506	1.60	456	456
$MgSO_4 \cdot 7H_2O$	1444	1525	5.33	-	-	-	1510	-

---

[2] The literature results are obtained using the displacement method.
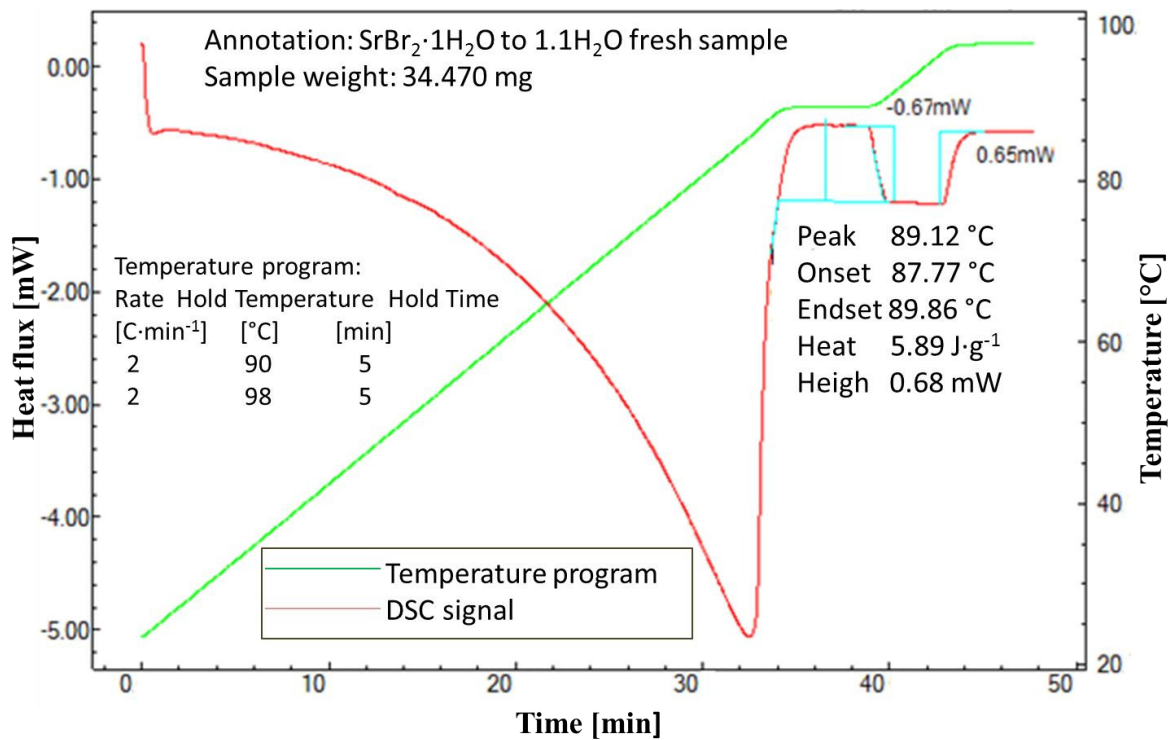
Figure 4.14. DSC scan of dried powder sample of 34.47 mg and melting after 40 °C.

Table 4.7. Comparison between the area at the isotherm from DSC scan and the calculated one from the displacement value.

| Material | Based on area at isotherm | | Calculating the area under the curve = displacement (mW) x 60 min / 2°C) x 10) | |
| | $J \cdot g^{-1}$ | $J \cdot g^{-1}$ | $J \cdot g^{-1}$ | $J \cdot g^{-1}$ |
	60°C	90°C	60°C	90°C
$CaCl_2 \cdot 6H2O$	19.73	17.81	19.95	19.47
$CaCl_2$	6.11	5.67	6.28	5.56
$MgCl_2 \cdot 6H2O$	10.15	10.57	10.47	10.19
$MgCl_2 \cdot 2H2O$	5.9	5.8766	5.79	5.85
$SrBr_2 \cdot 6H2O$	5.935	5.29	5.76	5.43
$SrBr_2 \cdot 1H2O$	4.81	5.273	4.59	5.34
$MgSO_4 \cdot 7H2O$	8.69	-	8.97	-

The obtained results allowed the knowledge of the storage capacity. Additionally, it was used as parameters to run the simulation with reliable values.

4.5.3. PERMEABILITY RESULTS

In the sample preparation, a sieve ws used to determine the grain size of the sample. The sieve with holes of diameter around 1.01 mm helped measuring only samples with the respective grain

139

size. In reality, the gas is a pure water vapour. However, precise flowmeter to detect the vapour flow is very expensive and nearly not available. That is why first measurements were done using Helium gas (He). Then, looking at a gas with physical properties close to water vapour, Nitrogen was used to perform new measurements. The position of the bed in the vessel effected the results, thought an optimal position (as it will be in the reactor i.e. far from the reactive gas entrance) was adopted. Bigger permeability was obtained when the bed was placed directly at the entrance of the tube then when it was on the middle. That difference lied on the flow surface strongly dependent on the diameter. So when directly placed at the entrance the considering diameter is 13 mm whereas in the middle, the considering diameter was 63 mm (see Figure 4.8). The bed size was determined using a sieve (diameter of about 1 mm). This means the samples were those subdued with the sieve. The sample bed porosity was represented by the void fraction.

Table 4.8. Experimental results and comparison for permeability measurement.

Materials	Void fraction (%)	He permeability (m^2)	N$_2$ permeability (m^2)	Theoretical permeability (m^2)	Literature
CaCl$_2$·6H$_2$O	27	6.1×10^{-10}	0.28×10^{-10}	0.03×10^{-10}	-
CaCl$_2$	16	56×10^{-11}	2.7×10^{-11}	0.01×10^{-11}	-
MgCl$_2$·6H$_2$O	23	3.9×10^{-10}	2.1×10^{-10}	0.05×10^{-10}	-
MgCl$_2$	16	4.9×10^{-11}	0.11×10^{-11}	0.01×10^{-11}	-
SrBr$_2$·6H$_2$O	24	5.6×10^{-11}	3.1×10^{-11}	0.04×10^{-10}	0.86×10^{-11} m^2 (Michel et al., 2012)[3]
SrBr$_2$ (*dried at 270 °C*)	11	0.15×10^{-10}	0.7×10^{-10}	0.32×10^{-10}	0.3×10^{-10} m^2 (Michel et al., 2012)
MgSO$_4$·7H$_2$O	27	0.31×10^{-11}	1.9×10^{-11}	0.003×10^{-11}	-

The obtained results based on Nitrogen showed bigger difference than the one with Helium and are closed to the formal results (Michel et al., 2012) under air flow in an open system concerning strontium bromide. However the results have an uncertainty around 25% due to the pressure loss in the ambient air caused by the thermal mass flow meter. The pressure compensation with calibration was difficult to reach due to the low differential pressure. Anyway the results were satisfactory for the closed system. The Table 4.8 resumes the obtained results.

---

[3] This is the result for the first hydration of the bed using air as gas flow, obtained with an uncertainty of 0.32×10^{-11} m^2. At the seventh hydration an average of 6.5×10^{-12} m^2 is obtained as the air-permeability of the bed.

Works on the determination of thermochemical material's permeability is still under study and only few researchers had performed it. That is why literature is limited. Table 3.8 exhibits the results of the permeability and highlights the overestimation made when using the Helium as the gas flow. The reason might be that Helium is lighter than Nitrogen and therefore passes easily through the voids of the bed. As of standard deviation matter, only $MgCl_2 \cdot 6H_2O$ and $SrBr_2 \cdot 6H_2O$ presented about 45% between the two gas utilisation. The others deviated of about 95% leading to big difference in the results. However, the N_2 permeability gives realistic and reliable results, especially in the case of strontium bromide. However, theoretical evaluation of this property shows a higher underestimation and might lead to a biased result during practical design or simulations. This conclusion is based on the particle size determination using a sieve which is normally not the appropriate device. In fact, salt particles going through the sieve could be small bulk of grains together. That may lead to an overestimation of the particle size. Further better knowledge on the particle size distribution may change this drawn conclusion.

4.5.4. CHEMICAL KINETICS RESULTS

The purpose of a kinetic analysis can have two objectives: 1. Find reaction conversion at given temperature conditions, if the chemical mechanism of reaction is unknown and not really important, 2. Determine and describe the kinetic mechanism if the chemical mechanism of reaction is unknown or partially unknown. From this latter, one can talk about reversibility.
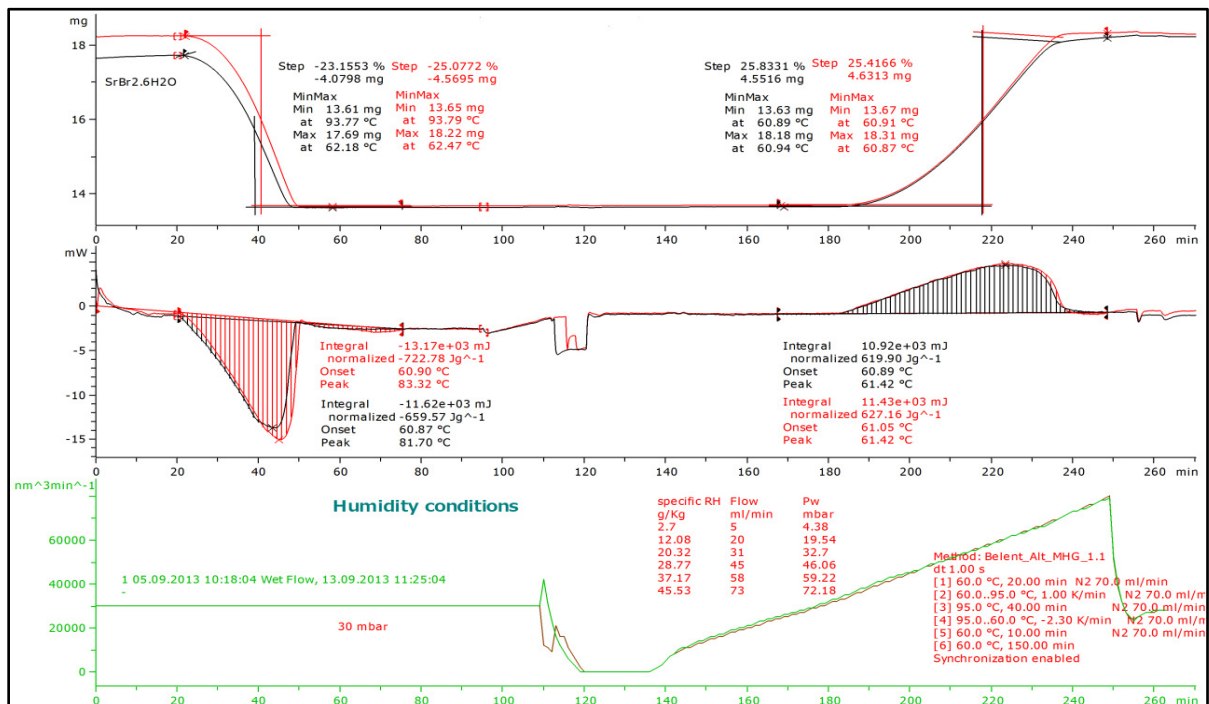
Figure 4.15. Thermal analysis of $SrBr_2 \cdot 6H_2O$ using the TGA/DSC device connected to a humidity generator in order to fulfil the realistic conditions.

Figure 4.15 illustrates reversibility under 95 °C and relative humidity (RH) up to 45 g·kg⁻¹ vapour when subjected to a heating rate of 1 °C·min⁻¹. Water losses and recoveries were about 25% relating to the reversibility. Slower heating rate was used here to observe water losses in multiple steps. This thermochemical material has been extensively studied and a temperature of 80 °C was already sufficient to insure the complete dehydration from the hexahydrate to the monohydrate (Michel et al., 2012). $SrBr_2 \cdot 6H_2O$ was among the three salts that could provide a net energy storage above 200 kWh·m⁻³ under 100 °C (N'Tsoukpoe et al., 2014). The maximum power generated by the sorbent, which corresponded to the heat flow difference between the sample (around 18.22 mg) and the reference in the oven, raises up to 7 mW. The total amount of energy released by the sample was 3.18 Wh, respectively 0.17 Wh·mg⁻¹.

These results reflected a very fast energy release. The results in Table 4.9 shows that the effective energy recovered during discharging was 0.17 Wh·mg⁻¹ of pure salt, representing 13.4% of the energy supplied to charge the system. This efficiency was linked to the fact that, the energy supplied to charge the system was not dedicated solely to dehydrate the material. A part of this energy corresponded to the sensible heat required to bring the sample temperature at 95 °C; this energy was lost during the 160 min of cooling following the charging and before the discharging.

From the Figure 3.16, the reaction rate can be obtained by linear fitting. The reaction rate is expressed as:

$$reaction\ rate\ =\ \pm\ \frac{d[\alpha]}{dt} =\ \pm\ \frac{d[salt]}{dt} \tag{4.22}$$

where [salt] is the molar concentration of the salt. The sign $\pm$ represents both the dehydration (-) and hydration (+). Results gave, $rate_{dehyd} =\ 0.0335$ mol·l⁻¹·s⁻¹ and $rate_{hyd} =\ 0.0675$ mol·l⁻¹·s⁻¹.
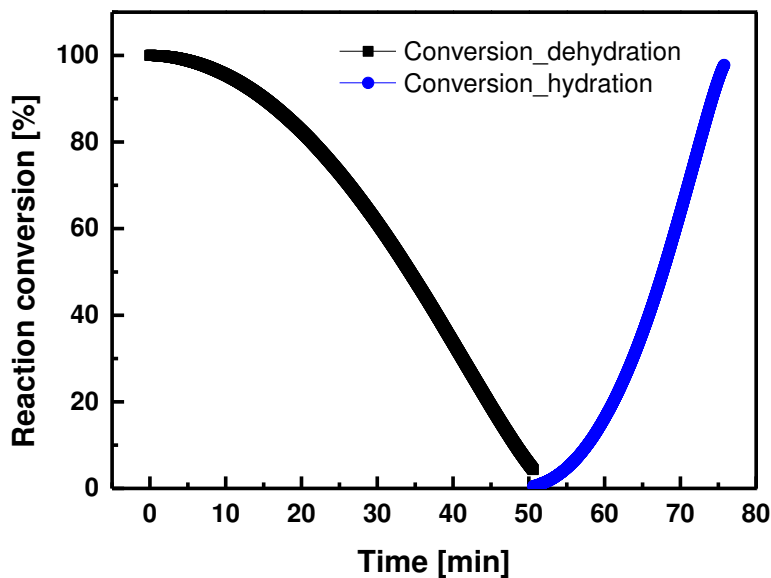
Figure 4.16. Degree of global conversion of the charging/discharging phase with $SrBr_2 \cdot 6H_2O$.

Returning at the first point of the kinetic analysis, the degree of conversion of the reaction is given at the Figure 4.16. The prepared materia $SrBr_2 \cdot 6H_2O$ weighted 18.22 mg and lost about 25% of water, which corresponded to the mass of the five water molecule involved during the reaction. Normalized conversion is presented in the figure in order to have percentage of conversion.

Table 4.9. Summary of experimental results for $SrBr_2 \cdot 6H_2O$ at the micro-scale.

Mode	Characteristics	Value
Charging	Peak power	16 mW ~ 0.9 W·g^{-1}
		3.66 Wh
	Stored energy	0.2 Wh·mg^{-1}
		480 MWh·m^{-3}
Discharging	Maximal released power	7 mW ~ 0.4 W·g^{-1}
		3.18 Wh
	Released energy	0.17 Wh·mg^{-1}
		606 MWh·m^{-3}

Even at this micro-scale, it can be shown that dehydration required more time than hydration (25 min for the hydration and 50 min for the dehydration) when using only pure salt. In this case disregarding isothermal-step (between charging/discharging) which might be regarded as the time when the system is resting, the dehydration time was around two times or more than the hydration time. This was also proven in the work of Michel (160 h for the hydration and 350 h for the dehydration) at the reactor-scale (Michel, 2012). These reaction times were very important for designing the prototype. However, a lab-scale experiment is more appropriate. Looking at the actual heat flow measurements under realistic conditions (Figure 4.15) to the reactor design point of view, storage energy density of the material was about 531 kWh·m^{-3} (porosity included) leading to a net prototype storage energy density of 115 kWh·m^{-3} (corresponding to 72% of the project target value, see Chapter 5, Table 5.1). Calculations can be found in the Appendix A3. This performance seemed lower at micro-scale with an equilibrium temperature at 60 °C and could be higher at the reactor-scale. Additionally, there is a heat exchanger within the bed of pure salt in order to recover the heat losses and optimise the energy released. However, only a lab-scale experiment could confirm this argumentation in order to have a closed idea of the prototype design.

4.6. CONCLUSION OF THE CHAPTER

In this chapter, the work focused on the thermal and kinetics characterization of storage materials, more exactly the determination of crucial parameters concerning thermochemical storage system. They are thermal conductivity, specific heat capacity, permeability and chemical kinetics. All those parameters were very important, numerically and experimentally. The thermal

and kinetics characterization were undertaken at both, microscopic- and macroscopic-scale, which helped to have an estimation of the system performances though a lab-scale would be more appropriate.

Concerning the thermal conductivity, two methods apparatus were used. The first, using the differential scanning calorimetry (DSC) at micro-scale, based on the determination of the heat flux through the sample in order to have the thermal resistance of the sample and therefore the thermal conductivity. The used method was an adaptation of previous method used on polymer samples. The second apparatus at macro-scale was designed and built in-house and called guarded hot cartridge (GHC). It was based on the direct determination of the thermal resistance by imposing different electrical loads through the cartridge and recording the bed temperature at different radial positions. The heat sink is the ambient air in the laboratory. The difference in using the both apparatus for evaluating thermal conductivity yielded a standard deviation less than 12%. Inorganic salts often used in thermochemical energy storage ($CaCl_2$, $MgCl_2$, Sr_2Br_2 and $MgSO_4$) and host matrices (activated carbon, expanded natural graphite and silica gel, vermiculite) were used as samples and the results on both system for only salts gave a thermal conductivity in the range of 0.3 – 1.3 $W \cdot m^{-1} \cdot K^{-1}$ with uncertainty less than 14%. These obtained data were within literature values range. Regarding the results, the need of composites design is a must to achieve great thermal performances in thermal storage systems, especially in closed systems. The specific heat capacity measurement at micro-scale also showed good agreement with the literature and between the different methods used for the evaluation.

For the permeability, the obtained results based on the nitrogen showed bigger difference than the one with Helium and were closed to some literature results under air flow in an open system. The reason might be that Helium was lighter than Nitrogen and therefore passed easily through the voids of the bed. As of standard deviation matter, only $MgCl_2 \cdot 6H_2O$ and $SrBr_2 \cdot 6H_2O$ presented about 45% between the two gas usages. The others deviate of about 95% leading to the difference in the results. However, the N_2 permeability gave realistic results, especially for strontium bromide. However the results had an uncertainty around 25% due to the pressure loss in air (the ambient) caused by the thermal mass flow meter.

The above parameters well determined under realistic conditions, will help for numerical investigations and performances evaluation. A thermal analysis based chemical kinetics was performed in order to have a trend on the storage material performances. At the material scale, the expectations were closed to the theoretical performances, however when related to the prototype, the performances were reduced. Only the lab-scale will help us correlating the micro- to macro-scale and then extending it to the prototype. Based on the previous results, numerical investigations will be done in the next chapter for performance analysis at the lab-scale before performing the experiment itself.

REFERENCES CHAPTER

Alrtimi, A., Rouainia, M., Manning, D.A.C., 2014. An improved steady-state apparatus for measuring thermal conductivity of soils. International Journal of Heat and Mass Transfer 72, 630–636. doi:10.1016/j.ijheatmasstransfer.2014.01.034

Archie, G.E., 1942. The electrical resistivity log as an aid in determining some reservoir characteristics. Transactions of the AIME (Am. Inst. Min. Metall. Eng.) 146, 54 – 62. doi:10.2118/942054-G

Barin, I., Knacke, D.O., Kubaschewski, O., 1977. Thermochemical properties of inorganic substances, in: Thermochemical Properties of Inorganic Substances, Inorganic Chemistry. Springer Berlin Heidelberg, Berlin, Germany, pp. 1–861.

Camirand, C.P., 2000. Etude de la chaleur spécifique et la conductivité thermique des hydrures métalliques par calorimétrie différentielle (Master Thesis). Université du Quebec à Trois-Rivières, Trois-Rivières, Cananda.

Camirand, C.P., 2004. Measurement of thermal conductivity by differential scanning calorimetry. Thermochimica acta 417, 1–4. doi:10.1016/j.tca.2003.12.023

Carman, P.C., 1956. Flow of gases through porous media. Academic Press, New-York, USA.

Chase, M.W., Davies, C.A., Downey, J.R., Frurip, D.J., McDonald, R.A., Seyverud, A.N., 1998. NIST–JANAF Thermochemical Tables, Fourth Edition. Journal of Physical and Chemical Reference Data, Monograph 9 25, 1–1951. doi:10.1063/1.555993

Colby College, C., 2007. Differential scanning calorimetry; first and second ordertransitions in polymers (Course No. http://www.colby.edu/chemistry/PChem/lab/DiffScanningCal.pdf). USA.

Degiovanni, A., 2012. Conductivité et diffusivité thermique des solides. Techniques de l'ingénieur, Traité-Mesures et Contrôle R2850, 17.

Druske, M.-M., Fopah Lele, A., Korhammer, K., Rammelberg, H.U., Wegscheider, N., Ruck, W., Schmidt, T., 2014. Developed Materials for Thermal Energy Storage: Synthesis and Characterization. Energy Procedia, International Conference on Applied Energy, ICAE2014 61, 96–99. doi:10.1016/j.egypro.2014.11.915

El-Dessouky, H., Al-Juwayhel, F., 1997. Effectiveness of a thermal energy storage system using phase-change materials. Energy Conversion and Management 38, 601–617. doi:10.1016/S0196-8904(96)00072-6

Ergun, S., Orning, A.A., 1949. Fluid flow through randomly packed columns and fluidized beds. Ind. Eng. Chem. 41, 1179–1184. doi:10.1021/ie50474a011

Flynn, J.H., Levin, D.M., 1988. A method for the determination of thermal conductivity of sheet materials by differential scanning calorimetry (DSC). Thermochimica Acta 126, 93–100. doi:10.1016/0040-6031(88)87254-X

Fopah Lele, A., Korhammer, K., Wegscheider, N., Rammelberg, H.U., Schmidt, T., Ruck, W.K.L., 2013. Thermal conductivity of salt hydrates as porous material using calorimetric (DSC) method, in: 8th World Conference on Experimental Heat Transfer, Fluid Mechanics, and Thermodynamics, R&D Document Type: BXXS. Presented at the ExHFT-8, A. Faria - Edicao Electronica Lda., Instituto Superior Técnico, Lisbon, Portugal, p. 5.

Freni, A., Tokarev, M.M., Restuccia, G., Okunev, A.G., Aristov, Y.I., 2002. Thermal conductivity of selective water sorbents under the working conditions of a sorption chiller. Applied Thermal Engineering 22, 1631–1642. doi:10.1016/S1359-4311(02)00076-5

Gascoin, N., Fau, G., Gillard, P., 2012. Determination of Darcian permeability of porous material by infrared spectrometry. Journal of Porous Materials 19, 317–331. doi:10.1007/s10934-011-9478-5

Genceli, F.E., Rodriguez Pascual, M., Kjelstrup, S., Witkamp, G.-J., 2009. Coupled heat and mass transfer during crystallization of mgso4·7h2o on a cooled surface. Crystal Growth & Design 9, 1318–1326. doi:10.1021/cg800377x

Gomez, J.C., Glatzmaier, G.C., Mehos, M., 2012. Heat capacity uncertainty calculation for the eutectic mixture of biphenyl/diphenyl ether used as heat transfer fluid, in: SolarPACES, Contract No. DE-AC36-08GO28308. Presented at the SolarPACES, NREL (National Renewable Energy Laboratory), Marrakech, Morocco, p. 9.

Guanghua, N., 2004. Measurement of the thermal conductivities of $Na_2SO_4 \cdot 10H_2O$ and $Na\_2CO\_3 \cdot 10H\_2O$. Inorganic Chemicals Industry, Chinese 6.

Guanghua, N., Zhi-ying, Z., 2002. Measurement of thermal conductivities of salt hydrates II. $FeCl_3 \cdot 6H_2O$, $FeSO_4 \cdot 7H_2O$. Journal of Hubei Institute For Nationalities 8.

Gurgel, J.M., Filho, L.S.A., Grenier, P., Meunier, F., 2001. Thermal Diffusivity and Adsorption Kinetics of Silica-Gel/Water. Adsorption 7, 211–219. doi:10.1023/A:1012732817374

Gurgel, J.M., Grenier, P., 1990. Mesure de la conductivite thermique du charbon actif ac-35 en presence de gaz. The Chemical Engineering Journal 44, 43–50. doi:10.1016/0300-9467(90)80052-E

Gurgel, J.M., Klüppel, R.P., 1996. Thermal conductivity of hydrated silica-gel. The Chemical Engineering Journal and the Biochemical Engineering Journal 61, 133–138. doi:10.1016/0923-0467(96)80020-0

Hakvoort, G., van Reijen, L.L., Aartsen, A.J., 1985. Measurement of the thermal conductivity of solid substances by DSC. Thermochimica Acta 93, 317–320. doi:10.1016/0040-6031(85)85081-4

Iverson, B.D., Cordaro, J.G., Kruizenga, A.M., 2011. Thermal property testing of nitrate thermal storage salts in the solid-phase. ASME 54686-5th International Conference on Energy Sustainability, Parts A, B, and C 495–502. doi:10.1115/ES2011-54159

Jiang, L., Wang, L.W., Jin, Z.Q., Tian, B., Wang, R.Z., 2012. Permeability and thermal conductivity of compact adsorbent of salts for sorption refrigeration. J. Heat Transfer 134, 104503–104503. doi:10.1115/1.4006751

Jiang, L., Wang, L.W., Wang, R.Z., 2014. Investigation on thermal conductive consolidated composite CaCl2 for adsorption refrigeration. International Journal of Thermal Sciences 81, 68–75. doi:10.1016/j.ijthermalsci.2014.03.003

Kaviany, M., 1999. Principles of Heat Transfer in Porous Media, 2nd edition. ed, Mechanical Engineering Series. Springer, New York.

Kiplagat, J.K., Wang, R.Z., Li, T.X., Oliveira, R.G., 2012. Enhancement of heat and mass transfer in solid-gas sorption systems. International Journal of Air-Conditioning and Refrigeration 20, 1130001 (1–16). doi:10.1142/S2010132511300011

Kristiansen, J., 2003. The Guide to expression of uncertainty in measurement approach for estimating uncertainty an appraisal. Clinical Chemistry 49, 1822–1829. doi:10.1373/clinchem.2003.021469

Kuhmichel Abrasiv GmbH, Glass beads physic-chemical properties, Glass Beads - GP. (2014). http://www.kuhmichel.com/116-1-Glass-Beads.html (accessed September 10, 2014).

Lahmidi, H., Mauran, S., Goetz, V., 2006. Definition, test and simulation of a thermochemical storage process adapted to solar thermal systems. Solar Energy 80, 883–893. doi:10.1016/j.solener.2005.01.014

Lei, Z., Pan, N., Zhu, S., 2009. Transient methods of thermal properties measurement on fibrous materials. J. Heat Transfer 132, 032601–032601. doi:10.1115/1.4000049

Lide, D.R. (Ed.), 2005. CRC Handbook of Chemistry and Physics, Internet Version 2005 <Thermal properties of Air (Page 6-175)>, 90th Internet Edition. ed, Thermal properties of Air (Page 6-175). CRC Press LLC, Boca Raton, Florida, USA.

Marcus, S.M., Blaine, R.L., 1994. Thermal conductivity of polymers, glasses and ceramics by modulated DSC. Thermochimica Acta 243, 231–239. doi:10.1016/0040-6031(94)85058-5

Mauran, S., Lahmidi, H., Goetz, V., 2008. Solar heating and cooling by a thermochemical process. First experiments of a prototype storing 60kWh by a solid/gas reaction. Solar Energy 82, 623–636. doi:10.1016/j.solener.2008.01.002

Melinder, A., 1997. Thermophysical properties of liquid secondary refrigerants; Proprietes thermophysiques des frigoporteurs liquides.

Menard, D., Py, X., Mazet, N., 2007. Activated carbon monolith of high thermal conductivity for adsorption processes improvement: Part B. Thermal regeneration. Chemical Engineering and Processing: Process Intensification 46, 565–572. doi:10.1016/j.cep.2006.07.013

Merzlyakov, M., Schick, C., 2001. Thermal conductivity from dynamic response of DSC. Thermochimica Acta, Frequency and Time-Dependent Heat Capacity. A collection of Papers from the 6th Lahnwitzseminar on Calorimetry Kuhlungsborn, Germany, 12-18 June 2000 377, 183–191. doi:10.1016/S0040-6031(01)00553-6

Michel, B., 2012. Procédé thermochimique pour le stockage intersaisonnier de l'énergie solaire : modélisation multi-échelles et expérimentation d'un prototype sous air humide (Doctorate/Ph.D). Université de Perpignan, Perpignan - France.

Michel, B., Mazet, N., Mauran, S., Stitou, D., Xu, J., 2012. Thermochemical process for seasonal storage of solar energy: Characterization and modeling of a high density reactive bed. Energy 47, 553–563. doi:10.1016/j.energy.2012.09.029

N'Tsoukpoe, K.E., Schmidt, T., Rammelberg, H.U., Watts, B.A., Ruck, W.K.L., 2014. A systematic multi-step screening of numerous salt hydrates for low temperature thermochemical energy storage. Applied Energy 124, 1–16. doi:10.1016/j.apenergy.2014.02.053

Olives, R., Mauran, S., 2001. A highly conductive porous medium for solid–gas reactions: effect of the dispersed phase on the thermal tortuosity. Transport in porous media 43, 377–394.

Parker, W.J., Jenkins, R.J., Butler, C.P., Abbott, G.L., 1961. Flash method of determining thermal diffusivity, heat capacity, and thermal conductivity. Journal of Applied Physics 32, 1679–1684. doi:10.1063/1.1728417

Presley, M.A., Christensen, P.R., 1997. Thermal conductivity measurements of particulate materials 1. A review. Journal of Geophysical Research 102, 6535. doi:10.1029/96JE03302

Schick, C., 2002. Chapter 16 Temperature modulated differential scanning calorimetry (TMDSC)-basics and applications to polymers, in: Stephen Z.D. Cheng (Ed.), Handbook of Thermal Analysis and Calorimetry, Applications to Polymers and Plastics. Elsevier Science B.V., pp. 713–810.

Smalc, M., Skandakumaran, P., Norley, J., 2007. Thermal performance of natural graphite heat spreaders with embedded thermal vias. ASME Proceeding InterPACK Conference, San Francisco, California USA, Heat Sink Modeling and Characterization 1, 607–617. doi:10.1115/IPACK2007-33215

Tanashev, Y.Y., Krainov, A.V., Aristov, Y.I., 2013. Thermal conductivity of composite sorbents "salt in porous matrix" for heat storage and transformation. Applied Thermal Engineering 61, 401–407. doi:10.1016/j.applthermaleng.2013.08.022

Teng, H., Zhao, T.S., 2000. An extension of Darcy's law to non-Stokes flow in porous media. Chemical Engineering Science 55, 2727–2735. doi:10.1016/S0009-2509(99)00546-1

Tian, B., Jin, Z.Q., Wang, L.W., Wang, R.Z., 2012. Permeability and thermal conductivity of compact chemical and physical adsorbents with expanded natural graphite as host matrix. International Journal of Heat and Mass Transfer 55, 4453–4459. doi:10.1016/j.ijheatmasstransfer.2012.04.016

Tsotsas, E., Martin, H., 1987. Thermal conductivity of packed beds: A review. Chemical Engineering and Processing: Process Intensification 22, 19–37. doi:10.1016/0255-2701(87)80025-9

Van Helden, W., Hauer, A., 2013a. Task 42 - Annex 24, Compact thermal energy storage: material development for system integration - Final Report (Research and Engineering No. IEA SHC/ECES Task 42/24 Final Report), IEA SHC/ECES Task 42/24. International Energy Agency, Europe.

Van Helden, W., Hauer, A., 2013b. 2012 Annual report-Feature article on advances in compact thermal energy storage - material development (Research and Engineering No. IEA Solar Heating

& Cooling Programme), IEA Solar Heating and Cooling Programme. International Energy Agency, Europe.

Vasques, A.R., Innocentini, M.D.M., Assis, O.B.G., 1999. A Simple apparatus for determining the permeability of thin- thickness porous materials by pressure-decay technique. Revista de Fisica Aplicada e Instrumentacao, Instruments 14, 4.

Wang, K., Wu, J.Y., Wang, R.Z., Wang, L.W., 2006. Effective thermal conductivity of expanded graphite–CaCl2 composite adsorbent for chemical adsorption chillers. Energy Conversion and Management 47, 1902–1912. doi:10.1016/j.enconman.2005.09.005

Wen, D., Ding, Y., 2006. Heat transfer of gas flow through a packed bed. Chemical Engineering Science 61, 3532–3542. doi:10.1016/j.ces.2005.12.027

Xamán, J., Lira, L., Arce, J., 2009. Analysis of the temperature distribution in a guarded hot plate apparatus for measuring thermal conductivity. Applied Thermal Engineering 29, 617–623. doi:10.1016/j.applthermaleng.2008.03.033

Yu, N., Wang, R.Z., Wang, L.W., 2013. Sorption thermal storage for solar energy. Progress in Energy and Combustion Science 39, 489–514. doi:10.1016/j.pecs.2013.05.004

Zalba, B., Marín, J.M., Cabeza, L.F., Mehling, H., 2003. Review on thermal energy storage with phase change: materials, heat transfer analysis and applications. Applied Thermal Engineering 23, 251–283. doi:10.1016/S1359-4311(02)00192-8

Zhang, X., Fujii, M., 2000. Simultaneous measurements of the thermal conductivity and thermal diffusivity of molten salts with a transient short-hot-wire method. International Journal of Thermophysics 21, 71–84. doi:10.1023/A:1006604820755

5. PERFORMANCE ANALYSIS OF THE THERMOCHEMICAL HEAT STORAGE SYSTEM

In this chapter, numerical and theoretical performances of the storage system are studied in order to develop a prototype. Based on the previous study at the micro-scale, thermal performances are highlighted and then extended with the lab-scale experiment, and finally a comparison for models (analytical and 3D) validation. The analytical models developed in Chapter 3 served to efficiently approach the optimal solution and greatly reduce the design for any 3D study (geometry design and meshing) and the number of simulations to achieve.

5.1. GENERAL ANALYSIS

Before starting analysis, the project target specifications are presented in order to define the needs and constraints and hence designing a prototype.

Table 5.1. Target specifications of the thermochemical storage system and reference values.

Specifications	Value
Storage capacity	80 kWh in 1 m^3 of prototype reactor
Energy storage density	576 kJ·l^{-1} = 160 kWh·m^{-3} for the prototype
Thermal power	10 kW
Heating rate	1-10 K·min^{-1} or higher according to (N'Tsoukpoe et al., 2014)
Pressure range	10 – 80 mbar
Temperature range	35 – 88 °C
Coefficient of performance (COP_{th})	> 0.5 (minimum COP for basis system using only one salt (Istria et al., 1996))
Thermal conductivity of the salt	0.56 ($SrBr_2·H_2O$), 0.71 ($SrBr_2·6H_2O$) (W·m^{-1}·K^{-1})
Permeability of the salt	0.7×10^{-10} ($SrBr_2·H_2O$), 3.1×10^{-11} ($SrBr_2·6H_2O$) (m^2)

Looking at the above table, one can understand that a prototype based on these specifications can run 8 hours per day in cold periods. From the preliminary studies at micro-scale, the required time to completely hydrate the salt in order to fulfil the above specification can be estimated. In fact, from the released power of the reactor and the stored energy, the following formula is used:

$$t_\alpha = \frac{stored\ energy}{released\ power} = \frac{E_{stored}}{P_{released}}$$

(5.1)

From the above formula and using data from Table 4.9, hydration time is about 22 days to completely hydrate the salt bed at prototype level. However, this time was based on the micro-scale study. The complete hydration time function of the reaction conversion or advancement at the reactor scale will be given using the sharp front model developed in chapter 4. The focus on this time is to justify the required simulation time for numerical studies. Therefore, the eight hours (28800 s) of running period has been chosen. The needed parameters as permeability, thermal conductivity, specific heat capacity and kinetic properties have been already determined in the previous chapter and will be used here. For charging, an inflow temperature of $\sim 100\ °C$ is set for the heat transfer fluid and condensation temperature to 25 °C, hence a condensing vapour pressure around 32 mbar. Since Eq. (3.6) normally stands for pure vapour system, equilibrium temperature of the salt bed can easily be deduced according to the condensing pressure. It is found to be $T_{eq}(p_{cond})$ = 58 °C. This temperature helps evaluating the temperature swing that the reactor will experience during a whole cycle. In fact, in practice, the reaction requires the reactive salt to be out of equilibrium (as mentioned in chapter 2, section 2.2.3) for heat and mass transfer to take place. For the discharging phase, the vapour should be generated at lower temperature such of 10 °C corresponding to a vapour pressure of about 13.2 mbar. Therefore an inlet pressure of about 14 mbar were chosen for the simulations. Following the same scheme to determine the equilibrium drop during discharging, it was found that $T_{eq}(p_{evap})$ = 45 °C. Based on this theoretical thermodynamic analysis, it can be sure that at least 45 °C can be produced by the thermochemical system based on strontium bromide with five water molecules involved. Still, this achievement depends on the reaction kinetic of the salt bed. In the following, numerical investigations are performed in order to point out the optimal parameter values to better hydrate the salt bed and hence, lead to optimal performances.

5.2. NUMERICAL INVESTIGATIONS

Since hydration corresponds to the discharging, hence the output that is need for the common user, the work is in general focused on it. From an engineering view, the question, how should the conversion be completed to offer great performances, find the answer in determining the appropriate vapour flow rate through the bed, the size of the bed, its optimal porosity and hydration time.

5.2.1. OPTIMAL PARAMETERS EVALUATION

From the sharp front model (Eq. (3.56)) and using the different experimental permeability (k_D from Eqs. (4.13)) of strontium bromide with the previous mentioned hypothesis in chapter 2, the needed hydration time, water vapour flow rate crossing the salt bed along with the bed size can be predicted and later compared with the experimentation on the prototype. Using the following constraints:

- water vapour pressure of 14 mbar, bed temperature of 45 °C and a pressure difference around the bed of 0.5 mbar,
- an enthalpy of formation of 67400 $J·mol^{-1}$, an entropy of 175 $J·mol^{-1}·K^{-1}$ with five water molecules involved,

- in this model, a bed with particle diameter of 100 μm and a total porosity of 0.75 (this value find its justification in the following) is assumed,
- and assuming a quasi-complete hydration ($\alpha \sim 0.9$),

the required time to totally hydrate the bed is given in Figure 5.1a (~ 22 days) which matches the theoretical value obtained with Eq. 5.1. On Figure 5.1a, it can be seen that less than one month is required to hydrate the bed.
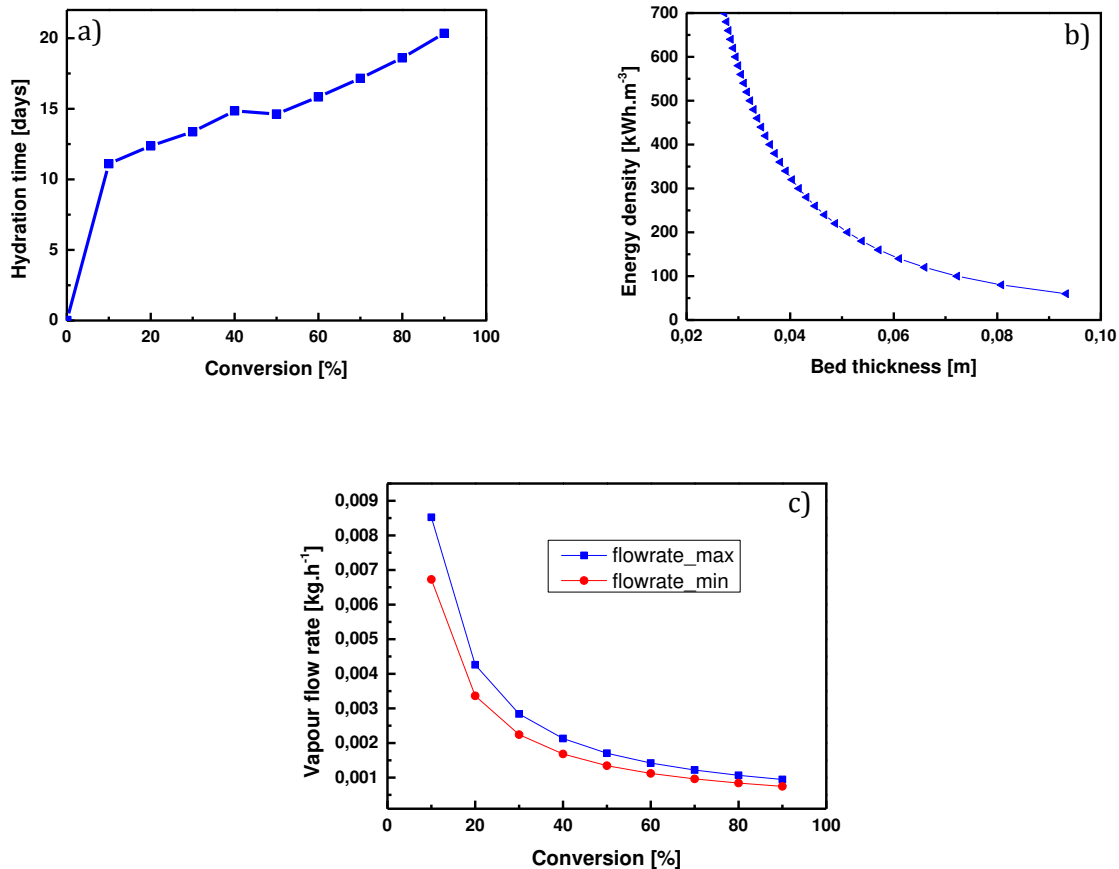
Figure 5.1. Numerical results of parameters: (a) hydration time as function of the reaction conver¬sion or advancement under pure water vapour; (b) energy density of the salt as function of the bed size (thickness); (c) vapour mass flow rate at the entrance of the salt bed as function of the reaction conversion.

Hydration strongly depends on the heat source for evaporation performance. A geothermal heat source can provide the 10 °C needed at a very low cost, so that any impact on the prototype cost is noticed. Unfortunately, no geothermal heat source was available.

Once hydration time is known, Eq. (3.57) helps to evaluate the salt energy density on the bed size. Fig. 5.1b shows the relationship between the energy density of the salt and the bed size. As already determined at micro-scale (531 kWh·m^{-3}) and comparing to theoretical value (629 kWh·m^{-3}), energy density should be between 500 and 650 kWh·m^{-3} in order to exhibit great performance at the prototype scale than latent and water storage systems. Hence to obtain that energy density, bed

thickness should be in the range of 0.028 – 0.033 m under pure vapour. According to that thickness range and still using the sharp front model, the corresponding mass flow rate of the vapour can be determined. Figure 5.1c shows vapour mass flow rate evolution function of the reaction conversion and one can observed that, to achieve quasi-complete hydration of the bed, mass flow rate should not be higher than 0.001 kg·h^{-1}. Such information consolidates the laminar regime mode within the bed (found in the chapter 3). This information helps when looking for the appropriate valve to connect the evaporator and the reactor. When compared to the mass flow rate at the micro-scale (chapter 4, Figure 4.15), it was very small, around 4×10^{-18} kg·h^{-1} of water vapour. As a recall, this flow rate strongly depends on the tubing. The flow rate maximum and minimum corresponds to the minimum and maximum bed thickness respectively. Large bed thickness required a lower vapour mass flow rate whereas a small bed thickness required a higher mass flow rate to achieve quasi-complete hydration.
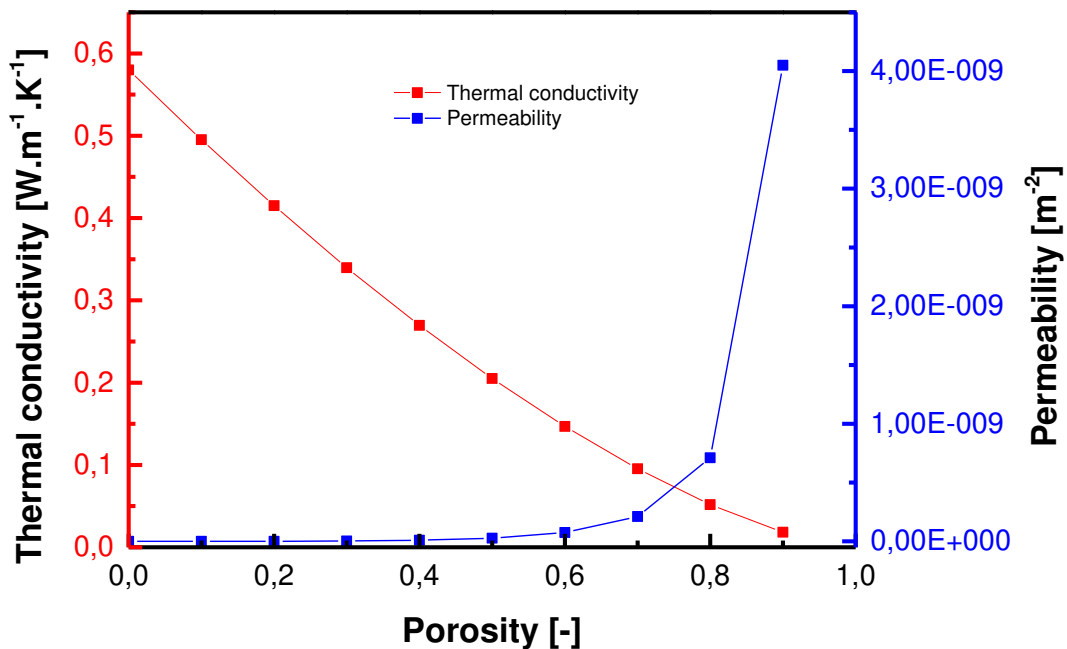
Figure 5.2. Numerical evaluation of the optimal porosity of strontium bromide for efficient heat and mass transfer.

Numerical evaluation of the optimal porosity is strongly related to the simultaneous heat and mass transfer. That means, looking for the porosity that allow simultaneously fairly good heat and mass transfer. Contrastingly, porosity also effects on the density of the salt. If the density of the salt is low and the porosity high, an efficient heat exchanger must be added to increase the heat transfer in the reactor. On the other hand, gas diffusers must be added to increase mass transfer in the reactor when the density of the salt is high and the porosity low. Some researchers (Azoumah et al., 2004) focused their interest on finding the optimal density for composites design. Figure 5.2 shows the confrontation of thermal conductivity (heat transfer characteristic) and permeability (mass

transfer characteristic) of the strontium bromide versus its total porosity. The chosen porosity value of 0.75 in the above section was taken from this analysis.

5.2.2. KINETICS ANALYSIS

Various geometrical scales characterise all phenomena which occur in a reactor. A description of the modelling process requires a precise definition of these different scales. We have deliberately set these scales from the size: micro (milligrams), where the reactor is a pan into a furnace and macro (some grams of salt), where the reactor is at labscale. This precision is necessary to show the difference with the prototype-scale where tons of salt are required. Figure 5.3 shows the validation of the analytical model and simulated model for the conversion. However, only hydration is presented at the reactor scale due to the fact that this phase determines the system performance.
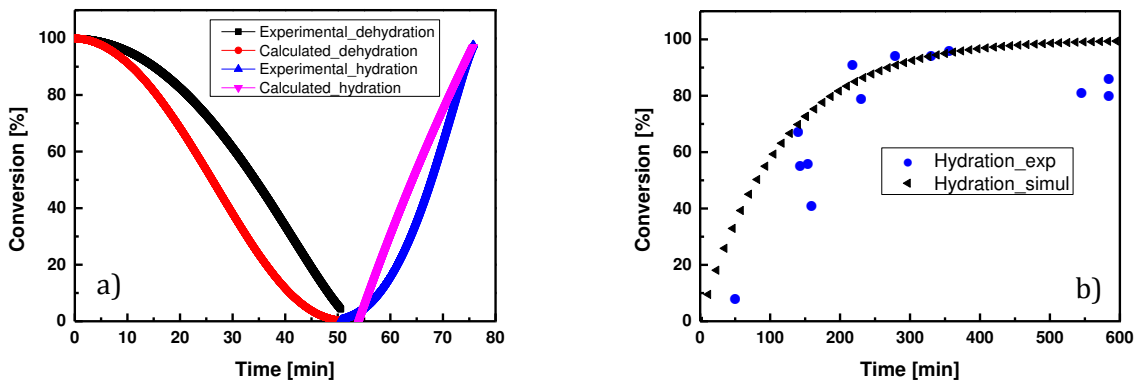
Figure 5.3. a) Micro-scale validation of the theoretical analysis of the kinetic curves under realistic conditions. b) Reactor-scale validation of the kinetic simulation for the coupled heat and mass transfer.

In both case, one can see that numerical results predict rapid conversion than experimental results and seems to closely fit when reaching the end of the reaction. Where the curves do not fit closely can be due to the pressure effect and the absence of thermal expansion or shrinking coefficient in the model. At the microscopic scale, the conversion is evaluated for a representative quantity of salt. By finite difference it is possible to derive the reaction rate $\frac{\partial \alpha}{\partial t}$ (Eqs. (3.17) - (3.18)), which allows calculating heat and mass sources produced by the reaction. Hence, heat source and mass source for the vapour presented in Eqs. (3.29) and (3.37).

Due to these sources terms, the chemical reaction at the microscopic scale impacts the spatial and temporal evolution of the thermodynamic processes at the reactor scale. Inversely since temperature and pressure changes modify the frequency of nucleation and the reactivity of growth (Favergeon et al., 2013), thermodynamic influences conversion of the reaction at microscopic scale. Previous work on a different salt has shown similar behaviour (Fopah Lele et al., 2015). Figure 5.4 shows the experimental and numerical kinetic rate of a cycle dehydration-hydration of the

strontium bromide. Numerical results account for the pressure effect, hence the slowness than the experimental. The first pick down corresponds to the dehydration and the pick up to the hydration, showing at which rate heat is stored and released, respectively. It can be observed that the cycle yields at magnitude of $\times 10^{-4}$. In addition, the crystallography systems (although it is not in the scope of this work) of $SrBr_2 \cdot 6H_2O$ and $SrBr_2 \cdot H_2O$ can be tetragonal or orthorhombic (Dyke and Sass, 1964), meaning large structure to receive water molecules. Hence gas pressure effect into the structure.
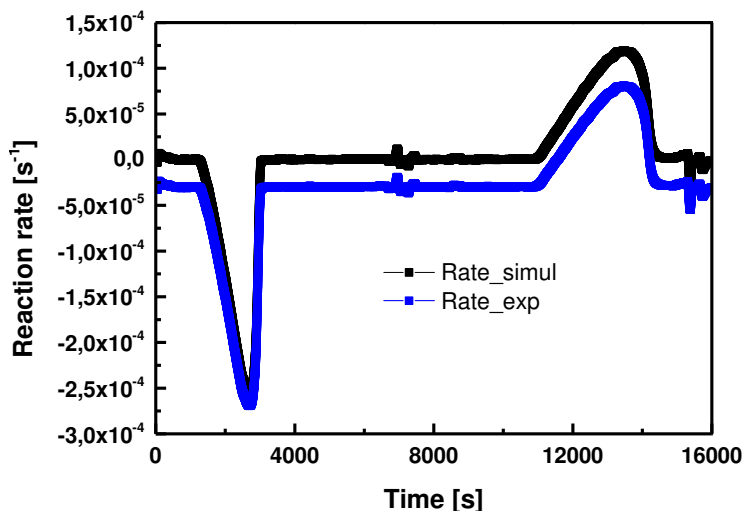
Figure 5.4. Experimental reaction rate of strontium bromide during decomposition and synthesis with their comparison with numerical result as functions of time.

The reaction rate versus the extent conversion on Figure 5.5 clearly should normally show the different hydrates during decomposition and synthesis of strontium bromide at the exact conversion or percentage of removed/gained water into the salt. The reaction rate is however showing a kind of dome (downward and upward face) corresponding to the direct formation of $SrBr_2 \cdot 1H_2O$ (Figure 5.5a) and $SrBr_2 \cdot 6H_2O$ (Figure 5.5b). Each analysis of the peak led to a first order kinetic. One can see that, conversion do not proceed step by step, I mean for example, in decomposition, it does not decompose to penta-, tetra- or dehydrate, it is an overall process until the anhydrous form ($SrBr_2 \cdot H_2O$). A question arises, why not obtaining $SrBr_2$ directly? The answer lies in term of stability. Dyke and Sass (Dyke and Sass, 1964) justified that answer stating that, the increase in coordination number of the strontium ion by water molecule allow great stabilization in crystal lattices. Taking into account the pressure effect shows slight discrepancy between numerical and experimental results. One can observe that during decomposition, energy is stored from 20% to 50% of conversion, and is released from 45% to 95% of conversion during synthesis. This justifies the assumption of the quasi-complete hydration adopted earlier in the analytical sharp front model.

Chemical kinetics is always a function of temperature, time and concentration. The conversion informs us about the decomposition and synthesis mechanisms and the reaction rate about the time effect, what happened during conversion and the reaction order. However a good understanding of other mechanisms (nucleation, growth, cracks, and dilatation-retraction) should involve scanning electronic microscopy (SEM) study of the material crystals damaged by heating and X-ray diffrac-

tion (XRD) for structural analysis, which is not in the scope of this thesis. These agreements between experimental and numerical results lead to validate the kinetic model
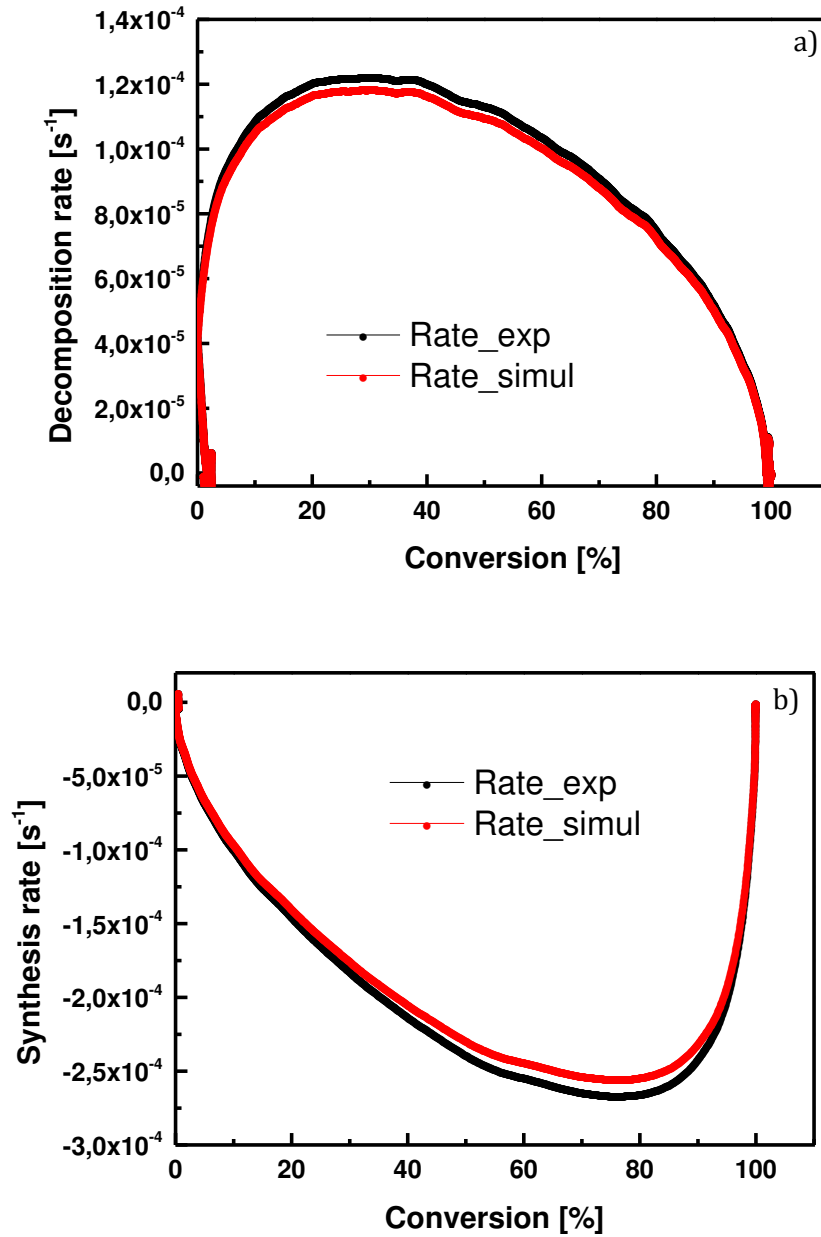
Figure 5.5. Experimental reaction rate of the strontium bromide during decomposition (a) and synthesis (b) and their comparison with numerical result as functions of the conversion.

The reaction rate is temperature and pressure dependent. This dependence is related to the kinetic factor $R_{kin} = A_f \exp\left(-\frac{E_a}{\mathcal{R}T}\right)$ in Eqs. (3.17) and (3.18). So, for different temperatures there is a variation of the kinetic factor of the reaction. Focusing only on the hydration, Fig. 5.6 shows that the conversion α strongly depends on R_{kin}. For the same value of α, for example α =0.7, we can observe

that the high temperature group (R_{kin} = 2×10⁻⁴ and 3×10⁻⁴) arrives much earlier than the low temperature group (R_{kin} = 9×10⁻⁵ and 1×10⁻⁴). That means high temperature has a rapid effect on the reaction rate. However, with a high reaction temperature, the amount of heat loss on the wall is too high. This heat loss reduces the energy efficiency of the thermal storage system. Therefore one has to find a compromise between the reaction rate and the energy efficiency. In the following, R_{kin}= 1×10⁻⁴ is adopted for further simulation and this value is justified on the Figure 5.4, besides, the kinetic of reaction may become a limiting factor to the hydration. The same Figure shows that, reaction advancement is not so sensitive to the vapour pressure *p*. For different pressures values, the results are similar. For an extremely low pressure value of *p* = 20 Pa, the evolution of the conversion (or advancement) becomes slightly slower than before.
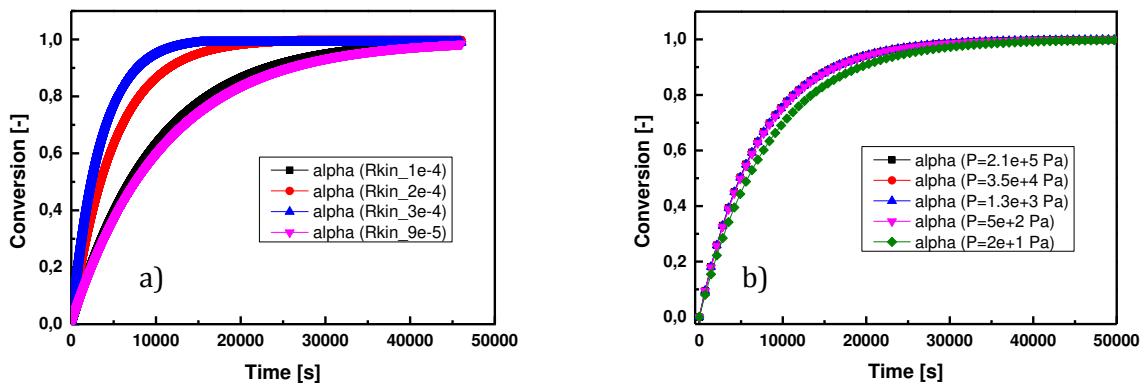
Figure 5.6. Influence of kinetic factor (a) and vapour pressure (b) on the reaction conversion of the strontium bromide during synthesis.

Since conversion expresses the water adsorption/desorption, another parameter to take into account is the grain size. N'Tsoukpoe et al. showed that the grain size can be a powerful tool to also manage the dynamic of water adsorption/desorption (K. Edem N'Tsoukpoe et al., 2014). The above results will allow an estimation of the accuracy of simulations depending on the detail to which the reaction kinetics of a material are known. This also helps validating the kinetic model under varying circumstances. The use of kinetics can significantly reduce experimental efforts for characterizing a reactive material to enable simulations of a larger system based on said material.

5.2.3. HEAT AND MASS TRANSFER RESULTS

Before discussing the results in this part, it is relevant to point out the parameters dependence. The main parameters (thermal conductivity, permeability, heat capacity, porosity) used for numerical investigation are independent of the conversion process (adsorption/desorption). Indeed, under vacuum, the dependence can be neglected with standard deviation lower than 2% on the results (Michel, 2012). This previous author demonstrated that under vacuum, heat transfer is the limiting factor to the conversion for effective thermal conductivity of the bed less than 50 W·m⁻¹·K⁻¹, and within the range (10.38 – 11) W·m⁻¹·K⁻¹, hydration time is reduced, hence released power increase. The non-taking into account of radiation (although radiation highlights the realty of enhanced

surface heat transfer) in the energy balance reduces the heat transfer coefficient. However the reduction is less than or equal to 10% but increases the charging time (Andreozzi et al., 2014). Well, we are expecting longer dehydration time and exact hydration (8 hours per day) time as predicted before. However, the increase of released power can be done using composites-based-salt (which is not in the scope of this work of course).

The investigation was then further performed at the lab-scale using the geometry of Figure 3.7 and Eq. (3.19) (numerical). Due to the long-time of numerical simulation, the dynamic of water adsorption or absorption is studied only during the hydration. The effect of the main parameters (permeability and thermal conductivity) is looked on the hydration conversion.
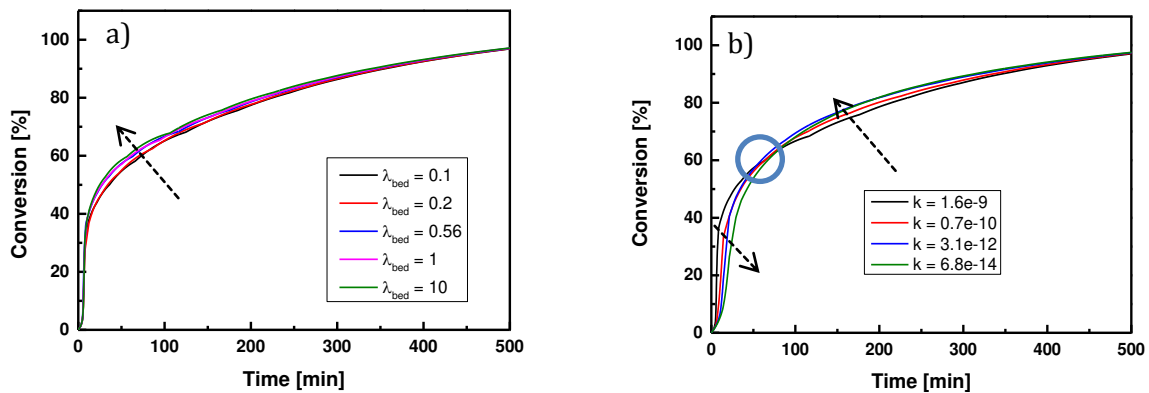
Figure 5.7. Influence of the thermal conductivity of the salt bed (a) and its permeability (b) on the hydration degree of the bed.

Figure 5.7 shows the impact of the two main parameters, when talking about heat and mass transfer, on the hydration of the salt bed in order to see the optimum value for a complete hydration. Figure 5.7a exhibits that high the thermal conductivity, fast is the hydration. However, between 25 and 80% of conversion we observe two main groups: (0.1 to 0.56 W·m^{-1}·K^{-1}) and (1 to 10 W·m^{-1}·K^{-1}). The standard deviation between those two groups is less than 7%, but it reveals that storage materials with higher thermal conductivity improve the hydration (respectively the dehydration).

Figure 5.7b shows the permeability effect. At the beginning of the hydration until reaching 60% of conversion, bigger permeability leads to faster hydration. Then the phenomenon is reversed after 60% of conversion until the complete hydration. This can be explained by water molecules absorption as follows: big voids in the salt structure are rapidly occupied and also react faster with solid, then become slower since the voids are no longer available. Small voids are progressive occupied, that is why the conversion is slower at the beginning and then become fast. The intersection on Figure 5.7b may explain the simultaneous adsorption at the salt surface and quasi-absorption in the salt volume (not entirely but a part). During the adsorption, voids are blocked by the adsorbed gas and the following gas flows through the supercritical voids (Kainourgiakis et al., 1998). Vapour is then condensed after a certain time inside the salt structure, leading to the absorption of those condensable (such as droplets in the liquid phase).

3D modelling of thermochemical heat storage is a complex problem where a simultaneous chemical reactions and heat and mass transfer through porous medium occur. In this thesis, fluid flow field was coupled to the heat and mass transfers inside salt bed. Numerical considerations involved solution of the hydrodynamic equations for the fluid followed by solving the equations of heat and mass transfers in salt as porous medium. Thus, heat was transferred from heating fluid to salt surface by convection and from surface to inside of the salt by conduction. Similarly, the water content was transferred to the surface from the inside by diffusion and from the salt surface to the gas by convection.
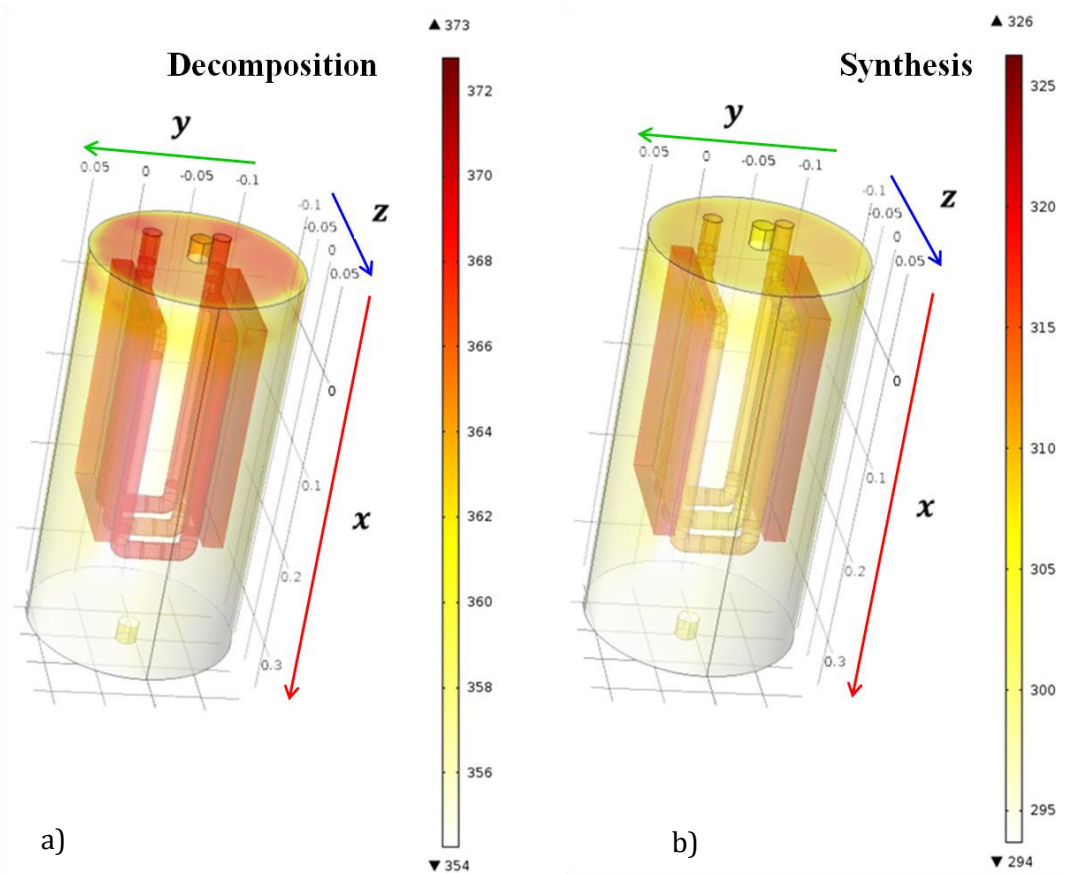
Figure 5.8. Numerical 3D view of the salt bed temperature during charging (a) and discharging (b) at a specific time of 150 min for the charging and 15 min for the discharging.

The following results on the 3D model (Figure 5.8) are based on the used parameters in appendix A3. The geometry of the simulation model is always a big issue in 3D. The resolution of fluid mechanics in the elbow parts of the tubes is a tough task in the charging process and the initial inlet fluid temperature is set to 105 °C. Inlet and inflow boundaries are set to the bottom of the reactor in the discharging process. The vapour steam arrives with a concentration fixed at 2500 mol·m^{-3}. At t=0, initial bed temperature is equal to 20 °C. Figure 5.8 exhibits storage and release heat process using a 3D model in order to be closed to the reality. The fluid (thermal oil) circulates into the tubes perfectly conductive, and transfers its heat to bed in order to dehydrate the salt bed. When heat is stored, water vapour leaves the bed and is condensed into a condenser, which is not simulated here.

One can see in Figure 5.8a that, the bed received the quasi-exact temperature from the heating fluid at about 373 K (100 °C). As already said, this temperature corresponds to what can provide the losses from a micro-CHP. In order to visualize distribution within bed, temperature at several space points (Appendix A7) of the bed is plotted and discussed.
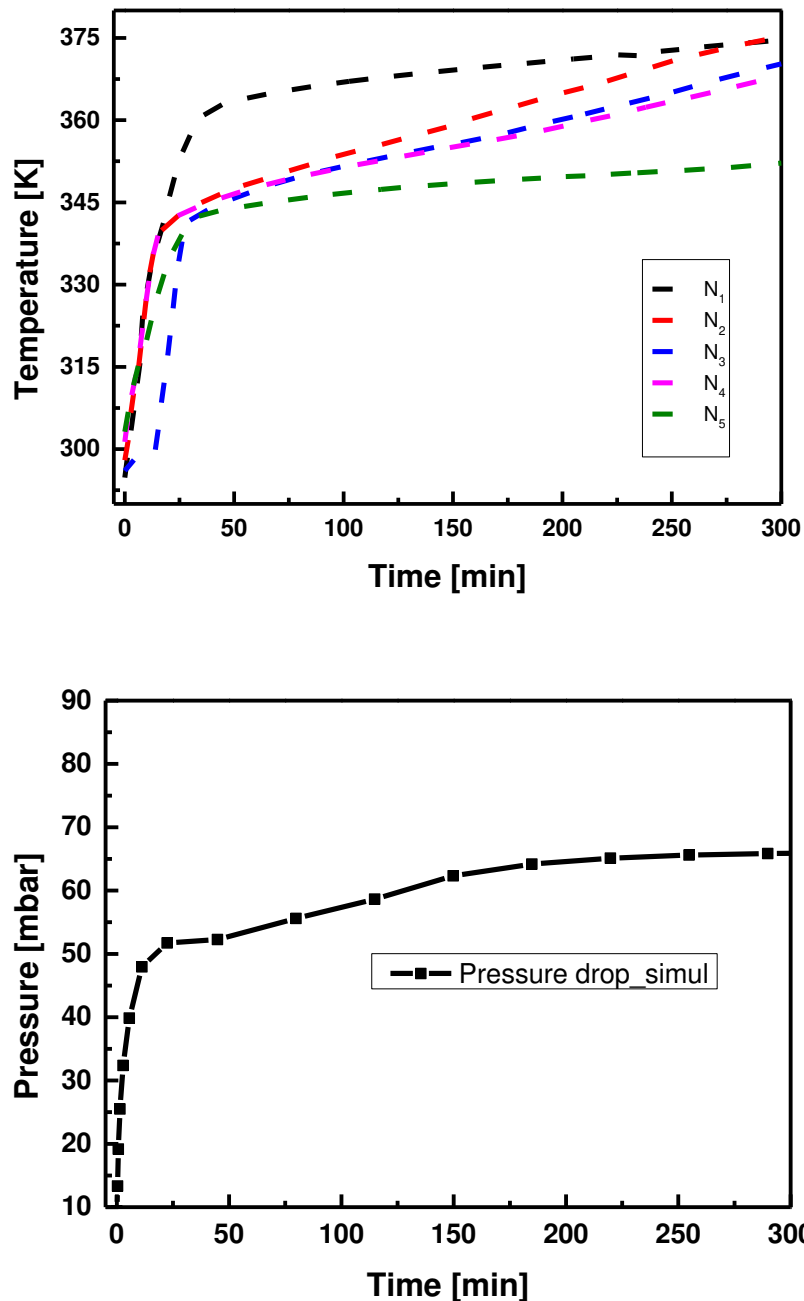
Figure 5.9. Numerical results of the charging process (bed temperature and pressure evolution).

During charging it can be observed in Fig. 5.9 how gradually bed temperature evolves. It shows two elbows at space positions N2 (0.1, -0.03, -0.025), N3 (0.08, -0.04, 0.02), N4 (0.2, -0.03, -0.025), the first at around 50 min actually explains the phenomenon when inside-water becomes vapour, and the second at around 250 min when the vapour is getting out of the bed. That second phenomenon is well explained using the pressure drop in the reactor which tends to be linear after 175 min of process. The quasi-linearity from 50 min on the pressure drop figure, brings an explanation to the first phenomenon. Once water is in the gas phase, pressure tends to reach reactor equilibrium. However, that equilibrium is at around 69 mbar, corresponding to the equilibrium temperature of around 362 K in Figure 3.6 to charge the bed.
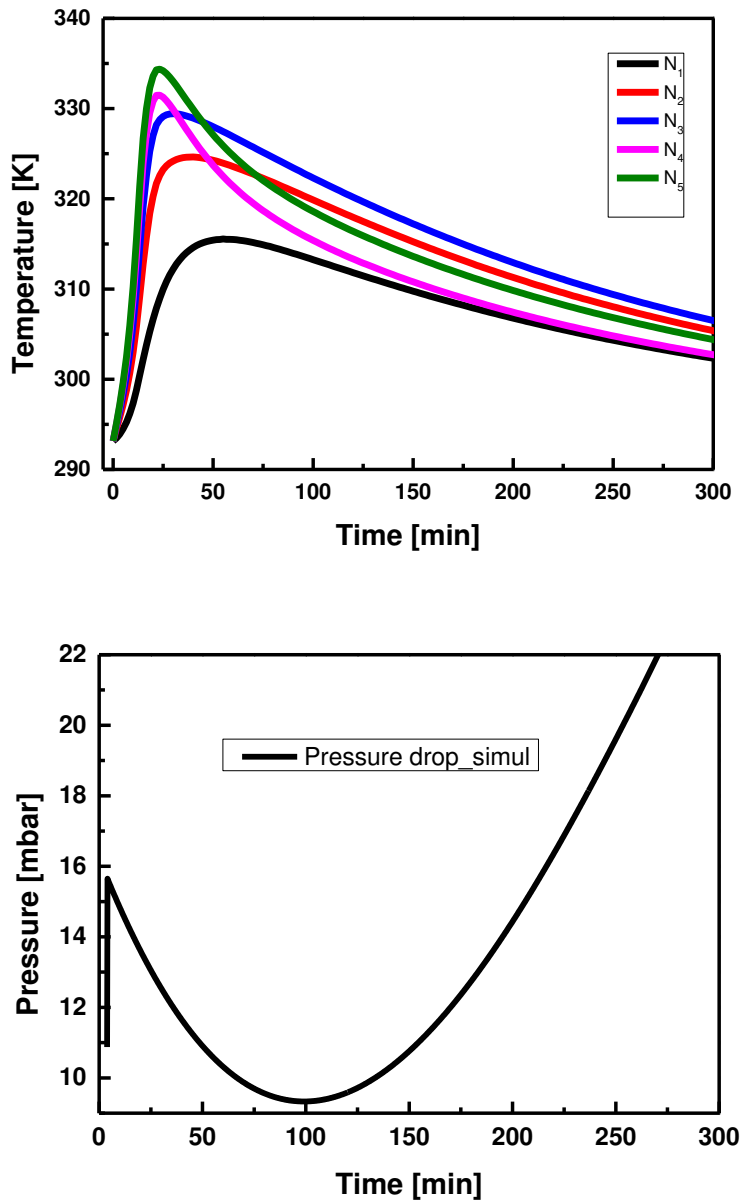
Figure 5.10 Numerical results of the discharging process (bed temperature and pressure drop).

From there (50 min), starts the endothermic dehydration of the $SrBr_2 \cdot 6H_2O$ with release of water vapour indicated by a drop in the gradient of the bed temperatures. After 12 min, temperature is at about 294 K (21 °C) and later at 30 min temperature of 338 K (65 °C) is reached. Hence, the heating rate higher at the beginning decrease from 24 $K \cdot min^{-1}$ to 1 $K \cdot min^{-1}$ as expected beyond the range. However from 30 min to the end the rate is in the target rate range as in Table 5.1.

Figure 5.10 shows the bed temperature and the pressure drop profiles during the discharging procedure. The reaction is initiated when water vapour at 14 mbar flows into the reactor. At position N5 (0.08, -0.04, 0.02), peak goes up to 335 K (62 °C) because of the proximity to the evaporator entrance, meaning salt react first at this position. At position N1 (0.1, -0.03, 0.025), peak goes up to 315 K (42 °C) since vapour arrives later at this position. An average at all points of the bed gives temperature peak at 325 K (52 °C). The peak temperature is obtained at a heating rate of about 27 $K \cdot min^{-1}$ but during the decreasing that value is between 1 and 10 $K \cdot min^{-1}$. As seen in Figure 5.10, bed temperature increases till the equilibrium temperature before starting to decrease slowly. This happens between 1 and 15 min and after that cooling starts. This cooling effect is linked to two phenomena: the cooling of the inflow vapour itself after the first input and the natural convective flux outside of the reactor.

In Comsol, the physics "reacting flow diluted species" calculates the pressure during the process. Figure 5.10 shows a small pressure drop variation of 13 mbar during the discharging process. This drop is closely related to the exothermic reaction. During this latter, salt adsorbs the vapour quite quickly in the beginning, then get slower and slower because it gets saturated and attempts to regain the equilibrium. The effect is directly coupled with the peak temperature happening at the beginning. However this drop is very small (for instance less than 0.1 mbar) across a hexagonal duct which compose the bed. It is verified using Eq. (3.6). After 100 min, pressure suddenly starts to increase. An explanation can be the bed temperature at some point (N5) of the bed, since N'Tsoukpoe et al. stated that, a vapour pressure above 40 mbar is required to reach 60 °C in the reactor (N'Tsoukpoe, 2014).

5.2.3.1. Cooling effect on bed temperature

This parametric study mostly concerns the discharging procedure. The cooling effect of the bed is investigated, considering a simulation run with only vapour cooling itself, meaning there is no natural convection ($h = 0$ $W \cdot m^{-2} \cdot K^{-1}$). Another case, where only natural convection is considered ($h = 4,05$ $W \cdot m^{-2} \cdot K^{-1}$ and diffusion coefficient neglected), and the both represents the formal numerical results.

Figure 5.11a exhibits the cooling effect on the bed temperature profile. It starts from 315 K (42 °C) and there can be seen that considering only the self-cooling of the vapour slightly increases the bed temperature but is reduced if only the outside convection is considered. This can be explained by the variation of the vapour temperature. While it cools down the side salt, the vapour is heated itself when reacting with the salt plus the generated sensible heat. So after a time period the vapour temperature is balanced with the side salt while the convective heat flux keeps decreasing the

temperature which tends to balance with the ambient temperature of the room. Another effect is the honeycomb made of aluminium, which tend to homogenise the bed temperature from the start of the reaction as seen in Figure 5.11b. On that figure, it can be seeing that the use of equivalent parameters on the simplified bed as done in chapter 3, do not affect the results.
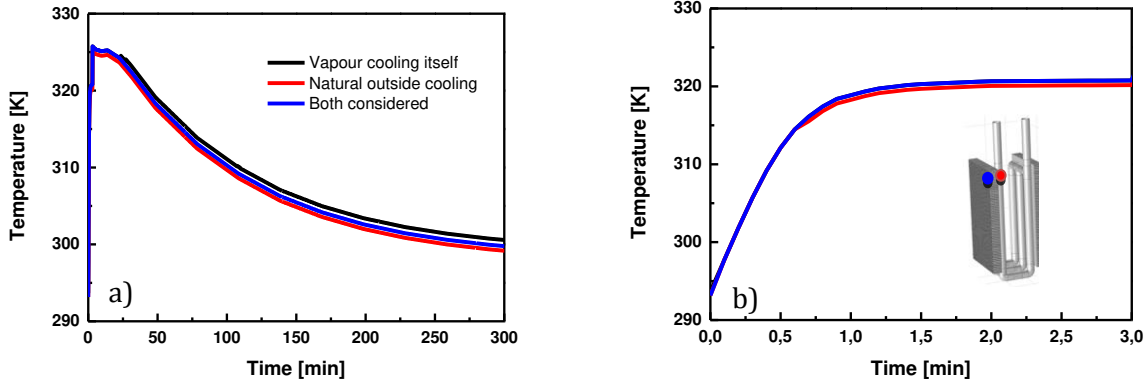
Figure 5.11. Cooling effect on the released temperature (a); and the aluminium effect during the first three minutes of the discharging (b).

5.2.4. THERMAL POWER AND EFFICIENCY

Expressions of thermal power evaluation in thermochemical heat storage are varying and strongly depend on the process. Most of them only focus on the synthesis (hydration or sorption) phase. The trivial condition determining the power of thermochemical reactors is the equilibrium deviation $\Delta T_{eq} = T_c - T_{eq\_bed}$, where T_c is the temperature at the heat exchanger layer in the case of closed process. The reason behind is that, this deviation initiates the synthesis or decomposition reaction. Stitou et al. proposed the average thermal power, involving the both the reaction power and the sensible power developed during the reaction phase as follows (Stitou et al., 1997):

$$P_{aver} = (1 + \sigma)\left(\chi C_{s0} V_{s0} \Delta H_r \frac{\Delta\alpha}{t_\alpha}\right) \quad \text{where } \sigma = \frac{\rho_{s0} C_p \Delta T_{eq}}{\chi n_{s0} \Delta H_r} \approx 2 - 10\% \tag{5.2}$$

The term σ represents the energy ratio between the sensible and the reaction energy, of a mean value of 5% adopted by the authors for the average power at the heat exchanger layer or wall. From the analytical sharp front model, the average volume power (Michel, 2012; Stitou, 2013) released by the reactive salt can be expressed in function of the reaction conversion or advancement:

$$P_{aver\_v} = (1 - \varepsilon)\left(\chi \Delta H_r \frac{\rho_{s0}}{M_{s0}}\right)\frac{\Delta\alpha}{t_\alpha} \tag{5.3}$$

163

Some researchers came out with other expressions. Li et al. proceeded by determining the amount of heat produced during discharging on the required hydration time, in which the sorption heat of every material involved is taken account (Li et al., 2014). This amount of heat is the sum of the reaction heat of the reactant, the sensible heat released by the reactant during transferring heat to the tube and the sensible heat released by the aluminium part of the reactor when it is cooled from the heat input to the heat transfer fluid. The average power of solid–gas thermochemical sorption heat storage during the discharging phase is calculated using the following equation:

$$P_{aver\_sht} = \frac{Q_{out}}{t_\alpha} = \frac{Q_r + Q_{s\_salt} + Q_{s\_Al}}{t_\alpha} \tag{5.4}$$

From the authors' definition of different heats, their amount can be obtained from the following equation:

$$\begin{cases} Q_r = \alpha \cdot \Delta H_r \\ Q_{s\_salt} = \int_{T_{eq\_dis}}^{T_{htf\_in}} C_{p_{s1}} \alpha m_{s1} dT + \int_{T_{eq\_dis}}^{T_{htf\_in}} C_{p_{s0}} (1-\alpha) m_{s0} dT + \int_{T_{htf\_out}}^{T_{eq\_dis}} C_{p_{s0}} m_{s0} dT \\ Q_{s\_Al} = \int_{T_{htf\_out}}^{T_{htf\_in}} C_{p_{Al}} \cdot M_{Al} dT \end{cases} \tag{5.5}$$

Eq. (5.4) can be adopted for experimentation calculation particularly for sorption, since it takes into account the heat capacitance, the reaction advancement and equilibrium conditions.

To determine the charging power, a simple operation is needed as the inlet and outlet of the heat transfer fluid to heat up the salt bed are known and a mass flowmeter available. An author (Stitou, 2013) proposed the following expression: $P_{stored\_1} = - m_{s1} E_{d_m} \Delta\alpha / t_\alpha'$. It can also be determined when knowing the mass flow rate and the temperature difference between the material and the heat transfer fluid.

$$P_{stored} = - \dot{m} C_{p\_htf} \Delta T_{in/out} \tag{5.6}$$

For the charging power determination, Li et al. (Li et al., 2014) also proposed a similar way as of the discharging. The thermal power consumption of solid–gas thermochemical sorption heat storage during the charging phase is calculated using the following equation:

$$P_{stored\_sht} = \frac{Q_{in}}{t_\alpha'} = \frac{1}{t_\alpha'} \left(Q_r + Q_{s\_salt} + Q_{s\_Al} \right) \tag{5.7}$$

The first term in the right hand side into bracket is the reaction heat of reactant. The second term is the sensible heat consumed by the reactant during the pre-heating and super-heating phases

when it is heated from heat output temperature T_{htf_out} to heat input temperature T_{htf_in} during the hydrate and dehydrate states.

$$\begin{cases} Q_r = \alpha \cdot \Delta H_r \\ Q_{s\_salt} = \int_{T_{htf\_out}}^{T_{eq\_ch}} C_{p_{s0}} \, m_{s0} \, dT + \int_{T_{eq\_ch}}^{T_{htf\_in}} C_{p_{s1}} \alpha \, m_{s1} \, dT + \int_{T_{eq\_ch}}^{T_{htf\_in}} (1-\alpha) C_{p_{s0}} \, m_{s0} \, dT \\ Q_{s\_Al} = \int_{T_{htf\_out}}^{T_{htf\_in}} C_{p_{Al}} \cdot m_{Al} dT \end{cases} \quad (5.8)$$

The third term is the sensible heat released by the metallic (Aluminium) part of reactor when it is heated from heat output temperature T_{htf_out} to heat input temperature T_{htf_in}. These amounts of heat can be obtained from Eq. (5.8).

The performance for heat production of the system is clearly demonstrated with the coefficient of performance (COP$_{th}$) and the thermal efficiency (η). For such of storage method of thermochemical energy, when operates under the heat recovery process to upgrade the system, heat is produced only during the synthesis reaction process. Hence the COP$_{th}$ and the thermal efficiency are respectively defined as follows:

$$COP_{th} = \frac{Useful\ heat\ production}{Heat\ consumption} = \frac{Q_{out}}{Q_{in}} \ \text{ and } \ \eta = \frac{P_{aver}}{P_{stored}} \quad (5.9)$$

Equation (5.9) can be re-written for each expression earlier mentioned; however a care has to be taken on the units. Indeed, the following chosen power for efficiency calculation is adopted since inconsistent values are obtained with the other expressions.

The following results on the evaluation of thermal power, efficiency and coefficient of performance rely on the thermodynamics data in Appendix A3. The value of salt volume could not be very accurate, however the value 0.054 m^3 found in chapter 2 is adopted. The stored power is determined using a salt weight of about 10 kg and a mass flow rate of 520 kg·h^{-1} and in the case involving heat transfer fluid, parameters in Table 5.2 is adopted. Literature proposed different method of power evaluation. Three of them, in accordance with the present application were gathered. Eq. (5.3) and of P_{stored_1}, underestimate the numerical power evaluation. Eqs. (5.4) and (5.7) show inconsistent results, whereas the one based on Eqs. (5.2) and (5.6) point out proper results. Therefore, the discussion will be based on this latter. Figure 4.12a shows thermal power evolution as function of the reaction conversion during dehydration and hydration. In dehydration, thermal power decreases from -420 W to -805 W between 0.1 and 0.9 of reaction advancement. The same phenomenon is observed in hydration from 630 W to about 130 W. Figure 5.12b shows thermal efficiency evolution with the reaction advancement. Efficiency (average of 0.7) evolution increases before slightly decreasing. This efficiency is about 0.78 for reaction advancement at about 0.9, which is quite good as upgraded system. This high efficient value supposes the heat of condensation is considered.

165
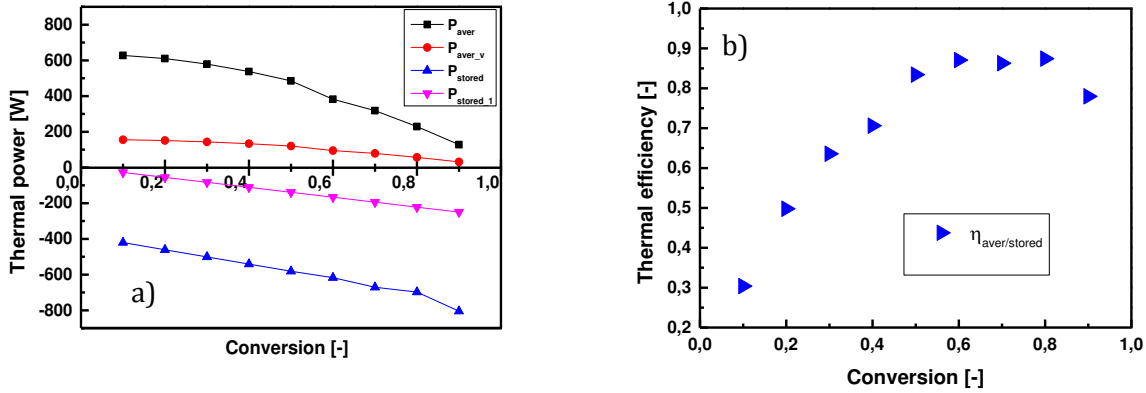
Figure 5.12 Evolution of the thermal power (a) and the thermal efficiency (b) obtained numerically as function of the reaction advancement.

Table 5.2. Parameters used in numerically power evaluation involving the heat transfer fluid.

Charging / dehydration			Discharging / hydration		
T_{eq_ch}	T_{htf_in}	T_{htf_out}	T_{eq_dis}	T_{htf_in}	T_{htf_out}
58 °C	100 °C	97 °C	45 °C	15 °C	50 °C

Figure 5.13 shows again thermal power function of time and heating COP$_{th}$ of solid–gas thermochemical sorption heat transformer at different global conversions. Whether in dehydration or in hydration, thermal power decreases with time. Peaks are obtained at the beginning and the reason can be explained by looking at the bed temperature profiles. A priori, during the discharging where after the peak is obtained, follows the cooling. This figure exhibits power profile on the eight hours of running per day.

In order to numerically evaluate the storage capacity of solid–gas thermochemical heat storage system, peak power at hydration output is used. The target storage capacity 80 kWh corresponds approximately to the heat demand (including the DHW) for four days of a single family house in a moderate central European climate with a heating load of 30 kWh·m^{-2}·year^{-1} (Heimrath and Haller, 2007; Lahmidi et al., 2006). Based on these four days and the output power at the hydration, a numerical storage capacity of 60 kWh is obtained, corresponding to 75% of the project target value. At micro-scale, it was demonstrated that 72% of the target value could be reach (chapter 4, section § 4.5.4.).
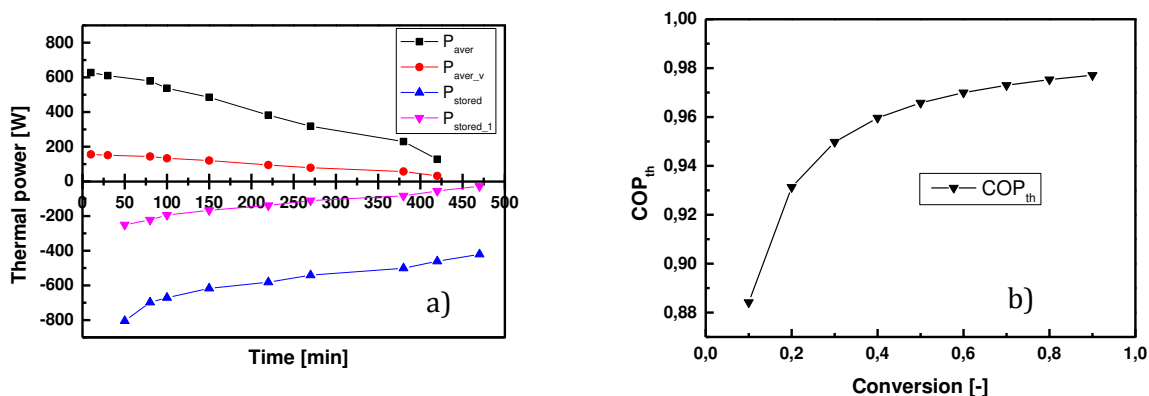
Figure 5.13. Thermal power as function of time (a) and heating COP_{th} of the solid-gas thermochemical heat storage system at different reaction advancement (b).

We can conclude at this level that, thermal management of thermochemical heat storage can be performed through micro-scale or macro-scale with minor standard deviation in results less than 4%. However, disregarding heat loss (to be in accordance with the numerical simulation), 1 m³ of water can store 44 kWh for a temperature change of 38 °C (temperature difference between charging and discharging in this application). A question arises then: is it worth such a system with performances closed to water storage? Experimental investigations can bring some answer elements.

The heating COP_{th} on Figure 5.13b increases with the increase in conversion of chemical reaction and is about 0.97 when the reaction advancement/conversion is 0.8. That value is higher than the ideal COP which is 0.5 as predicted in Table 5.1. Once again the performance of the system is numerically demonstrated.

5.3. EXPERIMENTAL INVESTIGATIONS

Previous modelling and simulation are meant to help sizing a prototype. Before building a prototype, a lab-scale is rather developed to test the system in known and controlled conditions so that the feasibility of the process can be proved. The results of the experiment will also be used in the validation of the model which has been developed in the previous chapter. The laboratory reactor has the target described in Table 4.1. During the instrumentation, the major challenge is to manage the vacuum state.

5.3.1. REACTOR CONCEPT

For the experiments in this work, an operated reactor based on a honeycomb heat exchanger concept is manufactured and integrated into the test bench. This choice of heat exchanger is based on the improvement of issue, such as agglomeration, expansion of the bed and diffusion. The honeycomb structure prevents the agglomeration as precedents studies have shown the need to change the exchangers for proper hydration (Fopah Lele et al., 2014, 2015a). Above, an optimal bed

thickness was assessed; however the bed has a three-dimensional character. The agglomeration occurs much more in width and length of the bed, hence the reduction of these dimensions by introducing the honeycomb, which involves equal-size cells of the order smaller than the bed thickness. The reactor is made of stainless steel and the exchanger of aluminium. Prior roughly corrosive tests were performed on aluminium. After 24 hours, strontium bromide does not affect the metal but it starts degrading the structure after five days. Since a cycle test does not last more than a day, corrosion problems are not expected.

5.3.2. TEST BENCH FOR THE LAB-SCALE EXPERIMENT

A laboratory test plant has been set up at the Institute of Environmental Chemistry (IEC) and a process flow diagram of the experiment is shown in Figure 5.14. It consists of three main units: the cylindrical reactor (Ø = 200 mm, L = 400 mm for an internal volume of 0.012 m³) containing the integrated honeycomb heat exchanger with strontium bromide, a thermal bath playing the role of an evapo-condenser and the Unistat, a temperature control engineering having both the role of a micro-CHP for the charging process and the households for the discharging process. All those units allow the supply of the HTF at demanded temperatures and mass flows, the reactive gas supply and the cooling and disposal of the vapour stream.
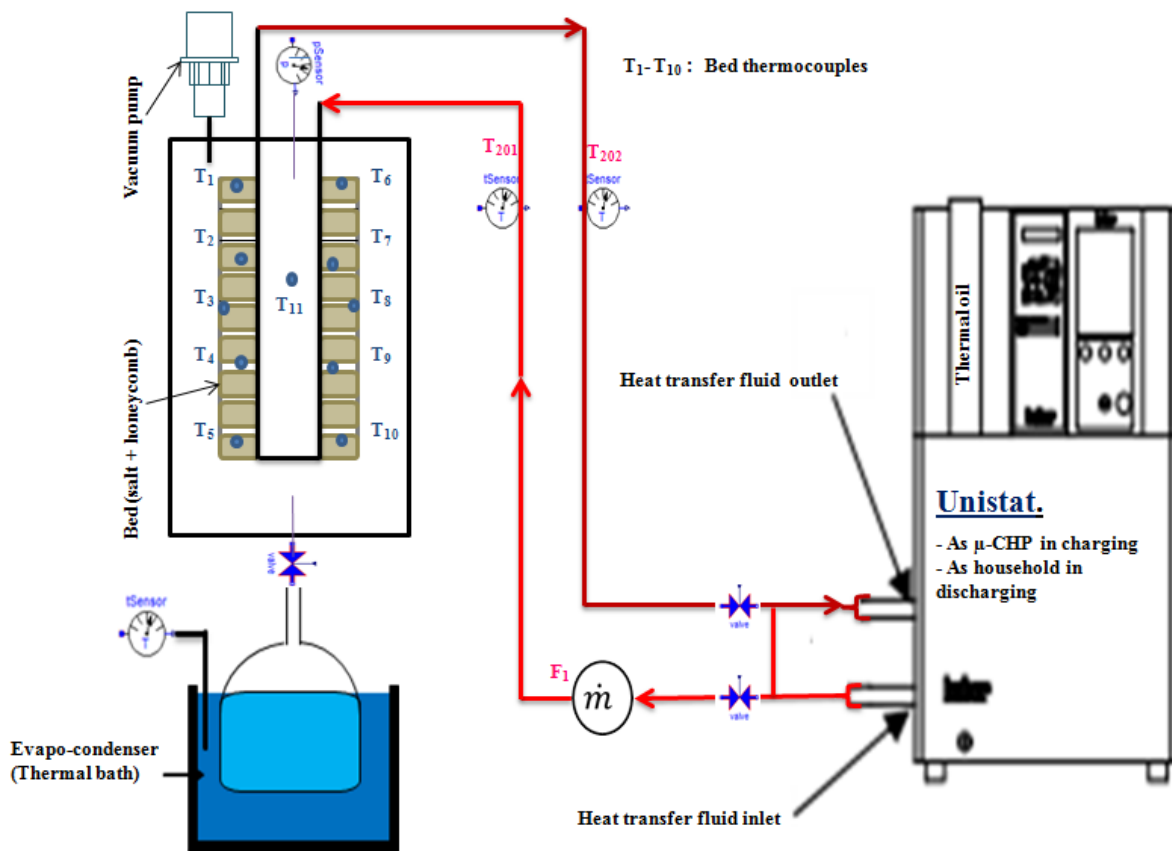
Figure 5.14. Lab-scale schematic and process flow diagram of the test bench for experimentation.

5.3.2.1. The heat exchanger montage

The heat exchanger description and parameters are presented in Appendix A1-3. The heat exchanger consists of two parts, a bundle tubes transporting the heat transfer fluid and the honeycomb bed structure containing strontium bromide. So the both parts are welded. However, welding do not insure a very good heat conduction between the tube and the plate as shown in Figure 5.15 and Figure 5.16. Therefore, a thermal conductive adhesive was impregnated between the two part by forming a powerful conductive thin layer (white color in Figure 5.16).
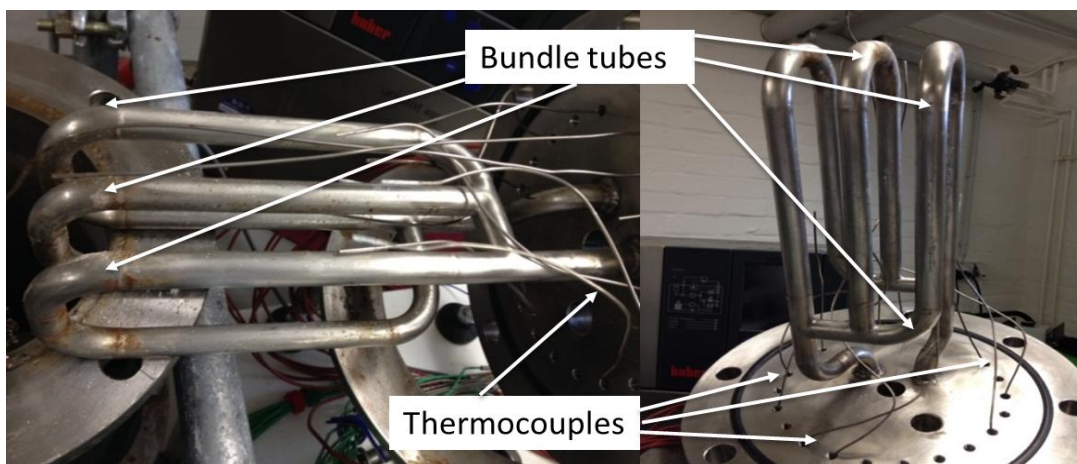
Figure 5.15. Fisrt part of the heat exchanger (bundle tubes) and thermocouples not yet inserted into the bed.

The 10 thermocouples were then inserted into the bed by making some holes. As already explained above, the use of this structure solves the agglomeration issue by dividing the bed into small hexagonal beds as presented in Figure 5.17. In order to maintain the bed fixed and not losing some salt particles, a diffusive mesh is technically bolted on the bed face. The diffusive mesh has a very high permeability ($\sim 10^{-4}$ m2) compared to the bed permeability.
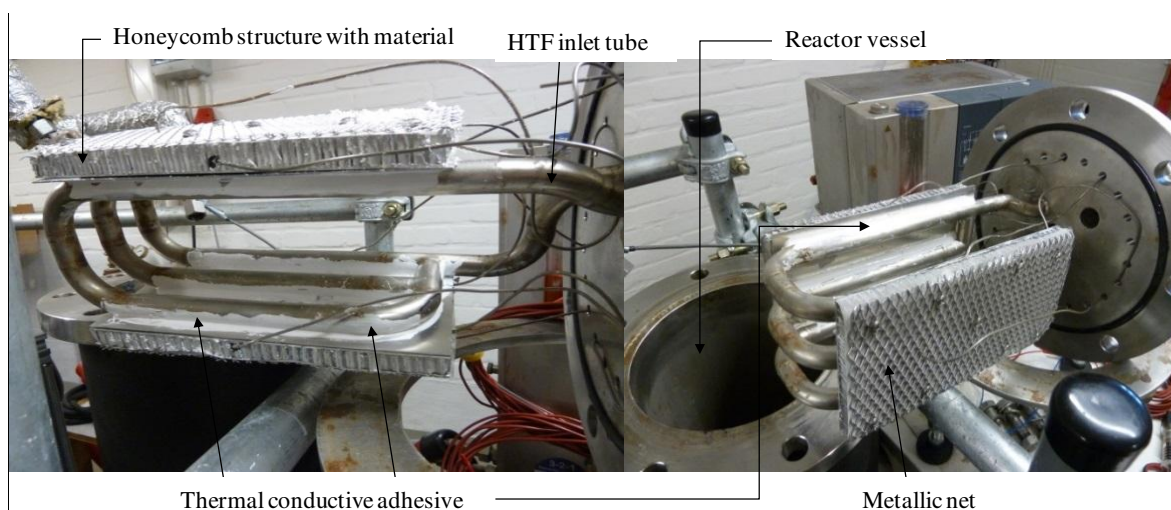
Figure 5.16. Final heat exchanger (bundle tubes + honeycomb bed) and inserted thermocouples.

5.3.2.2. The measurement elements

For performance evaluation of the lab-scale reactor, different values were obtained using the following measuring elements in Table 5.3. A vacuum pump was connected to the reactor in order to evacuate the system down to an absolute pressure (varying from 6 to 11 mbar) to enable a pure vapour atmosphere. The vacuum management is done through a rotary vane of the type RA 0025 F. An additional safety valve is installed before the reactor entrance. It is ensuring that the valves of the pump are always open before starting the system. Via a thermostatic bath (Julabo, Type c-5B/2, nominal power 1.1 kW) as an evapo-condenser, the temperature of the reactive gas to discharge the salt bed can be set at 30 °C. While charging of the storage material takes place in the reactor at a variable condensation temperature was difficult to adjust.

Table 5.3. Measured quantities, measuring instruments and features of the elements.

Measured quantity	Units	References	Characteristics
Bed temperature (T_1...T_{10}) and reactor ambient temperature T_{11}	°C	Sheathed thermocouple NiCr-Ni (Typ K) RM-Type AL-KE-3,0-L-2, TT-465. In-house calibration	Max. deviation: DIN EN 60584 class 1. Range: 0 to 350 °C. $\Delta T = \pm 0.2$ °C
HTF inlet and out-let temperature	°C	Sheathed resistance thermometer Pt 100 RM-Type WL-6, 0-1 Pt100-A-L-2 , 4-w., TT-465.	Max. deviation: DIN EN 60751 class A. Range: -50 to 200 °C. $\Delta T = 0.3 \pm 0.005\theta$ °C θ absolute value of T.
Reactor pressure	Pa	Pressure transmitter SD-37 (Rössler Messtechnik)	Precision : 0.1% Range : -1..0 bar (vacuum) with temperature decoupler to 200°C
Mass flow rate	kg·s^{-1}	Coriolis-Mass meter: Yokogawa RCCT34-AV0M02D4SL	At 70% of flow, 0.76 of pressure loss. Precision of 0.13%. See appendix A5.
Vacuum creation	Pa	Rotary vane Vacuum pumps series R5; Type RA 0025 F 5A3 GK-Aqua. From BUSCH GmbH.	Possibility of water vapour in the process. Vacuum limit: 0.5 mbar. Rate: about 25 m^3·h^{-1}.

L=represents the corresponding thermocouple length.

The mass flowmeter F_1 (capacity up to 3 tons/h) of type Yokogawa RCCT34-AV0M02D4SL recorded the mass flow of the heat transfer fluid during the both phases. A data calibration sheet is presented in the appendices (Appendix A5). To observe the reaction front and identify possible limitations due to heat and mass transfer of pure vapour, 10 sheathed thermocouples NiCr-Ni (type K of different lengths: 200, 300, 400, 500 and 600 mm) were installed inside the reaction bed and an eleventh thermocouple between the bed and the bed for the reactor temperature. Two sheathed platinum resistance thermometers (Pt-100, RM-Type from Rössel Messtechnik) T_{201} and T_{202} were plugged (perpendicularly to the flow) into the tube conducting the HTF to record inlet and outlet

temperatures. Temperature was recorded through these thermocouples connected to a BenchLink Data Logger software "Agilent". The heat transfer fluid in this experiment was the thermofluid (oil) DW-Therm HT P20.330.32. A pressure transmitter (SD-37 from Rössel Messtechnik) plugged in on the top cover of the reactor records the pressure evolution in the reactor. Data acquisition was done using Agilent 34970A/34972A Meilhaus LXi.

5.3.3. EXPERIMENTAL METHODOLOGY

An early description of the charging phase is described in chapter 3 (section 3.2). The volume flow of the HTF was kept constant for the whole cycle. In order to obtain a high temperature difference between the temperature of the HTF and the reaction bed, the system is evacuated (vacuum) and a constant temperature was applied in the condenser of the gas supply unit. To initiate the reaction, the temperature of the HTF was increased to 105 °C (after looping flow through the by-pass during about 20-45 min) and kept constant until the conversion of the material is complete. The mass flow rate is supposed to be constant. It slightly varied (± 2 kg·h⁻¹) due to the running into the by-pass.

However, to discharge the stored energy in the bed, a certain evaporation temperature was adjusted with the thermostatic bath. Thus, steam was generated in the evapo-condenser, flowed into the reactor and enabled the hydration reaction at constant pressure. Based on the measured change of the water level in the evapo-condenser, the overall rate of conversion in the reactor was determined. The conversion in percentage was calculated as the ratio of the amount of water absorbed or released during the reaction to the theoretical amount of water based on the stoichiometric reaction:

$$Conversion \; (\%) = \frac{\Delta m_{H_2O,evapo-cond}}{m_{H_2O,stoichiometric}} \tag{5.10}$$
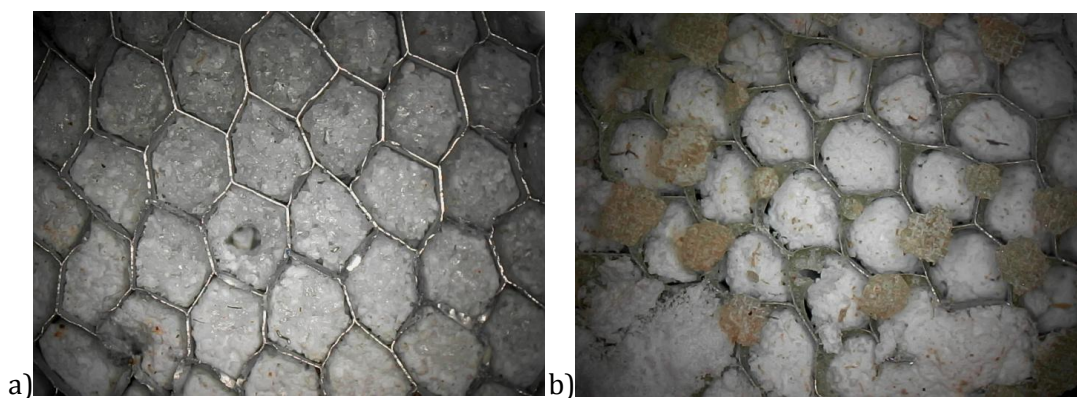
Figure 5.17. Strontium bromide in the (a) hydrate form and the (b) dehydrated form into the bed of honeycomb structure.

Table 5.4. Operating conditions and results of cycles performed.

Cycles	Dehydration (charging)						Hydration (discharging)					
	Conversion [%]	T_{bed_i} [°C]	T_{cond_i} [°C]	$p_{reactor}$ [mbar]	Mass flow rate [kg·h-1]	Time [min]	Conversion [%]	T_{bed_i} [°C]	T_{evap_i} [°C]	$p_{reactor}$ [mbar]	Mass flow rate [kg·h-1]	Time [min]
1	60	19.5	16.5	8	520	177	56	27	30	32	-	143
2	52	19.5	18	4.3	520	108[4]	57	30	30	22.5	-	154
3	74	18.1	18	6.3	520	217	92	19.6	30	18	-	218
4	96	16.8	18	9.3	520	342	95	19	30	18.4	520	330
5	95	17.9	18	9.3	520	340	97	18	30	17.5	170	356
6	86	24	16	9	520	540	82	17	30	19	220	545
7	15	19.3	20	8	521	45	9	21	30	20	30	50
8	73	15	16	11	520	529	81	20	30	20	11	584
9	37	24	16	11	521	141	42	16	30	18	11	159
10	82	17.5	16.5	10.2	520.4	566	87	20	30	16	188	584
11	100	18.4	17	9.5	520.5	411	80	20	30	16	225	230
12	66	18.4	17	9.5	520	158	95	19	30	13	190	279
13	63	26	16.5	6	520	140	68	18	30	15	-	140

During the discharging the evaporation temperature does not change from the starting until the end of the process.

---

[4] The experiment was interrupted due to leakage that breaks the vacuum.

The reactor was filled with an amount of 974 g of SrBr$_2$·6H$_2$O and the bed in the both state, hydrated and dehydrated form is shown in Figure 5.17. According to Eq. (3.2) and the molar masses of the reactants, the theoretical amount of water was calculated to $m_{H_2O,stoichiometric} = 247$ g. The numerator was obtained by weighting the amount of water (received from condensation during charging or leaving by evaporation) in the evapo-condenser.

From a hydraulic point of view, preliminary experimental tests showed that heat exchange was not working as expected in the evapo-condenser. Difficulty to stabilise the thermal bath at 25 °C during charging. However, it varied much between 16 and 26 °C.

The provided thermocouples were all consistent before the beginning of the test process (displayed out 18 ° C, during the test of empty closed reactor). Some incorrect values were obtained during the tests such as negative value or nil. Indeed, the mass flow F$_1$ was provided with accurate temperature probes at 0.2 °C, so each flow rate corresponds to a fluid temperature. There was also some salt loss from the bed during cycle tests, but remained at the mesh surface as shown in Figure 5.18. It is due to the thermal expansion of the bed during sorption and desorption of water vapour. From a temperature point of view this does not affect the bed temperature since that out-of-bed salt sticks at the surface and chemically reacts. However it had an effect on the bed reaction conversion. For example, during charging it will be difficult to heat that lost salt at the mesh surface.
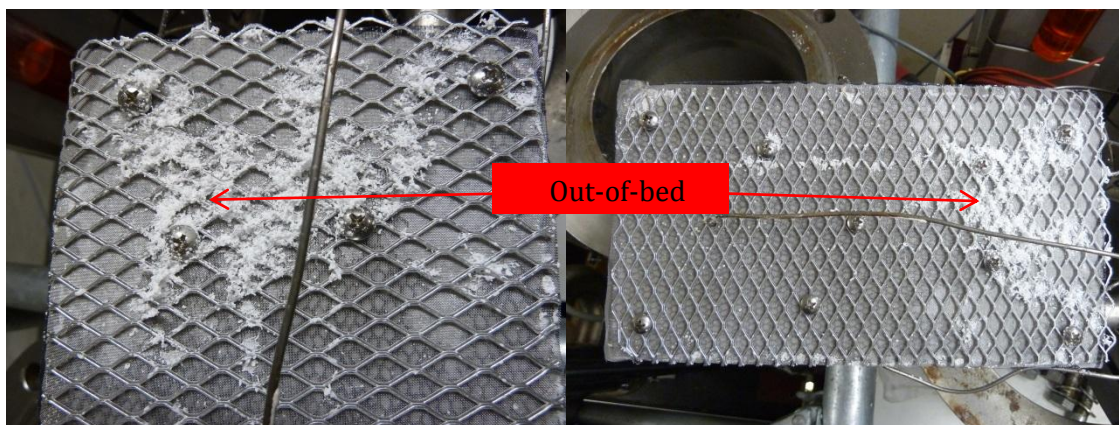
Figure 5.18. Out-of-bed salt (Strontium bromide) during a cycle test, showing some salt loss.

Search for leaks (air intakes in the process) was done at the connections (valves, thermocouples entrance, in and out of heat transfer fluid connections). The tightness had been mastered at these levels using "Ultra-Torr" vacuum connections (Swagelok), O-rings if necessary and polytetrafluoroethylene (Teflon). The inputs for thermocouples and transmitter were covered by a flexible sealant tape (AXSON SM 5127). The insulation was then put in place covering the reactor after the vacuum state is stabilized. It was done using a flexible insulating elastomer from KAIMANN GmbH (Kaiflex EPDM plus) 32 mm thick with a maximum allowable temperature of 175 ° C.

The preliminary tests with about 700 g were time consuming but necessary to know which problems were present and how to solve or avoid them. Every test was a full cycle (dehydration/hydration) and lasts between 100 and 570 min. During some tests, vacuum was

breaking and the experiment stopped. Also due to the non-stability temperature of the evapo-condenser, all the tests were not performed as initially (initial and final conditions) expected.

5.4. EXPERIMENTAL RESULTS

The lab-scale reactor was experimented during the period from 31.03.2014 to 02.05.2014 (33 days). Within this period, thirteen cycle tests were performed at varying operating conditions. Unfortunately the sorption evolution was not dynamic, hence punctual measurement and individual linear evolution. So formula such as of sorption where conversion was involved, will be globally determined (i.e. for the thirteen cycles) or time-dependent at constant value of conversion. Conversion effect on thermal power was difficult to argue here. The amount of water in the evapo-condenser was measured at the beginning and at the end of the test. This is why Figure 5.19 exhibits the overall reaction conversion (dehydration and hydration) for the thirteen tests. One can see that the longer cycle lasted about 600 min to process. Cycles that reach more than 70% of conversion also last longer. It was obvious that the time to charge and discharge the salt bed played a very important role if great performances were intended to be verified.
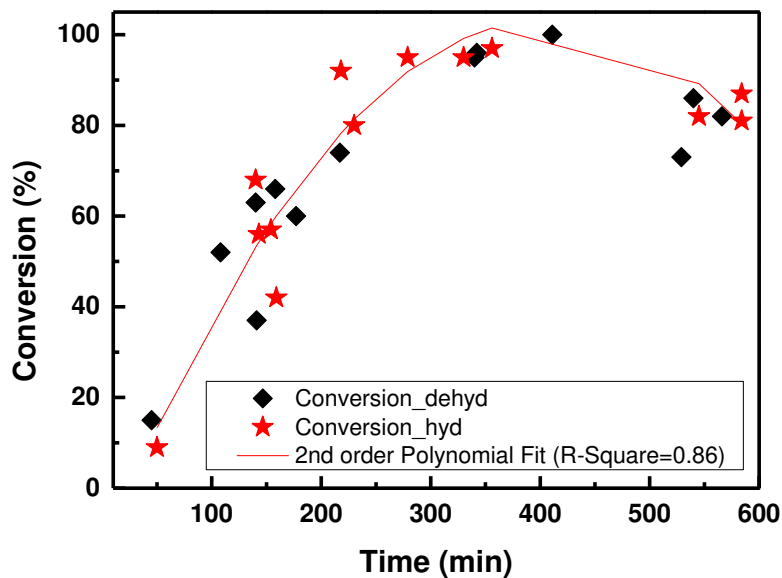
Figure 5.19. Experimental reaction conversion during dehydration and hydration for the thirteen cycle tests.

During the cycle number 1 and 2, the maximum conversion in the both phases did not exceed 60% at a relatively less time (more than 5 hours for the entire cycle), meaning a decreasing evolution from 100% to 40%. However the hydration at about 56% did not mean it is not completed since it starts at 40%. Though with the same salt without opening the reactor, the cycle tests number 3, 4, 5, 6, 8, 10 and 11 (Table 5.4) exhibit good performances. In the case, where the hydration conversion was higher, the dehydration conversion corresponded to an overhydration or

the presence of non-condensable water at the reactor wall and at the surface of the heat exchanger, which were not in the evapo-condenser to be weighted. Table 5.4 summarizes the operating conditions and the results of all tests performed. Initial conditions (bed temperature, evapo-condenser temperature, reactor pressure) of the experiment were put in that table too. Evapo-condenser pressure was determined using the theoretical formula since we have the corresponding temperature. The mass flow rate in this table was a dynamic measurement. In fact, the mass flow rate values observed at the display screen does not change much during a charging test, but inconsistent during the discharging.

In the following, the obtained results were detailed, particularly for the cycle test number 4. This cycle test has been chosen because physical phenomena that take place are representative of those of the other cycles. For the mass flow of the heat transfer fluid (which is not the reactive gas), note that the dehydrations were performed with a flow rate set to 520 kg·h⁻¹ and the hydration with a flow varying out-of-scale on some tests, so inconsistent values could have been recorded. However, for the calculation the value 520 kg·h⁻¹ of is adopted. Flow rate of the reactive gas was not measured due the difficulty to get a very accurate device for such of low gas velocity.

5.4.1. CYCLE (DEHYDRATION/HYDRATION) TEST N° 4 RESULTS

This cycle follows a quasi-completed hydrated bed (test number 4 in Table 5.4) due to the fact that much time was not allowed for the running. The bed is completely dehydrated at 96% and 4% remaining represents the non-condensable water at the reactor wall. Hydration is then completed at 99% of the dehydrated state. This test lasts 11 hours, hence the good performances.

Figure 5.20 shows pressure and temperature evolution during the fourth dehydration (Figure 5.20a and 5.20b) and hydration (Figure 5.20c and 5.20d). It presents temperature of the ten thermocouples inserted in the bed at different positions (as shown in Figure 5.14) in order to have the spatial bed temperature. The eleventh thermocouple gives the reactor temperature, the transmitter provides the reactor pressure and the two platinum type thermocouples shows the heat transfer fluid temperature. It is observed on Figure 5.20a that, from the opening of the by-pass, heat transfer fluid flows and salt bed temperatures T_1 to T_{10} increasing then tend to stabilize at a level, around 70 °C before increasing again, one after the other, to move toward the heat transfer temperature (at about 90 °C). At the final state (conversion around 0%), all the ten thermocouples tend to this temperature. These temperatures along with the HTF temperatures decrease forming two bearing before getting stable at around 76 °C. The eleventh thermocouple that gives the environmental reactor temperature follows the other thermocouples, except at the end it increases. It is because at the end, bed is releasing its temperature to the reactor environment.

These different bearings of the temperature evolution reveal the sharp front reactions, moving in two directions: parallel (i.e. T1, T2, T5, T6, T7 and T10) and perpendicular (i.e. T3 to T4 and T8 to T9) to HTF inlet due the bed position and the gravity effect (Appendix A7). Indeed, at the reaction front, dehydration of the salt, which is endothermic, resulting in a consumption of the sensible heat of the salt and the heat flow from HTF, explains the decreasing temperatures, until the bearing temperature.

Indeed, the parallel front is caused by the heating transfer fluid flow that imposes its temperature at the salt layer (corresponding to the first bearing at around 70 °C) closed to the heat exchanger and move horizontally until water is out. At the end of the reaction front, the endothermic reaction is complete, the salt is thus gradually brought to the thermal equilibrium with the heat transfer fluid circulating, where the gradual increase of the salt temperatures to the second bearing toward the inlet temperature of the HTF at around 90 °C. It should be noted that because of the HTF flow through the whole layer of salt bed closed to the exchanger and therefore controlling its temperature at the front, it is only possible to establish that the reaction is almost completed at a point when temperature tends towards that of the flowing HTF.
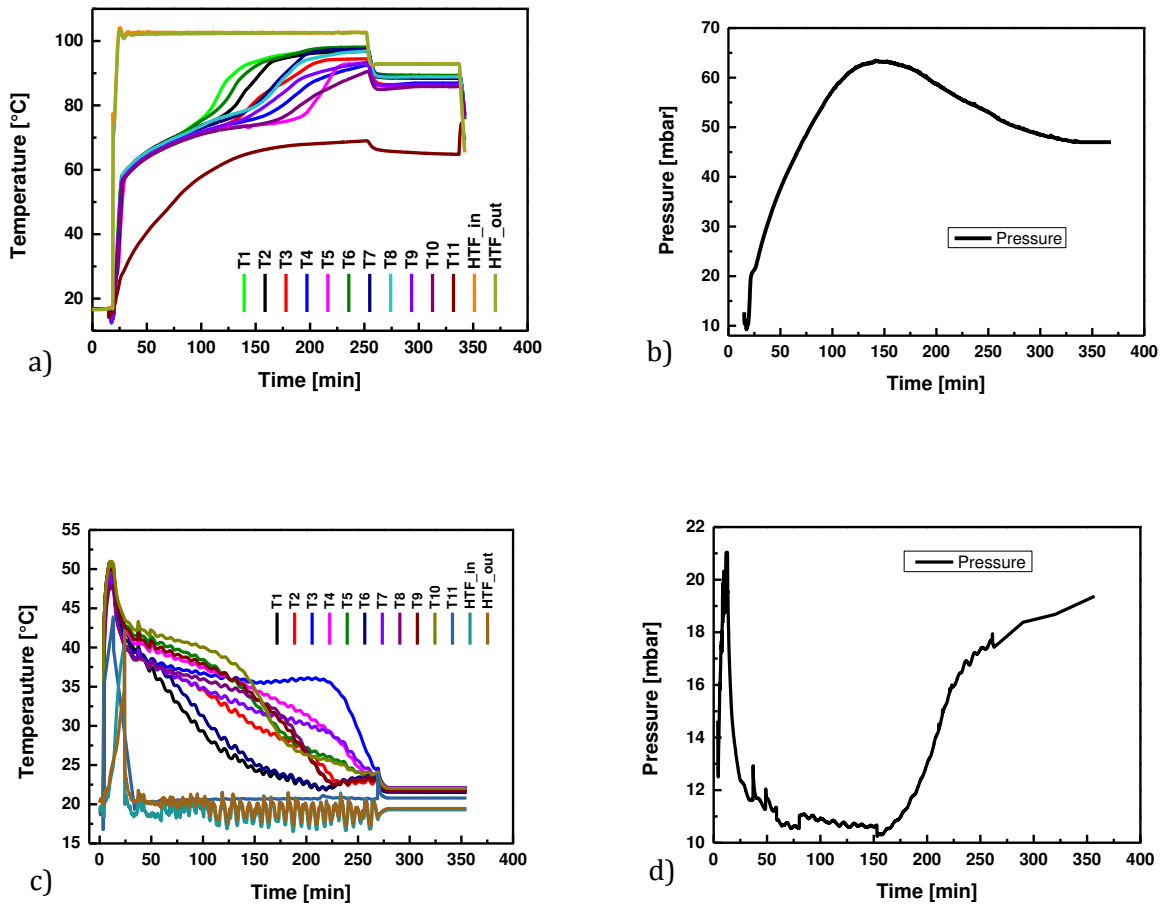
Figure 5.20. Experimental pressure and temperature evolution of the bed, of the heating transfer fluid and in the reactor as function of time during the 4th dehydration/hydration.

Figure 5.20b shows the pressure in the reactor environment. However, reactor pressure almost behaves like temperature evolution. An increase from the initial state until the bed received the corresponding charging temperature (dome at around 65 mbar) followed by a bearing that decrease until the stabilization at around 45 mbar.

Figure 5.20c also exhibits the similar measurement as previous, but for hydration during the fourth cycle test. The rapid initial increase during the first 2-3 min is ascribed to the physical sorption of water on the $SrBr_2 \cdot H_2O$. Parallel and perpendicular reaction front are also in evidence here when looking at the bed temperature evolution. For instance from T_3 to T_2 or T_4 (parallel front), bed temperature gradually increases according to the front displacement. The same increase is perpendicularly observed from T_5 to T_1 (respectively from T_{10} to T_6). The reason of this progression is due to the reactive gas from the bottom, so that reaction begins at the bed bottom and goes up gradually. However, it enters the bed in parallel, reacts with the first salt particles which cool a bit down when reaction takes place with the next particles into deep bed, hence the parallel front (see chapter 2, section 2.3.2). This front, much important than the perpendicular one, is modelled in chapter 3, section 3.5.3.3. Some thermocouples show a quasi-steady temperature state, particularly T_3. This might be due to the heat exchanger wall acting like a return effect of the reaction front or a heat accumulation at that layer level. The eleventh thermocouple follows the bed peak temperature but at lower temperature and suddenly drops to 20°C until the reaction is almost completed. An explanation to this behaviour is such as heat generated by the bed is absorbed somewhere, per example to the HTF or the metal part in the reactor. In fact, platinum thermocouples inserted in the HTF exhibit the same behaviour as the eleventh thermocouple with a peak at about 43 °C. This transient recovery of the heat produced by the bed by HTF might be due the heat capacity of the fluid, here the thermos-oil.

Table 5.5. Parameters obtained for power evaluation involving the heat transfer fluid.

Charging / dehydration			Discharging / hydration		
T_{eq_ch}	T_{htf_in}	T_{htf_out}	T_{eq_dis}	T_{htf_in}	T_{htf_out}
53 °C	105 °C	103 °C	61 °C	15 °C	43 °C

Water with very high capacity should be the HTF since the system is intended for household's application. Figure 5.20d shows the pressure in the reactor environment. In the first minutes a suddenly increase directly followed by a drop for more than two hours. This drop is closely related to the chemical reaction. During this latter, the salt absorbs the water vapour quite quickly at the beginning, then slower and slower because it gets saturated. The effect is directly coupled with the peak temperature happening in the beginning as shown in Figure 5.20c.

The reaction power and thermal efficiency of the lab-scale reactor for this precise cycle test will be determined in the following. The same methodology, already shown above, is using Eqs. (5.2)-(5.9) for purpose. As the reaction conversion is represents an average value, it is not possible to have time evolution of these system properties. Table 5.6 shows the experimental performance results for this cycle test. All the calculations of Table 5.6 are also based on Table 5.5 values.

Table 5.6. Experimental performance results of the cycle test number 4.

$\alpha \geq 0.9$	Dehydration	Hydration	Efficiency	COP$_{th}$
P_{stored} (W)	859	-		
P_{aver} (W)	-	662	0.78	0.97

For this test, the obtained efficiency and coefficient of performance are numerically predicted. The hydration power is calculated here using a real time to discharge the bed, i.e. about 21 days and the dehydration power only depends on the mass flow rate. These results are subjected to some possible errors such as the theoretical salt bed evaluation, the adopted energy ratio between sensible and reaction energy and mass flow rate. Concerning this latter source error, power is calculated using the HTF mass flow rate values measured at the inlet and outlet of the heat exchanger tubes. The problem with this evaluation is the accumulation of solution in the outlet tube where no flowmeter is installed. Indeed, the mass flow of outgoing fluid in this case is not really that out of the exchanger. However, the above table helps pointing out minimum expected performances of the system in the absence of dynamic measurement of the reaction conversion and necessary real time. Based on the four days heat demand as mentioned earlier and the output power at the hydration, an experimental storage capacity of 63 kWh is obtained, representing 79% of the target value. Once again, numerical model predicts the experimental results, though the target can be reach even at an experimental level. In addition, Figure 5.21 exhibits power evaluation at the corresponding time of the lab-scale experimentation. Results were based on Eq. (5.6) using heat transfer fluid temperature during the reversible process and the absolute value of temperature variation.
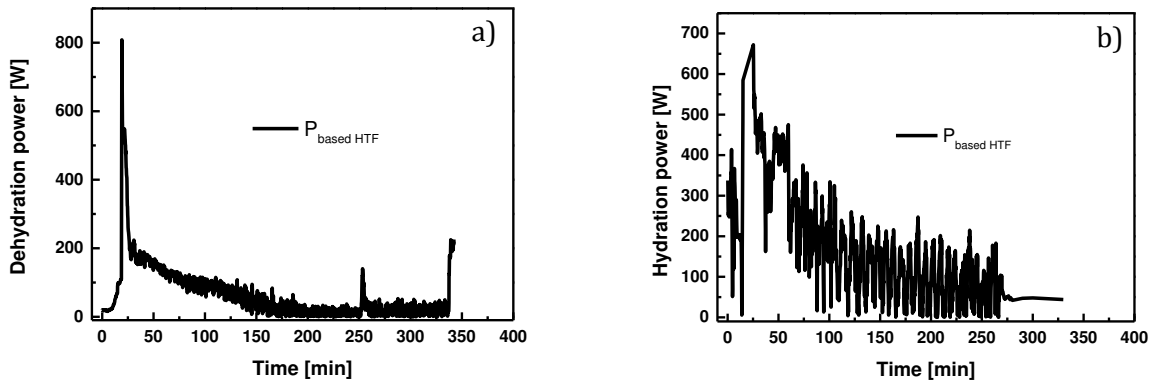
Figure 5.21. Experimental power determination based on the heat transfer flows during dehydration (a) and hydration (b).

The possible propagation of errors was the use of the same mass flow rate (520 kg·h^{-1}). However, results were closed to the one found in Table 5.6. For this specific case, heat transfer coefficient had been estimated using Eq. (3.10). Result showed high peak variation, but with an average around 100 W·m^{-2}·K^{-1}, far from the value of 200 W·m^{-2}·K^{-1} suggested by Rambaud (Rambaud, 2009). In the following, a global observation will be made in order to conclude the present assertion.

For the dehydration, Fig. 5.21a shows a sharp peak with a maximum power of 800 W, observed after only 25 minutes. That peak corresponds to the time where the bed has already absorbed a sufficient water vapour amount to initiate the exothermic reaction. The average charging power for the first 300 minutes is 400 W. In the evaluation of the hydration power (Fig. 5.21b), there are high fluctuations, due to the heat transfer between the bed and the heat transfer fluid. In fact, after 25 min, the bed is beyond his initial temperature (19 °C), which is different from the HTF inlet temperature of about 18 °C. So, as the bed is generating large amount of heat, the HTF outlet also becomes bigger. Therefore, bed temperature fluctuation leads to HTF outlet temperature fluctuation which make power fluctuate as it is based on HTF. However, an average discharging power of about 300 W is obtained after 300 min.

5.4.2. THE GLOBAL CYCLE (DEHYDRATION/HYDRATION) TEST RESULTS

In order to globally observe the overall cycle performances, representative tests had been chosen based on the consistence of the results. There were some issues such as vacuum broken and mass flowmeter not recording during some tests. Figure 5.22 presents temperature evolution for each cycle test. It represents the average bed temperature measured at the ten different points as presented earlier. All temperatures increased until a certain temperature before cooling very quickly. During the charging, the bed was heated beyond 80 °C excepted the tests Nr. 6, 8 and 10 where the bed was heated at temperature lower than 80 °C and which take longer time. Surprisingly, those three latter presented good sorption and desorption capacities. Some of the tests (test Nr. 4, 5 and 11) where the salt bed was heated above the melting temperature (88 °C) are those with best performances.
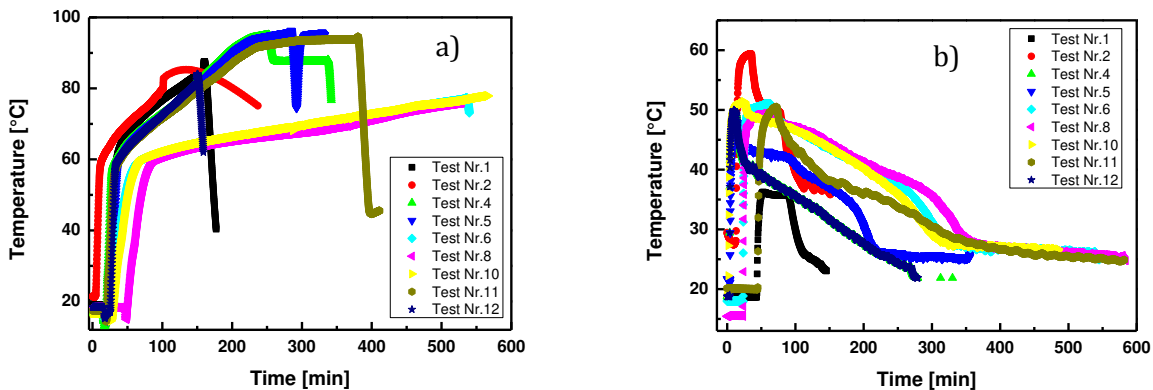
Figure 5.22. Experimental temperature profiles during dehydration (a) and hydration (b) representing the overall cycles.

The reason was of course the honeycomb structure that divided into small cells, so that even when the salt melted it remained in his cell and recrystallised thereafter. During discharging, the same test performances were observed. The different test numbers mentioned above, exhibited at least at peak temperature of 52 °C, except test number 2 which popped out very high peak at a relatively short time and test number 1 at 38 °C. The reason can be that material life is still good and

the stability establishment found during the test number 1 was already reached, or elapsed time between tests allowed the bed to be charged/discharged completely.
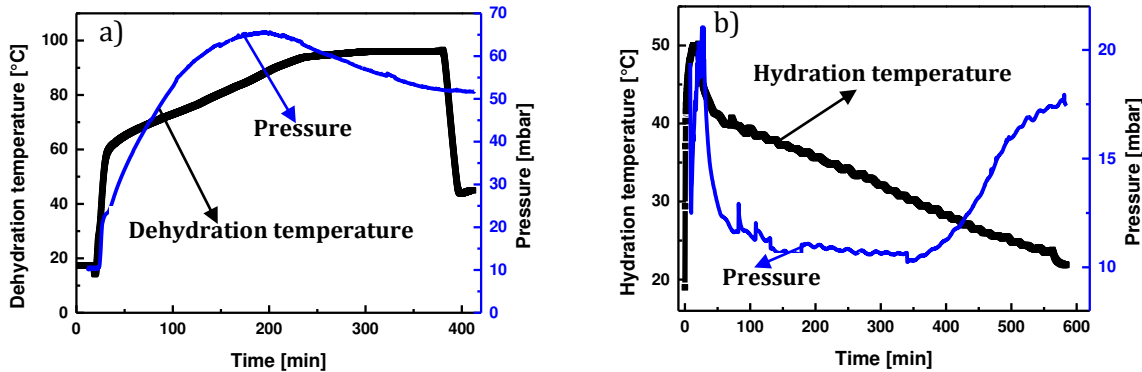
Figure 5.23. Average temperature and pressure evolution of global cycle test during dehydration (a) and hydration (b).

Figure 5.22b shows that reaction leads to high peaks that rapidly cool down. This rate was so high due to the temperature difference between the bed and the heat transfer fluid. In this case, about 30 °C of difference, hence the rapid heat rate transfers according to the heat transfer principle (from higher to lower temperature). Test number 8 exhibited good performances. During this hydration test, the cooling was slow and dropped to about 30 °C after 6 hours, which was a desirable discharging operation regarding the overall time.

In order to have a global view, meaning, seeing the significant tests as one, an average of temperature and reactor pressure is presented in Figure 5.23. In a global way, dehydration in well performed, even if at the end the bed is heated above the melting temperature, which is not an issue in this case study as mentioned earlier. The reactor pressure increases and tends to be stable at the end. It varies between 10 and 70 mbar. Hydration is also well done; with a peak at around 52 °C after 20 minutes of sorption and the cooling down under 30 °C is reached after more than 7 hours on a total of 10 hours processing. Considering the eight hours running per day in winter period, the present storage system is appropriate to cover the heat demand. The reactor pressure during hydration suddenly increases at the first 10 minutes and decreases thereafter before increasing again after 6 hours. The variation, not very high, is between 10 and 20 mbar.

Figure 5.24 shows the experimental thermal power during dehydration (a) and hydration (b) of the thermochemical heat storage system. The stored thermal power is normally a negative value, but it is presents here as absolute value in order to observe the heat transfer coefficient along with it. The stored power starts from 805 W to nil, with a nearly constant variation between 250 and nil. The released thermal power varies from 682 W to nil with high fluctuations such that it can be said this thermal power has a constant value of around 300 W.

Still globally, thermal efficiency based on the peak values on Figure 5.24, is about 0.77. This value in accordance with the above case value and the numerical value, allows validation of the theoretical and numerical modelling. The experimental coefficient of performance (COP$_{th}$) based on the above formula of Q_{in} and Q_{out} is about 0.97, highlighting the system performance level.
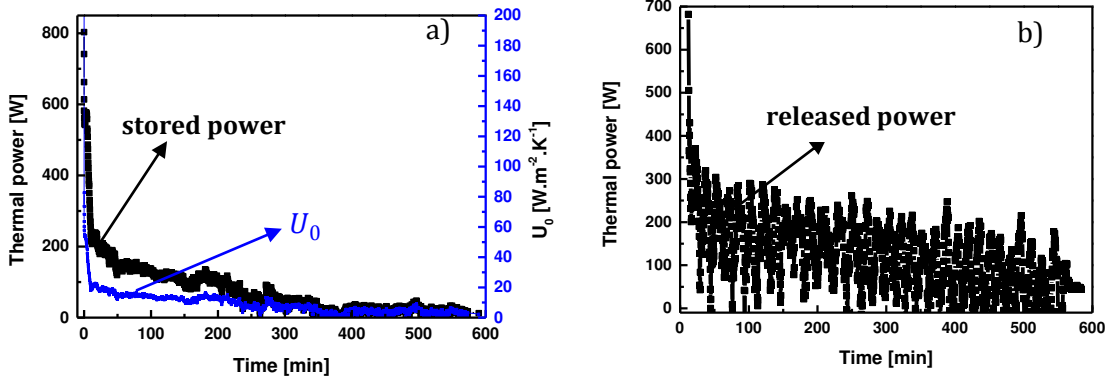
Figure 5.24. Experimental thermal power evaluation based on the heat transfer flows during dehydration (a) and hydration (b) for the overall cycles.

The storage capacity, calculated on the four days running as mentioned much earlier, is based on the released power. This value, representing the global energy storage capacity of the lab-scale is about 65 kWh. Even at this scale, the 80 kWh could not be reached. Other means should be considered and proof-checked in order to have such of performances based on thermochemical. Another fact to point out here is the evapo-condenser. Its temperature of about 30 °C during the hydration implies small vaporisation enthalpy of water leading to a higher net volume energy storage (about 140 kWh·m^{-3} instead of 115 kWh·m^{-3}). However the cost of producing this 30 °C reduces at the end the system efficiency and makes it not very worthy.

The overall heat transfer coefficient of the heat exchanger is also shown in Figure 5.24a. For the charging phase, it is inferred from the expression of the power exchanged adopted in Chapter 2, Eq. (3.10) and recall here as follows:

$$P_{stored} = U_0 \cdot A_0 \cdot \frac{\Delta T_1 - \Delta T_2}{\ln\left(\frac{\Delta T_1}{\Delta T_2}\right)} = \dot{m} \, C_{p\_htf} \left(T_{htf\_out} - T_{htf\_in} \right) \tag{5.11}$$

where $\Delta T_1 = \left| T_{htf\_in} - T_{bed_i} \right|$ and $\Delta T_2 = \left| T_{htf\_out} - T_{bed_f} \right|$. The term T_{bed_f} is considered as the average bed temperature measured at the ten thermocouples inserted in the bed. This coefficient on Figure 5.24a, starts at value around 200 W·m^{-2}·K^{-1} and rapidly decreases within the first ten minutes and is relatively constant between 0 and 20 W·m^{-2}·K^{-1}. However, an average value of 147 W·m^{-2}·K^{-1} is obtained. Once again this value is lower than the required value to expect good performances. It is

assumed that the layer between heat exchanger and bed is not enough heat conductive. A solution could be to coat that layer with salt first, before filling the rest of the bed with salt.

5.5. COMPARISON ANALYSIS BETWEEN EXPERIMENTAL AND NUMERICAL RESULTS

The experimental design was composed of a single reactor containing about 1 kg of $SrBr_2 \cdot 6H_2O$, fed by steam flow and heat using heat transfer fluid at controlled temperature. Initially, micro-scale experiment was performed to characterise the salt, in studying heat transfer (thermal conductivity and heat capacity), mass transfer (permeability) and reaction kinetics. The macro-scale (or lab-scale) experiment serves as performance analysis tool. The amount of energy released during the discharge phase was then estimated and translated into storage density term. In the second analysis, these experimental results are now compared to the predictions of the macroscopic model developed in Comsol Multiphysics, though roughly mentioned in the above sections. The experimental results presented in this section are used for validation of the mathematical model proposed in chapter 3. Given the number of tests performed (13, see Table 5.4), only few of them are presented as shown in Figure 5.22. Their average is then confronted to the numerical results.

5.5.1. MODEL VALIDATION AND DISCUSSION

From the application point of view of thermochemical storage heating for building, relevant criteria have been identified to assess the system performance. Three features have appeared essential to the design of the system: temperature generated during hydration reaction, heat power and thermal efficiency. So these criteria are compared, experimentally and numerically. The main parameters used for numerical study were experimental determined, such as thermal conductivity, heat capacity, permeability, kinetic factor (R_{kin}). The sharp front model helps determining parameters such as real time for hydration, but numerical study was performed on a time based lab-scale experiment, i.e. around 600 minutes. It also helps having the water vapor inlet flow rate according to the bed thickness and the bed porosity estimation.

Figure 5.25 presents the confrontation between the experiment and the simulation of the charging and discharging based on parameters in Appendix A4. Charging temperature curves evolution are similar with a standard deviation lower than 4%, except the cooling effect which was not numerically accounted. Numerical curve is above the experimental due to the fact that, theoretical considerations are virtually perfect, such as wall conduction and initial temperature.

Discharging prediction can be done using the numerical model until 100 min. If the agreement experiment-simulation is quite satisfactory in the early 30 min of the hydration reaction, the model tends to move lower away from experimental data during the cooling phase of the system. However, when extrapolating numerical profile, experimental and numerical curves will both closely tend to the final bed temperature. If the consistency between simulation and experience was quite satisfactory in charging phase, the results in discharging phase after a certain time show a discrepancy. Obviously, the physical and chemical phenomena occurring during the hydration reaction in the salt bed might not be correctly interpreted by the model. Model predictions prove

fairly accuracy at a short time, but the agreement experiment-simulation deteriorates over time. The reliability of the measurements can be questioned, such as no-measuring the reactor wall temperature to identify heat loss. However, the model can also be incriminated because of the incomplete representation of cycle tests. However, a linear fit between the numerical and experimental data was performed (Figure 5.26) in order clarify the interpolation mentioned above. Their relationship is linear ($y = 1.02x + 0.94$) and values are within the 90% confidence interval. Therefore the model is valid within the time ranging from 0 to 600 min.

Figure 5.25. Numerical and experimental comparison of charging (a) and discharging (b) temperature of the thermochemical heat storage system.

Discharging prediction can be done using the numerical model until 100 min. If the agreement experiment-simulation is quite satisfactory in the early 100 min of the hydration reaction, the model tends to move lower away from experimental data during the cooling phase of the system. However, when extrapolating numerical profile, experimental and numerical curves will both closely tend to the final bed temperature. If the consistency between simulation and experience was quite satisfactory in charging phase, the results in discharging phase after a certain time show a discrepancy. Obviously, the physical and chemical phenomena occurring during the hydration reaction in the salt bed might not be correctly interpreted by the model. Model predictions prove fairly accuracy at a short time, but the agreement experiment-simulation deteriorates over time. The reliability of the measurements can be questioned, such as no-measuring the reactor wall temperature to identify heat loss. However, the model can also be incriminated because of the incomplete representation of cycle tests. However, a linear fit between the numerical and experimental data was performed (Figure 5.26) in order clarify the interpolation mentioned above. Their relationship is linear ($y = 1.02x + 0.94$) and values are within the 90% confidence interval. Therefore the model is valid within the time ranging from 0 to 600 min.

Concerning the pressure in the reactor, Figure 5.27 also shows good agreement between simulation and experiment at a specific time. It can be seen here a consistency between experiment and simulation during the first 200 min. After that, there is a discrepancy between them. The reason is

that in numerical study, the convergence is mathematically programmed and the physico-chemical gas property in the reality does not follow the ideal gas law.
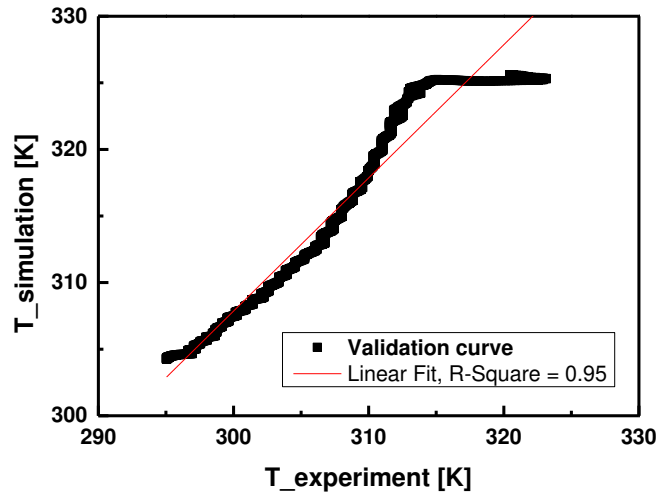
Figure 5.26. Validation of the model by the experience during discharging in the time range (0-600) min ($y = 1.02x + 0.94$; confidence interval: 90%).

In a global way, for both experiment and simulation, results are within 10 – 70 mbar during the charging and within 10 – 25 mbar during the discharging of the thermochemical system. Those results justify the so called "low pressure systems" in thermal energy storage. For such a closed system, Mauran et al. found reactor pressure in the range of 10 – 56 mbar for the charging and 10 – 20 mbar for the discharging, but the reactive salt strontium bromide was implemented with an expanded natural graphite in the form of a consolidated material which has acceptable thermal conductivity and permeability adapted to low pressure (Mauran et al., 2008). Could be it drawn that, composite materials in this application considerably improve the operating conditions? Anyway, only pure salt could not achieve the expected performances in order to concurrence the water storage system.
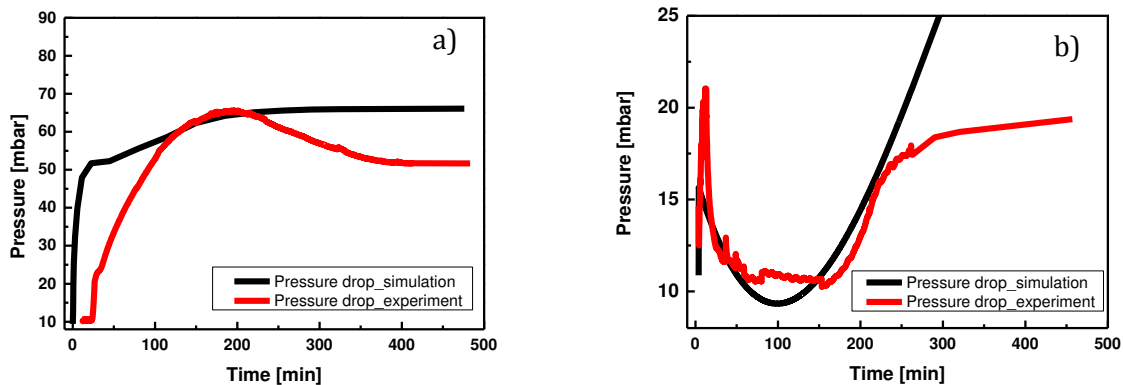
Figure 5.27. Numerical and experimental comparison of charging (a) and discharging (b) pressure of the thermochemical heat storage system.

184

To conclude on the model validation, an observation of the performance analysis realised earlier and summarized in Table 5.7, gives a broad and definitive overview. For a quasi-complete hydration, it can be seen the good agreement between the numerical and experimental results. However, a large discrepancy for the overall heat transfer coefficient is significant. Numerical result exhibits good value due to the perfect conduction at the layer of the bed and the heat exchanger.

Experiment shows lower values, causing bad heat transfer when recovery the produced heat for space heating and DHW for example. From the point of view of the bed, the application is more valuable than other thermal energy storage technique. Therefore more attention and care have to be brought in the reactor component and material design.

Parameter values in Table 5.7 are the main criteria on discussing the performance of such a system. Indeed, the Coefficient of Performance is representative of energy saving; the efficiency and the heat transfer coefficient to know how much recovery would be possible. Even with numerical modelling parameters, simulations results bring hopeful conclusion. Storage capacity level is lower than expected but storage process provides heating that lead to interesting energy saving.

Table 5.7. Numerical and experimental performance analysis comparison of the thermochemical heat storage system.

	Numerical ($\alpha = 0.9$)	Case cycle test Nr. 4 ($\alpha \geq 0.9$)	Global cycle tests ($\alpha = 0.9$)
Energy storage capacity	60 kWh	63 kWh	65 kWh
Thermal efficiency	0.78	0.78	0.77
Coefficient of performance (COP_{th})	0.97	0.97	0.97
Overall heat transfer coefficient (U_0)	182	100	147

Additional remark on the experimental power value is that, the presented result accounts with the salt losses during experimentation as shown in Figure 5.18. It also reduces the power amount of course, since the system power strongly depends on the salt quantity.

5.6. CONCLUSION OF THE CHAPTER

In this chapter, numerical results were presented followed with performance analysis of the system. A sensitive investigation regarding the chemical kinetic, heat and mass transfer was performed to analyse the process kinetic and hence the thermal power. It numerically shows that 76% of the target objectives can be achieved with an energy density of 115 kWh·m^{-3} of salt. As Emanuel Kant said "experience without theory is blind, but theory without experience is mere intellectual play", so a lab-scale experiment was developed in order to compare and prepare the prototype design. With about 1 kg of salt hydrate in a honeycomb bed structure, the thermal process was analysed and it

shows that 81% of the target objectives can be achieved with an energy density of 140 kWh·m^{-3} of salt disregarding the heat source cost. Considering only pure salt hydrates may not allow meeting the set target for the intended application (80 kWh·m^{-3} for the whole reactor including the water storage) since lab-scale power proved to be lower than what envisaged. This assertion is only based on lab-scale experiment where the total volume of the system is less than 1 m^3. Experimentally, temperature levels for dehydration and hydration were determined by their heat sources. Regeneration with micro-CHP heat losses is performed in a temperature range of 95 – 115 °C using a condensation temperature of 16 – 30 °C. Hydration takes place at about 20 °C (evaporator temperature of 30 °C) and has to fulfil a temperature lift of 30 °C getting the HTF inlet temperature of about 50 °C for both space heating and DHW. Both, evaporation and condensation are strongly influenced by their external heat source/heat sink which can be ground storage. The reaction front was experimentally put in evidence with the aid of thermocouples within the bed. It could not being shown through the mass transfer because of the absence of dynamical measurement of the sorption.

Different ways of evaluating thermal system power are presented and used for evaluation. Formulae involving the reaction conversion are relevant, since its evolution is dynamic. Reason why there is a non-consistency of using some formula. However, two of them help bringing meaningful conclusion for future prototype development. It shows thermal power variation with very high peaks. Numerically, the charging power with a peak at 805 W and the discharging power with a peak at 630 W do not vary much. Experimentally, the charging with a peak at 805 W also and the discharging with a peak at 682 W show very high variation. Comparison of the performances was quite similar, hence validating the numerical model. As already said by Mauran et al. (Mauran et al., 2008) the storage capacity and the power of the system are still insufficient because of the low heat transfer at the interface between the reactive layer and the exchanger wall leading to heat transfer coefficient lower than 200 W·m^{-2}·K^{-1}. Since bed is producing higher temperature which difficult to be transferred at a maximum temperature difference of 3 °C. That is why, coating layer should be considered and the development of efficient heat exchanger. Many other thermochemical energy storage using strontium bromide were performed, whether in closed or open systems (Marias et al., 2014; Mauran et al., 2008; Michel et al., 2014; Tanguy et al., 2012, 2010), but no closed system has already exhibited more than 65 kWh of storage capacity.

REFERENCES CHAPTER

Andreozzi, A., Buonomo, B., Manca, O., Tamburrino, S., 2014. Thermal energy storages analysis for high temperature in air solar systems. Applied Thermal Engineering 71, 130–141. doi:10.1016/j.applthermaleng.2014.06.036

Azoumah, Y., Mazet, N., Neveu, P., 2004. Constructal network for heat and mass transfer in a solid–gas reactive porous medium. International Journal of Heat and Mass Transfer 47, 2961–2970. doi:10.1016/j.ijheatmasstransfer.2004.03.022

Dyke, M., Sass, R.L., 1964. The Crystal structure of strontium bromide monohydrate. J. Phys. Chem. 68, 3259–3262. doi:10.1021/j100793a031

Favergeon, L., Morandini, J., Pijolat, M., Soustelle, M., 2013. A General approach for kinetic modeling of solid-gas reactions at reactor scale: application to kaolinite dehydroxylation. Oil & Gas Science and Technology – Revue d'IFP Energies nouvelles 68, 1039–1048. doi:10.2516/ogst/2012018

Fopah Lele, A., Hu, J., Kuznik, F., Schmidt, T., Ruck, W.K.L., 2015a. Numerical investigations of a thermochemical heat storage system during the discharging, in: ASME-ATI-UIT 2015 Conference on Thermal Energy Systems: Production, Storage, Utilisation and the Environment, Heat and Mass Transfer in Porous Media. Presented at the ASME-ATI-UIT 2015, ASME, Napoli, Italy, p. 8.

Fopah Lele, A., Kuznik, F., Rammelberg, H.U., Schmidt, T., Ruck, W.K.L., 2015b. Thermal decomposition kinetic of salt hydrates for heat storage systems. Applied Energy 154, 447–458. doi:10.1016/j.apenergy.2015.02.011

Fopah Lele, A., Rönnebeck, T., Rohde, C., Schmidt, T., Kuznik, F., Ruck, W.K.L., 2014. Modelling of heat exchangers based on thermochemical material for solar heat storage systems. Energy Procedia, International Conference on Applied Energy, ICAE2014 61, 2809–2813. doi:10.1016/j.egypro.2014.12.284

Heimrath, R., Haller, M., 2007. The reference heating system, the template solar system of Task 32 (IEA-A technical report of Subtask A), IEA Solar Heating and Cooling programme "Advanced storage concepts for solar and low energy buildings". IEA-SHC, Graz, Austria.

Istria, S., Castaing-Lasvignottes, J., Neveu, P., 1996. Energetic analysis, application field and performance of a new thermochemical sorption cycle: The multisalt system. Applied Thermal Engineering 16, 875–889. doi:10.1016/1359-4311(96)00007-5

Kainourgiakis, M.E., Kikkinides, E.S., Stubos, A.K., Kanellopoulos, N.K., 1998. Adsorption–desorption gas relative permeability through mesoporous media—network modelling and percolation theory. Chemical Engineering Science 53, 2353–2364. doi:10.1016/S0009-2509(98)00084-0

Lahmidi, H., Mauran, S., Goetz, V., 2006. Definition, test and simulation of a thermochemical storage process adapted to solar thermal systems. Solar Energy 80, 883–893. doi:10.1016/j.solener.2005.01.014

Li, T.X., Wang, R.Z., Yan, T., Ishugah, T.F., 2014. Integrated energy storage and energy upgrade, combined cooling and heating supply, and waste heat recovery with solid–gas thermochemical sorption heat transformer. International Journal of Heat and Mass Transfer 76, 237–246. doi:10.1016/j.ijheatmasstransfer.2014.04.046

Marias, F., Neveu, P., Tanguy, G., Papillon, P., 2014. Thermodynamic analysis and experimental study of solid/gas reactor operating in open mode. Energy 66, 757–765. doi:10.1016/j.energy.2014.01.101

Mauran, S., Lahmidi, H., Goetz, V., 2008. Solar heating and cooling by a thermochemical process. First experiments of a prototype storing 60kWh by a solid/gas reaction. Solar Energy 82, 623–636. doi:10.1016/j.solener.2008.01.002

Michel, B., 2012. Procédé thermochimique pour le stockage intersaisonnier de l'énergie solaire : modélisation multi-échelles et expérimentation d'un prototype sous air humide (Doctorate/Ph.D). Université de Perpignan, Perpignan - France.

Michel, B., Mazet, N., Neveu, P., 2014. Experimental investigation of an innovative thermochemical process operating with a hydrate salt and moist air for thermal storage of solar energy: Global performance. Applied Energy 129, 177–186. doi:10.1016/j.apenergy.2014.04.073

N'Tsoukpoe, K.E., Restuccia, G., Schmidt, T., Ruck, W.K.L., 2014. Regarding the size of sorbents in low pressure sorption and thermochemical energy storage systems: assessment and guidelines. In Progress.... 27 pages manuscript.

N'Tsoukpoe, K.E., Schmidt, T., Rammelberg, H.U., Watts, B.A., Ruck, W.K.L., 2014. A systematic multi-step screening of numerous salt hydrates for low temperature thermochemical energy storage. Applied Energy 124, 1–16. doi:10.1016/j.apenergy.2014.02.053

Rambaud, G., 2009. Problématique des transferts en milieu poreux réactif déformable pour procédés de rafraîchissement solaire (Doctorate/Ph.D). Université de Perpignan, France.

Stitou, D., 2013. Transformation, conversion, stockage, transport de l'energie thermique par procédés thermochimiques et thermo-hydrauliques (Habilitation (HDR)). Université de Perpignan, France.

Stitou, D., Goetz, V., Spinner, B., 1997. A new analytical model for solid-gas thermochemical reactors based on thermophysical properties of the reactive medium. Chemical Engineering and Processing: Process Intensification 36, 29–43.

Tanguy, G., Marias, F., Rouge, S., Wyttenbach, J., Papillon, P., 2012. Parametric studies of thermochemical processes for seasonal storage. Energy Procedia, 1st International Conference on Solar Heating and Coolingfor Buildings and Industry (SHC 2012) 30, 388–394. doi:10.1016/j.egypro.2012.11.046

Tanguy, G., Papillon, P., Paulus, C., 2010. Seasonal storage coupled to solar combisystem : dynamic simulations for process dimensioning, in: EuroSun_international Conference on Solar Heating, Cooling and Buildings. Presented at the EuroSun, ISES-EuroSun, Graz, Austria, p. 8.

6. CONCLUSION & GUIDELINES

The presented thesis, was performed within the European research project "Thermal Battery" with the main objective to develop a compact 1 m³ thermochemical heat storage system for micro-CHP efficiency upgrading and heating purposes. The presented research and development focused on the characterization of the most important and sensitive parameters and the performance analysis of the thermochemical system process. Their influence on the performance was numerically presented.

Such a system, based on the reversible reaction between an inorganic salt and pure water vapour, is defined as a closed system. Although this operating mode presents many advantages such as greater reaction efficiencies (Casey et al., 2015) and power released (Michel et al., 2014), it also deals with some technological constraints such as vacuum control. To demonstrate its feasibility, numerical and experimental investigations were performed.

At first, the interest of thermochemical systems over others such as absorption and adsorption systems was presented, followed by a comparative analysis of possible materials that can meet the expected requirements of the present system. A thermodynamics review also presents the real equilibrium temperatures and pressures diagram, because it is shifted from the theoretical process. Within the project framework, a systematic screening of over 125 inorganic salts was performed and it came out that $SrBr_2 \cdot 6H_2O$ (exchanging five water molecules) presented good theoretical properties such as energy storage density and good thermodynamic conditions corresponding to the application (N'Tsoukpoe et al., 2014). The state-of-art on upgrading the combined heat and power device with a thermal energy storage system highlights that, it is possible and that, it will bring more economical and technological benefits. Then a short review on the main important phenomena (heat, mass transfer and chemical reaction with sorption) involved during this process was highlighted. This first part of the thesis helps knowing which properties to characterise in order to analyse the thermochemical storage system performance.

The next chapter (chapter 3), based on the thermal management of the thermochemical heat storage system, numerically presents the investigation method. In order to talk about thermal management, the device (here the reactor) in which it will take place should be chosen. Therefore a critical analysis of different reactors used in thermal engineering was done, presenting the pros and cons for each thermal reactor. Fixed or packed bed is adopted due to their characteristics with the present work. The storage system was then methodologically and thermodynamically described followed by the main component investigation for such a closed system, the heat exchanger. The investigation, only numerical, was performed on three different heat exchangers, namely, helical coil, plate-fin and honeycomb. Using commercial software for geometry design and thermal simulation and based on criteria such as bed temperature, pressure drop and overall heat transfer coefficient, the honeycomb heat exchanger demonstrated to be more effective. Once the reactor and the heat exchanger were known, a 3D model was developed to describe and analyse in detail the dynamic behaviour from the porous media (salt hydrate) to the thermochemical reactor (lab-scale reactor). This model accounted for the heat and mass transfers through the porous bed of reactive salt, and used the phenomenological laws adapted to the flow types encountered in reactive porous media during thermochemical heat storage process. Another 1D model, purely analytical, based on the displacement of a front within the bed due the reaction advancement or conversion, was developed. It helps evaluating the required time for effectively discharging the system.

Characterization of thermal transfer and chemical reaction has been the main objective of the fourth chapter. Although the system used $SrBr_2\cdot6H_2O$ as the reactive salt, some characterization was extended to other salts generally used in thermochemical storage. Concerning the thermal conductivity, two methods were used. The first was realised by using the DSC present in the laboratory and the second was designed, built and tested. Specific heat capacity was transiently measured (using the DSC) according to the DIN 51007 at isothermal steps at 60 °C and 90 °C, approximatively corresponding to the discharge and charge temperature, respectively. Permeability was also measured through an in-house device, designed, constructed and tested, which operated under two different gases, namely, helium and nitrogen. Kinetics analysis was evaluated with a simultaneous thermogravimetric analysis (TGA) and a differential scanning calorimetry (DSC) device form Mettler Toledo. Besides those properties characterization, bed density and void fraction were determined. After calibration of the different devices, measurements were performed, the thermophysical properties evaluated along with uncertainties, and then validated with literature values. The determined properties were then inserted in the mathematic modelling such as thermal conductivity, specific heat capacity, permeability, porosity of the bed and reaction rate. Conductivity results exhibited low values, as expected for inorganic salts. Permeability results using nitrogen as gas were closed to air-permeability value concerning the chosen salt. Kinetics analysis was also treated as a micro-scale experiment. At this scale, the expected reactor energy storage density (115 kWh·m⁻³) representing 72% of the fixed objective, was obtained, disregarding the fact that the oven is an open system.

The above parameters, well determined under realistic conditions, helped for numerical investigations and performances evaluation. The first part of the fifth chapter concerns the numerical results. From general analysis to numerical investigation, objectives were presented and optimal parameters to achieve these latter found. A first validation of the model was done at micro-scale using the reaction conversion and rate as key factors since reaction efficiency leads to great performance. Sensitivity of permeability and thermal conductivity on the reaction efficiency was numerically demonstrated. Output reveals that bed with conductivity at around 10 W·m⁻¹·K⁻¹ and permeability of 0.7x10⁻¹⁰ should be efficient. At this level, simultaneous chemical reaction and sorption phenomena are highlighted. The 3D temperature results are presented and then plotted along with the pressure evolution in the reactor during charging and discharging. The cooling effect of the bed is also numerically considered and a controlled environment could slightly increase the bed temperature. The metal part of the reactor also effects on the bed temperature, but only during the first minutes and get thereafter homogeneous. Based on all those previous effects, different formulation of the thermal power was reviewed and adapted to the present work, followed by the thermal efficiency and the coefficient of performance. Some of the formulas concerning thermal power were consistent and the different results were presented, analyzed and discussed. It also came out that, only 75% of the fixed objectives could be reached based on the numerical investigations. Before the prototype, lab-scale was developed to test the system under known and controlled conditions so that, the feasibility of the process can be proved. Therefore a lab-scale reactor operating under vacuum was designed, built and tested, mimicking the association with a micro-CHP. It contains about 1 kg of salt hydrate inserted in the honeycomb cells. The bed energy density was found to be 531 kWh·m⁻³ of salt hydrate. Based on the condensation temperature

during the experimentation, a reactor energy density of 140 kWh·m^{-3} was obtained and a storage capacity of 65 kWh representing 81% of the fixed objectives.

Thirteen cycling tests were performed in order to check the stability of the system. The results show that a cycling stability can be reached also at this medium scale, even when some of the storage material melts during charging. A cycle test was separately analyzed and discussed, then confronted to the global (average) cycling test and the results showed very little difference. Experimental results are presented and discussed. The sharp front displacement was highlighted through temperature evolution at different thermocouple positions. This phenomenon is always present in such a thermochemical process, due to the equilibrium shift created to permit that reaction takes place. The confrontation of this front model and experiment value show that the hydration time is approximately the same. Around 22 days are needed to completely discharge the system at the prototype level. 3D model results confronted to experiments showed quite similar behavior with a standard deviation lower than 4%, except during the discharging where the cooling effect which was not numerically accounted deviates from the experimental temperature curve after a certain time. Using a linear fit between simulation and experiment for the hydration proved that the values were within the 90% confidence interval. However, released temperature of the bed reached about 52 °C during the hydration, which met the expected output temperature for heating and DHW application. Concerning the reactor pressure, experiment and simulation results were within 10 – 70 mbar during the charging and within 10 – 25 mbar during the discharging of the thermochemical system, ensuring again the model validation. The overall heat transfer coefficient, whether numerical or experimental, exhibited low heat transfer at the interface between the reactive bed layer and the exchanger wall. The recommended value of 200 W·m^{-1}·K^{-1} by Rambaud (Rambaud, 2009) was not obtained, and was one of the causes of not reaching a great performance. Anyway, in the last chapter, the simulation confronted with experimental results gave encouraging results, even if they are not finalized and are only at lab-scale.

Finally, this study demonstrated the feasibility of thermal energy storage by thermochemical process, for heating applications, and as addition to existing systems such as micro-CHP. For this, we have shown that it is possible to use inorganic salts as porous structure having both high energy density and fairly satisfactory heat and mass transfer parameters. As comparison, Lahmidi (Lahmidi et al., 2006) obtained 60 kWh·m^{-3} of reactor with 268 kg of composite material (Graphite+ $SrBr_2 \cdot 6H_2O$) and in this study, 65 kWh·m^{-3} of reactor with 1 kg of pure material ($SrBr_2 \cdot 6H_2O$) is obtained. In addition, a lab-scale system was designed and has achieved thermal powers as well as high energy densities closed to the project objective. Furthermore, a set of models from the reactive porous media and extended to the system, with different levels of complexity, was developed, particularly for vacuum operation, and was validated with experimental results. Offering therefore a design and analysis tools for such a thermochemical system.

Still, several issues remain to study or to deepen in the design of heat storage systems through thermochemical process. Although the developed model predicts reasonably well the dynamic behaviour of the process, more specific studies to establish a more accurate model are required. The study of the impact of heat and mass transfer and monitoring of chemical kinetics will be necessary during experimentation. Measurement of the reactor wall temperature was not performed, in order to evaluate the heat losses. At lab-scale, sorption was not dynamically studied, preventing dynamical

process observation. The evapo-condenser was not controllable, in order to fix the required temperature. Additional components are required to enhance the vaporization like borehole heat-exchangers, solar thermal assistance, or others. The following recommendations should be taken into consideration for the prototype development.

➢ Nevertheless the utilisation of pure salt hydrates for the purpose of heat storage may show material related problems.

Structural changes: Salt hydrates undergo structural changes during sorption (changes in volume, rheological behaviour). This can result in degradation and failure of the storage material. Thanks to the honeycomb structure, it can be avoided.

Phase change: During charging process the salt can solute in leaking crystal water (incongruent melting). Salt solutions can cause corrosion and mechanical damage to the system. The present study shows how this can be avoided, but for a very long time, corrosion is inevitable.

Reaction kinetics: The hydration of salts is a sequence of reactions forming successively higher grades of salt hydrates. Kinetic obstacle and thermodynamically stable intermediates can significantly reduce the reaction dynamics and output power of the overall process. This point should be deeper studied as a research project and extend the investigations to the system performances.

Temperature lift: Reaction temperature during hydration strongly depends on the vapour pressure (evaporator temperature). e.g. for seasonal storage minimum reaction temperatures of 40 - 60°C have to be reached with water evaporation temperatures around 0 -10°C (ground heat source).

➢ Improving the structural integrity of the material by composites or additives such as salts in matrix (SIM), salt inside porous matrix (CSPM), selective water sorbents (SWS) and coated salt layer (CSL) should improve the thermal transfers (Aristov et al., 2000; Casey et al., 2015; Gordeeva and Aristov, 2012). In some, development of compound materials, mixtures of salt hydrates with im-proved properties should be performed as already started in (Korhammer et al., 2015).

➢ Development of geometry optimisation for TES systems only for cylindrical shape as sug-gested by Azoumah in his thesis (Azoumah, 2005) by taking second thermodynamics principle as optimisation criteria.

From the experimental data, it will be worthy to perform, a study of the thermochemical storage system integration using TRNSYS software, so that, the system control from the power point of view will be mastered and its importance of upgrading electricity production of the micro-CHP shown. Finally, from an environmental point of view, a life cycle analysis is highly recommended.

REFERENCES OF THE CONCLUSION

Aristov, Y.I., Restuccia, G., Tokarev, M.M., Cacciola, G., 2000. Selective water sorbents for multiple applications, 10. Energy Storage Ability. Reaction Kinetics and Catalysis Letters 69, 345–353. doi:10.1023/A:1005616420331

Azoumah, Y.K., 2005. Conception optimale, par approche constructal, de reseaux arborescents de transferts couplés pour reacteurs thermochimiques (Doctorate/Ph.D). Université de Perpignan, France.

Casey, S.P., Aydin, D., Riffat, S., Elvins, J., 2015. Salt impregnated desiccant matrices for "open" thermochemical energy storage—Hygrothermal cyclic behaviour and energetic analysis by physical experimentation. Energy and Buildings 92, 128–139. doi:10.1016/j.enbuild.2015.01.048

Gordeeva, L.G., Aristov, Y.I., 2012. Composites "salt inside porous matrix" for adsorption heat transformation: a current state-of-the-art and new trends. International Journal of Low-Carbon Technologies 0, 1–15. doi:10.1093/ijlct/cts050

Korhammer, K., Druske, M.-M., Fopah-Lele, A., Rammelberg, H.U., Wegscheider, N., Opel, O., Osterland, T., Ruck, W., 2015. Sorption and thermal characterization of composite materials based on chlorides for thermal energy storage. Applied Energy. doi:10.1016/j.apenergy.2015.08.037

Lahmidi, H., Mauran, S., Goetz, V., 2006. Definition, test and simulation of a thermochemical storage process adapted to solar thermal systems. Solar Energy 80, 883–893. doi:10.1016/j.solener.2005.01.014

Michel, B., Neveu, P., Mazet, N., 2014. Comparison of closed and open thermochemical processes, for long-term thermal energy storage applications. Energy 72, 702–716. doi:10.1016/j.energy.2014.05.097

N'Tsoukpoe, K.E., Schmidt, T., Rammelberg, H.U., Watts, B.A., Ruck, W.K.L., 2014. A systematic multi-step screening of numerous salt hydrates for low temperature thermochemical energy storage. Applied Energy 124, 1–16. doi:10.1016/j.apenergy.2014.02.053

Rambaud, G., 2009. Problématique des transferts en milieu poreux réactif déformable pour procédés de rafraîchissement solaire (Doctorate/Ph.D). Université de Perpignan, France.

APPENDICES

APPENDIX – A1. HEAT EXCHANGERS CHARACTERISITICS

1- **Fine plate Heat Exchanger**

- Total heat surface area = 0.63 [m²]

- Tube inner diameter = 12 [mm]

- Tube outer diameter = 16 [mm]

- Tube length = 1193.4 [mm]

- Inner space U-tube = 36 [mm]

- External U-tube width = 68 [mm]

- U-tube curve diameter = 52 [mm]

- Distance between the U-tubes = 36 [mm]

- Plate (square) = 0.1*0.1 [m²]

- Plate thickness = 1[mm]

- Plate pitch = 10 [mm]

- 50 plates
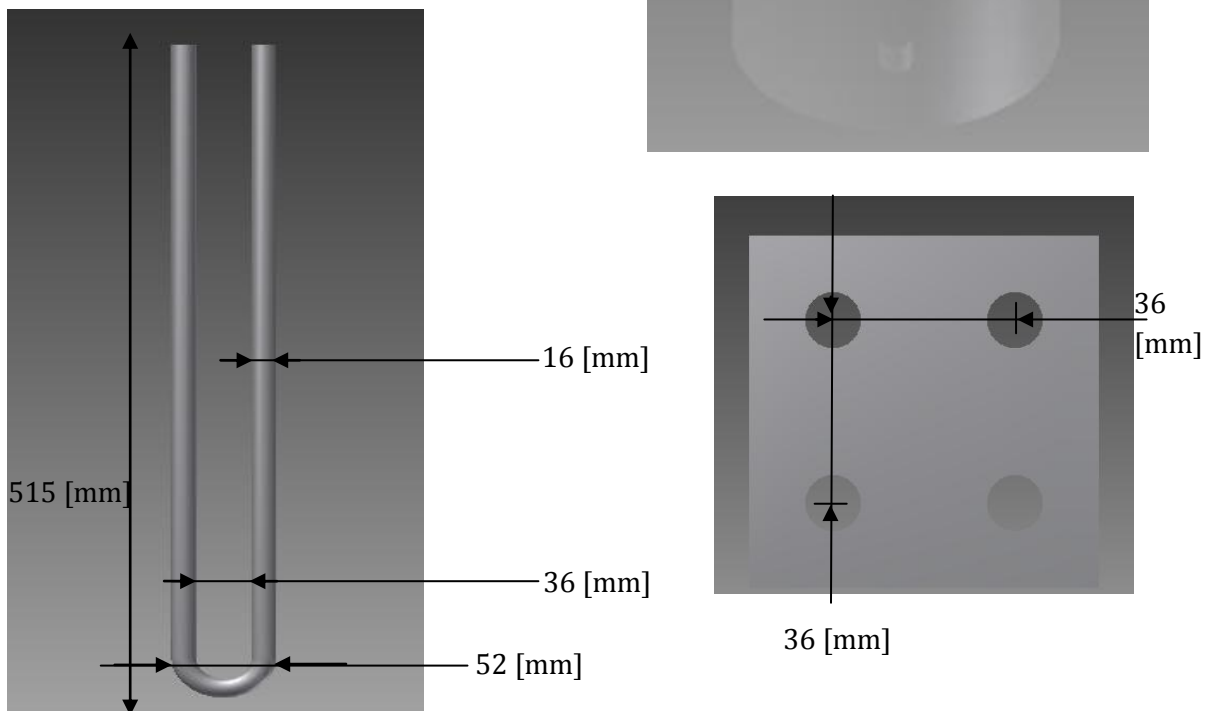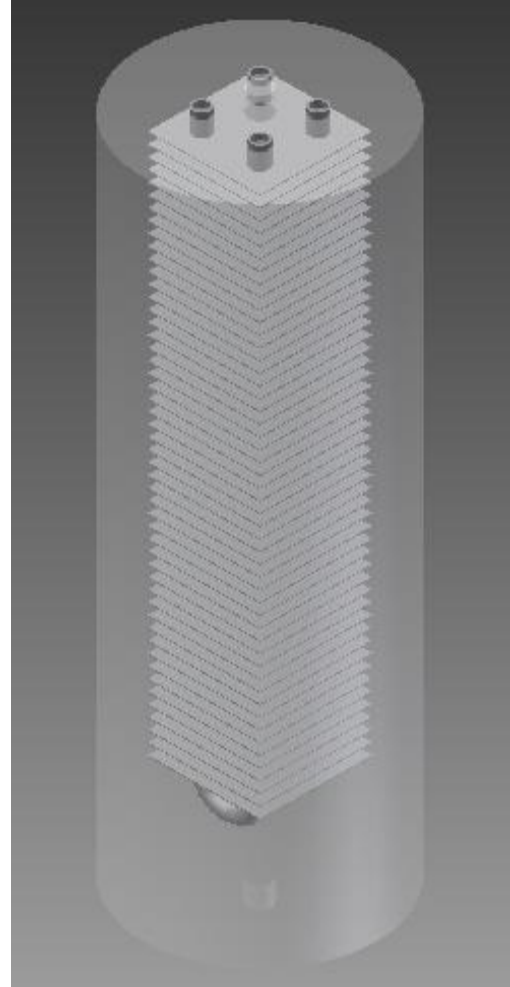
2- Helical coil Heat Exchanger

- Total heat surface area = 0.49 [m^2]

- Tube inner diameter = 12 [mm]

- Tube outer diameter = 16 [mm]

- Tube length = 4840 [mm]

- Coil pitch = 40 [mm]

- Coil diameter = 140 [mm]

- Curvature ration = 85 [mm]

- 10 turns
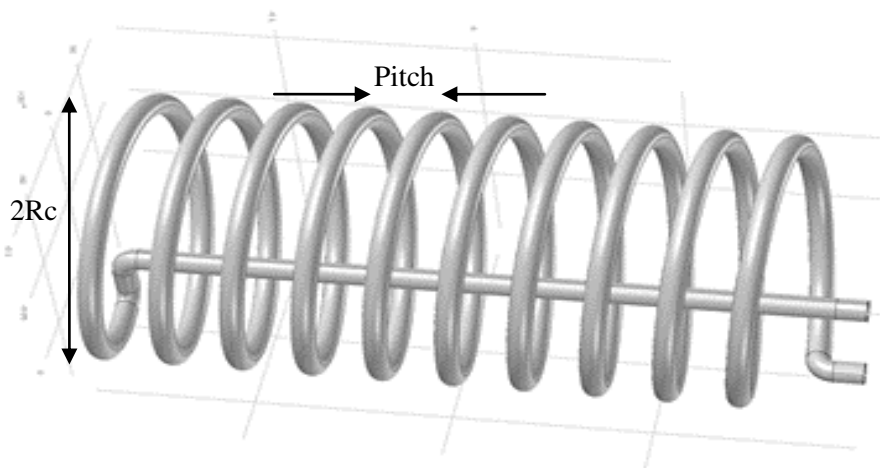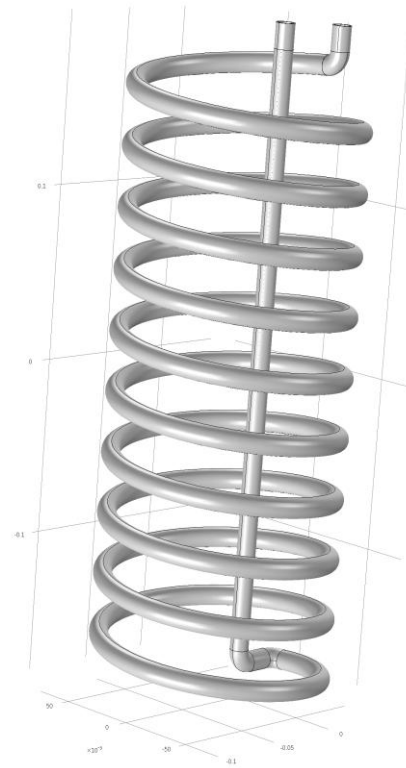
The curvature ratio, δ , is defined as the coil-to-tube diameter ratio, d/2Rc (tube diameter/2*curvature radius).

3- Honeycomb Heat Exchanger

- Total heat surface area = 0.17 [m²]

- Tube inner diameter = 12 [mm]

- Tube outer diameter = 16 [mm]

- Tube length = 1750 [mm]

- Inner space U-tube = 74 [mm]

- External U-tube width = 106 [mm]

- Elbow curve diameter = 5 [mm]

- Distance between the //-tubes = 175 [mm]

- Plate (square) = 0.13*0.235 [m²]

- Plate thickness = 1[mm]

- Plate pitch = 10 [mm]
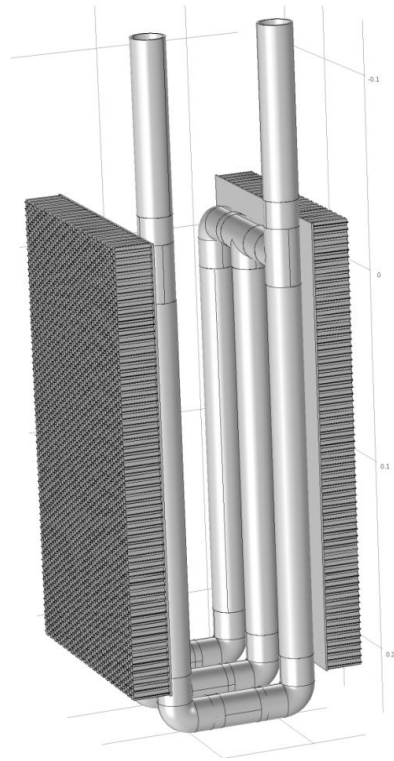
2D description of one side honeycomb heat exchanger   Honeycomb duct details
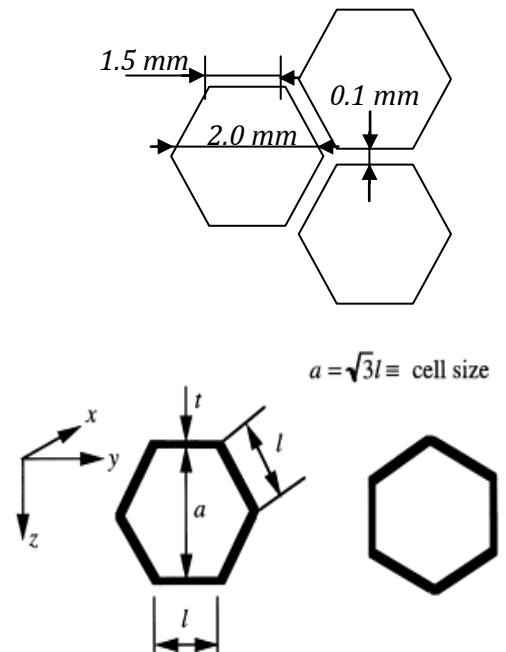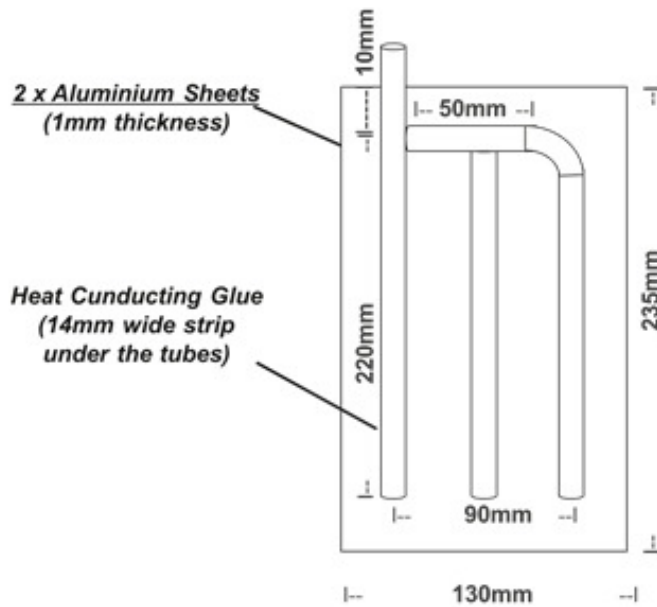
APPENDIX – A2. PARAMETERS EVALUATION FOR NUMERICAL INVESTIGATIONS

1- Knudsen number

The dimensionless Knudsen number (Kn = $^l/_d$, where l is the mean free path of the gas, i.e. the average distance between two consecutive molecular collisions, and d is the characteristic pore diameter) is used to determine the degree of appropriateness of applying continuum approach. For Kn < 0.01, the mean free path of the gas molecules is negligible compared to the characteristic dimension of the flow geometry (i.e. d parameter), the continuum hypothesis of fluid mechanics generally holds true and flow is of Darcy type. At Kn < 10 the gas molecules collide with the flow boundaries more often than inter-molecule collisions. Thus the molecules move independently of each other and in this condition the gas composition have no importance. This flow regime is known as Knudsen diffusion or free-molecule flow. The intermediate region in between 0.01 < Kn < 10 cannot be considered neither as a continuum flow nor a free-molecule flow. A further classification is done for that region is given by (Karniadakis et al., 2005):

- Slip flow (0.01 < Kn < 0.1)
- Transition flow (0.1 < Kn < 10)

In the slip flow regime (0.01 < Kn < 0.1) the no-slip boundary conditions doesn't hold true, and a layer of about one mean free path thickness, known as the Knudsen layer, starts to become dominant between the bulk of the fluid and the wall surface. This results in a finite particle velocity value at the wall, and the corresponding flow regime is known as the slip flow regime. As we increase the Knudsen number, either by increasing the mean free path of gas (i.e. gas flowing at very low pressure) or decreasing the pore size, the contribution of the Knudsen layer increases. It goes to a transition flow and then finally to pure Knudsen flow. However, the limits of the Knudsen number for each flow regime is purely empirical and are based on pipe flow experiment and will vary for other geometries and surface roughness (Karniadakis et al., 2005). Another important point we have to remember, that these theories were developed to explain rarefied gas flows at very low pressure. These models are experimentally verified or developed for sub-atmospheric (near vacuum) pressures. In our application, the gas flow happens at much smaller pore pressures. Hence one need to make this assumption that physics of the system remains the same at low pressure and is governed by Darcy law and there is no slip flow.

2- Convective heat flux coefficient, *h*

To have an idea about the convective heat flux coefficient h of the reactor with the ambient, an experimental correlation must be used. It leads to the calculation with dimensionless numbers. In the case of natural convection, Grashof and Rayleigh numbers developed some correlations (Kreith, 1999). Based on the diameter of the reactor, the Grashof number is given by:

$$Gr_d = \frac{g|T_{amb} - T_w|d^3}{T_{film}\nu^2}$$

(A2-1)

Rayleigh number is then given by:

$$Ra_d = Gr_d \cdot Pr = \frac{g|T_{amb} - T_w|d^3}{T_{film}\nu} \frac{\rho c}{\lambda} \tag{A2-2}$$

The ambient temperature is $T_{amb} = 295$ K and the temperature of the outer wall of the reactor in the discharging phase is $T_w = 313$ K. Hence the film (layer between the reactor and the ambient) temperature can be determined as follows:

$$T_{film} = \frac{295 + 313}{2} = 304 \text{ K} \tag{A2-3}$$

Then the film temperature is used to acquire the physical properties of air from the table given in the handbook of chemistry and physics (Lide, 2005):

- $\nu = 16.0 \cdot 10^{-6}$ m/s^2
- $\rho = 1.165$ kg/m^3
- $c = 1007$ J/kg. K
- $Pr = 0.7115$

d is the reactor diameter, $d = 0.200$ m.

Thus,

- $Gr_D = 2.01 \cdot 10^7$
- $Ra_D = 1.43 \cdot 10^7$

Here the convection is "natural over a vertical cylinder". Correlations for "natural convection over a vertical plate" are valid as long as:

$$\frac{L_r}{d_r} < 4 \cdot 10^{-4} Pr Gr_D \tag{A2-4}$$

L_r is the height of the reactor, equal to 0.4 m. d_r is the reactor diameter, equal to 0.207 m.

The calculation from Eq. (A1-4) leads to $1.93 < 5720.46$, validating the correlations.

For $10^4 < Ra_D < 10^9$, the flow is laminar. The Nusselt number is given by the Mc Adams correlation (Mac Adams, 1961):

$$Nu = C_T 0.13 Ra^{1/4} \tag{A2-5}$$

For Pr = 0.7115, $C_T = 0.516$ ➔ Nu = 31.7. Moreover,

$$\text{Nu} = \frac{h \cdot D}{\lambda} \text{ ➔ } h = \frac{\lambda \cdot \text{Nu}}{D} \qquad (A2\text{-}6)$$

Finally, $\qquad \mathbf{h = 4.05 \ W/m^2.K}$

3- Inlet pressure

Instead of the inlet velocity of steam, the inlet pressure is determined. This pressure is considered as equal as to the one at the outlet of the evaporator, which one can be calculated with the Clausius-Clapeyron equation (Lahmidi et al., 2006):

$$\log\left[\frac{P_{vi}}{P_{ref}}\right] = \frac{-\Delta h_{L/G}}{R_g \cdot T_{evap}} + \frac{\Delta s_{L/G}}{R_g} \qquad (A2\text{-}7)$$

$$P_{vi} = \exp\left[\frac{-\Delta h_{L/G}}{R_g \cdot T_{evap}} + \frac{\Delta s_{L/G}}{R_g}\right] \cdot P_{ref} \qquad (A2\text{-}8)$$

Δh_r is the reaction enthalpy of formation, equal to 40930 J/mol. Δs_r is the reaction entropy equal to 109.6 J/mol.K. The reference pressure P_{ref} is equal to 10^5 Pa. The steam from the evaporator has a temperature of 283.15 K.

Thus,

$$P_{vi} = \exp\left[\frac{-40930}{8.314 \cdot 283.15} + \frac{109.6}{8.314}\right] \cdot 10^5 \quad \Longrightarrow \quad P_{vi} = 1494 \ \text{Pa} \qquad (A2\text{-}9)$$

References A2:

Karniadakis, G., Beskok, A., Aluru, N., 2005. Microflows and Nanoflows - Fundamentals and Simulation, 1ed ed, Interdisciplinary Applied Mathematics. Springer London, USA.

Kreith, F., 1999. The CRC Handbook of Thermal Engineering, 1st ed, Mechanical Engineering. Springer Jointly published with CRC Press, USA.

Lahmidi, H., Mauran, S., Goetz, V., 2006. Definition, test and simulation of a thermochemical storage process adapted to solar thermal systems. Solar Energy 80, 883–893. doi:10.1016/j.solener.2005.01.014

Lide, D.R. (Ed.), 2005. CRC Handbook of Chemistry and Physics, Internet Version 2005 <Thermal properties of Air (Page 6-175)>, 90th Internet Edition. ed, Thermal properties of Air (Page 6-175). CRC Press LLC, Boca Raton, Florida, USA.

McAdams W.H., 1961. Détails pour transmission de la chaleur (heat transfer), Translation into French from A. Beaufils. Paris Dunod, 585 pages.

APPENDIX – A3. ENERGY STORAGE DENSITY CALCULATIONS

1. The different energy storage densities calculation of salt hydrate and prototype (N'Tsoukpoe et al., 2014)

The volume energy storage density

It is evaluated in relation to the highest involved hydrates in the reaction (initial salt to be dehydrated). The volume energy density $\Delta H_{r,V}$ is calculated as the product of the mass energy density $\Delta H_{r,m}$ and the density of the particles of the salts d_s (it is not the bulk density and therefore, the required porosity is not considered here). The highest hydrates have usually the lowest particle density.

$$\Delta H_{r,V} = \frac{\Delta H_r}{M_s} \cdot d_s = \Delta H_{r,m} \cdot d_s \tag{A3.1}$$

ΔH_r is the molar enthalpy of the reaction per mole of the salt hydrate; M_s is the molar mass of the hydrate and d_s is the particle density.

The enthalpy of the reaction per mole of the salt hydrate ΔH_r is calculated based on the enthalpy of formation of the concerned hydrates. The reaction enthalpy is measured by TGA/DSC in this work and the value of 285 kJ·mol⁻¹ is obtained. The specific energy storage is 801 J·g⁻¹.

The net molecule energy storage density

It has to be noticed that the previous definition of energy storage density (either ΔH_r or $\Delta H_{r,V}$), which is widely used in the literature, characterised a heat pump rather than a heat storage unit because it does not actually account the actual amount of heat that is stored. Indeed, during the discharging phase, the evaporation energy has to be provided, though at low temperature. This evaporation energy is barely free, because even when a borehole is used to take it from the environment, the investment and the operation cost are to be considered. Therefore, it makes sense[e] to take this into account in the evaluation of storage density of the salt by diminishing the reaction enthalpy ΔH_r by the vaporisation energy required at the evaporator:

---

[e] This is very important in particular when the evaporation energy is not "free". Actually, this evaporation energy is barely free, because even when a borehole is used to take it from the environment, the investment and the operation cost are to be considered.

$$\Delta H_{netmo} = \Delta H_r - n \cdot L_v \tag{A3.2}$$

L_v corresponds to the vaporisation enthalpy of water, here at 15 °C, that is 44.6 kJ·mol^{-1} (an error less than ± 0,5 % is made if an evaporator at 10 or 20 °C were considered). Strictly speaking, ΔH_{netmo} corresponds to the actual energy storage potential and it is called here the "net molecule energy storage density".

The net volume energy storage density

The net volume energy storage density $\Delta H_{n,V}$ (kWh·m^{-3}) could then be evaluated as follow:

$$\Delta H_{n,V} = \frac{\Delta H_{netmo} \cdot d_s}{M_s} \tag{A3.3}$$

In case a comparison with another storage process is needed, the necessary volume for the storage of the condensed water (close processes) has also to be considered. The reduced net volume energy storage density is then:

$$\Delta H_{n,V*} = \frac{\Delta H_r}{\frac{1}{d_s} + \frac{M_w}{M_s} \cdot \frac{n}{d_w}} \tag{A3.4}$$

The first term of the denominator of the right side of the equation (A3.4) corresponds to the minimum volume required for the salt. The second term corresponds to the required volume for the storage of the condensed water. This term give actually the net storage capacity regarding the prototype volume (comprising the material bed, heat exchanger and the evapo-condenser).

Table A3.1. Energy storage densities calculation for the strontium bromide.

SrBr$_2$·6H$_2$O $\updownarrow$ SrBr$_2$·1H$_2$O	$\Delta H_{r,V}$ [kWh·m^{-3}]	ΔH_{netmo} [kWh·mol^{-1}]	$\Delta H_{n,V}$ [kWh·m^{-3}]	$\Delta H_{n,V*}$ [kWh·m^{-3}]
Molar mass [g·mol^{-1}]	355.5	Theoretical:	Theoretical:	Theoretical:	Theoretical:
Density [kg·m^{-3}]	2.390	531.77	61.75	115.32	71.85

Water moles	5			
Reaction enthalpy [kJ·mol⁻¹]	285	Lab-scale: 532	Lab-scale: 75	Lab-scale: 140.06	Lab-scale: 87.26

The net volume energy storage density obtained from the lab-scale is still lower than the required value as shown in Table 4.4. The lab-scale value is obtained under evapo-condenser temperature about 30 °C which is costly in term of system efficiency. One can conclude that, fulfilling the target objective also consists of additional energy source for the evapo-condenser.

APPENDIX – A4. PARAMETERS USED FOR THERMAL SIMULATIONS

Table A4.1. Parameters used for discharging simulation.

Parameter	Value	Unit	Description
c_0	2500	[mol·m⁻³]	Initial concentration
Cp_s	456	[J·kg⁻¹·K⁻¹]	Heat capacity of salt
Cp_v	f(T) ≈ 2478	[J·kg⁻¹·K⁻¹]	Heat capacity of steam
d_g	0.0001	[m]	Grains diameter
ΔH_r^0	67400	[J·mol⁻¹]	Enthalpy of formation
ΔS_r	175	[J·mol⁻¹·K⁻¹]	Reaction entropy of formation
E_a	55000	[J·mol]	Activation energy of salt
h	4.05	[W·m⁻¹·K⁻¹]	Convective heat flux coefficient
M_s	0.247	[kg·mol⁻¹]	Molar mass of salt (SrBr2)
M_v	0.018	[kg·mol⁻¹]	Molar mass of vapor
P_{vi}	1404	[Pa]	Inlet pressure of vapor
P_{vo}	90	[Pa]	Outlet pressure of vapor
P_{eq}	90	[Pa]	Equilibrium pressure
R	8.314	[J·mol⁻¹·K⁻¹]	Ideal gas constant
β	10	[K·min⁻¹]	Heating rate
ε	0.74	[-]	Porosity
k	0.7 x 10⁻¹⁰	[m²]	Permeability of the salt bed
λ_v	0.026	[W·m⁻¹·K⁻¹]	Steam thermal conductivity

λ_s	0.56	[W·m^{-1}·K^{-1}]	Salt thermal conductivity (SrBr2)
λ_p	0.71	[W·m^{-1}·K^{-1}]	Reaction Product thermal conductivity
ρ_v	f(p,T) ≈ 0.015	[kg·m^{-3}]	Density of steam
ρ_s	1209	[kg·m^{-3}]	Density of salt (porous)
ρ_{SrBr2}	4216	[kg·m^{-3}]	Density of srbr2
μ_v	8.90 x 10^{-4}	[Pa.s]	Viscosity of steam
χ	5	[-]	Stoichiometric coefficient

Table A4.2. Parameters used for charging simulation.

Paramters	Value	Unit	Description
β	10	[K·min^{-1}]	Heating rate
ΔH_r	337000	[J·mol^{-1}]	Reaction enthalpy
A_f	5.5 x 10^5	[s^{-1}]	Frequency factor in Arrhenius' equation
E_a	55000	[J·mol^{-1}]	Activation energy in Arrhenius' equation
$E_{a,w}$	50000	[J·mol^{-1}]	Activation energy of water
D_g	1 x 10^{-9}	[m^2·s^{-1}]	Gas diffusion coefficeint
T_{ext}	303	[K]	External temperature to the bed, but still in reactor
R	8.314	[J·mol^{-1}·K^{-1}]	Ideal gas constant (J/mol·K)
h	4.05	[W·m^{-1}·K^{-1}]	Convective heat transfer coefficient
k	3.1 x 10^{-11}	[m^2]	Permeability

Table A4.3. Thermodynamics data of strontium bromide (Michel, 2012).

Designation	Units	State/phase	SrBr$_2$	SrBr$_2$·H$_2$O	SrBr$_2$·6H$_2$O
Molar mass	[kg·mol^{-1}]		0.2474	0.2654	0.3555
Density	[kg·m^{-3}]		3700 / 4216	3480	2390
Molar volume or concentration	[mol·m^{-3}]		14955.5074	13112.3466	6723.1411
Heat capacity	[J·mol^{-1}·K^{-1}]	Solid	75.3 / 79.55	121	344
Reaction enthalpy	[J·mol^{-1}]		n.a.	67400 / 58000	

Formation enthalpy	[J·mol⁻¹]	Solid	-718000 /	-1033302 /	-2530502 /
			-716000	-1032611	-2531002
		Liquid	705000	n.a.	n.a.
Melting enthalpy	[J·mol⁻¹]		20100	n.a.	n.a.
Melting entropy	[J·mol⁻¹·K⁻¹]		22	n.a.	n.a.
Formation entropy	[J·mol⁻¹·K⁻¹]	Solid	135.1 / 142	n.a.	175
		Liquid	154.84	n.a.	n.a.
Melting temperature	[K]		916.15	618	361 / 361.15
Boiling temperature	[K]		1655	n.a.	n.a.

Most of these data were collected in Refs. (Gmelin, 1997; Lahmidi, 2005; Rambaud, 2009; van Ekeren, 1998).

Table A4.4. Equivalent parameters used for numerical simulations.

$SrBr_2 \cdot 1H_2O$		$SrBr_2 \cdot 6H_2O$	
m_{s0} (kg)	0.677	m_{s1} (kg)	0.973
m_{Al} (kg)	0.118	m_{Al} (kg)	0.118
V_{Al} (m³)	4.39×10^{-5}	V_{Al} (m³)	4.39×10^{-5}
V_{salt} (m³)	5.37×10^{-4}	V_{salt} (m³)	5.37×10^{-4}
V_t (m³)	5.80×10^{-4}	V_t (m³)	5.80×10^{-4}
ρ_{Al} (kg·m⁻³)	2700	ρ_{Al} (kg·m⁻³)	2700
ρ_{salt} (kg·m⁻³)	3480	ρ_{salt} (kg·m⁻³)	2390
λ_{bed} (W·m⁻¹·K⁻¹)	0.56	λ_{bed} (W·m⁻¹·K⁻¹)	0.71
λ_{Al} (W·m⁻¹·K⁻¹)	160	λ_{Al} (W·m⁻¹·K⁻¹)	160

C_{p_Al} (J·kg^{-1}·K^{-1})	900	C_{p_Al} (J·kg^{-1}·K^{-1})	900
C_{p_s0} (J·kg^{-1}·K^{-1})	456	C_{p_s1} (J·kg^{-1}·K^{-1})	968
C_{p_v} (J·kg^{-1}·K^{-1})	1410	C_{p_v} (J·kg^{-1}·K^{-1})	1410
C_{p_bed} (J·kg^{-1}·K^{-1})	1171.5	C_{p_bed} (J·kg^{-1}·K^{-1})	1198.5
ε (-)	0.75	ε (-)	0.86
$(\rho \cdot C_p)_{Al}$ (J·m^{-3}·K^{-1})	2430000	$(\rho \cdot C_p)_{Al}$ (J·m^{-3}·K^{-1})	2430000
$(\rho \cdot C_p)_{bed}$ (J·m^{-3}·K^{-1})	4076820	$(\rho \cdot C_p)_{bed}$ (J·m^{-3}·K^{-1})	2864415
γ_{Al} (-)	7.56 x 10^{-2}	γ_{Al} (-)	7.56 x 10^{-2}
γ_{bed} (-)	9.24 x 10^{-1}	γ_{bed} (-)	9.24 x 10^{-1}
ρ_{eql} (kg·m^{-3})	3421.06	ρ_{eql} (kg·m^{-3})	2413.42
$(\rho \cdot C_p)_{eql}$ (J·m^{-3}·K^{-1})	3952384.98	$(\rho \cdot C_p)_{eql}$ (J·m^{-3}·K^{-1})	2831590.26
λ_{eql} (W·m^{-1}·K^{-1})	12.61	λ_{eql} (W·m^{-1}·K^{-1})	12.71

APPENDIX – A5. FLOW METER CHARACTERISTICS

ROTA *MASS* Data sheet   **YOKOGAWA**

Version of the program: Vers. 4.3/k/kg/j   Date: 14-03-2013
Modell: **RCCx34**
Client: Universität Lüneburg   Tests bench

Flange: DN25 PN40 SL (02D4)
Medium: (Liquid)   Thermöl
Temperature: 20 °C
Pressure: 0.90000 bar overpressure
Viscosity: 5.4000 mPa·S
Operating density: 0.99400 kg/l
Density option: standard
Density specification: 3.0000 g/l
Flow type: Mass flow

Flow		Pressure loss	Accuracy	Velocity	Reynolds number
%	kg/h	mbar	% of rate	m/s	-
100	700	129	0.12	2.10	2977
90	630	110	0.12	1.89	2679
80	560	92.7	0.12	1.68	2382
70	490	76.4	0.13	1.47	2084
60	420	61.3	0.13	1.26	1786
50	350	47.4	0.14	1.05	1489
40	280	34.8	0.15	0.84	1191
30	210	23.6	0.16	0.63	893.1
20	140	13.9	0.20	0.42	595.4
10	70	5.8	0.29	0.21	297.7

APPENDIX – A6. UNCERTAINTIES CALCULATION

A6-1: Uncertainty calculation for the GHC

The determination of the thermal conductivity is based on the measurement of the average temperature gradient through the sample bed by a known axial heating power q_e (heating power determined by the electric current of central cartridge heater and the voltage generator) under steady-state conditions. When the working conditions are set up and the equilibrium is reached, the thermal conductivity (W·m^{-1}·K^{-1}) is given by the Eq. (4.5). The heating power is calculated by the current intensity and the voltage, in which the voltage has the relative uncertainty of ±1% after calibration and the electric current, is controlled by the stabilized power supply which has the relative uncertainty of ±3%. The height of the sample is measured using a meter with the uncertainty of ±0.01 mm, and the height of the sample in the experiments varies from 5 to 7.5 mm, the minimum value of temperature difference across the sample is 2.7 °C.

The error calculation of thermal conductivity under steady state measurement is:

$$\left|\frac{d\lambda}{\lambda}\right| = \left|\frac{dq_e}{q_e} - \frac{dL_s}{L_s} - \frac{d(slope)}{slope}\right| \leq \left|\frac{dq_e}{q_e}\right| + \left|\frac{dL_s}{L_s}\right| + \left|\frac{d(slope)}{slope}\right| \tag{A6-1}$$

The slope expression as mentioned below the Eq. (4.5) and its relative uncertainty are automatically obtained during the fitting process.

A6-2: Uncertainty calculation for the DSC

The determination of the thermal conductivity is based on the measurement of the heat flux through the sample and the corresponding temperature difference with the reference pan. That heat flux or thermal power has a standard deviation or systematic uncertainty of 0.0006 W. The temperature measurement has a standard deviation of 0.03 °C. The height and diameter of the sample is measured using a digital calliper (Powerfix) with the uncertainty of ±0.02 mm.

The error calculation of thermal conductivity under transient state measurement is obtained via Eqs. (4.3) and (4.4):

$$\left|\frac{dslope}{slope}\right| = \left|\frac{dq_t}{q_t} - \frac{dT}{T}\right| = \left|\frac{dR_s}{R_s}\right| \leq \left|\frac{dq_t}{q_t}\right| + \left|\frac{dT}{T}\right| \tag{A6-1}$$

$$\left|\frac{d\lambda}{\lambda}\right| = \left|\frac{dL_s}{L_s} - \frac{dA}{A} - \frac{dR_s}{R_s}\right| \leq \left|\frac{dL_s}{L_s}\right| + \left|\frac{dA}{A}\right| + \left|\frac{dR_s}{R_s}\right| \tag{A6-2}$$

APPENDIX – A7. ALUMINIUM HONEYCOMB HEAT EXCHANGER PLATES: THERMOCOUPLES POSITION AND THEIR PARALLEL AND PERPENDICULAR DIRECTION TO HTF FLOW.

N_1 (0.1; -0.03; -0.025)

N_2 (0.1; -0.03; -0.025)

N_3 (0.08; -0.04; 0.02)

N_4 (0.2; -0.03; -0.025)

N_5 (0.08; -0.04; 0.02)
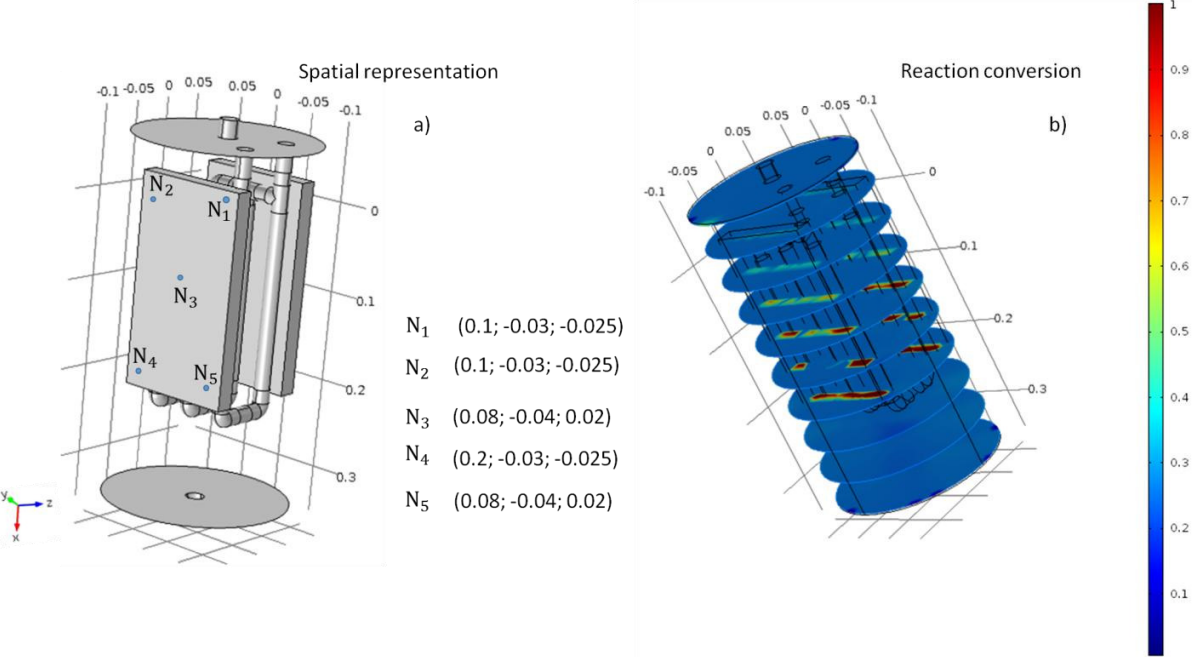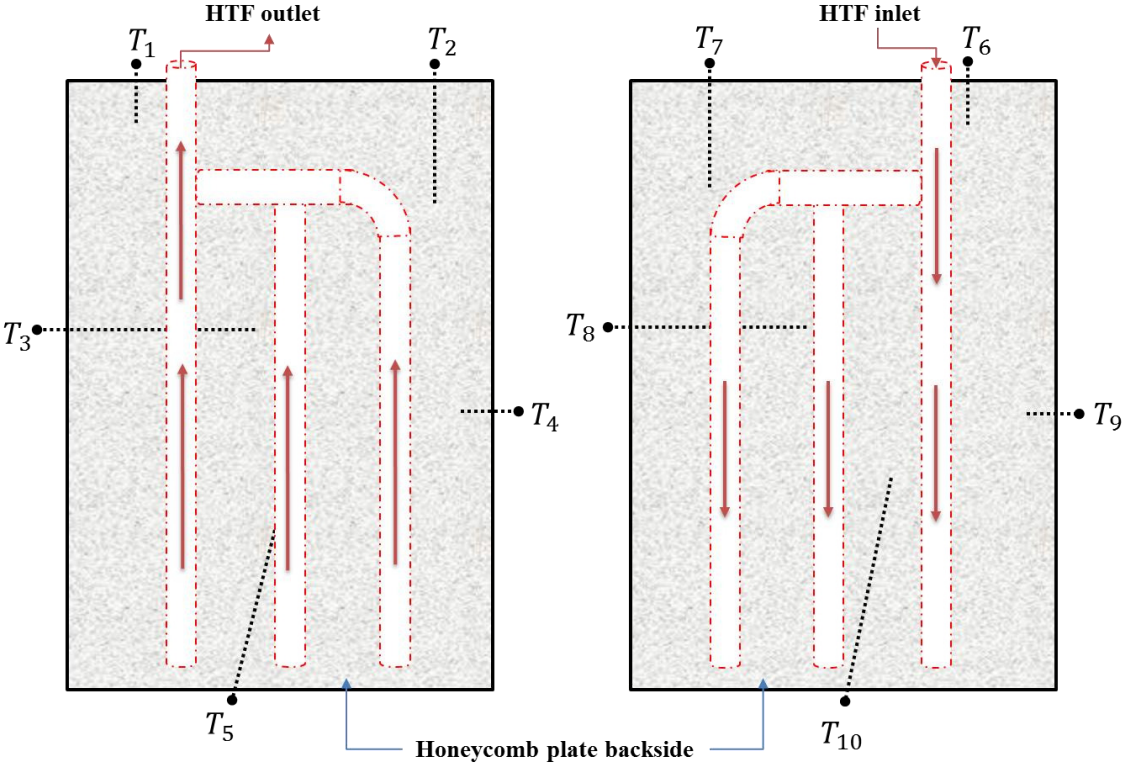
SIGMA-ALDRICH

sigma-aldrich.com

SAFETY DATA SHEET

according to Regulation (EC) No. 1907/2006
Version 5.0 Revision Date 18.12.2012
Print Date 09.09.2013
GENERIC EU MSDS - NO COUNTRY SPECIFIC DATA - NO OEL DATA

---

1. IDENTIFICATION OF THE SUBSTANCE/MIXTURE AND OF THE COMPANY/UNDERTAKING

1.1 Product identifiers

Product name : Strontium bromide hexahydrate

Product Number : 433438
Brand : Aldrich
CAS-No. : 7789-53-9

1.2 Relevant identified uses of the substance or mixture and uses advised against

Identified uses : Laboratory chemicals, Manufacture of substances

1.3 Details of the supplier of the safety data sheet

Company : Sigma-Aldrich Chemie GmbH
Riedstrasse 2
D-89555 STEINHEIM

Telephone : +49 89-6513-1444
Fax : +49 7329-97-2319
E-mail address : eurtechserv@sial.com

1.4 Emergency telephone number

Emergency Phone # : +49 7329-97-2323

---

2. HAZARDS IDENTIFICATION

2.1 Classification of the substance or mixture

Classification according to Regulation (EC) No 1272/2008 [EU-GHS/CLP]
Skin irritation (Category 2)
Eye irritation (Category 2)
Specific target organ toxicity - single exposure (Category 3)

Classification according to EU Directives 67/548/EEC or 1999/45/EC
Irritating to eyes, respiratory system and skin.

2.2 Label elements

Labelling according Regulation (EC) No 1272/2008 [CLP]
Pictogram

Signal word Warning

Hazard statement(s)
H315 Causes skin irritation.
H319 Causes serious eye irritation.
H335 May cause respiratory irritation.

Precautionary statement(s)
P261 Avoid breathing dust.
P305 + P351 + P338 IF IN EYES: Rinse cautiously with water for several minutes. Remove contact lenses, if present and easy to do. Continue rinsing.

Supplemental Hazard none
Statements

CCX

According to European Directive 67/548/EEC as amended.

Hazard symbol(s)

R-phrase(s)

R36/37/38   Irritating to eyes, respiratory system and skin.

S-phrase(s)

S26   In case of contact with eyes, rinse immediately with plenty of water and seek medical advice.

S36   Wear suitable protective clothing.

2.3 Other hazards - none

---

3. COMPOSITION/INFORMATION ON INGREDIENTS

3.1 Substances

Formula   : $Br_2Sr \cdot 6H_2O$

Molecular Weight   :   355,52 g/mol

Component			Concentration
Strontium bromide hexahydrate			
CAS-No.	7789-53-9		-
EC-No.	233-969-5		

---

4. FIRST AID MEASURES

4.1 Description of first aid measures

General advice

Consult a physician. Show this safety data sheet to the doctor in attendance.

If inhaled

If breathed in, move person into fresh air. If not breathing, give artificial respiration. Consult a physician.

In case of skin contact

Wash off with soap and plenty of water. Consult a physician.

In case of eye contact

Rinse thoroughly with plenty of water for at least 15 minutes and consult a physician.

If swallowed

Never give anything by mouth to an unconscious person. Rinse mouth with water. Consult a physician.

4.2 Most important symptoms and effects, both acute and delayed

Exposure to large amounts can cause:, Central nervous system depression, Nausea, Vomiting, To the best of our knowledge, the chemical, physical, and toxicological properties have not been thoroughly investigated.

4.3 Indication of any immediate medical attention and special treatment needed

no data available

---

5. FIREFIGHTING MEASURES

5.1 Extinguishing media

Suitable extinguishing media

Use water spray, alcohol-resistant foam, dry chemical or carbon dioxide.

5.2 Special hazards arising from the substance or mixture

Hydrogen bromide gas, Strontium oxides

5.3 Advice for firefighters

Wear self contained breathing apparatus for fire fighting if necessary.

5.4 Further information

no data available

CCXI

6.	**ACCIDENTAL RELEASE MEASURES**

6.1 Personal precautions, protective equipment and emergency procedures
Use personal protective equipment. Avoid dust formation. Avoid breathing vapors, mist or gas. Ensure adequate ventilation. Evacuate personnel to safe areas. Avoid breathing dust.

6.2 Environmental precautions
Do not let product enter drains.

6.3 Methods and materials for containment and cleaning up
Pick up and arrange disposal without creating dust. Sweep up and shovel. Keep in suitable, closed containers for disposal.

6.4 Reference to other sections
For disposal see section 13.

7.	**HANDLING AND STORAGE**

7.1 Precautions for safe handling
Avoid contact with skin and eyes. Avoid formation of dust and aerosols.
Provide appropriate exhaust ventilation at places where dust is formed.Normal measures for preventive fire protection.

7.2 Conditions for safe storage, including any incompatibilities
Store in cool place. Keep container tightly closed in a dry and well-ventilated place.

7.3 Specific end use(s)
no data available

8.	**EXPOSURE CONTROLS/PERSONAL PROTECTION**

8.1 Control parameters

Components with workplace control parameters

8.2 Exposure controls

Appropriate engineering controls
Handle in accordance with good industrial hygiene and safety practice. Wash hands before breaks and at the end of workday.

Personal protective equipment

Eye/face protection
Safety glasses with side-shields conforming to EN166 Use equipment for eye protection tested and approved under appropriate government standards such as NIOSH (US) or EN 166(EU).

Skin protection
Handle with gloves. Gloves must be inspected prior to use. Use proper glove removal technique (without touching glove's outer surface) to avoid skin contact with this product. Dispose of contaminated gloves after use in accordance with applicable laws and good laboratory practices. Wash and dry hands.

The selected protective gloves have to satisfy the specifications of EU Directive 89/686/EEC and the standard EN 374 derived from it.

Body Protection
Impervious clothing., The type of protective equipment must be selected according to the concentration and amount of the dangerous substance at the specific workplace.

Respiratory protection
For nuisance exposures use type P95 (US) or type P1 (EU EN 143) particle respirator.For higher level protection use type OV/AG/P99 (US) or type ABEK-P2 (EU EN 143) respirator cartridges. Use respirators and components tested and approved under appropriate government standards such as NIOSH (US) or CEN (EU).

CCXII

9. PHYSICAL AND CHEMICAL PROPERTIES

9.1 Information on basic physical and chemical properties

a)	Appearance	Form: Crystals with lumps Colour: white
b)	Odour	no data available
c)	Odour Threshold	no data available
d)	pH	no data available
e)	Melting point/freezing point	no data available
f)	Initial boiling point and boiling range	no data available
g)	Flash point	not applicable
h)	Evaporation rate	no data available
i)	Flammability (solid, gas)	no data available
j)	Upper/lower flammability or explosive limits	no data available
k)	Vapour pressure	no data available
l)	Vapour density	no data available
m)	Relative density	no data available
n)	Water solubility	no data available
o)	Partition coefficient: n-octanol/water	no data available
p)	Auto-ignition temperature	no data available
q)	Decomposition temperature	no data available
r)	Viscosity	no data available
s)	Explosive properties	no data available
t)	Oxidizing properties	no data available

9.2 Other safety information
no data available

10. STABILITY AND REACTIVITY

10.1 Reactivity
no data available

10.2 Chemical stability
no data available

10.3 Possibility of hazardous reactions
no data available

10.4 Conditions to avoid
no data available

10.5 Incompatible materials
Strong oxidizing agents

10.6 Hazardous decomposition products
Other decomposition products - no data available

11. TOXICOLOGICAL INFORMATION

11.1 Information on toxicological effects

Acute toxicity
no data available

Skin corrosion/irritation
no data available

Serious eye damage/eye irritation
no data available

Respiratory or skin sensitization
no data available

Germ cell mutagenicity
no data available

Carcinogenicity

IARC: No component of this product present at levels greater than or equal to 0.1% is identified as probable, possible or confirmed human carcinogen by IARC.

Reproductive toxicity
no data available

Specific target organ toxicity - single exposure
Inhalation - May cause respiratory irritation.

Specific target organ toxicity - repeated exposure
no data available

Aspiration hazard
no data available

Potential health effects

Inhalation	May be harmful if inhaled. Causes respiratory tract irritation.
Ingestion	May be harmful if swallowed.
Skin	May be harmful if absorbed through skin. Causes skin irritation.
Eyes	Causes serious eye irritation.

Signs and Symptoms of Exposure
Exposure to large amounts can cause:, Central nervous system depression, Nausea, Vomiting, To the best of our knowledge, the chemical, physical, and toxicological properties have not been thoroughly investigated.

Additional Information
RTECS: WK8225000

12. ECOLOGICAL INFORMATION

12.1 Toxicity
no data available

12.2 Persistence and degradability
no data available

12.3 Bioaccumulative potential
no data available

12.4 Mobility in soil
no data available

12.5 Results of PBT and vPvB assessment
no data available

12.6 Other adverse effects
no data available

13. DISPOSAL CONSIDERATIONS

13.1 Waste treatment methods

Product
Offer surplus and non-recyclable solutions to a licensed disposal company. Contact a licensed professional waste disposal service to dispose of this material. Dissolve or mix the material with a combustible solvent and burn in a chemical incinerator equipped with an afterburner and scrubber.

Contaminated packaging
Dispose of as unused product.

14. TRANSPORT INFORMATION

14.1 UN number
ADR/RID: -   IMDG: -   IATA: -

14.2 UN proper shipping name
ADR/RID: Not dangerous goods
IMDG: Not dangerous goods
IATA: Not dangerous goods

14.3 Transport hazard class(es)
ADR/RID: -   IMDG: -   IATA: -

14.4 Packaging group
ADR/RID: -   IMDG: -   IATA: -

14.5 Environmental hazards
ADR/RID: no   IMDG Marine Pollutant: no   IATA: no

14.6 Special precautions for user
no data available

15. REGULATORY INFORMATION

This safety datasheet complies with the requirements of Regulation (EC) No. 1907/2006.

15.1 Safety, health and environmental regulations/legislation specific for the substance or mixture
no data available

15.2 Chemical Safety Assessment
no data available

16. OTHER INFORMATION

Further information
Copyright 2012 Sigma-Aldrich Co. LLC. License granted to make unlimited paper copies for internal use only.
The above information is believed to be correct but does not purport to be all inclusive and shall be used only as a guide. The information in this document is based on the present state of our knowledge and is applicable to the product with regard to appropriate safety precautions. It does not represent any guarantee of the properties of the product. Sigma-Aldrich Corporation and its Affiliates shall not be held liable for any damage resulting from handling or from contact with the above product. See www.sigma-aldrich.com and/or the reverse side of invoice or packing slip for additional terms and conditions of sale.